Mitochondrial function in the neonatal rat cochlea

Zoë Francesca Mann

A Thesis submitted for the Degree of Doctor of Philosophy

Department of Physiology
and
UCL Ear Institute
University College London

January 2008

ProQuest LLC
789 East Eisenhower Parkway
P.O. Box 1346
Ann Arbor, MI 48106-1346

Declaration

I, Zoë Mann, confirm that the work presented herein is my own. In any place where information has been obtained from other sources, it has been fully referenced and indicated in the thesis.

Abstract

The cochlea is a specialised structure that contains the cells responsible for transducing mechanical sound stimuli into neural code within the auditory nerve. Mutations in the mitochondrial genome have been associated with hearing loss, suggesting that they play a key role in cochlear physiology. Alongside ATP production, mitochondria are also intimately involved in processes such as calcium homeostasis and the regulation of cell death. The precise role for mitochondria in inner ear physiology is at present poorly defined.

I used neonatal cochlear explants and confocal microscopy to study aspects of mitochondrial physiology. The dye TMRM was used to investigate differences in $\Delta\psi_{mt}$ between basal and apical inner (IHC) and outer (OHC) hair cells and supporting cells. Data reveal a base-to-apex difference in mitochondrial function specific to inner hair cells. Mitochondrial function was investigated further using the endogenous autofluorescence of NADH and flavoproteins and revealed a base-to-apex difference in cell redox state, again in the IHCs but not OHCs. Differences in intracellular metabolism were also investigated using fluorescence lifetime imaging of NAD(P)H and revealed metabolic differences between OHCs and supporting cells consistent with a metabolism that is more glycolytic in supporting cells and more oxidative in OHCs.

The role of mitochondria in cochlear Ca^{2+} homeostasis was also investigated. The amplitude and spatiotemporal properties of intercellular Ca^{2+} waves initiated by ATP were studied. Blocking mitochondrial Ca^{2+} ($[Ca^{2+}]_{mt}$) uptake using Ru360 increased the wave amplitude, propagation velocity and extent of spread in cochlear supporting cells, showing that mitochondrial Ca^{2+} buffering plays a role in shaping calcium signals in the cochlea.

Finally, neomycin was used to investigate $[Ca^{2+}]_c$ and $[Ca^{2+}]_{mt}$ during neomycin toxicity. Neomycin induced a rapid bi-phasic response in OHC $[Ca^{2+}]_c$ leading to cell loss of $\Delta\psi_{mt}$ and cell permeabilsation, which correlated with ATP-dependent intercellular Ca^{2+} waves in the surrounding supporting cells.

Acknowledgements

First and foremost, I would like to thank my supervisors Dr Jonathan Gale and Professor Michael Duchen for their continued support, guidance and encouragement throughout my Ph.D. I would also like to thank Professor Jonathan Ashmore for all his help and scientific input to my project and Dr Dan Jagger for introducing me to the wonderful world of cochlear slicing.

My thanks also go to my lab members and most of all friends at the Centre for Auditory Research, in particular Manu and Helen for their continued patience and friendship even in the hardest of times. I would also like to thank all the members of the Duchen lab for always keeping my spirits up.

I would like to give a special thanks to my wonderful family and to Jonathan, for their never wavering support, love and perspective during these past few years. I couldn't have done it without you all.

This thesis is dedicated to John and Julia Summerfield, you will always be in my heart.

TABLE OF CONTENTS

List of Figures

Chapter 1 - Introduction

Chapter 2 – Materials and Methods

Chapter 3 – Base-to-apex differences in mitochondrial function in the cochlea

Chapter 4 – Mitochondrial Ca^{2+} buffering influences $[Ca^{2+}]_c$ signalling

Chapter 5 – Early signalling events in neomycin-induced hair cell death

Chapter 6 – General discussion

List of Tables

List of abbreviations

AIF	apoptosis inducing factor
ANT	adenine nucleotide translocase
ATP	Adenosine triphosphate
Bcl2	B-cell leukemia/lymphoma 2
$[Ca^{2+}]_c$	cytosolic calcium
$[Ca^{2+}]_{mt}$	mitochondrial calcium
CCCP	carbonyl cyanide-m-chlorophenylhydrazone
CV	coefficient variation
CyP-D	cyclophilin D
Cyt c	cytochrome c
DMEM	Dulbecco's Modified Essential Medium
$DiIC_1(5)$	1,1'-dimethyl-3,3,3',3'-tetramethylindodicarbocyanine, iodide
ER	endoplasmic reticulum
ERK1/2	extracellularly regulated kinase 1/2
ETC	electron transfer chain
FAD^{2+}	Flavin adenine dinucleotide
FCCP	carbonyl cyanide p-trifluoromethoxyphenyl hydrazone
FM1-43	N-(3-triethylammoniumpropyl)-4-(4-(dibutylamino-styryl) pyridiniumdibromide
HEPES	4-(2-hydroxyethyl)-1-piperazineethanesulfonic acid
HBSS	Hanks balanced salt solution
ICRAC	store-operated calcium current
IHCs	inner hair cells
IMM	inner mitochondrial membrane
IP_3	inositol 1,4,5-triphosphate
IP_3R	inositol 1,4,5-triphosphate receptor
JNK	C-Jun N-terminal kinase
K^+	potassium
LSM	laser scanning microscope
MAPK	mitogen-activated protein kinase

MCU	mitochondrial calcium uniporter
MET channel	mecahnoelectrical transducer channel
mPTP	mitochondrial permeability transition
mtDNA	mitochondrial DNA
mRNA	messenger RNA
NADH	nicotinamide adenine dinucleotide
NAD(P)H	nicotinamide adenine dinucleotide phosphate
$NaHCO_3$	sodium hydrogen carbonate
NaOH	sodium hydroxide
nDNA	nuclear DNA
OHCs	outer hair cells
OMM	outer mitochondrial membrane
P (2,3 etc)	post natal day (2,3 etc)
P2X	ionotropic purinergic receptor
P2Y	metabotropic purinergic receptor
PFA	paraformaldehyde
Rh123	Rhodamine 123
ROI	region of interest
ROS	reactive oxygen species
Ru360	ruthenium 360
SEM	standard error of the mean
SOC	store-operated calcium channel
TMRM	tetramethyl rhodaminemethylester
UCP	uncoupling protein
VDAC	voltage-dependent anion channel

ΔR	change in ratio
$\Delta\psi_{mt}$	mitochondrial membrane potential

1 Introduction

Mutations are known to occur in the mitochondrial genome, which result in hearing loss. Patients carrying these mutations can present with any of the following; aminoglycoside hypersensitivity, sudden onset hearing loss and accelerated presbyacusis. Cells carrying mitochondrial mutations are likely to exhibit impaired ATP production, which in turn is detrimental to the physiology of tissue. Little is known about the physiology of mitochondria in the cochlea, making it difficult to determine how impaired ATP production would occur. Aside from ATP production, mitochondria are also intimately involved in numerous physiological processes within the cell, including Ca^{2+} homeostasis, regulation of cell redox state and the control of cell life and death all of which are essential for normal tissue function. It is likely therefore that mitochondrial dysfunction can disrupt the physiology of hearing through means other than simply reduced production of ATP.

1.1 Structure and function of the cochlea

1.1.1 The mammalian inner ear

The ear is comprised of the outer ear, middle ear and inner ear. The cochlea and vestibular organs are located in the inner ear, encased together within the otic capsule forming a structure known as the bony labyrinth (Moller, 2000). The cochlea is a coiled structure that contains the sensory organs for hearing and the vestibular system, contains the organs necessary for balance. Within the cochlea, complex sound stimuli are transduced into coded neural signals in the auditory nerve. The cochlea itself is comprised of three fluid-filled compartments; the scala media, the scala tympani and the scala vestibuli. The scala media, located in the middle of the cochlea is separated from the scala vestibuli by the Reissner's membrane and from the scala tympani by the basilar membrane (see Figure 1.1). The ionic composition of the fluids in these compartments are different, and their maintenance is essential for hearing. The scala tympani and vestibuli contain perilymph, the composition of which is similar to extracellular fluid. The scala media contains endolymph, whose composition more closely resembles intracellular fluid (See Table 2).

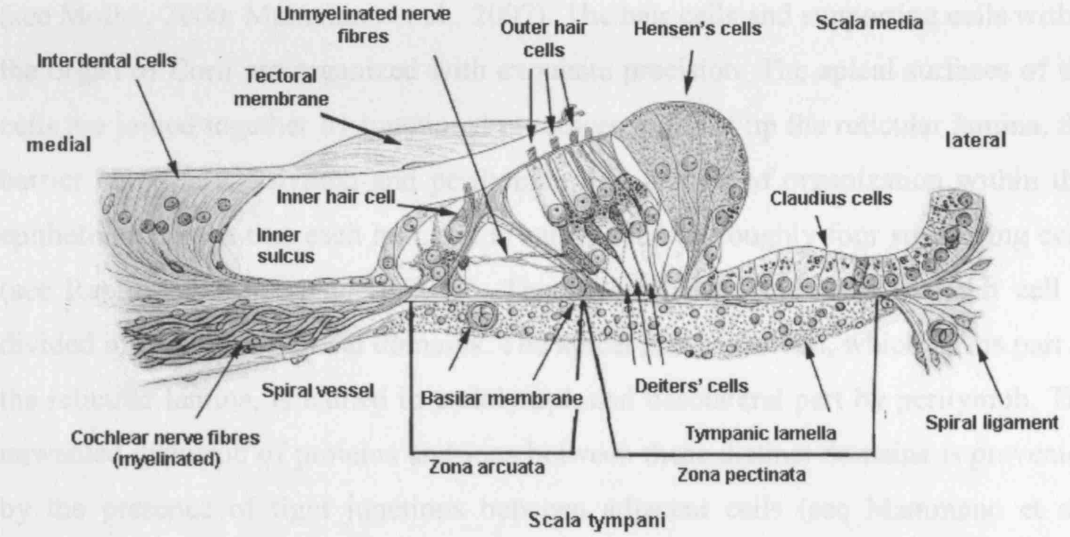

Figure 1. 1 Scematic representation of the human cochlea.

The diagram depicts the different cell types and specialised extracellular components existing in the organ of Corti. The outer hair cells (OHCs) and inner hair cells (IHCs) comprise the sensory cells. The Claudius cells, Deiters' cells, Hensen's cells and cells of the inner sulcus make up some of the various non sensory supporting cell populations. The scala media contains the specialised cochlear fluid, the endolymph and the scala tympani the perilymph. *Schematic adapted from Raphael & Altschuler 2003.*

Table 1 Ionic composition of the inner ear fluids. ***Adapted from Wangemann 2006***

Ion	Unit	Scala media endolymph	Scala tympani perilymph	Scala vestibuli perilymph	Plasma
Na^+	mM	1.3	148	141	145
K^+	mM	157	4.2	6.0	5.0
Ca^{2+}	mM	0.023	1.3	0.6	2.6
Cl^-	mM	132	119	121	106
HCO_3^-	mM	31	21	18	18
Glucose	mM	0.6	3.6	3.8	8.3
Protein	mg/dl^{-1}	38	178	242	4238
pH	pH units	7.4	7.3	7.3	7.3

Mechanosensory transduction in the inner ear is carried out by the sensory hair cells. Hair cells are found in three types of sensory organ; the organ of Corti, and the maculae and the cristae of the vestibular system. The organ of Corti comprises the epithelium of the cochlea and the maculae and cristae those of the vestibular system

(see Moller, 2000; Mammano et al., 2007). The hair cells and supporting cells within the organ of Corti are organized with exquisite precision. The apical surfaces of the cells are joined together by junctional processes to make up the reticular lamina, the barrier between endolymph and perilymph. The pattern of organization within this epithelium is such that each hair cell is surrounded by roughly four supporting cells (see Raphael and Altschuler, 2003). The hair cells are polarised i.e each cell is divided into basal and apical domains. The apical part of the cell, which forms part of the reticular lamina, is bathed in endolymph and basolateral part by perilymph. The unwanted diffusion of proteins and ions between these distinct domains is prevented by the presence of tight junctions between adjacent cells (see Mammano et al., 2007).

1.1.2 Hair cells

Hair cells are the mechanosensory cells of the cochlea and vestibular systems. There are two types of sensory hair cells within the cochlea, the inner hair cells (IHCs) and the outer hair cells (OHCs). The IHCs are the true sensory receptors of the cochlea, converting mechanical sound stimuli into nerve impulses. The OHCs on the other hand are responsible for establishing the sensitivity and selectivity of the cochlea to given sound stimuli (see Raphael and Altschuler, 2003).

The stereocilial bundle located at the apical end of the hair cell is necessary for the reception of sound stimuli and mechanoelectrical transduction and is comprised of around 20-300 actin-filled stiff microvilli (Pickles, 1988). The individual cilia are arranged in rows of graded heights, giving a staircase pattern (Lin et al., 2005). Actin turnover within these structures has the characteristics of a treadmill model, in which the rate of treadmilling corresponds to the length of each individual stereocilium. This highly regulated process of actin turnover is thought to maintain stereocilial lengths over long periods of time (Lin et al., 2005). The basolateral end of hair cells can be contacted by both afferent and efferent nerve fibres. Supporting cell lateral membranes enclose the inner hair cells and their associated axons and nerve terminals enabling each hair cell to be successfully isolated from its neighbours (Moller, 2000).

This epithelial surface is overlaid by an extracellular matrix. This matrix exists in two forms; the otoconial membrane in the vestibular system and the tectoral membrane in the cochlea. These matrices permit the delivery of sound and mechanical stimuli to the hair cell bundles, by providing a stable structure against which they can react.

1.1.3 The cochlear amplifier

Mechanosensory transduction in the inner ear refers to the highly specialised process by which mechanical stimuli perceived by hair cells are converted into electrical signals in the auditory nerve (for review see Fettiplace and Ricci, 2006). The walls of the cochlea are lined with epithelial cells, which collectively make up the membranous labyrinth. This population of cells includes sensory hair cells and non-sensory supporting cells, both of which are polarised (see Raphael and Altschuler, 2003). High frequency sounds are transduced at the base of the cochlea and low frequency sounds at the opposite end, referred to as the apex (see Russell and Sellick, 1978). This results in a tonotopic distribution of sound frequencies from the base to the apex of the cochlea.

Sound energy induces pressure changes within the cochlea fluids and elicits specific patterns of vibration on the basilar membrane (BM) (Pickles, 1988). The motion of the BM elicited by a given sound stimulus is determined by the intrinsic properties of the membrane (stiffness and mass) itself. The stiffness of the membrane decreases from base to apex of the cochlea thus enabling it to act as a spectral analyser.

Sound-induced deformations of the BM result in deflection of the stereocilial bundle towards the tallest stereocilia (excitatory stimulus). This processes results in the opening of mechanosensitive transduction channels at the apical pole of the cell. Opening of these cation-selective channels causes an influx of K^+ ions from the extracellular fluid, the endolymph. It is the endocochlear potential in the endolymph, (+80 to +100 mV with respect to perilymph) (Salt et al., 1987) established through the activity of marginal and intermediate cells within the stria vascularis that drives this K^+ influx (Takeuchi and Ando, 1997; Marcus et al., 2002; Wangemann, 2006). The electrical activity occurring within the hair cells subsequent to K^+ entry is then

relayed to the higher brain areas via the auditory nerve. Potassium (K^+) is the predominant charge carrier in the process of sensory transduction, (see section 1.1.3) given that it is the most abundant ion in the scala media (Wangemann 2006), however a small proportion of the transduction current has been attributed to Ca^{2+} (Ricci and Fettiplace, 1998).

Hearing in mammals, (achieved through mechanosensory transduction) can be amplified by up to 40 dB, by means of an active feedback mechanism intrinsic to the mammalian ear. Cochlear amplication of sound stimuli relies on the electromotile responses intrinsic to OHCs. The latter refer to the process in which transmembrane voltage induces length changes in OHCs at specific sound frequencies (Ashmore, 1987; Mammano et al., 1995; Liberman et al., 2002). These electromotile responses are thought to provide feedback to the basilar membrane thus allowing mechanical amplification of sound stimuli by the OHCs (Dallos et al., 1997). Cochlear amplification by the OHCs establishes the high frequency tuning and discrimination of the cochlea (Geleoc and Holt, 2003). Bundle motion in response to a given acoustic stimulus is shaped by the intrinsic stiffness or compliance of the bundle. Bundle compliance displays both passive and active elements. The passive component results from flexibility at the stereocilial ankles and interstereocilial connections (Fettiplace et al., 2001). The active component, also referred to as the channel gating compliance is linked to the opening and closing of the MET channels themselves (Howard and Hudspeth, 1988). This phenomenon centres around the idea that channels can undergo conformational changes as they open and close. These conformational changes can generate force sufficient to actively move the bundle and modulate its motion (Howard and Hudspeth, 1988). Bundles movements have been measured at values ranging from 1-100 nm in a variety of species (Crawford and Fettiplace, 1985; Martin and Hudspeth, 1999) and following bundle deflection with compliant probes (Crawford and Fettiplace, 1985; Howard and Hudspeth, 1987; Ricci et al., 2000; Kennedy et al., 2005). Amplification could thus result from a combination of the electromotile response and the bundle movement itself.

It has also been suggested, that amplication can occur as a result of non-linearity within the channel gating of transduction itself (Hudspeth et al., 2000; Fettiplace et al., 2001). Data suggesting cochlear amplification to originate from within the bundle

have come from studies in lower vertebrates (Crawford and Fettiplace, 1985). The precise role of these bundle movements is as yet unclear, although it has been suggested that they act by amplifying mechanically-induced oscillation of bundles to sound stimuli (Martin and Hudspeth, 1999). It has also been suggested that these active bundle movements are closely associated with MET channel adaptation (Ricci et al., 2000).

1.1.4 Cochlear adaptation

Adaptation of sensory auditory hair cells is defined as a reduction in transducer current during periods of prolonged bundle stimulation. The adaptation process is achieved by shifting the sensitivity of the bundle to a point where the degree of tension perceived by the MET channels is reduced (Eatock et al., 1987; Crawford et al., 1989).

Adaptation has been studied predominantly in lower vertebrates such as turtle (Ricci et al., 2000) and bullfrog (Eatock et al., 1987) although there is recent evidence suggesting the presence of a similar mechanism in neonatal (Kros et al., 1992) and adult (Kennedy et al., 2003) rodents. The adaptation or immediate closure of the MET channel subsequent to excitatory stimulation occurs via a two-stage process. Fast adaptation takes place over a sub-millisecond time scale and is most prominent for smaller mechanical stimuli (Corey and Hudspeth, 1983; Crawford and Fettiplace, 1985; Kros et al., 1992; Ricci and Fettiplace, 1998; Holt and Corey, 2000). Slow adaptation on the other hand occurs over tens of milliseconds and is predominant for larger stimuli (Wu et al., 1999). Slow adaptation has been shown to arise as a result of a myosin 1ß/1c-dependent process (Garcia et al., 1998; Steyger et al., 1998; Holt et al., 2002; Gillespie, 2004). It has been suggested that the rate of fast adaptation is directly proportional to the degree of Ca^{2+} from the endolymph during transduction. The precise mechanisms underlying fast adaptation remain as yet undefined.

1.2 Calcium in cochlear physiology

1.2.1 Purinergic signalling pathways in the inner ear

There is substantial evidence that nucleotide signalling plays an important role in the physiology of multiple sensory systems (Burnstock, 1972, 2007). This section will focus on the role of the purine nucleotide Adenosine 5'-triphosphate (ATP) in various signalling pathways of the inner ear. Extracellular ATP exerts it physiological and pathophysiological effects by activating purinergic receptors expressed widely throughout a number of tissues. Purinoceptors can be divided into two main subtypes, the P2X ligand-gated ion channels (ionotropic) and the P2Y G-protein coupled (metabotropic) receptors (see Burnstock, 2007). The P2X receptor family is comprised of seven members ($P2X_1$-$P2X_7$). These ligand-gated cation channels have structures that closely resemble that of the inwardly rectifying K^+ channel family (see North and Barnard, 1997; Housley et al., 2006). The P2Y receptor family consists of 8 members; $P2Y_1$, $P2Y_2$, $P2Y_4$, $P2Y_6$, $P2Y_{11}$, $P2Y_{12}$, $P2Y_{13}$, $P2Y_{14}$. Each receptor functions by binding to a single heterotrimeric G-protein. $P2Y_{1,2,4,6}$ bind to $G_{q/11}$, $P2Y_{11}$ associates with both $G_{q/11}$ and G_s, $P2Y_{12\&13}$ couple to G_i and $P2Y_{14}$ to $G_{i/o}$ (see Burnstock, 2007).

ATP can act as a co-transmitter or neuromodulator and has been shown to influence the sensitivity of the auditory system (see Mammano et al., 2007). The source of extracellular ATP in the cochlear has been confined to vesicular structures within the marginal cells of the stria vascularis (White et al., 1995). Using the luciferin-luciferase bioluminescent assay, vesicular release of ATP has been shown to exhibit Ca^{2+} dependence. ATP is known to modulate hearing sensitivity through its actions in the cochlea (Housley et al., 1999). Purinergic signalling is known to modulate numerous processes within the cochlea including K^+ transport, micromechanics, cochlear blood flow and can act as a neurotransmitter (see Housley, 2000).

Alongside the MET channel, OHCs express P2Rs on the stereocilial membranes (Mockett et al., 1994) suggesting a role for purinergic signalling in OHCs. Pharmacological studies on OHCs have shown that ATP can modulate cochlear mechanics (Skellett et al., 1997). Local application of ATP to isolated OHCs has

been shown to evoke inward rectifying, non-desensitising depolarisations (Nakagawa et al., 1990; Housley et al., 1992). These currents originated from purinergic receptors which localise to the apical surface of the OHCs (Figure 1.2 and Housley et al., 1992). Further pharmacological studies in guinea pig cochleae revealed the assembly of ATP-gated ion channels from $P2X_2$ receptor subunits with the highest expression found in hair cell stereocilia (Housley et al., 1999). It is proposed that these subunits assemble to form the splice variant $P2X_{2/3}$ (Greenwood et al., 2007). Apically localised ATP-activated conductances resulting in elevated cytoplasmic Ca^{2+} ($[Ca^{2+}]_c$) have also been revealed in chick cochlear hair cells (Shigemoto and Ohmori, 1990), guinea pig cochlear outer hair cells (Ashmore and Ohmori, 1990) and guinea pig inner hair cells (Dulon et al., 1991).

Elevations in endolymphatic ATP results in P2XR activation in OHCs and Deiters' cells (see Housley, 2000) establishing a shunt conductance of K^+ ions across the reticular lamina. The ATP-activated conductance depolarises the hair cell thus reducing the OHC receptor potential (Housley et al., 1992). Typically, the ATP concentration in both endolymphatic and perilymphatic compartments is maintained in the nanomolar range through the activity of ecto-nucleotidases. These nucleotidases are thought to be the primary mechanism by which purinergic signalling is terminated in the cochlea (Vlajkovic et al., 1998). Fluctuations in resting ATP levels are thought to signal important physiological or pathophysiological changes to the purinergic receptors (P2R) expressed widely throughout the cochlea (Housley et al., 1992).

The ATP-induced increases in $[Ca^{2+}]_c$ seen in isolated OHCs and Deiters' cells have been attributed to both intracellular and extracellular Ca^{2+} sources (Mammano et al., 1999; Lagostena et al., 2001). Recent work by Mammano and colleagues has shown extracellular application of ATP to the OHC bundle to elicit a bi-phasic increase in $[Ca^{2+}]_c$. The initial rise originates from Ca^{2+} influx through P2XRs. The second and more pronounced increase in $[Ca^{2+}]_c$ is due to IP_3-gated Ca^{2+} release (Mammano et al., 1999).

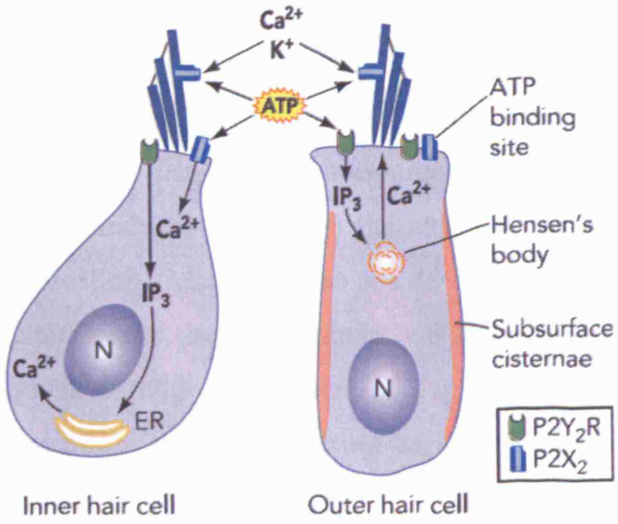

Figure 1. 2 P2 receptor expression in cochlear hair cells.

P2X receptors are ligand-gated cation channels allowing Ca^{2+} influx (from external sources). P2Y receptors are G-protein coupled receptors that bring about increases in $[Ca^{2+}]_c$ through release from intracellular stores. P2X receptors reside on the apical membranes of OHC and IHC stereocillia. P2X and P2Y receptors localise to the base of the hair cell bundle. OHCs possess a specialised structure at their apical pole, the Hensen's body. This structure consists of mitochondrial and ER membranes and is thought to function as an IP_3-gated Ca^{2+} store. *Figure from Mammano et al., 2007.*

It has been suggested that the site of Ca^{2+} release resides below the cuticular plate, at the base of the OHC bundle. This region contains a specialised structure comprised of ER and mitochondria, known as the Hensen's body (Mammano et al., 1999). Immuno-labelling studies have shown IP_3R expression to correlate with this structure suggesting it may act as an IP_3-sensitive Ca^{2+} store (Mammano et al., 1999). At present, there is no literature describing the physiological role of the mitochondria associated with this structure. There is however a vast body of evidence from a variety of other cell types supporting a pivotal role for mitochondria in $[Ca^{2+}]_c$ signalling (see Section 1.5). It is likely therefore that Hensen's body mitochondria are involved in $[Ca^{2+}]_c$ homeostasis and/or regulating the spatiotemporal properties of $[Ca^{2+}]_c$ waves in hair cells. Elevations in hair cell $[Ca^{2+}]_c$ in reponse to ATP are

thought to be restricted to the apical portion of the cell. The containment of such $[Ca^{2+}]_c$ signals is suggested to result from the function of numerous Ca^{2+} binding proteins expressed throughout the cochlea (Pack and Slepecky, 1995; Nomiya et al., 1998) and could also be regulated by the Hensen's body situated below the cuticilar plate (Mammano et al., 1999). It has also been suggested that this ATP-dependent Ca^{2+} increase regulates processes specific to the hair cell bundle, such as cochlear adaptation and amplification (Mammano et al., 1999). The ATP-induced $[Ca^{2+}]_c$ changes seen in Deiters' cells are predominantly P2Y mediated. The increase in $[Ca^{2+}]_c$ has been shown to reduce the extent of gap junctional coupling and thus intercellular communication, potentially acting as a protective mechanism during periods of cell stress (Lagostena et al., 2001)

1.2.2 A role for Ca^{2+} in cochlear adaptation

Transducer adaptation refers to the reduction in transduction current seen during prolonged bundle stimulation (Holt and Corey, 2000). This process is thought to be regulated by the rise in $[Ca^{2+}]_c$ that occurs during bundle deflection (Ricci and Fettiplace, 1998). This hypothesis emerged in light of evidence showing the slowing or absence of adaptation in conditions of reduced Ca^{2+} entry (Corey and Hudspeth, 1983; Eatock et al., 1987; Crawford et al., 1989). It has also been shown, that fast adaptation in the turtle is proportional to the extent of Ca^{2+} influx to the stereocilia (Ricci and Fettiplace, 1998) thus supporting the notion that adaptation is regulated by a rise in $[Ca^{2+}]_c$. Additional evidence supporting this hypothesis comes from work investigating the role of intracellular Ca^{2+} buffering on adaptation and from studies using photolysis of caged Ca^{2+} compounds (Kimitsuki and Ohmori, 1992). Raising the intracellular buffering capacity using BAPTA had similar effects to those seen under conditions of reduced external Ca^{2+} whereby both speed and extent of adaptation were decreased (Ricci and Fettiplace, 1997). It is somewhat puzzling that the adaptation mechanism would depend on Ca^{2+} influx, as the concentration of Ca^{2+} in the endolymph is unusually low (Bosher and Warren, 1978). Having entered the stereocilia, Ca^{2+} is thought to exert a feedback effect which acts to reset the opening range of the MET channels (Eatock et al., 1987; Eatock, 2000). It is subsequently bound by endogenous buffers within the stereocilia and recycled back to the

endolymph via the plasma membrane Ca^{2+} ATP-ases (PMCAs), namely PMCA-2a (Dumont et al., 2001; Mammano et al., 2007).

1.2.3 Ca^{2+} regulation of the cochlear amplifier

The amplification process intrinsic to OHCs is subject to modulation by changes in free $[Ca^{2+}]_c$. The stiffness of OHCs is controlled through the phosphorylation of cytoskeletal and prestin proteins. Polymerisation of cytoskeletal filaments is subject to modulation by $[Ca^{2+}]_c$ (see Mammano et al., 2007). Elevations of $[Ca^{2+}]_c$ into the millimolar range have been linked with decreases in OHC axial stiffness and OHC elongation (Frolenkov et al., 2003). Dallos and colleagues (1997) have also shown a reduction in OHC axial stiffness following application of acetylcholine (ACh) to the basal pole of the OHC (Dallos et al., 1997). The reduction in OHC axial stiffness in response to elevated $[Ca^{2+}]_c$ has been suggested to control the gain and operating point of the cochlear amplifier (Frolenkov et al., 2003).

1.2.4 The role of Ca^{2+} in synaptic function

The functional role of inner hair cells in the cochlea is twofold. They function as both the transducers of sound stimuli and as the presynaptic terminals that encode auditory signals in the afferent neurons (Fuchs et al., 2003). Opening of MET channels results in the flow of current into the apical portion of the hair cell. This current flow creates a graded receptor potential across the hair cell basolateral membrane, thus initiating the process of neurotransmission. Hair cells can therefore be divided into two distinct functional compartments, the apex, dedicated to mechanosensory transduction and the base, the site of synaptic transmission (Fuchs et al., 2003; reviewed by Mammano et al., 2007).

The mode of transmitter release occurring at the auditory synapse permits the exquisite precision of both sound location and frequency. The neural wiring of the auditory system is such that each auditory neuron receives input from only a single hair cell (Pickles, 1988). Deflection of the IHC stereocilia in response to a sound stimulus results in depolarisation of the IHC (see Section 1.2). The subsequent Ca^{2+}

influx at the ribbon-type active zones triggers the exocytosis of synaptic vesicles from a readily releasable pool, which is thought to consist of about 300 vesicles (Moser and Beutner, 2000). Vesicle fusion is followed by the release of glutamate onto glutamate receptors situated on the postsynaptic terminal of the afferent synapse (Kataoka and Ohmori, 1994). Depolarisation-induced exocytosis is observed in a variety of neurosecretory cells (Voets et al., 1999) and is typically biphasic in nature. The faster phasic component precedes and corresponds to opening of Ca^{2+} channels and mobilization of an immediately releasable pool (Voets et al., 1999). The mechanisms underlying the slower more sustained component are less clear. There are numerous physiological processes that could underlie the sustained release of vesicles during transduction. One mechanism describes a 'fire and reload' model of exocytosis, in which there is a rapid supply of vesicles to the readily releasable pool throughout the duration of the stimulus, which acts to prevent depletion of the pool (von Gersdorff et al., 1996; Griesinger et al., 2005). Vesicles are released at a rate of 3 per millisecond during depolarisation and are replenished at roughly 1.9 per millisecond The sustained endocytosis observed at the IHC ribbon depends on $[Ca^{2+}]^5$ (Beutner et al., 2001) and is sensitive to the slow Ca^{2+} chelator EGTA (Moser and Beutner, 2000).

Following the activation of voltage-gated Ca^{2+} channels the IHC becomes Ca^{2+} loaded. This Ca^{2+} load could be cleared through a number of mechanisms. These include Na^+/Ca^{2+} exchange (shown in frogs by Chabbert et al., 1995), the ATP-dependent PMCA (Kennedy, 2002) and mitochondrial Ca^{2+} buffering (Kennedy, 2002). The role of Na^+/Ca^{2+} exchange in hair cell Ca^{2+} regulation has been investigated in both OHCs, IHCs and in vestibular hair cells. Na^+/Ca^{2+} exchange plays an important role in the regulation of resting Ca^{2+} levels and recovery from prolonged Ca^{2+} loads in OHCs (Ikeda et al., 1992) but not IHCs (Kennedy, 2002). It is also thought to contribute mildly to the recovery from Ca^{2+} loads in vestibular hair cells (Chabbert et al., 1995). In contrast to OHCs, Ca^{2+} regulation in IHCs relies on the activity of ATP-dependent PMCAs, namely PMCA-1 (Furuta et al., 1998) and mitochondrial Ca^{2+} buffering. This is supported by evidence showing recovery of IHCs from Ca^{2+} loads is prolonged in the absence of PMCA activity and in the presence of FCCP (Kennedy, 2002). Taken together, these data support the idea that Ca^{2+} plays a vital regulatory role in neurotransmission at the IHC afferent synapse.

1.3 Mitochondrial structure and function

1.3.1 The mitochondrion

Mitochondria have evolved from prokaryotic microorganisms (Margulis, 1996) and occupy a significant volume of the cell cytoplasm. They have played a central role in the evolution of complex organisms and without the mitochondrion animals would depend solely on anaerobic glycolysis for all energy (ATP) production. Mitochondria are the site of oxidative phosphorylation in eukaryotic cells, the process by which electrons are extracted from complex foodstuffs and converted from chemical energy to electrical energy and subsequently to the chemical energy essential for cellular function, ATP (for a recent review see Hosler et al., 2006). Alongside ATP production, mitochondria play an intricate role in cellular Ca^{2+} homeostasis and $[Ca^{2+}]_c$ signalling; are involved in steroid and haem biosynthesis; and are key in regulating the delicate balance between cell life and cell death (Jacobson and Duchen, 2001; Duchen, 2004).

1.3.2 Structure

In many cases mitochondria are portrayed as elongated rod-like structures measuring between 0.5 and 1 μm in diameter. Time-lapse microscopy however presents a large body of evidence in which mitochondrial networks are shown to be plastic and mobile (see Alberts *et al.*, 1994). Together, these membranes establish two distinct compartments within the mitochondrion: the matrix and the intermembrane space. The mitochondrial inner membrane is highly impermeable allowing it to act as the primary barrier between the cell cytosol and the mitochondrial matrix. Molecules required for the function of mitochondrial matrix enzymes are permitted entry via specific transporter proteins in the inner membrane. The mitochondrial enzymes are concentrated in the matrix space and are necessary for functioning of the citric acid cycle (see Alberts et al., 1994). The intermembrane space is thought to hold a number of proteins involved in mitochondrial energetics, cell death and cell physiology. The most notorious proteins inhabiting this micro-environment are cytochrome c and creatine kinase (Duchen, 2000b). The structure and function of the

outer membrane is less clear, although it is thought to be permeable to small molecules and ion species.

Advances in light microscopy, fluorescent dye technology and genetic engineering have been pivotal in furthering our understanding of mitochondrial internal structure and physiology (see Frey & Mannella 2000). The mitochondrial inner membrane is portrayed as a highly invaginated structure in which the mitochondrial electron transfer chain resides. The structural organization of the inner membrane can vary from complex lamellar to elongated tubular structures and appears to be cell-specific (Frey and Mannella, 2000). The functional implications of such structural differences however remain to be elucidated. The structural stability of the cristae network is at present an area of debate. The well known textbook depiction as being an organized arrangement of parallel folds is now brought in to question following recent evidence suggesting that cristae are continuously fusing and dividing (Frey and Mannella, 2000).

The mitochondrial structure exists as a dynamic and delicate balance between fission and fusion (Collins and Bootman, 2003). The question of whether the mitochondrial network undergoes predominantly fission to form networks or fusion to form individual organelles persists. There is also evidence to suggest tissue-specific differences in the mitochondrial network itself (Rutter and Rizzuto, 2000). Mitochondrial networks can therefore exist as two separate entities, one a mobile homogeneous population closely associated with the endoplasmic reticulum (ER) (Rizzuto et al., 1998; De Giorgi et al., 2000) and the other a morphologically heterogeneous population throughout the cell (Zorov et al., 2000; Collins et al., 2002).

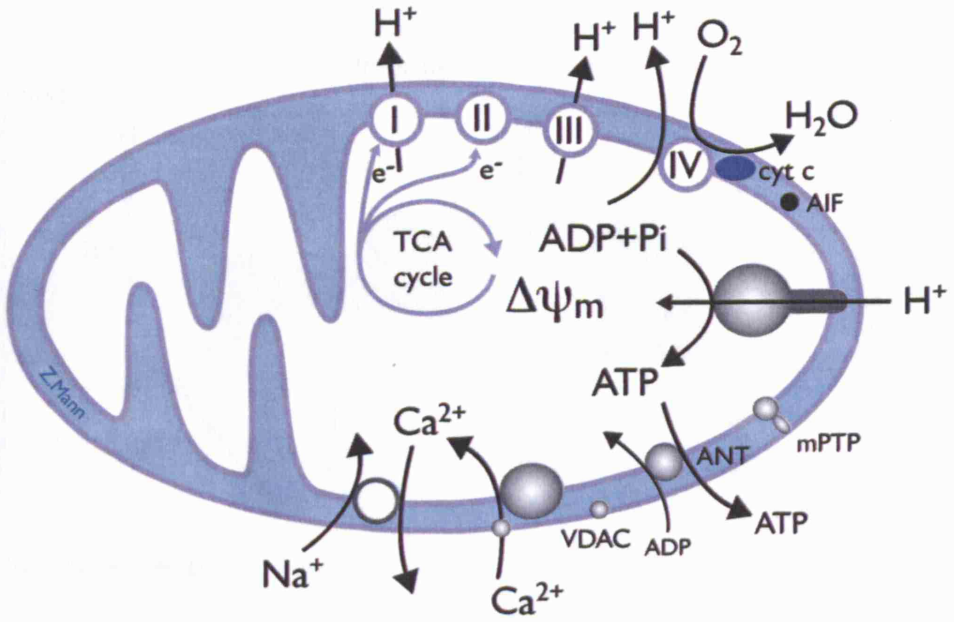

Figure 1. 3 The mitochondrion.

The schematic above illustrates the different functional compartments of the mitochondrion. The double membraned structure is highlighted in blue. The complexes of the mitochondrial electron transfer chain are labelled I-IV. Complex I: NADH dehydrogenase, complex II: succinate dehydrogenase, complex III: cytochromeQ oxidoreductase, complex IV: cytochrome oxidase. **VDAC**: voltage-dependent anion transporter, **ANT**: adenine nucleotide translocator, **mPTP**: mitochondrial permeability transition pore, **AIF**: apoptosis inducing factor, **cyt c**: cytochrome c. *Figure adapted from Duchen 2004.*

1.3.3 The chemiosmotic theory

The chemiosmotic theory proposed by Peter Mitchell in 1961 refers to the principles underlying the process of oxidative phosphorylation. This hypothesis proposed that oxidation and phosphorylation were coupled by a proton gradient established across the mitochondrial inner membrane (Mitchell, 1961; Tager et al., 1966).

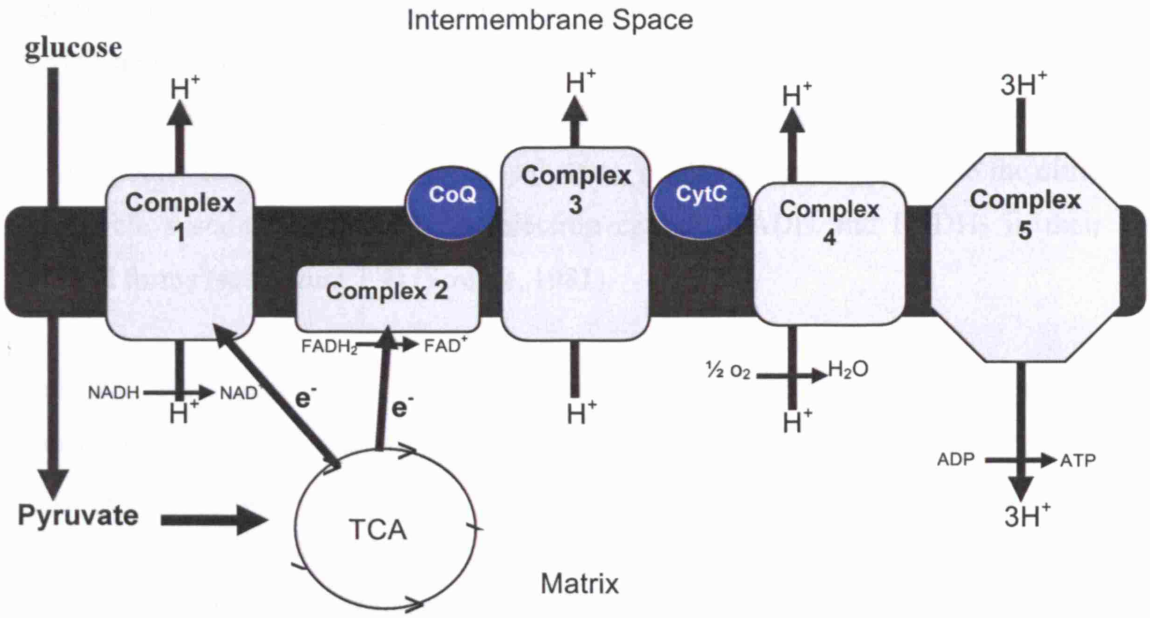

Figure 1. 4 The mitochondrial electron transfer chain (ETC).

This refers to a series of metalloprotein complexes in the mitochondrial inner membrane, that use the process of electron transfer to establish an electrochemical potential gradient. Substrates from glycolysis are fed into the citric acid cycle, in order to maintain the reduced pools of pyridine nucleotides (NADH) and flavoproteins ($FADH_2$). Reducing equivalents are then supplied to the mitochondrial electron transfer chain (ETC); NADH to complex I (NADH dehydrogenase) and FAD to complex II (succinate dehydrogenase). Electrons pass from complexes I and II to complex III (cytochrome c) via CoenzymeQ and finally combine with molecular oxygen at complex IV (cytochrome c oxidase). As electrons are passed along the (ETC), H^+ ions are transported from the mitochondrial matrix into the intermembrane space. Translocation of protons generates an electrochemical proton gradient referred to as the mitochondrial membrane potential ($\Delta\psi_{mt}$). This potential provides the necessary driving force for the generation of ATP at complex V (the F_1F_0-ATP synthase). Once generated, ATP is transported into the cell cytosol. *Schematic adapted from* www.gwu.edu/mbp/r/rxn900.gif.

Reduced pyridine nucleotides (NADH) and flavoproteins ($FADH_2$) are the major electron carriers employed in the oxidation of fuels. In their oxidised forms however NAD^+ and FAD^{2+} are the major electron acceptors. The process of oxidative phosphorylation relies on the maintenance of reduced NADH and flavoproteins (FAD) pools. The sustained supply of substrate, predominantly Pyruvate to the citric acid cycle sustains the pool of the electron carriers NADH and $FADH_2$ in their reduced forms (see Figure 1.4) (Streyer, 1981).

From the citric acid cycle, NADH and $FADH_2$ enter the mitochondrial electron transfer chain. NADH enters at complex one (NADH dehydrogenase) and $FADH_2$ from succinate-linked substrates at complex two (succinate dehydrogenase). Electrons from NADH and $FADH_2$ pass from either complex I or complex II to complex III (ubiquinol-cytochrome c reductase) via ubiquinone and are finally transferred to oxygen at complex IV (cytochrome c oxidase) (see Alberts *et al.*, 1994). As electrons pass along the electron transfer chain, protons (H^+ ions) are translocated from the mitochondrial matrix into the intermembrane space. This proton translocation generates an electrochemical potential gradient referred to as the mitochondrial transmembrane potential ($\Delta\psi_{mt}$) and is estimated to be 150-200 mV negative with respect to the cell cytosol (see Figure 1.4). $\Delta\psi_m$ provides the driving force required for the production of ATP at complex V, the F_1F_0-ATP synthase. This is a large enzyme complex assembled as a rotary motor. The F_0 subunit behaves as a proton conductance and permits the movement of electrons down their electrochemical potential gradient. The F_0 subunit uses the proton gradient established during electron transfer to drive the rotary motor in the F_1 subunit and thus ADP phosphorylation (Capaldi and Aggeler, 2002; Chan, 2006).

1.4 Mitochondrial genetics

As discussed previously (Section 1.3.3) mitochondria are the primary site of ATP production and are also extensively involved in cell signalling pathways such as those regulating cell death and calcium homeostasis. In light of their central role in eukaryotic cell function, mitochondrial defects can have catastrophic effects on

normal cell physiology (Wallace, 1999; Duchen, 2004; McKenzie et al., 2004; Beal, 2005; Chan, 2006).

1.4.1 Mitochondrial replication

Mitochondria possess their own DNA (mtDNA), which in humans is a circular double-stranded molecule around 16.6 Kb in length. Mitochondrial biogenesis is dependent on numerous genes, a large proportion of which are encoded by the nuclear genome (nDNA). Only 13 of the 80 proteins required for the process of oxidative phosphorylation are encoded by the mtDNA (Scarpulla, 2002). Although mtDNA synthesis can occur independently of the cell cycle (Taanman *et al.*,2003), mitochondria rely on the nuclear-derived enzymes mtDNA polymerase (POLG), thymidine kinase 2 and deoxyguanosine kinase for replication (Schapira, 2006). Mitochondrial DNA is transcribed and translated on mitochondrial ribosomes and the latter are necessary in order for successful replication to occur. In order to prevent cells with high turnover rates from becoming depleted of mtDNA, mitochondrial division and replication must be linked in some way to the replication of the cell. An attractive hypothesis is that mitochondrial replication is under the control of the nucleus and consequently associated with replication of nuclear DNA (Davis and Clayton, 1996). This hypothesis remains debatable however, in light of previous work showing replication of mtDNA to be independent of nuclear DNA (Bogenhagen and Clayton, 1977). MtDNA replication does not occur solely in accordance with the cell cycle. In addition to the hypotheses mentioned previously, mtDNA transcription and replication have also been associated with physiologicl changes within the cell (see Scarpulla, 2002). Reactive oxygen species (ROS) produced as a bi-product of cellular respiration can drive nuclear expression of the mitochondrial transcription factor A (Tfam) which in turn, regulates mtDNA copy number, aggregation and packaging. Tfam expression is modulated by two classes of nuclear transcriptional regulators. The first includes the nuclear transcription factors (NRF-1 and 2) and the second, the nuclear coactivator peroxisome proliferator-activated receptor-γ coactivator-1α (PGC1-α). A unique feature of this coactivator, is that its expression is determined by physiological signals including those involved in proliferation, thermogenesis and gluconeogenesis. In addition, PGC1-α can stimulate transcriptional activity of NRF-1 on the Tfam promoter. Both classes of

transcriptional regulator do not interact directly with DNA. Instead, they exert their effects through interactions with DNA-bound transcription factors (see Scarpulla, 2002). The PGC1-α coactiviator family has been implicated in the integration of various signalling pathways and DNA binding transcription factors, suggesting that this method of mtDNA replication can act as a pro-survival mechanism by matching cellular energy supply and demand (Piantadosi and Suliman, 2006).

Mitochondrial DNA is derived entirely from the oocyte at fertilization. The maternal inheritance means that mitochondrial replication follows the principals of population genetics rather than those typical to Mendelian genetics (DiMauro, 2007). During cell division, mitochondria are randomly distributed among daughter cells. Mutations in mtDNA present as a single copies of mtDNA in the egg and can be transmitted to developing tissues. In normal tissues, all mtDNA is identical or homoplasmic. In disease states associated with mitochondrial mutations, tissues contain a combination of both mutant and wild-type mtDNA and is therefore referred to as heteroplasmic (DiMauro, 2007). The clinical phenotype resulting from a given mtDNA mutation will depend on the proportions of mutant versus wild-type mtDNA within the tissue. In addition, the severity of the disease is determined by the energetic requirements of the tissues. In most cases tissues with a high dependence on oxidative phosphorylation have lower thresholds required for the expression of a disease phenotype. The complex genetic distribution of mtDNA is still not fully understood. It does however provide an explanation for the wide variation in disease expression patterns. Variation in phenotype expression is a common feature of many mitochondrial mutations however the precise mechanisms underlying this phenomenon remain to be elucidated.

1.4.2 Mitochondrial mutations associated with hearing loss

Mutations occurring in the mitochondrial genome underlie a wide variety of maternally inherited pathologies one of which is hearing loss (Casano et al., 1998; Fischel-Ghodsian, 1999; Zwirner and Wilichowski, 2001; Matsunaga et al., 2004). Mitochondrial diseases result in respiratory chain defects. The respiratory chain within the mitochondrion is unique in that it is the only metabolic pathway in the cell under the dual control of the mtDNA and the nuclear genome (nDNA) (DiMauro,

2004). Mitochondrial diseases can also be defined as those that interfere with mitochondrial protein synthesis and those that effect one of the 13 respiratory chain subunits necessary for ATP production. The highest abundance of mitochondrial diseases is in those occurring due to mutations in nDNA. The nucleus not only encodes the majority of respiratory chain subunits, but also the processes which determine their correct assembly and function (DiMauro, 2004). In diseases associated with mitochondrial mutations, the highest number of mtDNA mutations is found in tissues with high metabolic demand. Such tissues include nerve, muscle, liver and the ear. Due to the high energy demand of these tissues, mitochondrial dysfunction can be particularly harmful.

There are a number of mitochondrial diseases that present with hearing loss as a clinical symptom (see Table 1). Such diseases include systemic neuromuscular syndromes; Kearns-Sayre syndrome; mitochondrial encephalomyopathy, lactic acidosis and stroke-like episodes (MELAS) and myoclonus epilepsy and ragged red fibres (MERRF) (Fischel-Ghodsian, 1999). Similarly, the cells of the auditory system require a continuous supply of ATP in order to sustain the active process of sensory transduction. ATP consumption is particularly high in cells of the stria vascularis, whose primary function is to maintain the ion gradients in the cochlea and generate the endocochlear potential (Section 1.1) (Marcus et al., 1978; Salt et al., 1987; Wangemann, 2006). When considering the high energy demand of the auditory system, it is by no means surprising that a number of mitochondrial diseases are associated with hearing loss.

There is an abundance of patients that present with syndromic sensorineural hearing loss. This refers to hearing loss occurring in association with other syndromes (see Table 2. and Figure 1.5). Additionally, patients present with non-syndromic sensorineural hearing loss. In the latter, the mutation is present in all copies of the mtDNA but it is exclusively in the ear that the phenotype is expressed.

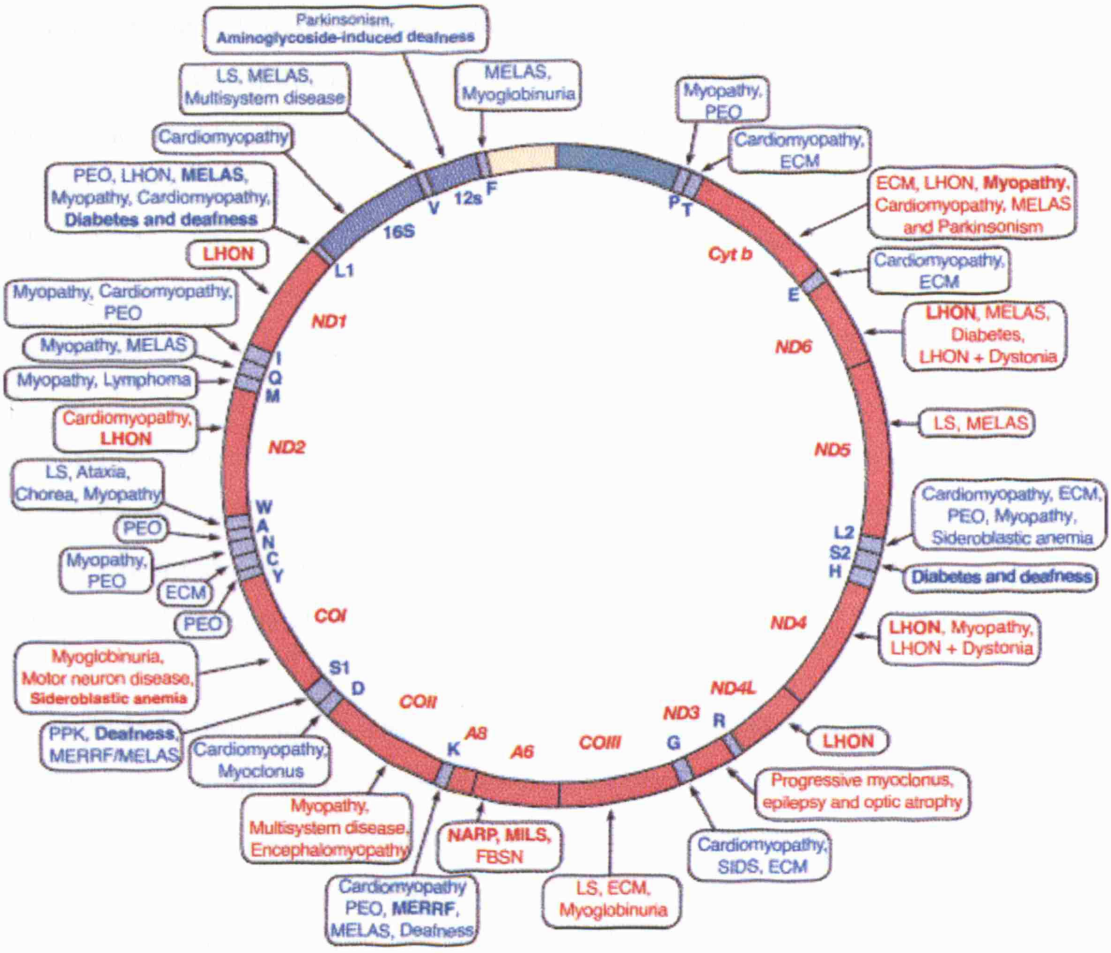

Figure 1. 5 Disease loci of the human mitochondrial genome.

The disease mutations occurring in the human mitochondrial genome as of January 2004. The $_{mt}$DNA measures 16.569 Kb. The protein coding sequences of the 7 subunits of complex 1, the three subunits of cytochrome oxidase, cytochrome b, the two subunits of the ATP synthase, the 12S and 16S ribosomal RNAs and the 22 transfer RNAs are represented by the coloured area. Each gene is identified by triplicate letter code and its corresponding amino acid. Blue areas indicate diseases resulting from mutations in protein synthesis genes. Diseases associated with mutations in protein coding genes are shown in red. *Figure from DiMauro 2004.*

Homoplasmic mitochondrial mutations resulting in -syndromic sensorineural hearing loss include the A1555G, T7511C and C1444T mutations. What is it therefore about the auditory system that makes it so susceptible to these mutations?

The first molecular defect linked with non-syndromic sensorineural hearing loss was identified in the mitochondrial 12S ribosomal RNA gene (12SrRNA) (Fischel-Ghodsian et al., 1993; Prezant et al., 1993). The two major hot spots for mitochondrial mutations associated with hearing loss are the 12S ribosomal RNA (12SrRNA) gene (Guan et al., 1996; Li et al., 2004) and the $tRNA^{Ser(UCN)}$ gene ((Zhao et al., 2005). There are four deafness mutations in $tRNA^{Ser(UCN)}$ gene associated with non-syndromic hearing loss and two with the 12S rRNA gene (see Table 1). One of the most prominent mitochondrial mutations linked with non-syndromic sensorineural hearing loss and aminoglycoside hypersensitivity is the homoplasmic A1555G mutation in the 12SrRNA gene. This mutation has been identified in patients with hearing loss from multiple ethnic backgrounds (Casano et al., 1998; Matsunaga et al., 2004; Noguchi et al., 2004).

The A1555G mutation is one of the most extensively studied deafness-associated mtDNA mutations. In 1996, Guan and colleagues used a lymphoblastoid cell line derived from patients carrying the mutation, to characterize some of the associated biochemical consequences (Guan et al., 1996; Fischel-Ghodsian, 1999). Those with the homoplasmic mutation exhibited marked reductions in mitochondrial protein synthesis, oxygen consumption and activity of ETC complexes I, III and IV (Guan et al., 1996). In association with an autosomal cochlea mutated gene, the A1555G mutation is thought to result in a tissue-specific impairment of mitochondrial transcription leading to hearing loss (Prezant et al., 1993).

The mechanism(s) underlying heightened sensitivity to aminoglycosides was also examined. The A1555G mutation occurs at a highly conserved region of the small ribosomal RNA, in which aminoglycosides are also known to bind. Classically, aminoglycosides interfere with bacterial replication, though binding to this region and stabilizing mismatched aninoacyl tRNAs. There are in fact, a number of sequences within this binding domain capable of aminoglycoside binding (Hornig et al., 1987). It has therefore been suggested that the mitochondrial ribosome is a major target in aminoglycoside-induced ototoxicity, since this is the naturally occurring target of these antibiotics in bacteria. It has been suggested, that the A1555G mutation introduces an additional G-C basepair, which causes the secondary structure of the rRNA binding domain to more closely resemble that of bacteria. This

would therefore enhance aminoglycoside binding and thus increase the sensitivity of the cell (Prezant et al., 1993).

Alongside aminoglycoside hypersensitivity, the A1555G mutation has also been linked with cases of sudden onset hearing loss and accelerated age-related hearing loss, both of which have been shown to occur in the absence of aminoglycoside treatment. This suggests therefore, that this mutation can exert its effects at different sites within the mitochondria to those linked with aminoglycoside toxicity.

Table 2 Mitochondrial mutations and diseases associated with hearing loss

Mutation	Gene	Phenotype	Reference
C1444T	12SrRNA	Aminoglycoside hypersensitivity, nonsyndromic hearing loss	Zhao *et al.*, 2005
A1555G	12SrRNA	Sensorineural hearing loss	Guan *et al* ., 1996
A7445G 747insC T7510C T7511C	$tRNA^{ser(UCN)}$	Nonsyndromic deafness	Fischel-Ghodsian *et al.*, 1995 Verhoeven *et al.*, 1999 Hutchin *et al.*, 2000 Li *et al.*, 2004 delCastillo *et al.*, 2002 Sue *et al.*, 2002 Chapiro *et al.*, 2002
A2343G	$tRNA^{Leu(UUR)}$	MELAS & associated deafness MERRF Optic atropy Kearns-sayre syndrome Leigh syndrome	Van den Ouweland *et al.*, 1992
T14709C	$tRNA^{Glu}$	Diabetes and deafness	Ballinger *et al.*, 1992
A8296G	$tRNA^{Alys}$	Diabetes and deafness	Vialettes *et al.*, 1997
OPA1 R445H	OPA1	Dominant optic atropy Sensorineural hearing loss	Payne *et al.*, 2004
8344A	$tRNA^{Lys}$	MERRF & associated deafness	Sivestri *et al.*, 1992

1.5 Mitochondria and calcium homeostasis

Alongside ATP production, the mitochondria possess a well established system permitting them to accumulate Ca^{2+} across its inner membrane (Crompton et al., 1976; Nicholls and Crompton, 1980). It has been well documented that mitochondria sequester significant amounts of Ca^{2+} from the cytosol in a number of cell types (see Nicholls and Crompton, 1980; Rizzuto et al., 1994; Boitier et al., 1999; Hajnoczky et

al., 1999; Hajnoczky et al., 2000a; Camello-Almaraz et al., 2002; Duchen, 2004; Andrade et al., 2005). The mitochondrial Ca^{2+} uptake pathway is important in both physiological and pathophysiological processes within the cell including; the spatio-temporal patterning of cytosolic Ca^{2+} signals, the rate of ATP production and execution of cell death pathways (see Rizzuto et al., 2000).

1.5.1 The mitochondrial Ca^{2+} uptake pathway

Mitochondrial Ca^{2+} transport is facilitated by a series of carriers, all with distinct characteristics and functions. Uptake of Ca^{2+} into mitochondria can occur via either the Ca^{2+} uniporter (Gunter and Pfeiffer, 1990; Gunter and Gunter, 1994) or through rapid mode uptake (RaM) (Sparagna et al., 1995).

1.5.2 The mitochondrial Ca^{2+} uniporter

The mitochondrial Ca^{2+} uniporter (MCU) utilises both electrochemical potential gradient to sequester Ca^{2+}. Uptake of Ca^{2+} into mitochondria is therefore dependent partly on $\Delta\psi_{mt}$ and also on maintenance of a low intramitochondrial Ca^{2+} ($[Ca^{2+}]_{mt}$) (see Duchen, 2004). Mitochondrial Ca^{2+} uptake is an electrogenic process meaning that Ca^{2+} influx across the inner mitochondrial membrane (IMM) into the mitochondrial matrix will elicit a depolarisation of $\Delta\psi_{mt}$ (Peuchen et al., 1996; Duchen et al., 1998; Boitier et al., 1999; Duchen, 2000a). The uptake of Ca^{2+} via the MCU exhibits second order dynamics whereby uniporter activity is regulated by both its activation and transport sites (Gunter et al., 2000). Despite its nomenclature, the Ca^{2+} uniporter does exhibit permeability to other bivalent cations with the following order of selectivity: $Ca^{2+} > Sr^{2+} > Mn^{2+} > Ba^{2+} > Fe^{2+} > La^{3+}$ (Drahota et al., 1969). The activity of the MCU appears unaltered by inhibitors of the mitochondrial electron transfer chain or ATP-synthase, including cyanide, antimycin A or oligomycin (Scarpa and Azzone, 1970). The uptake pathway does however exhibit a high sensitivity to hexavalent cations such as Ruthenium red (Reed and Bygrave, 1974).

Until recently, there has been some discrepancy regarding the structure and function of the MCU (Gunter and Pfeiffer, 1990). This has centred predominantly on whether

it acts as a carrier or a channel. Patch clamping studies of the IMM led to identification of a Ca^{2+} selective ion channel with a high sensitivity to inhibitors of mitochondrial Ca^{2+} uptake. The high affinity Ca^{2+} binding exhibited by this channel permits high Ca^{2+} selectivity irrespective of low cytosolic Ca^{2+} concentrations ($[Ca^{2+}]_c$). The inward rectifying nature of the uniporter permits only the inward movement of Ca^{2+} ions from the cytosol into the mitochondria, making it particularly effective for Ca^{2+} sequestration. The strong inward rectification means the process of Ca^{2+} uptake is voltage dependent. This therefore limits the efflux of Ca^{2+} from the mitochondria to the cytosol during periods of $\Delta\psi_{mt}$ depolarisation (Kirichok et al., 2004).

One of the major controversies over the past decade has focused around whether mitochondria have the ability to sequester sufficient Ca^{2+} from physiological-type pulses (Sparagna et al., 1995). Numerous experiments have been conducted to address this question (Miyata et al., 1991; Wendt-Gallitelli and Isenberg, 1991; Rizzuto et al., 1992; Sparagna et al., 1995; Buntinas et al., 2001), leading to the consensus that in a majority of cell types, significant increases in $[Ca^{2+}]_{mt}$ occur as a result of physiological type pulses. There is also evidence to suggest an additional mode of Ca^{2+} uptake into the mitochondria, referred to as rapid mode uptake (RaM). This pathway has been to rapidly sequester significant amounts of Ca^{2+} from the cytosol during rising phase of physiological Ca^{2+} pulses (Buntinas et al., 2001).

1.5.3 Mitochondrial Ca^{2+} efflux pathways

In addition to their Ca^{2+} uptake pathway, mitochondria also encompass a carrier system permitting Ca^{2+} efflux to the cytosol across their inner membrane (Nicholls and Crompton, 1980). There are two pathways associated with Ca^{2+} efflux; the Na^+-dependent pathway (Crompton et al., 1976), characterised initially in heart, skeletal muscle, brain, adrenal cortex and brown adipose tissue and the Na^+ independent pathway, observed in liver, kidney and smooth muscle (see Nicholls and Crompton, 1980). In addition to these, mitochondria can also release Ca^{2+} following loss of $\Delta\psi_{mt}$ As Ca^{2+}uptake is an electrogenic process, loss of $\Delta\psi_{mt}$ will eliminate the driving force behind it (Beatrice et al., 1980).

1.5.4 Mitochondria in physiological Ca^{2+} signalling

Intramitochondrial metabolism is known to be regulated by matrix Ca^{2+} levels (McCormack et al., 1990). There are numerous metabolic enzymes, whose activity is upregulated following an increase in matrix Ca^{2+}. These include pyruvate dehydrogenase, isocitrate dehydrogenase, phosphate phosphatase, 2-oxoglutarate dehydrogenase and α-ketoglutarate dehydrogenase (McCormack and Denton, 1984; Hajnoczky et al., 1995). Mitochondrial Ca^{2+} uptake during $[Ca^{2+}]_c$ signalling could therefore be considered as a means of matching cellular energy production with demand.

In order to establish the successful propagation of a Ca^{2+} wave, focal Ca^{2+} release must first be initiated by inosotiol triphosphate (IP_3) acting on endoplasmic reticulum (ER) Ca^{2+} release channels. Subsequent to this initial Ca^{2+} release, neighboring ER pools become sensitised to IP_3 by Ca^{2+}, therefore allowing the signal to propagate throughout the cell by means of an IP_3-sensitive Ca^{2+}-induced Ca^{2+} release (CICR) (Sheppard et al., 1997). These Ca^{2+} waves propagate via focal amplification regions, in which Ca^{2+} release kinetics are elevated. Cross-correlation analysis of mitochondrial-rich sites with regions in which the peak amplitude and rate of rise of Ca^{2+} waves occur have highlighted a central role for mitochondria in wave propagation (Simpson and Russell, 1996).

An elegant model of mitochondrial Ca^{2+} buffering was put forward by Nicholls and Crompton in 1980. Here, they describe Ca^{2+} cycling between cytosol and matrix as a delicate equilibrium sensitive to perturbations in either compartment. In accordance with this concept, an increase in $[Ca^{2+}]_c$ would therefore disturb this equilibrium and elicit a homeostatic response in which the mitochondria act to restore steady-state. The re-establishment of this equilibrium will consequently cause the distribution of Ca^{2+} across the IMM to change.

By means of flux studies in isolated mitochondria, Nicholls and Crompton also described the influence of mitochondrial Ca^{2+} uptake on resting $[Ca^{2+}]_c$ levels, a phenomenon known as the *set-point*. Through these experiments, they showed that mitochondria will accumulate Ca^{2+} from the cytosol following small perturbations in

$[Ca^{2+}]_c$. Under such conditions, the activity of the sodium/calcium (xNa^+/Ca^{2+}) exchanger is sufficient to prevent a net increase in matrix Ca^{2+}. Changes in $[Ca^{2+}]_c$ exceeding 400-500 nM will override the capacity of this extrusion mechanism, seen as a net increase in $[Ca^{2+}]_{mt}$.

It has been shown in a majority of cell types, that mitochondria will take up Ca^{2+} during $[Ca^{2+}]_c$ signalling. The functional consequences of Ca^{2+} accumulation are multiple, ranging from regulating spatio-temporal properties of Ca^{2+} signals (Boitier et al., 1999) to the control of cellular metabolism (Duchen, 1992; Hajnoczky et al., 1995; Robb-Gaspers et al., 1998). Changes in $[Ca^{2+}]_{mt}$ can be monitored directly using various methods. These include site directed expression of the Ca^{2+}-sensitive, fluorescent protein aequorin (Rizzuto et al., 1992) and use of the fluorescent indicators Rhod2-AM or XRhod1-AM (Hajnoczky et al., 2000a; Hajnoczky et al., 2000b; Camello-Almaraz et al., 2002; see Duchen, 2004). The ability of mitochondria to act as a spatial buffer becomes important when considering the many intracellular processes that are Ca^{2+}-sensitive. The fact that disruption of the mitochondrial Ca^{2+} uptake pathway has such profound effects on $[Ca^{2+}]_c$ signalling highlights the sensitivity of Ca^{2+} channels involved in these signalling events. Here, I will dwell briefly on the pathways of IP_3-mediated Ca^{2+} release from the ER and capacitative Ca^{2+} entry.

The combined action of Ca^{2+} and IP_3 on the IP_3 receptor (IP_3R) Ca^{2+} release channel is imperative for the evolution and development of $[Ca^{2+}]_c$ waves and oscillations (Hajnoczky et al., 1999). IP_3R-mediated $[Ca^{2+}]_c$ signals are associated with large increases in $[Ca^{2+}]_{mt}$ (Rizzuto et al., 1994) and IP_3R-mediated $[Ca^{2+}]_c$ oscillations can be transmitted to the mitochondria where they activate Ca^{2+}-sensitive dehydrogenases (Hajnoczky et al., 1995). This sophisticated signal transmission between ER and mitochondria is made possible by the close association of the two organelles (Rizzuto et al., 1998). In addition to the local transfer of Ca^{2+}, mitochondria have also been shown to modulate the $[Ca^{2+}]_c$ levels in microdomains close to the IP_3R Ca^{2+} release channels. This consequently allows the mitochondria to determine the threshold for IP_3R-dependent $[Ca^{2+}]_c$ signalling (Hajnoczky et al., 1999).

The open probability of IP_3-gated Ca^{2+} channels displays a high Ca^{2+} dependence, whereby subtle changes in $[Ca^{2+}]_c$ can enhance channel open probability (Hajnoczky et al., 1999). The open probability of different IP_3R Ca^{3+} channels differs with receptor subtype. The open probabilities of subtype I declines when $[Ca^{2+}]_c$ increases above μM levels (Bezprozvanny et al., 1991) whereas those II and III however continue to increase with $[Ca^{2+}]_c$ (Ramos-Franco et al., 1998). By modulating $[Ca^{2+}]_c$ around the mouth of the IP_3R channel, mitochondria can either amplify or restrict the development of $[Ca^{2+}]_c$ signals, in different cell types, based on the IP_3R expression profiles (for a recent review see Duchen, 2000a).

Agonist-induced activation of the IP_3 pathway elicits a biphasic increase in $[Ca^{2+}]_c$ involving IP_3-induced Ca^{2+} release from stores and Ca^{2+} influx from the extracellular space (Berridge, 1995). Initially, a given agonist acting on IP_3R Ca^{2+} release channels leads to Ca^{2+} release from intracellular stores. Subsequent to store depletion, Ca^{2+} influx from the extracellular space is initiated through the activation of store-operated Ca^{2+} channels (SOCs) (Putney, 1986; Hoth and Penner, 1992; Parekh, 2003). This store-operated Ca^{2+} influx manifests as a non voltage-gated current referred to as Ca^{2+} release-activated Ca^{2+} current (I_{CRAC}) (Bakowski et al., 2003). The increase in $[Ca^{2+}]_c$ established through SOC Ca^{2+} influx permits the re-filling of depleted Ca^{2+} stores (Parekh, 2003). The capacitative regulation of Ca^{2+} entry provides the predominant pathway by which Ca^{2+} influx from extracellular space can replenish depleted stores or enhance $[Ca^{2+}]_c$ signals (Putney, 1986). The precise pathway linking store depletion with SOC opening has until recently remained a mystery. Recent data suggest a local interaction between the ER protein STIM1 and the SOC subunit Opai1 (Wu et al., 2007). STIM1 is a membrane spanning protein with an unpaired Ca^{2+} binding EF hand. It has been proposed as the principle Ca^{2+} sensor in stores (Spassova et al., 2006). Subsequent to store release, the protein accumulates in sub-region within the ER, about 10-25 nm from the plasma membrane. STIM1 is proposed to activate SOC Ca^{2+} influx via local interaction with Orai1. Additionally, it has been suggested that the process is modulated by long range diffusible mediators (see Wu et al., 2007).

The I_{CRAC} current will only be activated in conditions of reduced SERCA pump activity and increased store emptying. Parekh (2000) proposed a model in which the

activation of I_{CRAC} is achieved through the activation of additional intracellular Ca^{2+} uptake pathways such as that seen in the mitochondria. By regulating the $[Ca^{2+}]_c$ levels in microdomains close to IP_3Rs, mitochondria reduce the Ca^{2+}-dependent inactivation of IP_3Rs thus maintaining conditions favourable for store depletion and I_{CRAC} activation.

In summary, mitochondria have the ability to regulate the mechanisms involved in the evolution and development of $[Ca^{2+}]_c$ waves. They are also important in restoring $[Ca^{2+}]_c$ levels to normal following intracellular signalling events. Impairment of the mitochondrial Ca^{2+} uptake pathway can therefore significantly influence the spatiotemporal characteristics, propagation and magnitude of $[Ca^{2+}]_c$ waves (Jouaville et al., 1995; Boitier et al., 1999). Mitochondrial Ca^{2+} uptake can also enhance the range over which IP_3 can control Ca^{2+} influx from the extracellular space. With this in mind, removal of mitochondrial Ca^{2+} accumulation will impair the process involved in intracellular store re-filling and enhancement of $[Ca^{2+}]_c$ signals.

1.6 Mitochondria and cell death

1.6.1 An overview of cell death

There are currently two well recognised mechanisms of cell death, necrosis and apoptosis, each with characteristic biochemical and physical hallmarks. Necrosis refers to cell death that is commonly linked with inflammation. This process is often thought of as passive in that it does not exhibit a requirement for ATP. Trademarks of necrosis include organelle swelling, cell membrane rupture and the release of cellular contents into the surrounding milleu (Orrenius, 2004). The phenomenon of apoptosis was described initially by John Kerr in 1972 and refers to the programmed destruction of a cell. Apoptosis is an ATP-dependent process (Eguchi et al., 1997) the characteristic features of which include cell shrinkage, cytoplasmic and nuclear condensation and phagocytosis (see Hengartner, 2000). Apoptosis can be divided into two pathways, receptor mediated apoptosis and mitochondrial-mediated apoptosis (the intrinsic pathway), the latter of which I shall now discuss.

1.6.2 The mitochondrial apoptotic pathway

Despite having been well documented that mitochondrial dysfunction and subsequent depletion of cellular ATP result in necrotic cell death, there is additional evidence implicating these organelles as major players in the apoptotic pathway (Orrenius, 2004). The mitochondrial apoptotic pathway can be triggered by both intracellular and extracellular stresses. Common activators of this pathway include oxidative stress and cytotoxic drugs, which result in apoptosis through a variety of mechanisms including: impaired functioning of the electron transfer chain; release of proteins which trigger caspase activation and dysregulation of intracellular redox state (Green and Reed, 1998).

1.6.3 Mitochondrial permeability transition and cell death

Loss of $\Delta\psi_{mt}$ is an event common to both apoptosis and necrosis (Susin et al., 1996; Green and Reed, 1998; Kroemer and Reed, 2000). In apoptosis, loss of $\Delta\psi_{mt}$ occurs relatively late in the process and in most cases as a result of cytochrome c depletion within the electron transfer chain (Green and Reed, 1998). Collapse in $\Delta\psi_{mt}$ is also thought to trigger activation of the mitochondrial permeability transition pore (mPTP) or mitochondrial megachannel (Marchetti et al., 1996; Green and Reed, 1998). Permeability transition refers to a sudden increase in the permeability of the inner mitochondrial membrane and has been closely linked with changes in $\Delta\psi_{mt}$ and matrix pH (Bernardi et al., 1992; Szabo et al., 1992). Although the precise structure and physiological role of this channel are at present unclear, it is thought to have two modes of conductance and function: a low level conductance, suggested to participate in both Ca^{2+} signalling and regulation of mitochondrial Ca^{2+} release (Ichas et al., 1997; Ichas and Mazat, 1998; Petit et al., 1998) and a high level conductance, leading to sustained mPTP opening, irreversible swelling of mitochondria, loss of $\Delta\psi_{mt}$ and cell death (Ichas and Mazat, 1998; Petit et al., 1998). The dissipation of $\Delta\psi_{mt}$ during mPTP activation occurs due to the equilibration of H^+ ions between the mitochondrial matrix and the intermembrane space. In addition, opening of the pore establishes hyperosmolarity within the matrix and thus dysregulation of mitochondrial volume (see Green and Reed, 1998). Mitochondrial

swelling due to entry of water results in permeabilisation of the outer mitochondrial membrane and release of pro-apoptotic matrix proteins such as cytochrome c (Green and Kroemer, 2004).

There are three distinct processes associated with induction of mPTP: initiation, decision and degredation. During the initiation phase effector molecules build up within the cell where they act directly on the mitochondria to induce mPTP. Throughout the decision phase mPTP activation and mitochondrial permeability transition are established, thus committing the cell to its apoptotic or necrotic fate. The specific mechanism of mPTP activation is thought to be determined by the nature of the death-inducing stimulus (Kroemer and Reed, 2000). The mPTP complex is regulated by numerous agents including peroxidants, caspases, cyclophillin D ligands, Ca^{2+} and Bcl-2-like proteins (Marzo et al., 1998). Elevated levels of peroxidants, Ca^{2+} and caspases (1,2,3,4,6) result in cytotoxicity and increased pore permeability. In contrast, the proteins Bcl-2 and Bcl-X_L are suggested to play a cytoprotective role by counteracting the activity of Bax, Bak and Bid (Yang et al., 1997; Marzo et al., 1998). Degradation refers to the engulfment or catabolic phase of cell death. Following mPTP activation, mitochondrial apoptogenic factors are released into the cytosol. These consist of apoptosis inducing factor (AIF), cytochrome c and Smac/Diablo (Ly et al., 2003). There are additional models however where apoptogenic factors are released in the absence of mPTP activation. Apoptosis also occurs normally in the cyclophilin D (CyP-D) knock out model (Nakagawa et al., 2005). The precise mechanism by which these factors are released remains at present unclear.

The permeability transition pore is thought to consist of the matrix protein CyP-D, the adenine nucleotide translocator (ANT) on the inner mitochondrial membrane and the voltage-dependent anion channel on the outer mitochondrial membrane (Figure 1.6) (Halestrap et al., 2002; Crompton, 2003; Galluzzi and Kroemer, 2007). Of these components, CyP-D is the only established component (Baines et al., 2005). Activation of mPTP is still observed in the absence of VDAC (Baines et al., 2007; Galluzzi and Kroemer, 2007) or ANT (Kokoszka et al., 2004). CyP-D is the target for mPTP inhibition by cyclosporine A. It is also thought to modulate the sensitivity of mPTP to Ca^{2+}. Although in some cases an important factor in mPTP activation,

CyP-D is not essential in its activation. Studies in mitochondria are devoid of CyP-D show that the protein is necessary for the sensitivity of the pore to Ca^{2+} and oxidative stress, but not essential in the execution of cell death (Baines et al., 2005; Basso et al., 2005).

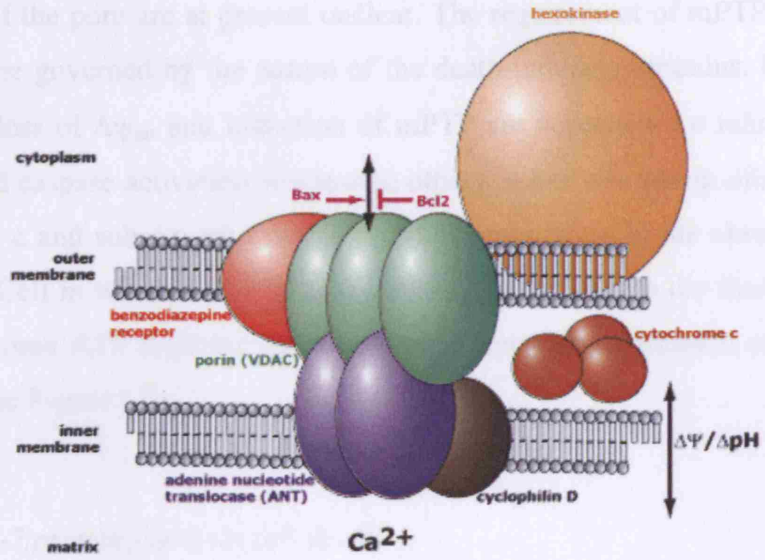

Figure 1. 6 Proposed structure of the mitochondrial permeability transition pore.

During apoptosis, numerous proteins combine to form the permeability transition pore. Proteins commonly associated with this structure include cytosolic hexokinase; the outer membrane protein porin or voltage-dependent anion channel (VDAC); adenylate cylase from the intermembrane space; cyclophilin D from the matrix and the adenine nucleotide translocase (ANT) from the inner membrane. *From www.molecularprobes.com*

The Ca^{2+} sensitivity of mPTP induction is also highlighted by experiments showing the phenomenon to be abolished in the presence of ruthenium red (Petronilli et al., 1993). The spread of permeability transition across a mitochondrial population increases in accordance with Ca^{2+} load. The induction of mPTP also varies with age and nature of the preparation studied (see Gunter and Pfeiffer, 1990).

The role of VDAC in cell death has been investigated using genetic manipulation and was found to be dispensable in mPTP induction. Additionally, it has been suggested that the Vdac1 and 2 isoforms of VDAC can function as receptors for the pro-apoptotic Bcl-2 proteins Bax and Bak (Galluzzi and Kroemer, 2007).

In summary, mPTP induction plays an important role in cell death in a number of cells types in response to multiple death-promoting stimuli. The precise structure and activation of the pore are at present unclear. The requirement of mPTP in cell death appears to be governed by the nature of the death-inducing stimulus. Under certain conditions loss of $\Delta\psi_{mt}$ and induction of mPTP are necessary for release of matrix proteins and caspase activation whereas in others, it has whereas in others release of cytochrome c and subsequent caspase activation can occur in the absence of mPTP activation. Cell in which mPTP is activated are more likely to die through necrosis, as they become ATP depleted and thus cannot support progression of the apptotic pathway (see Figure 1.7).

1.6.4 BCl-2 protein family in cell death

Members of the Bcl-2 family modulate a number of mitochondrial events. Certain members of the family, namely Bcl-2 and Bcl-X_L play a protective role during apoptosis and periods of cell stress, whereas others such as Bax or Bak can act as principal inducers of cell death. A majority of Bcl-2 proteins are often situated on the outer mitochondrial membrane, where they are known to modulate copious processes within the organelle (see Green and Reed, 1998). The biochemical changes required for the initiation of apoptosis are comprised of Ca^{2+} flux, caspase activation, production of ROS, loss of $\Delta\psi_{mt}$ and release of matrix proteins all of which are modulated by Bcl-2 proteins (Vander Heiden et al., 1997). One hypothesis is that Bcl-2 and Bcl-X_L interact with proteins of the inner mitochondrial membrane including both those associated with the mPTP and involved in ion transport (see Green and Reed, 1998). This lead the premise that Bcl-2 and Bcl-X_L are involved in the regulation of mitochondrial pH and the proton extrusion necessary for maintaining $\Delta\psi_{mt}$ (Shimizu et al., 1998). Overexpression of Bcl-2 and Bcl-X_L

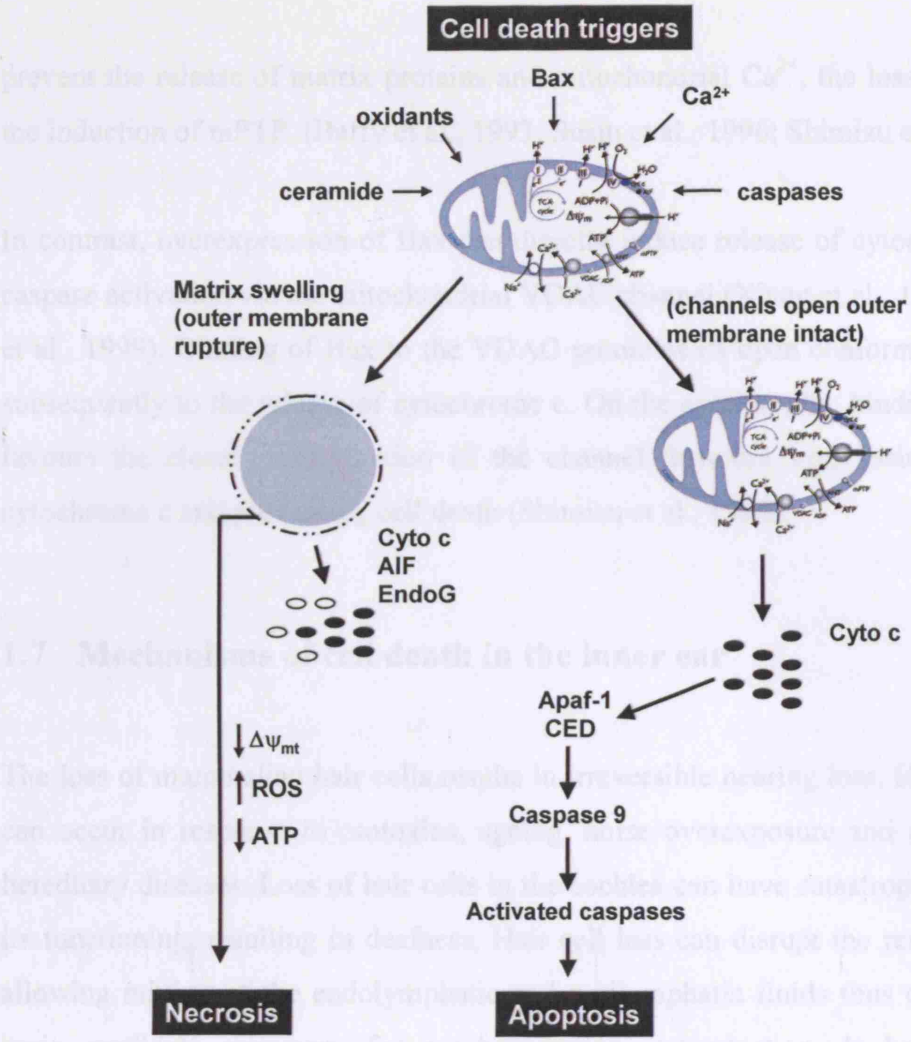

Figure 1. 7 Mitochondrial activation of caspases.

Release of caspase-activating proteins like cytochrome c (dark circles), Apoptosis inducing factor (AIF) and EndoG (empty circles) from mitochondria is triggered by multiple stimuli including Bax, Ca^{2+} and ROS. The two models explaining release of these proteins are 1) mitochondrial swelling and outer membrane rupture (left) and 2) the opening of channels in the outer membrane in the absence of mitochondrial swelling (right). In both cases cytochrome c relase occurs. Cytochrome c subsequently binds to Apaf-1, activates caspase 9 and initiates the protelytic cascade associated with apoptosis. Mitochondrial swelling and rupture results in a much slower progression towards cell death referred to as necrosis. This process does not require ATP and occurs due to loss of $\Delta\psi_{mt}$, elevated ROA and depletion of cellular ATP. *Figure adapted from Green & Reed 1998.*

prevent the release of matrix proteins and mitochondrial Ca^{2+}, the loss of $\Delta\psi_{mt}$ and the induction of mPTP (Baffy et al., 1993; Susin et al., 1996; Shimizu et al., 1998).

In contrast, overexpression of Bax can directly induce release of cytochrome c and caspase activation via the mitochondrial VDAC channel (Xiang et al., 1996; Shimizu et al., 1999). Binding of Bax to the VDAC promotes its open conformation leading subsequently to the release of cytochrome c. On the contrary, the binding of Bcl-X_L favours the closed conformation of the channel therefore suppressing release of cytochrome c and preventing cell death (Shimizu et al., 1999).

1.7 Mechanisms of cell death in the inner ear

The loss of mammalian hair cells results in irreversible hearing loss. Hair cell death can occur in response to ototoxins, ageing, noise overexposure and as a result of hereditary diseases. Loss of hair cells in the cochlea can have catastrophic effects on its functioning, resulting in deafness. Hair cell loss can disrupt the reticular lamina allowing mixing of the endolymphatic and perilymphatic fluids thus disrupting the ionic gradients necessary for mechanosensory transduction. It has been well documented that supporting cells are able to form *scars* that repair the cochlear epithelium (Forge, 1985; Raphael, 2002). Investigating the mechanisms involved in hair cell death is a challenging task. The complexity of the cochlea and the limited numbers of hair cells within it limit restrict the number of techniques that can be used to study the biochemical processes underlying cell death.

1.7.1 Aminoglycoside-induced hair cell death

Aminoglycosides are the most commonly used antibiotics worldwide for the treatment of gram negative bacterial infections. Their broad antibacterial spectrum and bactericidal properties allow them to kill and prevent the growth of bacteria. Aminoglycoside treatment results in the selective loss of auditory and vestibular hair cells. Hair cells exhibit a base-to-apex gradient of cell death in response to aminoglycosides. This phenomenon is observed both in neonatal (Richardson and Russell, 1991) and mature culture systems (Sha et al., 2001) and in *in vivo models*

(Kamimura et al., 1999). A similar gradient is observed in the aged cochlea (Usami et al., 1997) and in response to noise damage (Henderson et al., 2006). There are also multiple studies in both cochlear and vestibular hair cells, showing aminoglycoside antibiotic treatment to result in caspase activation and cell death via apoptosis (Forge, 1985; Richardson and Russell, 1991; Forge and Li, 2000; Cunningham et al., 2002). It is not surprising therefore that hair cell death can be prevented following administration of broad-spectrum caspase inhibitors (Forge and Li, 2000; Forge and Schacht, 2000; Cheng et al., 2005). Activation of upstream caspases 8 and 9, downstream caspase 3 and release of cytochrome c (Mangiardi et al., 2004) have been reported in avian hair cells in response to aminoglycosides (Matsui et al., 2004). In addition, inhibition of caspase 9 but not 8 protects against hair cell death (Cunningham et al., 2002). These data suggest that the death receptor pathway does not play a central role in aminoglycoside-induced toxicity and highlight the involvement of the mitochondrial death pathway. The mechanisms underlying aminoglycoside-induced hair cell death in the mammalian cochlea have been less well studied. Data in utricle however suggests that under *in vitro* conditions hair cell death occurs independently of the death receptor pathway (Bodmer et al., 2003). Data obtained from *in vivo* studies reveals nuclear translocation of AIF and EndoG (Figure 1.7) (Jiang et al., 2006) and cytochrome c (Wang et al., 2004) in cochlear hair cells following systemic treatment with kanamycin and cisplatin. In addition, there have been reports implicating the involvement of the Bcl-2 protein family (Cunningham et al., 2004; see Cheng et al., 2005; Vicente-Torres and Schacht, 2006) and oxidative stress (Kopke et al., 1997; Rybak et al., 1999; see Forge and Schacht, 2000) in aminoglycoside toxicity in the mammalian cochlea. Data from *in vitro* and *in vivo* systems reveal a role for MAP-kinase signalling in aminoglycoside toxicity. Activation of the transcription factor c-Jun N-ternimal Kinase (JNK) is found in vestibular hair cells following aminoglycoside treatment both *in vitro* (Sugahara et al., 2006) and *in vivo* (Ylikoski et al., 2002). Blocking this MAPK pathway has been shown to attenuate aminoglycoside-induced hair cell death *in vivo* (Ylikoski et al., 2002) but under *in vitro* conditions, JNK inhibitors were only effective at low aminoglycoside doses (Sugahara et al., 2006).

Taken together, these data show mitochondrial death pathways to be important in termination of both mammalian and avian hair cells in response to aminoglycoside

antibiotics. The upstream events subsequent to mPTP induction or activation of the mitochondrial apoptotic pathway are not well characterised.

1.7.2 A role for mitochondria in hair cell death

Mitochondria are key players in the execution of cell death pathways in a number of cell types (see Section 1.7). As discussed previously (Section 1.7.1), there is evidence supporting the involvement of mitochondria in aminoglycoside-induced hair cell death. There is also data linking mitochondria with noise-induced hair cell death. Activation of caspases 3, 8 and 9 and nuclear translocation of AIF, EndoG and cytochrome c have been reported in noise damaged cochleae (Nicotera et al., 2003; Yamashita et al., 2004; Han et al., 2006). There is also recent data reporting the coincident down regulation of Bcl-2 and up-regulation of Bax in both aged and cisplatin treated auditory hair cells (see Cheng et al., 2005). This therefore suggests an involvement of the Bcl-2 protein family and thus mitochondria in the regulation of hair cell death. It is well established that overexpression of Bcl-2 can protect against apoptosis (see Section 1.7.4). Similarly, overexpression of Bcl-2 prevented caspase-9 activation and hair cell death in utricular hair cells (Cunningham et al., 2004). Another key feature of apoptosis is induction of mPTP (see Section 1.7.3). Activation of mPTP and loss of $\Delta\psi_{mt}$ have been reported in gentamicin treated OHCs and are both prevented in the presence of the mPTP inhibitor cyclosporine A (Dehne et al., 2002).

More recently, it has been hypothesised that the mitochondrial uncoupling proteins UCPs) may be involved in aminoglycoside toxicity (Kitahara et al., 2005). The uncoupling proteins 1, 2, 3, 4 and 5 are members of the anion carrier family located on the inner mitochondrial membrane. It has been shown that tissues with high UCP expression levels exhibit increased respiratory rates and mitochondrial uncoupling. UCP-mediated proton leak reduces the number of protons flowing through the ATP synthase and consequently dissipates the $\Delta\psi_{mt}$ (for a recent review see Echtay, 2007). There are a number of physiological roles proposed for UCPs including export of fatty acids, protection against ROS (Echtay, 2007) and more recently, the regulation of mitochondrial Ca^{2+} (Trenker et al., 2007). The mRNA expression of UCPs has been detected in ganglion cells. mRNA expression of UCP 2 & 3 were

found to increase significantly subsequent to systemic kanamycin treatment and are suppressed by antioxidant administration (Kitahara et al., 2005). This study proposes that increased expression of UCP 2&3 mRNA plays a neuroprotective role in the cochlea, by attenuating the levels of mitochondrial superoxide production. Precise interpretation of the data is more complicated however, as there is no evidence showing a corresponding increase in UCP 2 or 3 protein expression.

In summary, there is substantial evidence implicating mitochondria in both aminoglycoside and noise-induced hair cell death. In most cases, cell death is consistent with apoptosis involving caspase activation and release of mitochondrial matrix proteins. The exact order in which these events occur however remains undefined. Additonally, the majority of data come from studies in avian vestibular and basal papilla hair cells and *in vivo* studies in mature mammalian cochleae. This makes it difficult to determine the specific mechanisms of hair cell death in neonatal cochlea cultures. Both aminoglycosides and noise damage result in an increase in levels of ROS in inner tissues, which could in turn act directly on mitochondria to initiate cell death via mPTP induction or membrane depolarisation. It is also a possibility that mPTP induction and loss of $\Delta\psi_{mt}$ result form Ca^{2+} overload in the hair cells (Matsui et al., 2004). The underlying mechanisms of hair cell death in the neonatal cochlea will be investigated as part of this thesis. The neonatal cochlear preparation provides a stable system that can be maintained *in vitro* over long periods of time. This makes it a useful model with which to study mitochondrial signalling during aminoglycoside-induced hair cell death.

2 Materials and Methods

2.1 General reagents

Unless stated otherwise, all reagents were purchased from SIGMA Aldrich, UK. All fluorescent dyes were purchased from Molecular Probes (Invitrogen, UK). Cell culture media and foetal bovine serum were purchased from GIBCO (Invitrogen, UK).

2.2 Cell culture

2.2.1 Dissection and isolation of the organ of Corti

This study used post-natal days 2-3 male and female rats. Animals were killed by rapid cervical dislocation followed by decapitation. Subsequent to decapitation, the head was immediately bisected along the midline exposing the brain and location of the temporal bone (bulla tympanica). Dissection forceps were used firstly to remove the brain and second, to cut the bulla away from the skull and surrounding tissues. Connective tissue was removed from the bulla using forceps (Richardson and Russell, 1991). The bulla from the opposite side was removed using the same technique. Bullae were then placed into M199. One was dissected immediately and the second left un-opened in M199 at room temperature. Under a dissecting microscope, a small incision was made in the bulla using fine forceps. Using two pairs of fine forceps as scissors, the remainder of the bulla was cut away. Extra care was taken when detaching the cochlea from base of the bulla to prevent tearing the cochlea. At this age, the bulla is easy to remove, as it is a soft cartilaginous structure. Once isolated, the nervous tissue was teased away from the centre of the cochlea revealing the coiled structure. To remove the stria vascularis, the cochlea was held down by gripping the remaining nervous tissue at the base and the stria then peeled away from base-to-apex. Cochleae were then cut into basal, middle and apical turns using iridectomy scissors. Cochlea turns were transferred into Cell-Tak® coated MatTek® dishes. Dishes were coated with Cell-Tak® at a dilution of 1 in 20 (of a 0.9 mg/ml stock) in 0.1M of sodium hydrogen carbonate buffer ($NaHCo_3$) at least 1 hour before culturing. Before plating, dishes were washed three times using

DMEM/F-12 containing 0.5% fetal bovine serum pre-incubated at 37^0C. Cultures were incubated overnight at 37^0C.

2.2.2 Assessment of cultures

Following 24 hours of culture, cochlea explants were studied using an inverted microscope (Nikon Eclipse TS 100). Cultures were examined for presence of rows of stereocilia. In outer hair cells, stereocilia are characteristically v-shaped (Pickles 1988). The presence of intact bundles running along the length of the cochlea piece was used as an indication of how healthy they were.

2.2.3 Cochlea slice preparation

Cochlear slices were obtained from P2-P12 rats using the technique pioneered by (Jagger et al., 2000). Bullae were isolated as described in section 2.4.1, in cold HBSS. Cochlea were placed on ice cold mounting blocks on a microtome (Vibratome Series 1000) and held in place using cyanoacrylate adhesive (super glue). The bulla was angled in such a way that the modiolar axis of the cochlea was parallel to the microtome blade (double edge, Boots, UK) and the oval window faced downwards, away from the cutting edge. Positioning of the bulla in this way produced planar slices in the modiolar plane which transected the three scalae radially. Cochleae were sliced using vibration 4 and slow advance. Slice thicknesses varied between 350-400 μm; in most cases slices used were 350μm. Slices were kept in ice cold HBSS before imaging. Greater care was taken when slicing cochlea from older animals, due to the advancing ossification of both the cochlea capsule and modiolus.

2.3 Imaging methods

2.3.1 Live imaging of mitochondrial membrane potential

$\Delta\psi_m$ was measured using either TMRM (tetramethylrhodamine methyl ester),$DiIC_1(5)$ (1,1',3,3,3',3'-hexamethylindodicarbocyanine iodide) or Rhodamine 123 (Rh123). For experiments with TMRM cultures (plated in Matek dishes) and slices were loaded for 45 minutes at concentrations ranging from 50-700nM in Hepes-buffered HBSS at room temperature. After loading, all experiments were

carried out at room temperature, using 150-200 nM of TMRM in the recording media throughout the experiment. TMRM fluorescence was excited at 543 nm and emission (peak around 575 nm) captured using a long pass 560 filter. Experiments with $DiIC_1(5)$ were carried out using the same loading protocol. $DiIC_1(5)$ fluorescence was excited at 633 nm and emission captured using a long pass 650 filter.

The dyes described previously are lipophillic cations that cross cell membranes and partition between cellular compartments in response to electrochemical potential gradients (Johnson et al., 1981; Scaduto and Grotyohann, 1999). In this study, the dyes have been used in two modes, redistribution mode and de-quench mode. When using redistribution mode, one assumes that at low concentrations (~ 150-200 nM) the fluorescence signal exhibits a linear relationship with the dye concentration. Under such circumstances, the dye concentration should follow Nernstian distribution between cellular compartments. The distribution of potassium (K^+) ions across the plasma membrane and establishment of the Nernst potential for K^+ ions is analogous to the equilibration of TMRM into the mitochondrion. The Nernst potential refers to the potential at which there is no net movement of ions across the membrane. Descriptions of the Nernst equation for both K^+ ions and TMRM are shown below.

$$V_m = -\frac{RT}{2f} \log_{10} \frac{[K^+]_{out}}{[K^+]_{in}}$$

$$\Delta\Psi_{mt} = -\frac{RT}{2f} \log_{10} \frac{[TMRM]_{cytosol}}{[TMRM]_{nucleus}}$$

R – is the universal gas constant

T – temperature in Kelvin

F – Faraday constant

V_m – membrane potential

In this example, the value for $RT/2f$ will be estimated at 60. If we assume the mitochondria to have a $\Delta\psi_{mt}$ value of approximately -180 mV with respect to the cytosol, this is equal to roughly 3 x RT/f (given that 180/3 = 60). In order to balance

the equation, a value of $3\log_{10}$ is used. This means that the concentration of dye used in the recording media will be concentrated by at least 1000 fold into the mitochondria.

In order to estimate a value for $\Delta\psi_{mt}$, the concentrations of dye in the cytosol (extracellular TMRM ions) and mitochondrial matrix (intracellular TMRM ions) are used in place of K^+ ions. In accordance with Nernstian distribution, one would expect the dye to concentrate by approximately 1000 fold into the mitochondria if $\Delta\psi_{mt}$ is estimated at 150 to -180 mV (Duchen et al., 2003; Duchen, 2004). Due to the large dynamic range of this dye (intensities from 3-4000) imaging systems require digitization of the signal to at least 12 bits (4096 grey levels). When using redistribution mode, a drop in $\Delta\psi_{mt}$ was seen as a reduction in mitochondrial TMRM fluorescence. The dye was not lost from the cell, but instead redistributed between mitochondrial and cytosolic compartments. Measurements of TMRM fluorescence intensity using regions of interest (ROIs) therefore showed no overall change in TMRM fluorescence when placed over the whole cell. Quantifiable changes in fluorescence were only obtained when measuring from clearly separated mitochondrial and cytosolic compartments.

When using the de-quench mode, higher dye concentrations were used (> 700 nM). This creates such a high concentration of dye in the mitochondria, that a substantial proportion of the fluorescence is quenched. In this case, a reduction in $\Delta\psi_{mt}$ was seen as an increase in fluorescence (Duchen et al., 2003; Duchen, 2004). When using de-quench mode the value of $\Delta\psi_{mt}$ cannot be estimated. This method of dye loading was used to only observe dynamic changes in $\Delta\psi_{mt}$ under various conditions.

For experiments done using the redistribution mode, cultures were loaded with TMRM or $DiC_1(5)$ (150-200 nM in HBSS) at room temperature for 45 minutes in order to reach equilibrium. Dye was also present in all recording solutions (150-200 nM) throughout the duration of the experiment. For these experiments, basal, middle and apical turns were turns were cultured in a single dish to ensure that all were exposed to the same experimental conditions. For experiments done using de-quench mode, cultures were loaded at 700-800 nM in HBSS for 30 minutes at room temperature followed by washing. Once again dye was present in all recording

solutions at 150-200 nM. The presence of dye in recording media enabled the TMRM equilibrium between mitochondrial and cytosolic compartments to be maintained.

2.3.2 Visualising mitochondria using Mitotracker dyes

Mitotracker dyes are membrane permeant dyes that accumulate selectively into actively respiring mitochondria. In comparison to TMRM and $DiIC_1(5)$ some Mitotrackers (Mitotracker 633) contain a thiol-reactive chloromethyl allowing them to bind with sulphydryl groups within the mitochondria. The strong binding with these groups prevents the redistribution of dye between compartments thus allowing the dye to remain associated with the mitochondria subsequent to loss of $\Delta\psi_{mt}$ (Hallap et al., 2005). Other Mitotracker probes however do exhibit fluorescent changes subsequent to loss of $\Delta\psi_{mt}$ (Poot et al., 1996).

Cultures were incubated with 200nM of Mitotracker 633 in HBSS (molecular probes) for 45 minutes at room temperature. Cultures were then washed with HBSS. Fluorescence images were obtained with a Zeiss 510 LSM confocal using a 40x Plan-Neofluar (NA 1.3) oil objective. Mitotracker 633 was excited using the 633 laser line and emission (peak 675 nm) collected using a long pass 650 emission filter. Alternatively images were captured using a Zeiss multiphoton confocal (Axioskop 2 FS Mot) with a Zeiss 63x Vis-IR dipping objective (NA 1.0). The dye was again excited at 633 nm and collected using a long pass 650 emission filter.

2.3.3 Dual labelling of mitochondria using Mitotracker and membrane potential dyes

Slice preparations and explant cochlea cultures were incubated in HEPES buffered HBSS containing 200nM $DiIC_1(5)$ and 200nM Mitotracker green for one hour at room temperature. For the slice preparation, loading solutions were bubbled with oxygen. Preparations were then washed three times in HEPES buffered HBSS containing 100nM of TMRM and subsequently imaged. The same protocol was used when loading with Mitotracker 633 and TMRM.

2.3.4 *Labelling of mitochondria using immunocytochemistry*

To study cellular distribution of mitochondria in the cochlea, tissue preparations were labelled with a mouse monoclonal antibody raised to the beta (ß)-subunit of the of the mitochondrial ATP synthase (see Section 2.3.3).

2.3.5 *Dynamic measurements of changes in $\Delta\psi_{mt}$*

Dynamic measurements of fluorescence were used in order to observe depolarization or hyperpolarisation of $\Delta\psi_{mt}$ *in situ*. Depolarisation of $\Delta\psi_{mt}$ resulted re-distribution of the dye (see section 2.5.1) from the mitochondrial compartment into the cytosolic compartment. Depending on the mode in which the dye was used (see section 2.5.1), this was seen as either an increase or decrease in the fluorescent signal. Three metabolic inhibitors were used to manipulate $\Delta\psi_{mt}$; the protonophore carbonylcyanide-p-trifluoromethoxyphenylhydrazone (FCCP, Fluka), sodium cyanide (NaCN,) and oligomycin (Fluka).

The FCCP was used to dissipate $\Delta\psi_{mt}$ by uncoupling oxidative phosphorylation from the mitochondrial electron transfer chain. FCCP (5 µM) was applied extracellularly to the recording media or under pressure from a micropipette and the subsequent changes in fluorescence (TMRM, Rh123 or mitotracker) recorded. For experiments using FCCP, TMRM was used in redistribution mode (see section 2.5.1) between 150-200 nM or in de-quench mode at 800 nM. Rh123 was used only in de-quench mode, at a concentration of 1 µM. Cultures were loaded with 1 µM Rh123 in HBSS for 20 minutes at room temperature. Cultures were subsequently washed three times using HBSS and then placed on the microscope stage. For these experiments, no additional dye was present in the recording media.

NaCN was used as a reversible inhibitor of complex IV (see section 1.4.3) in the mitochondrial electron transfer chain. NaCN was dissolved in MilliQ water and the pH adjusted to 7.3 using 4M NaOH. NaCN was used at a final concentration of 3 mM. NaCN was applied from a micropipette under pressure induced transient depolarisation in $\Delta\psi_{mt}$. Subsequent to application, the NaCN diffused away from the application site into the excess bath volume so that only a transient depolarisation

was observed. For experiments with NaCN, TMRM was used between 150-200 nM, meaning that depolarisations were observed as a decrease or redistribution of TMRM fluorescence.

Oligomycin (Fluka) was used to irreversibly block the proton channel of the mitochondrial ATP-synthase. Oligomycin (2.5 mg/ml) was dissolved in 100% ethanol and used at a final concentration of 12.5 μg/ml in HBSS. For experiments with oligomycin, TMRM was used in redistribution mode (150-200 nM).

BAPTA-AM was used at a final concentration of 50 μM at a 1 in 1000 dilution and used to study the effects of Ca^{2+} chelation on the $\Delta\psi_{mt}$. Baseline TMRM fluorescence was recorded over 20 minutes, after which BAPTA-AM was added and subsequently, $\Delta\psi_{mt}$ was monitored for a further 35-40 minutes. In these experiments, TMRM was used in redistribution mode (150-200 nM).

2.4 Imaging of endogenous autofluorescence

2.4.1 Measurement of NAD(P)H and FAD autofluorescence

Cultures were placed on the stage of an inverted Zeiss 510 laser scanning confocal microscope. All experiments were carried out in HBSS pH 7.3 at room temperature, unless stated otherwise. Reduced pyridine nucleotide (NAD(P)H) fluorescence (blue) was excited with UV 351 nm light using the UV laser line of the Enterprise™ UV laser.

Emitted fluorescence was collected using a 435-485 nm band pass filter (Duchen et al., 2003; Dumollard et al., 2007). Oxidised flavoprotein (FAD^{++}) fluorescence (green) was excited using the 458 nm line of the argon laser and collected using a long pass 505 filter (Duchen et al., 2003). Images were acquired using a Plan-Neofluar 40x oil immersion objective (NA 1.3).

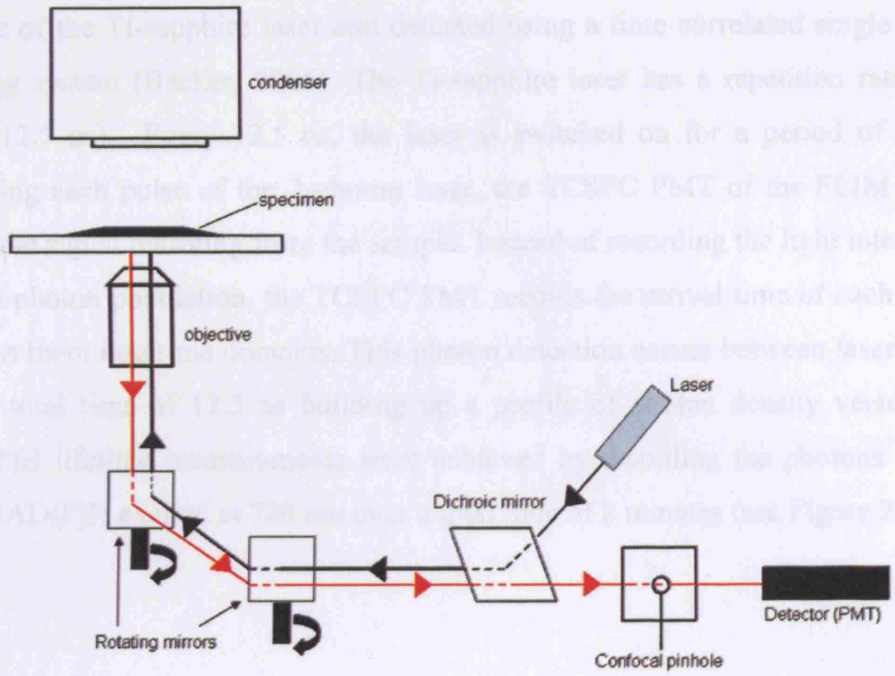

Figure 2. 1 The laser scanning confocal microscope.

This confocal microscope utilises a single spot scanning system that uses a laser beam and rotating mirrors placed strategically in aperture planes to achieve a scanning motion. Laser light enters the system and is reflected of a beam-splitting plate (dichroic mirror). The light is then directed into a mirror-based scanning system where it is scanned in two perpendicular directions. The scanned (polarized) light is subsequently focused on a region in the specimen. Emitted light coming from the illuminated area of the specimen is then descanned by the same system. The now unpolarised light then passes back thorough the beam-splitter to the confocal detector. The detection of the confocal system will be confined to region of illumination in the specimen

2.4.2 2-photon and lifetime imaging (FLIM) of NAD(P)H auto-fluorescence

All tissue was imaged using a 63x water dipping objective (Achroplan IR, NA 0.9). Blue auto-fluorescence from NADH and NAD(P)H was excited using the 720 nm line of a Ti-sapphire laser (Coherent, UK) pulsed at 80mHz (12.5 ns). Emitted fluorescence was detected using a 435-485 nm IR blocking band pass filter. For

lifetime imaging, auto-fluorescence from NAD(P)H was again excited using the 720 nm line of the Ti-sapphire laser and detected using a time correlated single photon counting system (Becker, 2006). The Ti-sapphire laser has a repetition rate of 80 MHz (12.5 ns). Every 12.5 ns, the laser is switched on for a period of 140 fs. Following each pulse of the 2-photon laser, the TCSPC PMT of the FLIM system awaits the signal returning from the sample. Instead of recording the light intensity of a given photon population, the TCSPC PMT records the arrival time of each photon and bins them into time domains. This photon detection occurs between laser pulses, over a total time of 12.5 ns building up a profile of photon density verses time. NAD(P)H lifetime measurements were achieved by recording the photons emitted from NAD(P)H excited at 720 nm over a total time of 2 minutes (see Figure 2.3).

2.5 Assessment of intermediary metabolism

2.5.1 Imaging of dynamic changes in NAD(P)H and FAD

To assess the resting redox state of cochlear cells, we employed a dynamic assay using the metabolic inhibitors NaCN (SIGMA) and the uncoupler carbonylcyanide-p-trifluoromethoxyphenylhydrazone (FCCP). NaCN blocks respiration at complex IV of the mitochondrial electron transfer chain and induces a state of maximal reduction meaning that throughout the duration of this period NAD(P)H and FAD are maximally reduced (Duchen et al., 2003). This switch in redox state alters the fluorescent properties of these two molecules. NAD(P)H is fluorescent when reduced and therefore addition of NaCN causes an increase in blue fluorescence and a decrease in green fluorescence (Dumollard et al., 2007).

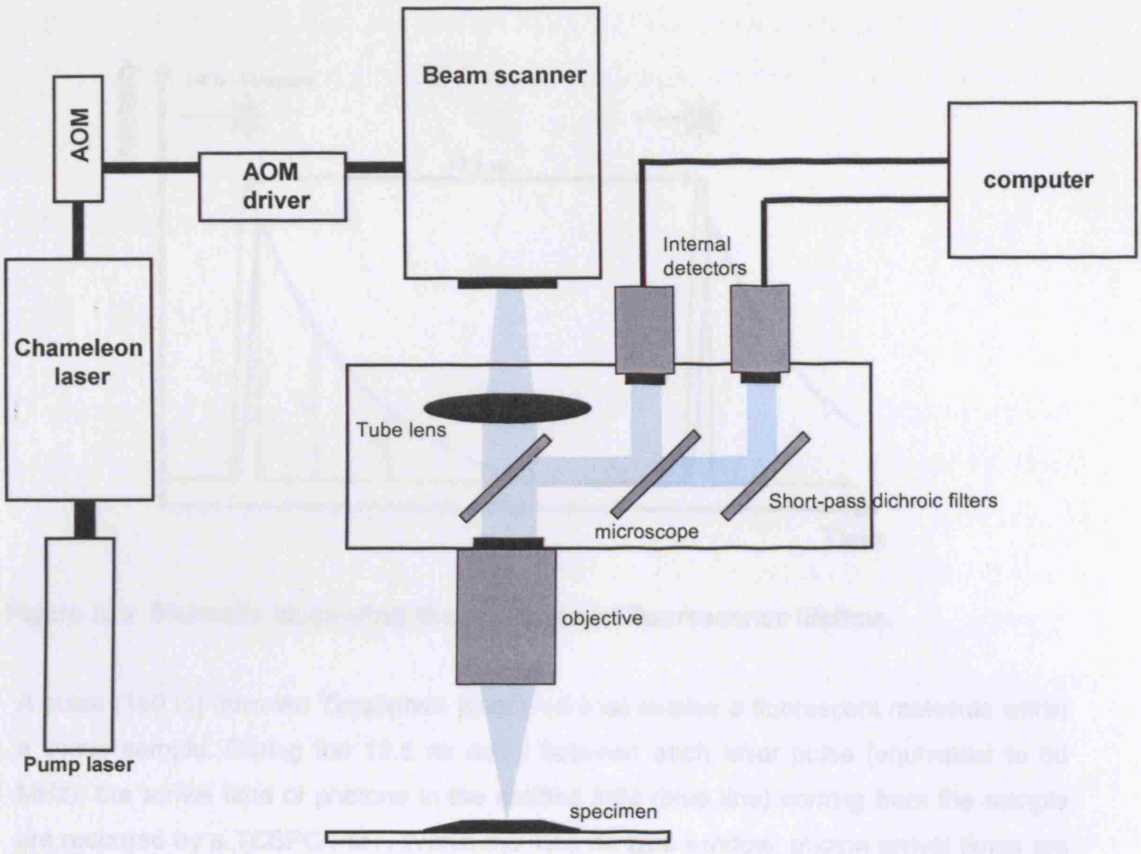

Figure 2. 2 Multiphoton confocal microscope.

Multiphoton microscopy uses localized, nonlinear excitation to excite fluorescence within a thin raster scanned plane (Zipfel, Williams & Webb 2003). Non linear excitation refers to the process by which 2 single photons will combine. In two or multiphoton microscopy, fluorescent dyes are excited with rapid, intense pulses of IR light (usually at ~ double the wavelength required for single photon excitation). Longer wavelengths of the IR laser also allow deeper tissue penetration. The dichroics used in the multiphoton system function in the opposite way to those used on the standard confocal system. The dichroics reflect long wavelength light coming from the excitation source and pass shorter wavelengths emitted from fluorescent molecules within the tissue sample. The system shown above consists of a laser scanning confocal coupled to a femtosecond pulsed infared (IR) laser. The laser module on this system contains both the pump laser and the Chameleon oscillator. Having both components in a single unit gives the system has a wider tuning range (690-1020). The excitation wavelength of the 2 photon laser is adjusted by means of acousto-optical modulator (AOM). The non-descanned detectors (NDDs not shown in Figure) collect the fluorescence signal before the scanning lens and are designed to gather heavily scattered light from deep within tissues.

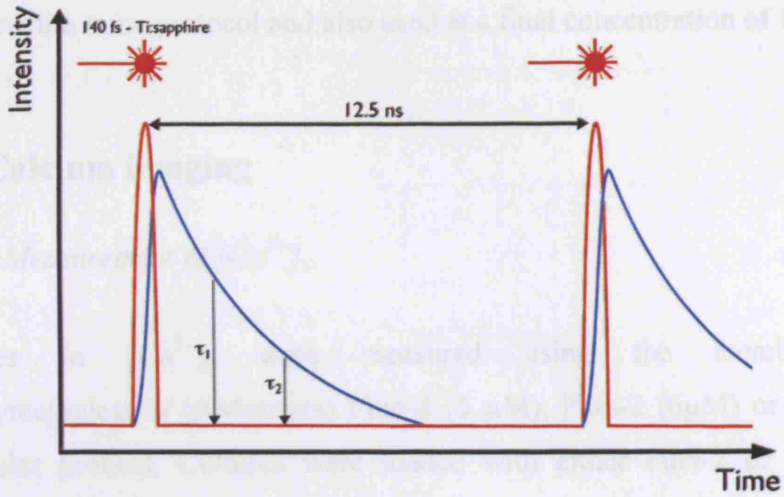

Figure 2. 3 Shematic illustrating the principles of fluorescence lifetime.

A pulse (140 fs) from the Ti:sapphire laser (red line) excites a fluorescent molecule within a tissue sample. During the 12.5 ns delay between each laser pulse (equivalent to 80 MHz), the arrival time of photons in the emitted light (blue line) coming from the sample are recorded by a TCSPC PMT. Within the 12.5 ns time window, photon arrival times are binned into specified time domains enabling a histogram (lifetime image) of photon density verses time and spatial position to be produced. In the case of NAD(P)H, the lifetime can be fit with double exponential decay.

Addition of FCCP induces a state of maximal oxidation. FAD is optimally fluorescent when reduced. This redox switch is therefore seen as an increase in green fluorescence and a reduction in blue fluorescence. The relative differences in the fluorescence of the two signals between there maximally oxidized and reduced state can then be used to calculate the resting redox state of the cell (Duchen et al., 2003; Duchen, 2004).

NaCN was dissolved in HBSS and the pH adjusted to 7.3 using 4M NaOH. NaCN was applied extracellularly from a glass micropipette under a pressure (10 psi) at 5mM.

The metabolic substrates pyruvate (Calbiochem) and lactate (Calbiochem) were also employed to study dynamic changes in NAD(P)H and FAD autofluorescence. Pyruvate was dissolved in HBSS and the pH adjusted to 7.3 using 4M NaOH.

Pyruvate was used at final concentration of 10mM. Lactate was prepared and used following the same protocol and also used at a final concentration of 10mM.

2.6 Calcium imaging

2.6.1 Measurement of $[Ca^{2+}]_c$

Changes in $[Ca^{2+}]_c$ were measured using the membrane-permeable acetoxymethylesters (AM-esters) Fluo-4 (5 μM), Fura-2 (6μM) or Fura-FF (6μM, Molecular probes). Cultures were loaded with either Fura-2 or Fura-FF in the presence of 0.01% pluronic for 40 minutes at room temperature. Subsequent to loading, cultures were washed three times over a period of 5 minutes in HBSS and left to equilibrate for a further 20 minutes before imaging thus allowing for complete cleavage of the AM ester. Fluorescence measurements were obtained using an epifluorescence inverted microscope (Axiovert S100 TV). Images were captured using a 20x Fluar objective (NA 0.75). Fura-2 and Fura-FF fluorescence were excited alternatively at 340nm and 380 nm by means of a fast switching monochramator (Kinetic Imaging). Fluorescence was collected using a 500 nm dichroic mirror and a 510 nm long pass filter producing images on a 12 bit cooled CCD camera (PCO Sensicam Pulse Photonics). The protocol consisted of 300-350 frames of 256 x 300 pixel (4x4 binning) images. The 340 and 380 channels were exposed sequentially for a period of 300 ms.

For confocal imaging, Fluo-4 was excited using the 488 nm laser line of the LSM Zeiss 510 confocal and emitted fluorescence collected using a 505-550 nm band pass filter. Fura-2 and Fura-FF were excited using the 405 nm line of the blue diode laser and emitted fluorescence collected using a 420 nm long pass filter.

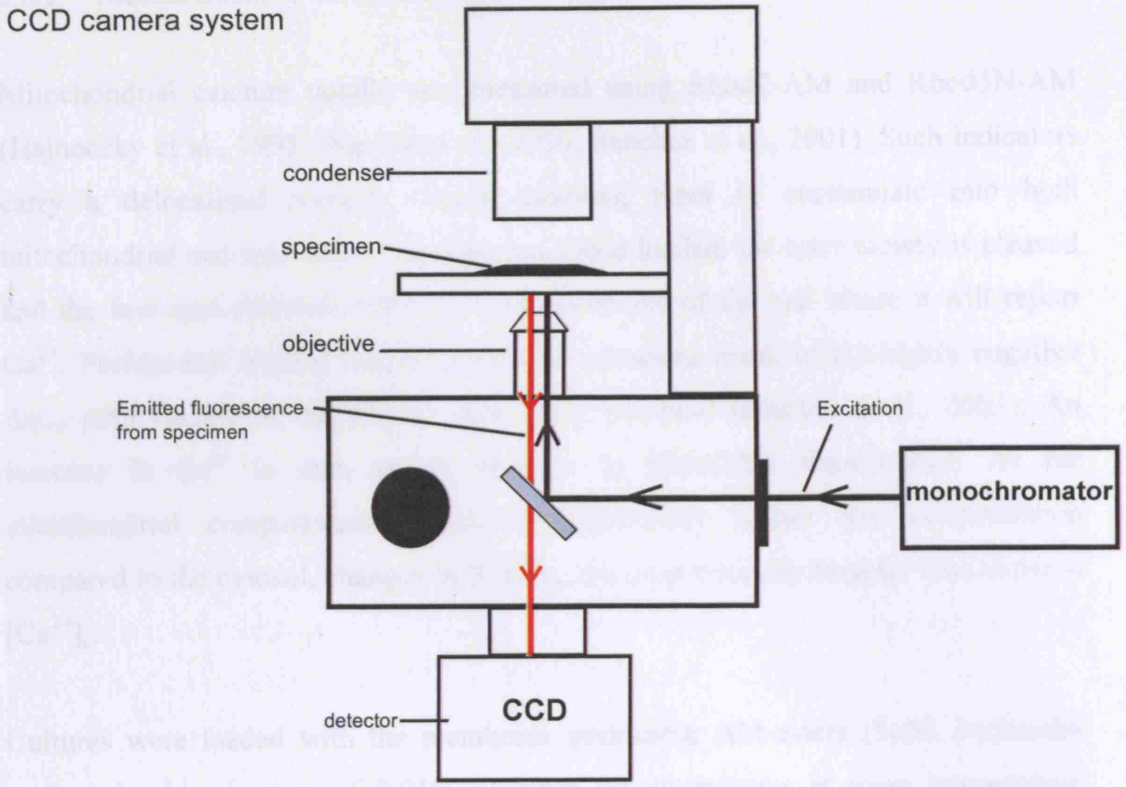

Figure 2. 4 CCD (charge coupled device) camera system.

Shows an inverted microscope connected to a CCD camera. Fluorescent dyes are excited by light of varying wavelengths coming from a fast-switching monochromator. Excitation light from the monochromator is reflected up towards the sample by a dichroic mirror (a mirror that reflects light with short wavelengths and passes that with longer wavelengths). Emission fluorescence from the sample is then passed back through the dichroic mirror to the detector, which in this case is the CCD camera. Photons (emitted light from the specimen) hit a silicon plate (CCD chip) comprised of a series of electrodes within the CCD camera and are trapped in the form of electrons in a silicon-oxide/*p*-type silicon junction. Electrons will accumulate here during the integration time of the CCD. The integration time is controlled electronically and can vary from microseconds to tens of milliseconds or tens of seconds. A change in voltage is then used to shift the gathered electrons underneath the electrodes thus giving the camera read-out. Only the electrodes that were bombarded with photons will correspond to the pixels in the resulting fluorescence image.

2.6.2 *Measurement of mitochondrial Ca^{2+} uptake*

Mitochondrial calcium uptake was measured using Rhod2-AM and Rhod5N-AM (Hajnoczky et al., 1995; Sharma et al., 2000; Sanchez et al., 2001). Such indicators carry a delocalized positive charge enabling them to accumulate into both mitochondrial and cytosolic compartments. Once loaded, the ester moiety is cleaved and the free acid retained within the compartments of the cell where it will report Ca^{2+}. Preferential loading into mitochondria occurs as result of the highly negative $\Delta\psi_{mt}$ with respect to the plasma membrane potential (Duchen et al., 2003). An increase in Ca^{2+} is seen as an increase in Rhod2/5N fluorescence. As the mitochondrial compartment retains a significantly higher dye concentration compared to the cytosol, changes in $[Ca^{2+}]_{mt}$ are proportionally brighter than those in $[Ca^{2+}]_c$.

Cultures were loaded with the membrane permeable AM-esters (5μM, Molecular probes) in the presence of 0.01% pluronic for 40 minutes at room temperature. Cultures were then washed and left to equilibrate for 15 minutes prior to imaging. Fluorescent images were acquired with the Zeiss 510 LSM confocal microscope using a 40x plan-neofluar (NA 1.3) oil objective. Dyes were excited at 543 nm and emitted fluorescence (peak at 575 nm) was captured using a 560 nm long pass filter.

2.6.3 *Inhibition of mitochondrial Ca^{2+} uptake using CCCP in combination with oligomycin*

The uptake of Ca^{2+} into mitochondria is governed by two factors. Firstly it depends on $\Delta\psi_{mt}$ meaning that Ca^{2+} can only be sequestered by actively respiring mitochondria. Uptake also relies on the maintenance of a low intramitochondrial Ca^{2+} thus permitting Ca^{2+} to move from the cytosol into the mitochondrial matrix when $[Ca^{2+}]_c$ is raised (Duchen, 2004). The protonophore carbonyl cyanide 3-chlorophenylhydrazone (CCCP, 5 μM) was used to dissipate $\Delta\psi_{mt}$ and thus remove the driving force for mitochondrial Ca^{2+} uptake. In the presence of CCCP the mitochondrial ATP-synthase can function in reverse-mode and consume cellular ATP in attempt to maintain $\Delta\psi_{mt}$. Oligomycin acts to prevent the reverse-mode

function of the mitochondrial ATP-synthase. Thus all experiments using CCCP were done in the presence of oligomycin.

2.6.4 Inhibition of mitochondrial Ca^{2+} uptake using Ru360

Mitochondrial Ca^{2+} uptake via the Ca^{2+} uniporter was blocked using the oxo-bridged ruthenium complex Ruthenium 360 (Ru360). Ru360 is an analogue of ruthenium red (a well characterised blocker of mitochondrial Ca^{2+} accumulation) and can be used to selectively block Ca^{2+} uptake into actively respiring mitochondria (Matlib et al., 1998). In this study, Ru360 was used to block mitochondrial Ca^{2+} uptake in response to extracellular ATP application or mechanical damage. Ru360 (Calbiochem) was dissolved in de-oxygenated water and used at a final concentration of 80 μM in HBSS. Cultures were incubated with RU360 (80 μM) for 20 minutes at room temperature. An additional 80 μM Ru360 was added at the start of the experiment in order to reduce the effects of oxidation on the ruthenium complex.

2.6.5 Agonist-induced Ca^{2+} mobilisation

To study the relationship between mitochondrial and cytoplasmic Ca^{2+} in cochlear cultures, we used the purine nucleotide adenosine 5'-triphosphate (ATP) to mobilise $[Ca^{2+}]_c$. Nucleotide solutions were prepared at 100 mM in 18 MilliQ water. ATP was used at concentrations ranging from 10 nM up to 100 μM in Hepes buffered HBSS. A micropipette was positioned approximately 10 μm above the second row of outer hair cells and ATP applied locally for a period of 30 seconds from a picospritzer system at a pressure of 10 psi. In these experiments ATP was used only as a method of eliciting changes in $[Ca^{2+}]_c$. The changes in $[Ca^{2+}]_c$ (see Section 2.8.1) and $[Ca^{2+}]_{mt}$ (see Section 2.8.2) were measured at each ATP concentration. To assess the influence of mitochondrial Ca^{2+} buffering on ATP-induced $[Ca^{2+}]_c$ signals, the Ca^{2+} uniporter was blocked using a cocktail of 5 μM CCCP plus 12.5 μg/ml oligomycin (see Section 2.8.3).

2.6.6 Damage-induced Ca^{2+} waves

Mechanical damage was induced using a glass micropipette. The micropipette was positioned roughly 15 μm above the second row of outer hair cells and lowered onto the outer hair cell region using a micromanipulator. In most cases lesions consisted of two outer hair cells. To ascertain the role of mitochondrial Ca^{2+} uptake on the spatiotemporal properties of the damage-induced signal, the uniporter was blocked using 80 μM Ru360 (see Section 2.8.4).

2.7 Aminoglycoside experiments

2.7.1 Measurement of neomycin-induced Ca^{2+} transients using Rhod2-AM

Cultures of the basal cochlea turn were incubated with the Ca^{2+} indicators Rhod2-AM (to measure $[Ca^{2+}]_{mt}$) and Fura-2-AM (to measure $[Ca^{2+}]_c$) for 40 minutes at room temperature. Cultures were subsequently washed three times over a period of five minutes, allowed to equilibrate for a further 20 minutes and placed on the microscope stage where they were imaged over 20-30 minutes in HBSS to allow for aclimatisation and recording of steady baseline fluorescence. Baseline fluorescence was also used as an estimate of resting $[Ca^{2+}]_c$ and $[Ca^{2+}]_{mt}$. The control HBSS solution was then replaced with HBSS containing 1 mM neomycin and the tissue then imaged for a further 6 hours at room temperature. Images were acquired with the Yokagowa Nipkow spinning disc system (PerkinElmer) using an Ixon EM CCD camera (Andor IQ, UK) using a 63x Apochromat oil immersion objective, apochromat (NA 1.4). Rhod2 was excited using the 565 nm laser line of the spinning disc confocal system. For experimental controls cultures were treated and imaged as described above, in the absence of neomycin.

2.7.2 Measurement of neomycin-induced Ca^{2+} transients using Fura-2-AM

Basal cochlear cultures were incubated with 6 μM Fura-2 in HBSS at room temperature for 45 minutes. Cultures were subsequently washed three times over a period of 20 minutes and then imaged as described previously in Section 2.8.1 Dishes were imaged for an initial period of 30 minutes in order to record baseline

Ca^{2+} levels. The recording media was then switched from HBSS to HBSS containing 1 mM of neomycin sulfate. The preparation was subsequently imaged over a period of up to 6 hours with an interval of 2 minutes between successive monochromator illuminations.

2.7.3 Experiments in low external Ca^{2+}

For all experiments, cultures were imaged in HEPES buffered HBSS solution in which the Ca^{2+} had been reduced to be nominally free (estimated at ~ 20 μM). The $[Ca^{2+}]$ was estimated as 20 μM, as solutions were made up without EGTA. The Ca^{2+} was substituted by magnesium (Mg^{2+}). Mg^{2+} was used at a final concentration of 2 mM.

2.7.4 Apyrase experiments

Apyrase was used to degrade extracellular ATP and thus investigate the role for ATP in the establishment of $[Ca^{2+}]_c$ waves. Apyrase was dissolved in HEPES buffered HBSS to give a final concentration of 400 U/ml. Cultures were incubated with 80 U/ml of apyrase in HBSS at room temperature for a period of 20 minutes prior to the start of the experiment. A further 80 U/ml were added after a period of 2 hours, to rule out any discrepancies due to degredation of the drug.

2.7.5 Neomycin-induced changes in $\Delta\psi_{ml}$ measured using TMRM

Basal cochlea explants were loaded with TMRM (200 nM) for one hour at room temperature in HBSS. TMRM (200 nM) was present in all recording media for the duration of the experiment. Cultures were treated and processed as described in section 2.7.1. TMRM fluorescence was excited using the 546 laser line of the spinning disc confocal system.

2.7.6 Neomycin-induced changes in $\Delta\psi_{ml}$ measured using Rhodamine 123

Basal cochlea explants were loaded with 1 μM Rhodamine 123 (Molecular Probes, Invitrogen) in HBSS at room temperature for 30 minutes. Cultures were subsequently washed three times in HBSS and imaged using the 488 nm laser line of

the spinning disc confocal system. Baseline was recorded over 20-30 minutes prior to neomycin addition.

2.7.7 Measurement of extracellular ATP

Extracellular ATP release in whole mount cochlea explants was measured using the luciferin-luciferase bioluminescence assay (Newman, 2001). ATP release was measured in response to treatment with 1 mM neomycin over a period of six hours. DMEM/F-12 culture media was replaced with HBSS (100 µl) containing 12.5 µl Luciferase (SIGMA L1759) from a 10mg/ml stock and 1mM of D-luciferin (SIGMA L6882). A baseline level of bioluminescence was recorded over a period of 5 minutes to check stability of the system. Resting ATP levels were then monitored over 30 minutes, after which 1 mM neomycin was added to the culture. Luminescence was then recorded over a period of up to 5-6 hours (see Figure 2.5).

2.7.8 Nominally Ca^{2+}-free experiments

In all nominally Ca^{2+}-free experiments, HBSS was prepared as stated in Section 2.2.1. Cultures were loaded in Fura-2 (6µM) for 45 minutes at room temperature after which they were washed three time in normal HBSS solution. Cultures were switched into nominally Ca^{2+}-free HBSS at the start of the experiment.

2.7.9 Detrmining cell permeabilisation

The permeabilisation of OHCs in reponse to 1 mM neomycin was detrmined using the DNA dye TOTO-3. This dye will label cellular DNA following permeabilsation of the cell or severe disruption of the cell membrane. TOTO-3 was added to cochlea cultures at a final concentration of 1 µM subsequent to loading with Rh123. TOTO-3 was present at 1 µM in the HBSS recording media throughout the duration of the experiment.

2.8 Selective labelling of cochlea hair cells

[N-(3-triethylammoniumpropyl)-4-(4-(dibutylamino-styryl)pyridiniumdibromide) FM1-43 is a styryl dye commonly used to study endocytosis and exocytosis in cells. Following brief (10-20 seconds) exposure to the dye hair cells can be selectively labelled due to its rapid entry at the apical surface (Gale et al., 2001).

Cultures were incubated for 20 seconds with 3μM FM1-43 in HBSS (Molecular probes, MW 611.55) and then washed immediately three times with HBSS. FM1-43 fluorescence was excited with the 488 nm line of the argon laser on the Zeiss 510 LSM confocal and emitted fluorescence collected (peak at 600 nm) using a long pass 505 filter.

2.9 Image analysis

2.9.1 Estimation of $\Delta\psi_{mt}$ using TMRM fluorescence

One hypothesis tested in this study, was whether there are differences in $\Delta\psi_{mt}$ between basal and apical hair cells and basal and apical supporting cells. In order to quantify the TMRM fluorescence, confocal images were analysed using Metamorph software. Estimates of $\Delta\psi_{mt}$ were made by analysing the intensity and staining pattern of TMRM fluorescence.

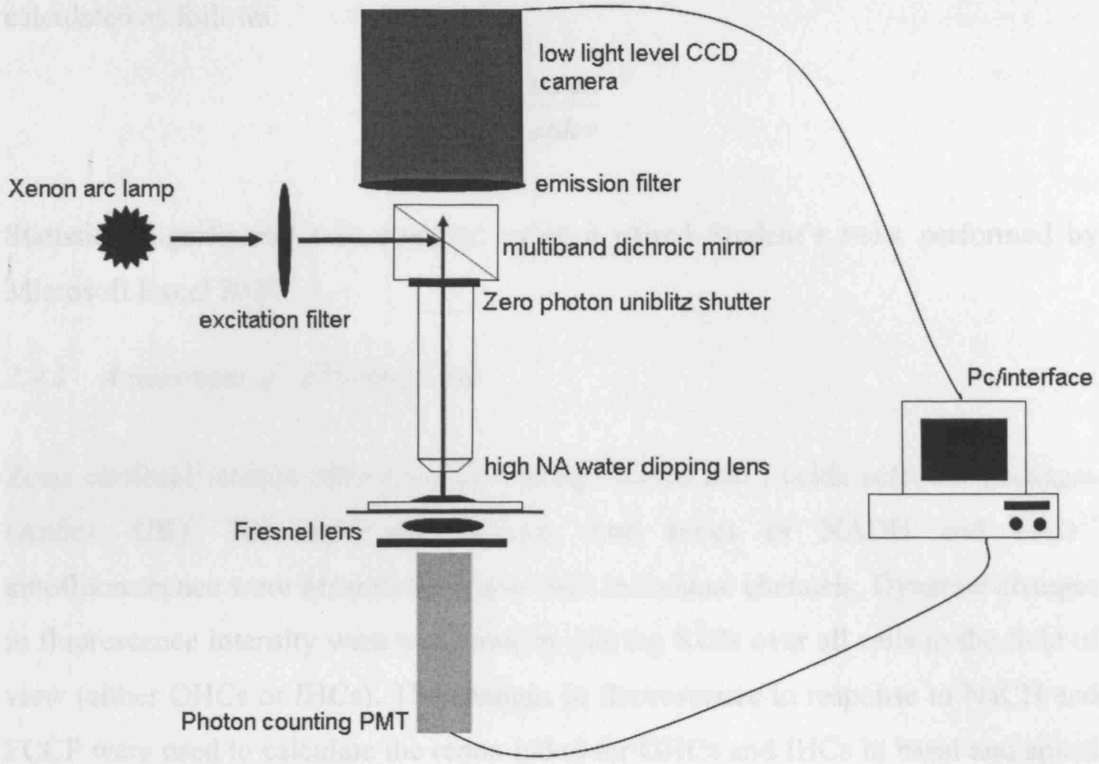

Figure 2. 5 Schematic to illustrate the principles of the fluoro-luminometer imaging system. ***Courtesy of Professor Michael R. Duchen, UCL***

The TMRM fluorescence intensity was quantified using average images of OHC and IHC regions taken from four individual focal levels (four individual z-planes) of confocal stacks through the organ of Corti. Images were then thresholded using a constant value of 350 pixels in order to reduce the inclusion of background fluorescence in the analysis protocol. Regions of interest (ROIs) were drawn around all OHCs or IHCs in the field of view and the mean fluorescence intensity measured. Intensity data were then exported to Microsoft Excel, where intensity data for each cell type and cochlear region were pooled.

The staining pattern of TMRM was determined using measurements of coefficient variation (CV) (Goldstein et al., 2000; Toescu and Verkhratsky, 2000). Lipophilic dyes exhibit a high amount of spatial heterogeneity when loaded into energised mitochondria. The level of spatial heterogeneity in basal versus apical cultures and

between different cochlear cell types was determined by calculating the spread of pixel intensity around the mean. This value was defined as the CV and was calculated as follows:

$$CV = \frac{mean}{stdev}$$

Statistical significance was assessed using a paired Student's *t*-test performed by Microsoft Excel 2000.

2.9.2 Assessment of cell redox state

Zeiss confocal images were processed using AQM6 and Lucida software packages (Andor, UK). The near simultaneous time series of NADH and FAD^{2+} autofluorescence were separated out into their individual channels. Dynamic changes in fluorescence intensity were measured by placing ROIs over all cells in the field of view (either OHCs or IHCs). The changes in fluorescence in response to NaCN and FCCP were used to calculate the redox index for OHCs and IHCs in basal and apical cultures. In order to quantify this index, autofluorescence signals were scaled as follows:

The NADH signal was scaled between 0, for maximally oxidised in the presence of FCCP and 1, for maximally reduced in the presence of NaCN. The same scaling was used for the FAD^{2+} signal, however in this case 0 corresponded to maximal reduction with NaCN and 1, to maximal oxidation by FCCP. The relative differences in signal between the states of fully oxidized and fully reduced were used to estimate the resting redox state of the cell by means of the following formula:

$$\text{Resting redox state} = \frac{\text{(baseline autofluorescence intensity – min)}}{\text{relative difference}}$$

2.9.3 Analysis of changes in cytosolic Ca^{2+} changes

The Fura-2 ratio images were processed from the raw traces. The Fura-2 ratio reflects the $[Ca^{2+}]_c$ level and changes in $[Ca^{2+}]_c$ will be seen as either an increase or

decrease in the Fura-2 ratio. Images were processed using AQM6 and Lucida software packages. In order to obtain a ratio that most accurately represents the $[Ca^{2+}]_c$ background signal associated with the camera noise floor background fluorescence must first be subtracted from each channel. For Fura-2 imaging the baseline subtractions were 69 (out of 4095 camera noise floor ~ 55) for the 340 channel and 70 for the 380 channel. For Fura-FF, the values were 65 for the 340 channel and 70 for the 380 channel.

For ATP-induced Ca^{2+} waves, changes in fluorescence intensity were measured using ratio images. The ratio change (ΔR) was obtained by placing regions of interest in the Claudius cell area (see Section 1.1). Ratio data were subsequently exported to Excel 2000 and converted to percentage change in fluorescence as follows:

$$\Delta R = ((R - R0)/R0) \times 100$$

In the above equation, ΔR is the ratio change, R is the ratio at time x and R0 the baseline ratio. The effects of CCCP + oligomycin on the Ca^{2+} signal were determined by comparing the peak ratio values (R_{max}) and duration of the Ca^{2+} signal between control and drug-treated cultures. The duration was calculated using the time taken to fall to half of R_{max} and was defined as $t_{1/2}$.

Response numbers for each ATP concentration were determined by counting the number of cells responding to a given ATP application and expressing this number as a percentage of the total number of cells in the field of view.

Changes in fluorescence intensity following mechanical damage were quantified using the same analysis protocol as that described for agonist-induced Ca^{2+} waves. The extent of wave spread and propagation velocity were measured from subtracted ratio images. Subtracted ratios were made by deducting the baseline ratio value (R0) from all sequential images in the time series.

$$R_{subtracted} = R\text{-}R0$$

The extent of wave spread was measured using line scan analysis. Lines were drawn from the site of damage to the edge of the field of view in the Claudius cell region, the outer hair cell/Deiters' cell region and the inner sulcus region. The extent of wave spread was defined as furthest point reached by the wave-front. To quantify propagation velocity, data were exported to Excel 2000 and the differential ratio (δR) for each line scan was calculated.

$$\delta R = R\text{-}R_{t+1}$$

δR_{max} corresponded to the onset of the Ca^{2+} transient so for each ROI, the time to δR_{max} was calculated. This method of analysis made it possible to measure the time at which the wave-front reached 20, 40, 60, 80 and 100 μm from the damage site in Claudius, Deiters' and inner sulcus regions. The velocity was then obtained from a plot of distance versus time using linear regression ($y=mx+c$). The velocity was equivalent to the slope of the line ($m=dx/dt$). The influence of mitochondrial Ca^{2+} buffering on the damage-induced Ca^{2+} signal was determined using the methods described previously.

2.9.4 Analysis of mitochondrial Ca^{2+} changes

Rhod-2 confocal time series were processed using AQM6 and Lucida software packages. Subtracted images were used to select ROIs, which were placed over mitochondrial compartments in Claudius cells (see Figure 2.6). The same ROIs selected using subtracted images were then superimposed onto raw data images in order to measure changes in mitochondrial Ca^{2+}. Data were exported to Excel 2000 and mitochondrial Ca^{2+} changes were expressed as percentage change in fluorescence. The duration of the mitochondrial Ca^{2+} transient was again defined as the time taken to reach 50 percent of the peak fluorescence.

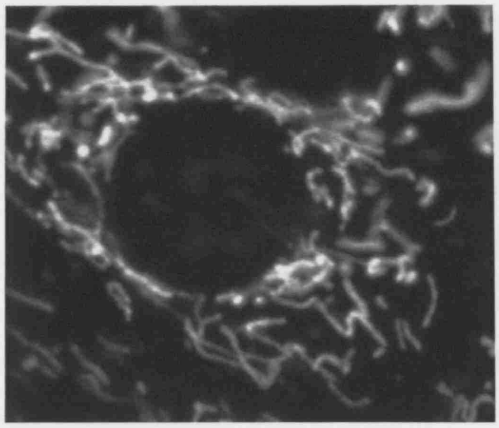

Figure 2. 6 Calcium-loaded mitochondria in a Claudius cell.

Image shows Ca^{2+} loaded mitochondria in response to application of 50 μM ATP. Mitochondrial Ca^{2+} measured using the AM ester Rhod-2. Changes in mitochondrial Ca^{2+} following extracellular ATP application or mechanical damage were determined by placing ROIs over mitochondrial compartments. The image above clearly depicts the mitochondrial compartments (bright rod structures) and cytosolic compartments (dark areas).

2.9.5 Analysis of neomycin-induced Ca^{2+} transients

Fura-2 images were converted to 340/380 ratios using Lucida software. Time series were analysed for Ca^{2+} waves originating form the outer hair cell region as a result of OHC death. Hair cell permeabilisation assumed to be death, was determined using the un-ratioed 340 and 380 signals. The criteria used to define OHC death was the coincident loss of Fura-2 fluorescence excited at 340 and 380 nm. Images were then analysed for correlation between loss of 340 fluorescence (OHC death) and the onset of a $[Ca^{2+}]_c$ wave. The times at which each correlated event occurred was noted and then subdivided into 30 minute time bins following neomycin addition. Time bins: 0-30 minutes, 30-60 minutes, 60-90 minutes, 90-120 minutes, 120-150 minutes, 150-180 minutes, 180-210 minutes and 210-240 minutes. Data were then plotted as a histogram of event frequency versus time in hours.

2.9.6 Analysis of ATP events using luciferin-luciferase

Raw data traces were analysed using Origin and Microsoft Excel software packages. Traces were smoothed in Origin using a running averaging of 10. From the smoothed traces, a running differential was calculated using the formula $n\text{-}n_{+10}$. In order to visualize events occurring above the baseline noise, the differential data were smoothed using an adjacent averaging of 4. The time at which an event occurred was noted and binned into the time domains specified in section 2.11.5. All events were again plotted as a histogram of frequency versus time and any correlation with the timing of OHC death and Ca^{2+} waves was determined.

2.9.7 Analysis of hair cell death using Rh123

Images were processed using Lucida software. ROIs were placed over OHCs in which a de-quenching of the Rh123 occurred. A de-quenching of the dye was seen as an increase in Rh123 fluorescence (see Section 2.5.1) followed by a rapid loss of fluorescence from the cell. The time at which a de-quenching event occurred was noted and used to generate a frequency histogram as described in sections 2.11.5 and 2.11.6

3 Results

3.1 Base-to-apex differences in mitochondrial function in the cochlea

3.1.1 Assessment of $\Delta\psi_{mt}$ using TMRM fluorescence

Measurement of the mitochondrial membrane potential ($\Delta\psi_{mt}$) can be used as a direct indicator of mitochondrial function. The transfer of electrons down the respiratory chain is coupled to the translocation of H^+ ions from the mitochondrial matrix into the intermembrane space. This process establishes an electrochemical gradient for protons which is expressed as a mitochondrial membrane potential. The application of lipophillic, cationic fluorescent dyes allow $\Delta\psi_{mt}$ to be monitored in live cells. It has been well documented, that basal hair cells are more susceptible than apical hair cells to noise insult (see Henderson et al., 2006), ototoxic drugs (Richardson and Russell, 1991) and aging (McFadden et al., 1999) although the precise mechanisms underlying these differences are at present unclear. It is possible that this variation results from differences in mitochondrial function between basal and apical hair cells, which could be reflected by differences in $\Delta\psi_{mt}$. In this chapter, I describe a series of experiments in which I have explored differences in mitochondrial function between cochlear cells in basal and apical turns of the cochlear explants.

The lipophillic cationic dye tetramethylrhodamine methyl ester (TMRM) was used to monitor $\Delta\psi_{mt}$. When used in re-distribution mode, TMRM fluorescence can be used to estimate the value of $\Delta\psi_{mt}$, as the fluorescence intensity is a simple function of dye concentration which in turn is a logarithmic function of potential (see Section 2.11.1). Analysis of TMRM fluorescence intensity from confocal images of P3 cochlear cultures revealed a significantly brighter fluorescence signal in apical IHCs compared to basal IHCs ($p = 0.004$, Student's paired *t*-test) (Figures 3.1, 3.2). TMRM fluorescence (measured as pixel intensities) was 587 ± 52 in basal IHCs compared to 840 ± 47 in apical IHCs. Quantification of TMRM fluorescence in basal and apical OHCs showed no significant differences ($p = 0.28$, Student's paired *t*-test) in signal (Figures 3.1, 3.2). These data indicate a difference in mitochondrial function between the base and apex of the cochlea that is specific to the IHCs. To

rule out a base-to-apex difference in mitochondrial number, cultures were stained with an antibody to beta subunit of the mitochondrial ATP-synthase. No significant differences were apparent in antibody staining between basal and apical hair cells (data not shown).

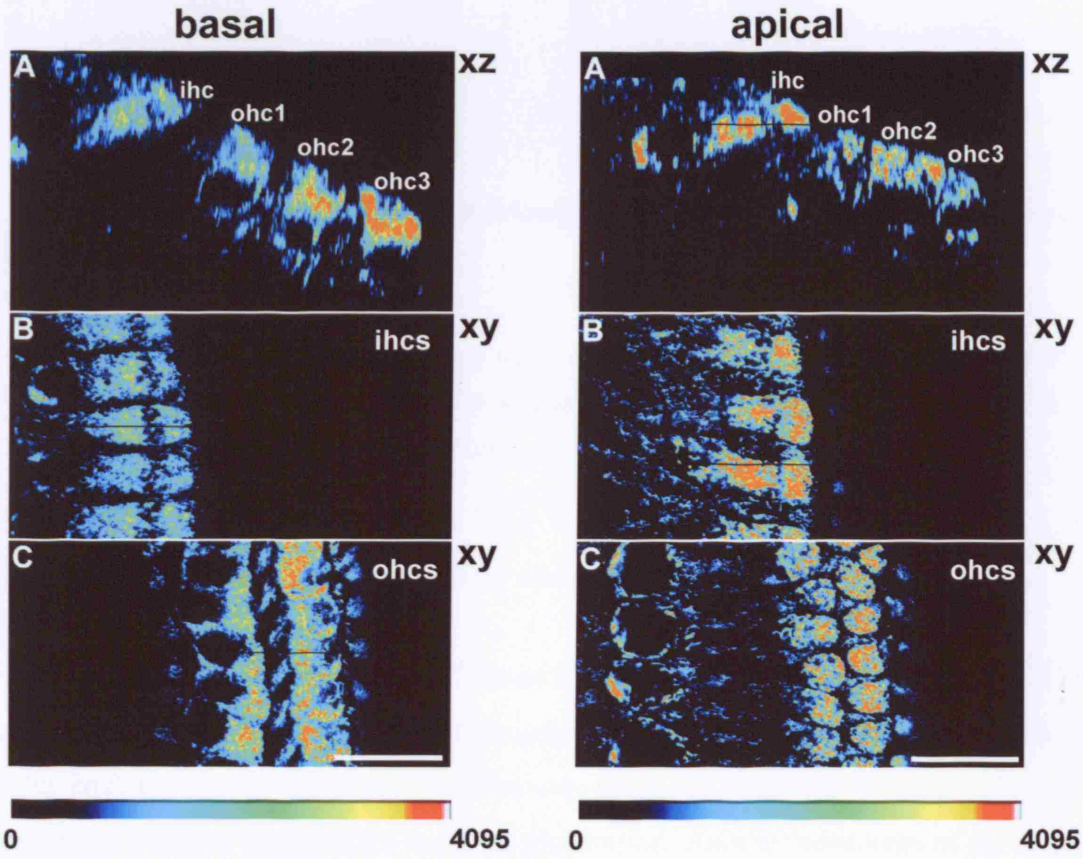

Figure 3. 1 TMRM loading in neonatal cochlear cultures.

Basal and apical cochlear explants loaded with 200 nM TMRM. Loading in inner (IHC) and outer (OHC) hair cells. Left and right panels show loading in basal and apical hair cells respectively. **(A)** Orthogonal (XZ) projections constructed from confocal stacks of basal and apical cultures with an optical section of 1 µm. Orthogonals depict the orientation of the OHCs and IHCs in the organ of Corti. **(B)** Averages of 4 z-planes from a confocal stack (effective optical section = 4 µm) , focused at the level of the IHCs. **(C)** Averages of 4 z-planes from a confocal stack, at the level of the OHCs. Images are mapped according to the look-up table displayed at the bottom of each panel. Scale bars are 20 µm.

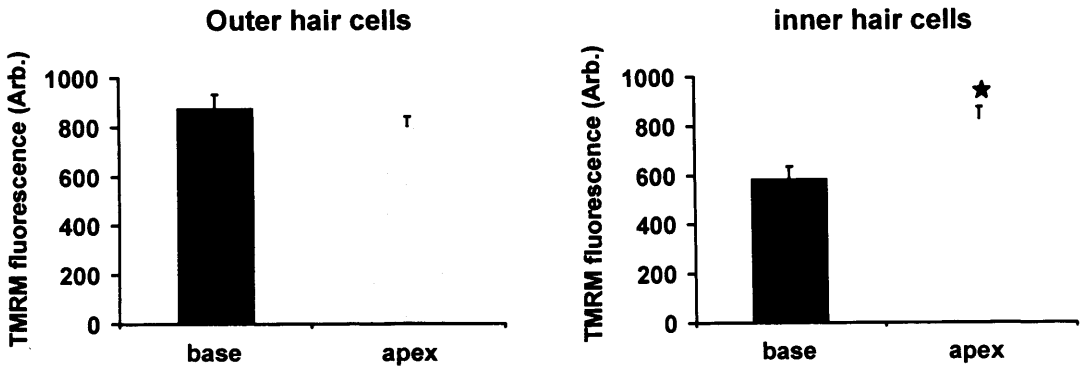

Figure 3. 2 Quantification of TMRM fluorescence reveals differences in $\Delta\psi_{mt}$ between basal and apical cochlear turns.

Charts show pooled data for OHCs and IHCs at the base and apex of the cochlea. For OHCs, data are mean ± SEM from 7 experiments, p = 0.28, Student's paired *t*-test. For IHCs, data are mean ± SEM from 7 cultures, p = 0.004, Student's paired *t*-test.

3.1.2 Measurement of $\Delta\psi_{mt}$ in cochlear slices

Having identified a base-to-apex difference in TMRM signal and thus $\Delta\psi_{mt}$ in IHCs of the explant culture model, TMRM fluorescence intensities were also investigated in the cochlear slice preparation. The slice was chosen as it permits the study of basal and apical cochlear turns within the same preparation. Another advantage of the slice preparation is that unlike the culture model, it allows one to study the physiology of cochlear cells in older animals. Initially, attempts were thus made to measure mitochondrial function in slices from young animals (P2), with the aim of later using these techniques in hearing animals (P12). The TMRM loading in P2 cochlear slices was strikingly different to that observed in explant cultures. Loading in the IHCs was difficult to detect with the same microscope settings as those used for imaging in cochlear explants. In contrast to the culture model, the TMRM signal was much brighter in the supporting cells compared to the hair cells (Figure 3.3). Although attempts were made to obtain tissue from P12 animals, samples were often too damaged from the slicing process to obtain accurate measurements of $\Delta\psi_{mt}$.

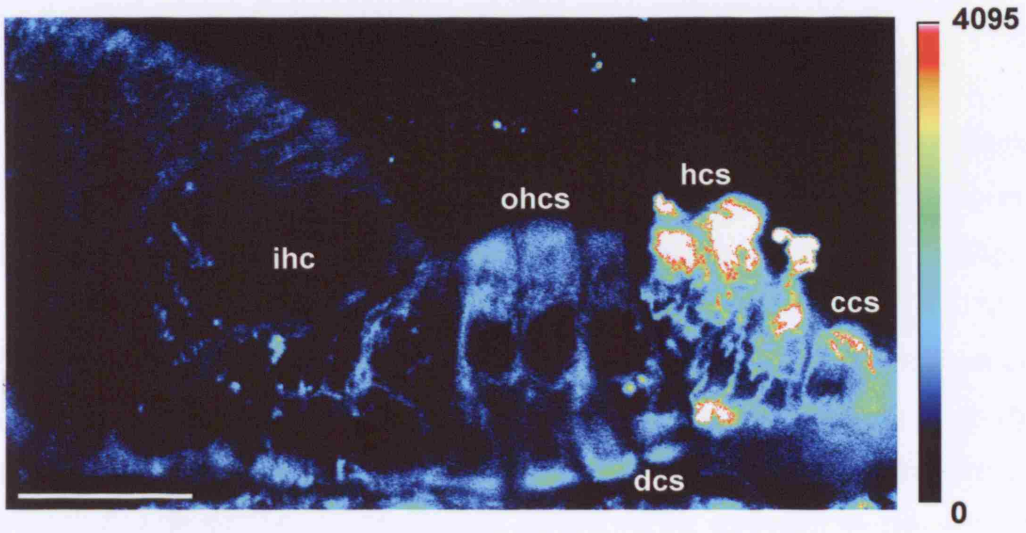

Figure 3. 3 TMRM loading in the cochlear slice preparation.

Image shows a transverse section through the apical turn of the organ of Corti at post-natal day 2 (P2). The slice is loaded with 200 nM TMRM. Image is an average of 3 z-planes from a confocal stack, focused 25 µm below the cut surface. **IHCs** – inner hair cell, **OHCs** – outer hair cells, **dcs** – Deiters' cells, **hcs** – Hensen's cells, **ccs** – Claudius cells. Scale bar is 50 µm. Image is mapped according to the scale indicated on the right

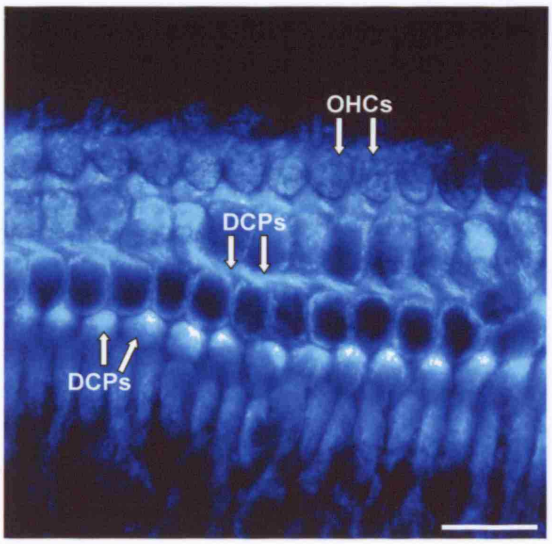

Figure 3. 4 NADH fluorescence in the cochlea.

Image shows the NADH autofluorescence (excited at 351 nm) in cochlear cells of a P3 explant culture. **OHCs** – outer hair cells, **DCPs**- Deiters' cell processes. Scale bar is 20 µm.

3.1.3 *Assessment of mitochondrial function using endogenous NADH and (flavoprotein) FAD^{2+} autofluorescence*

As the differences in $\Delta\psi_{mt}$ could be due to a number of mechanisms I sought an alternative measure of mitochondrial function both to confirm these differences and to understand the underlying mechanisms for this variation. The endogenous autofluorescence from reduced nicotinamide adenine dinucleotide (NADH) and flavoproteins (FAD^{2+}) can be used as an indicator of mitochondrial metabolism. As described in Section 1.3.3, these are electron donors, whose function is to shuttle electrons produced during the citric acid cycle into the electron transfer chain. Modulations in the redox state of either compound are conveyed by changes in their fluorescent properties.

NADH is fluorescent when reduced and non-fluorescent when it becomes oxidized to NAD^+. In contrast, flavoproteins are fluorescent in their oxidized form, FAD^{2+} and non-fluorescent when reduced to $FADH_2$. Further, their spectral properties are quite distinct, with both excitation and emission spectra separated by ~ 100 nm thus allowing them to be measured sequentially and independently on the UV confocal microscope. Using the autofluorescence of these two compounds, mitochondrial function in OHCs, IHCs and Deiters' cells was compared between basal and apical cultures. It was first necessary to establish the dynamic range of the signal in order to interpret the resting level in terms of redox activity.

To this end, NaCN (3 mM), which blocks respiration at complex IV and drives the mitochondria to a maximally reduced state was applied. Under such conditions, the NADH is no longer oxidized by the electron transfer chain, generating a maximally fluorescent signal. NaCN is subsequently washed out and FCCP (5 μm) applied to generate a maximally oxidized signal. FCCP stimulates maximal respiration, which leads to a maximal rate of oxidation of reduced NADH. The fluorescent signals were normalised between 100% for maximally reduced and 0% for maximally oxidized, giving a redox index for the resting redox state.

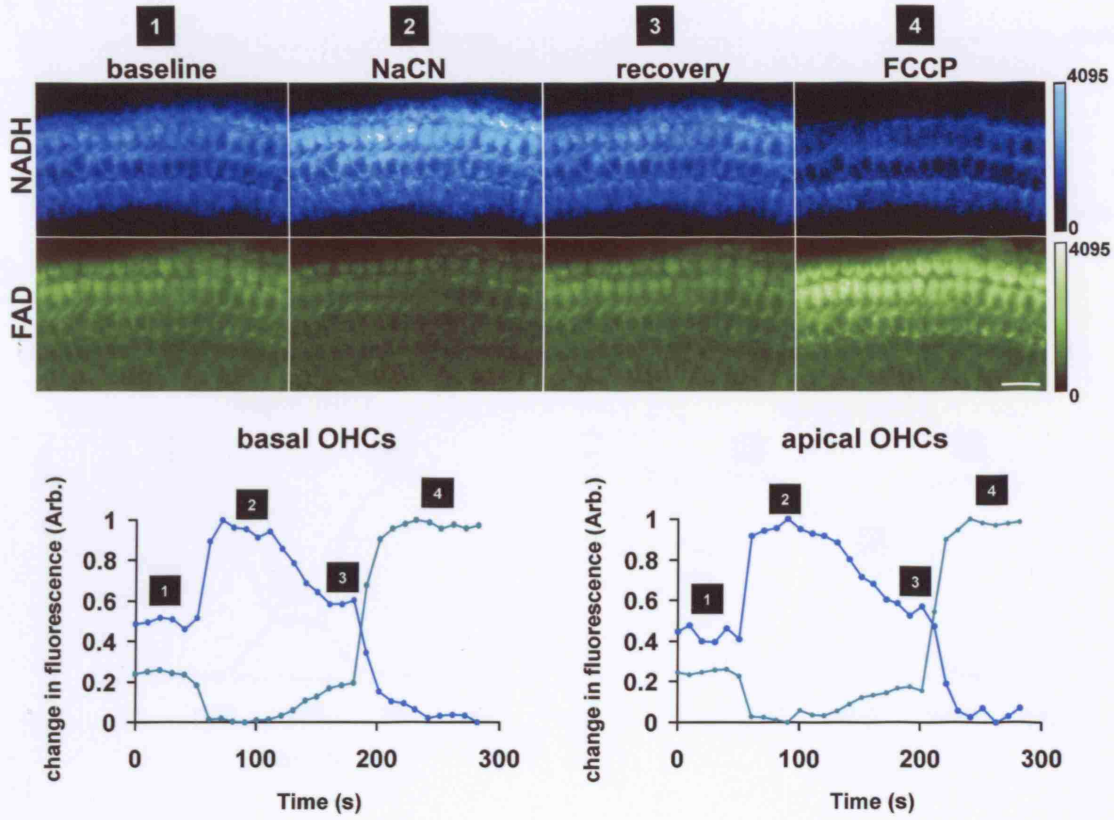

Figure 3. 5 Dynamic changes in NADH and FAD^{2+} autofluorescence measured in OHCs and Deiters' cells.

Top panel, image stills indicating the changes in NADH (blue) and FAD^{2+} (green) autofluorescence in response to the metabolic inhibitors NaCN (2) and FCCP (4). Images are presented 4 frame averages from successive points in a confocal time series and are focused at the level of the OHCs. At this focal plane, the Deiters' cells are represented by the phalangeal processes. Images are mapped according to the scales indicated right. Scale bar is 20 µm.

Bottom panel, traces recorded from basal (left) and apical (right) OHCs, showing changes in NADH (blue) and FAD^{2+} (green) autofluorescence with NaCN and FCCP. **Stage 1**: resting redox state estimated for the cell, **stage 2**: maximal reduction due to NaCN, **stage 3**: recovery phase, **stage 4**: maximal oxidation due to FCCP.

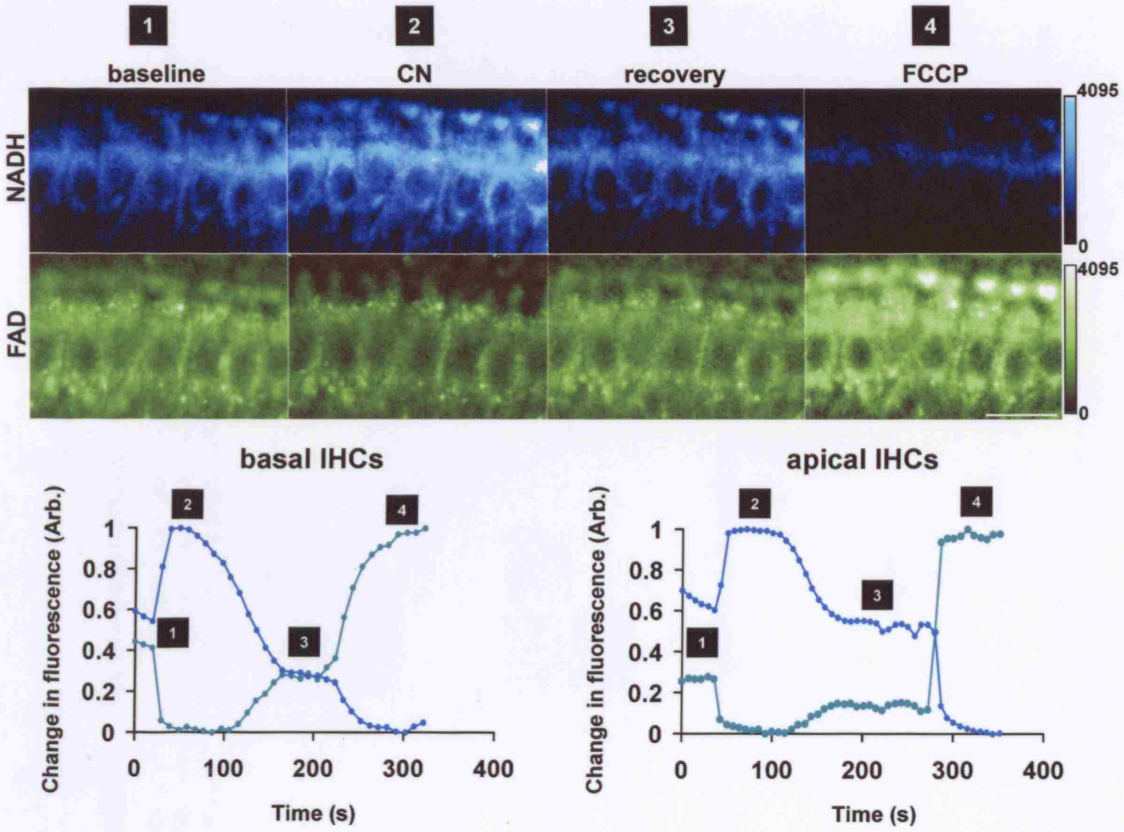

Figure 3. 6 Dynamic changes in NADH and FAD^{2+} autofluorescence measured in IHCs

Top panel, image sequence indicating the changes in NADH (blue) and FAD^{2+} (green) autofluorescence in response to the metabolic inhibitors NaCN (2) and FCCP (4). Confocal images taken from a time series focused at the level of the IHCs. Images are mapped according to the scales indicated right. Scale bar is 20 µm.

Bottom panel, traces recorded from basal (left) and apical (right) IHCs, showing changes in NADH (blue) and FAD^{2+} (green) autofluorescence with NaCN and FCCP. **Stage 1**: resting redox state estimated for the cell, **stage 2**: maximal reduction due to NaCN, **stage 3**: recovery phase, **stage 4**: maximal oxidation due to FCCP.

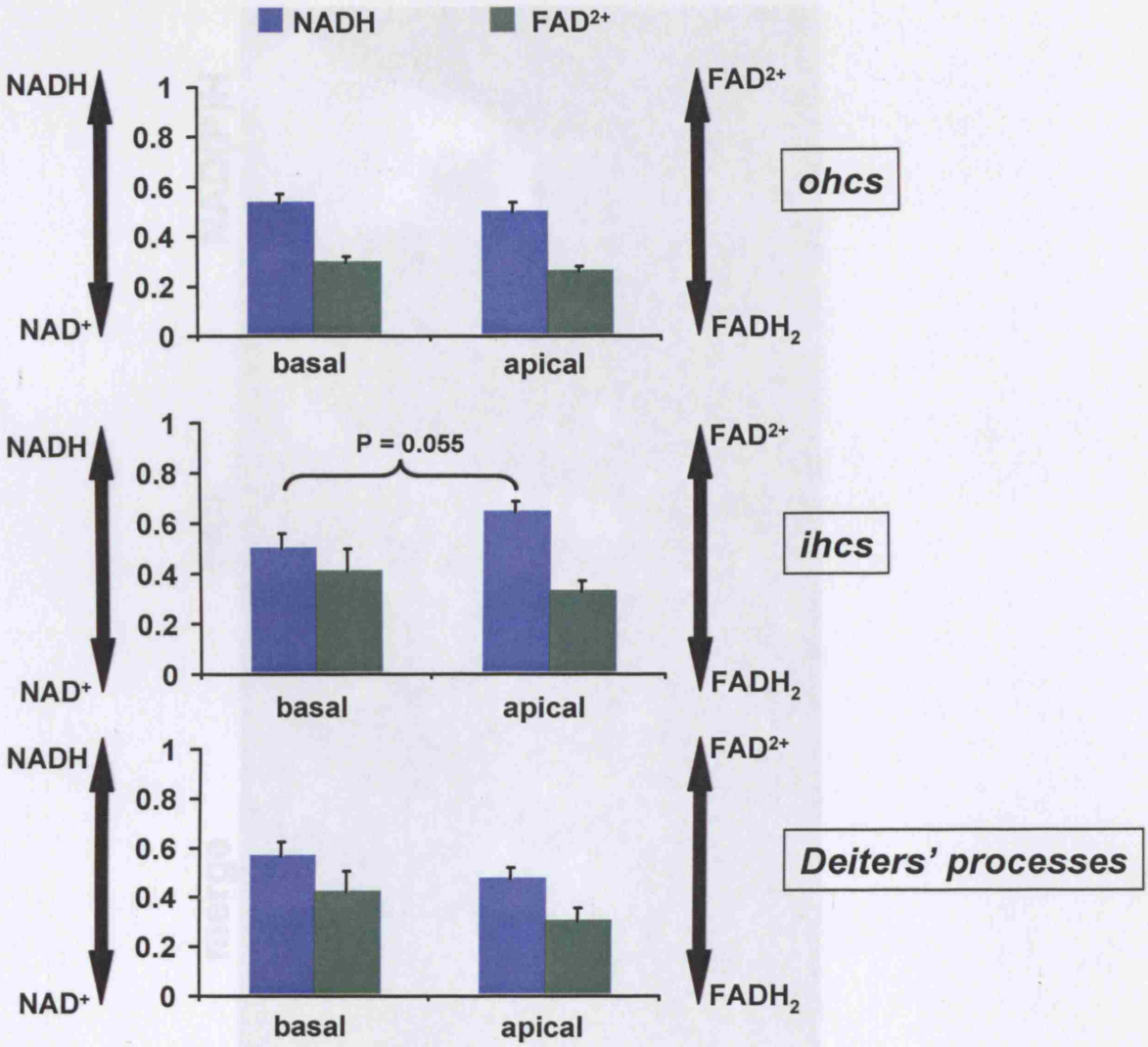

Figure 3. 7 Estimated redox index for cochlear hair cells and Deiters' processes.

The redox indices (indicated by the black arrows) of NADH (blue bars) and FAD^{2+} (green bars) between basal and apical OHCs, IHCs and Deiters' processes. Data are presented as mean ± SEM from 12, 8, 9 and 6, 6, 5 experiments in basal and apical OHCs, IHCs and Deiters' processes respectively. For NADH redox between base and apex: p = 0.48, 0.055 and 0.20 for OHCs, IHCs and Deiters' processes respectively. For FAD^{2+} redox index between base and apex: p = 0.24, 0.5 and 0.4 for OHCs, IHCs and Deiters' processes respectively. Data for OHCs and Deiters' processes were from the same time series.

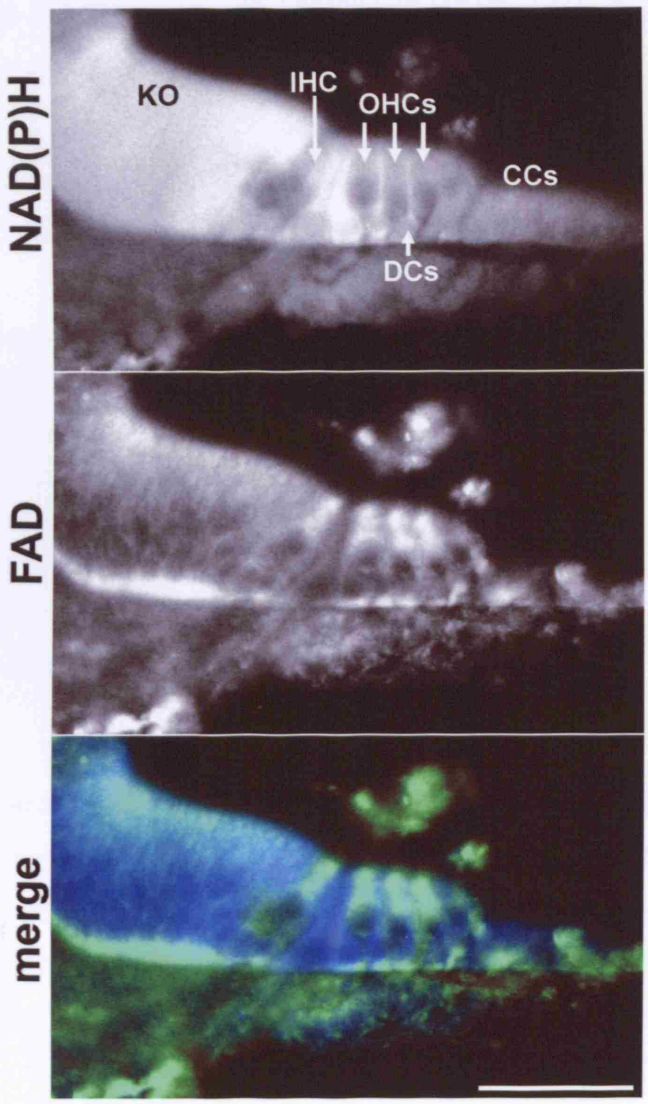

Figure 3. 8 NAD(P)H and FAD^{2+} autofluorescence in the cochlear slice preparation.

Images depict the NAD(P)H and FAD2+ autofluorescence intensities in a P2 cochlear slice. Top panel, NAD(P)H autofluorescence, middle panel FAD^{2+} autofluorescence and bottom panel the composite image of both signals where NAD(P)H is blue and FAD^{2+} is green. Images are taken 20-25 µm below the cut surface. KO – Kolliker's organ, OHCs – outer hair cells, IHC – inner hair cell, DCs – Deiters' cells and CCs – Claudius cells. Scale bar is 50 µm.

The same assay was used for flavoproteins although in this case, NaCN will give 0% and FCCP 100%. For each cell type, the baseline fluorescence of NADH and FAD^{2+} were calculated as a percentage of the response to NaCN (100% NADH, 0% FAD^{2+}) and FCCP (0% NADH and 100% FAD^{2+}) (Duchen and Biscoe, 1992; Duchen et al., 2003). I will refer to this value as the resting redox state or redox index of the cell

(Figures 3.5, 3.6 & 3.7). A consistent observation throughout these experiments was that the NADH signal in Deiters' cells appeared brighter than that in the OHCs (Figures 3.4 & 3.5). In addition, responses of NADH and FAD^{2+} autofluorescence to NaCN and FCCP in Deiters' cell processes were less than those occurring in the hair cells (Figure 3.5 **(stages 2 & 4)).**

Table 3 Comparison of resting redox states between basal and apical cochlear cells types

Cell type	NADH	FAD^{2+}
basal OHCs	53 ± 3%	29 ± 2%
apical OHCs	49 ± 3%	26 ± 1%
basal IHCs	50 ± 5%	41 ± 8%
apical IHCs	65 ± 4%	35 ± 3%
basal Deiters' cells	57 ± 5%	43 ± 4%
apical Deiters' cells	47 ± 5%	31± 5%

Another observation was that in OHCs and IHCs, FAD^{2+} autofluorescence changed by a greater amount in response to FCCP than with NaCN (Figures 3.5 & 3.6) suggesting the cells to be more reduced at rest. The resting redox states for OHCs, IHCs and Deiters' cells are shown in Table 3 and Figure 3.9. There were no significant differences between base and apex in any of the three cell types (see Figure 3.7).

3.1.4 Resting redox state in cochlear slices

NADH and FAD^{2+} autofluorescence were used to investigate mitochondrial function in cochlear slices from 2 day old rats. In agreement with data from P3 cultures, confocal images taken from 5 separate slices (from 2 animals) suggest NADH autofluorescence to be brighter in Deiters' processes compared to hair cells (Figure 3.10). A bright NADH signal was also observed in cells of the Kölliker's organ (Figure 3.8). In contrast to the explant culture model however, images showed a brighter flavoprotein signal in IHCs and OHCs compared to supporting cells (Figure 3.8).

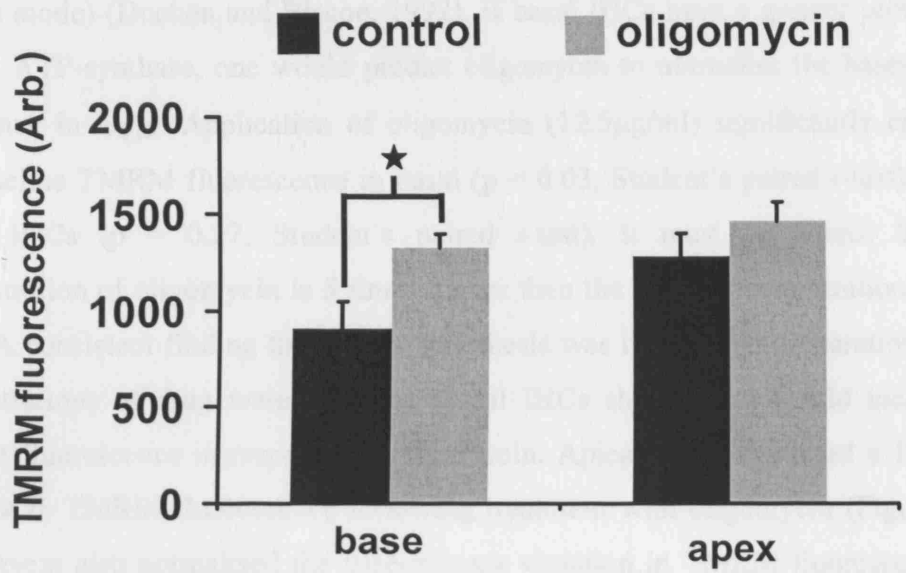

Figure 3. 9 Oligomycin hyperpolarises $\Delta\psi_{mt}$ in basal and apical IHCs.
Black bars: fluorescence intensity of TMRM loaded IHCs from basal and apical cultures under control conditions. **Grey bars**: effects of oligomycin on TMRM fluorescence intensity of basal and apical IHCs. Data are mean ± SEM from 6 cultures. p = 0.03 for basal IHCs and 0.27 for apical IHCs, Students' paired *t*-test.

3.1.5 Effects of oligomycin of $\Delta\psi_{mt}$

The more depolarised $\Delta\psi_{mt}$ (Section 3.1.1) and oxidised NADH (Section 3.1.3) in basal IHCs could be due to an increased ATP turnover and greater proton leak via the ATP-synthase. To investigate this hypothesis, I treated basal and apical IHCs with oligomycin and recorded the changes in $\Delta\psi_{mt}$ (using TMRM in redistribution mode) with time. Oligomycin is an antibiotic which acts by blocking the proton channel of the mitochondrial ATP-synthase, preventing the proton leak through it and consequently suppressing the respiration (state III respiration) required to balance it. Oligomycin has no effect has no direct effect on the mitochondrial electron transfer chain. In most cells oligomycin causes hyperpolarisation of $\Delta\psi_{mt}$ which in turn will impair respiration resulting in reduced activity of the electron transfer chain (Nicholls, 1982).

Oligomycin has been shown to cause hyperpolarisation of $\Delta\psi_{mt}$, represented by an decrease in Rh123 fluorescence (as in these experiments the dye was used in de-

quench mode) (Duchen and Biscoe, 1992). If basal IHCs have a greater proton leak via the ATP-synthase, one would predict oligomycin to normalise the base-to-apex difference in $\Delta\psi_{mt}$. Application of oligomycin (12.5µg/ml) significantly enhanced the baseline TMRM fluorescence in basal ($p = 0.03$, Student's paired *t*-test) but not apical IHCs ($p = 0.27$, Student's paired *t*-test). It must be noted, that this concentration of oligomycin is 5 times higher then the normal concentration used *in vitro*. A consistent finding throughout this thesis was that in this preparation higher concentrations of drug were required. Basal IHCs showed a 1.4 fold increase in TMRM fluorescence in response to oligomycin. Apical IHCs displayed a 1.13 fold increase in TMRM fluorescence following treatment with oligomycin (Figure 3.9). Oligomycin also normalised the base-to-apex variation in TMRM fluorescence and thus $\Delta\psi_{mt}$ (Figure 3.9). The p values calculated for basal verses apical TMRM fluorescence in IHCs were 0.06 and 0.3 (Student's paired *t*-test) for controls and oligomycin treated cultures.

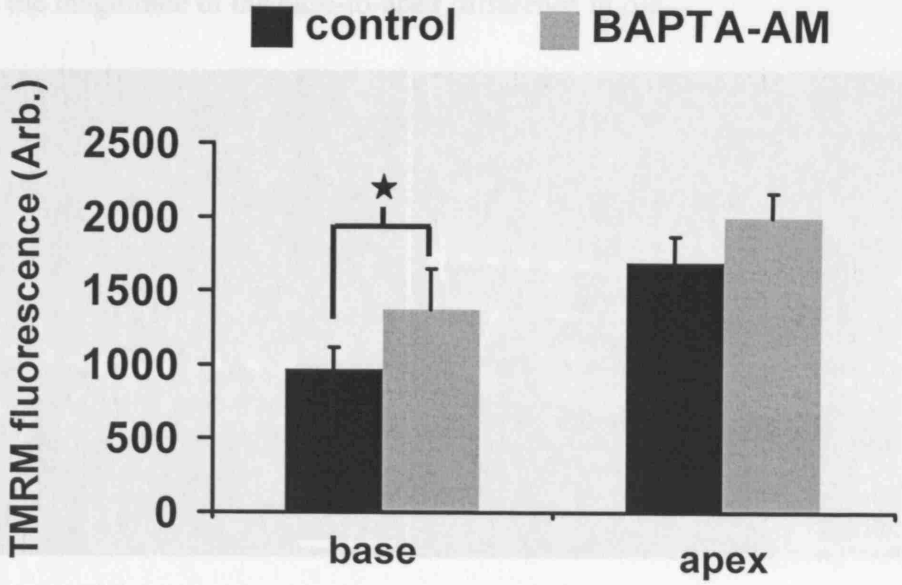

Figure 3. 10 BAPTA-AM causes hyperpolarisation of $\Delta\psi_{mt}$ in basal and apical IHCs.

Black bars: fluorescence intensity of TMRM loaded IHCs from basal and apical cultures under control conditions. **Grey bars**: effects of BAPTA-AM (50 µM) on TMRM fluorescence intensity of basal and apical IHCs. Data are mean ± SEM from 7 cultures. p = 0.03 for basal IHCs and 0.1 for apical IHCs, Students' paired *t*-test.

3.1.6 *BAPTA-AM causes hyperpolarisation of $\Delta\psi_{mt}$ in cochlear IHCs*

In addition to an increased proton leak via the mitochondrial ATP-synthase, the less polarised $\Delta\psi_{mt}$ in IHCs could result from a greater rate of Ca^{2+} cycling across the mitochondrial membrane at rest. If basal IHCs had higher resting $[Ca^{2+}]_c$ levels, it is possible that mitochondria in these cells would take up a greater amount of Ca^{2+} at rest compared to those in apical IHCs. As uptake of Ca^{2+} into mitochondria results in depolarisation of $\Delta\psi_{mt}$ (Nicholls, 1982) an increased basal Ca^{2+} load may contribute to the base-to-apex difference in TMRM fluorescence. To test this hypothesis, I treated cultures with the membrane permeant Ca^{2+} chelator BAPTA-AM and monitored the changes in TMRM fluorescence. Following application of BAPTA-AM (50 μM) TMRM fluorescence increased by 1.4 fold and 1.18 fold in basal and apical IHCs respectively (Figure 3.10). Similarly to oligomycin, treatment with BAPTA-AM significantly enhanced basal ($p = 0.03$, Student's paired *t*-test) but not apical ($p = 0.1$, Student's paired *t*-test) TMRM fluorescence. BAPTA-AM also reduced the magnitude of the base-to-apex difference in $\Delta\psi_{mt}$.

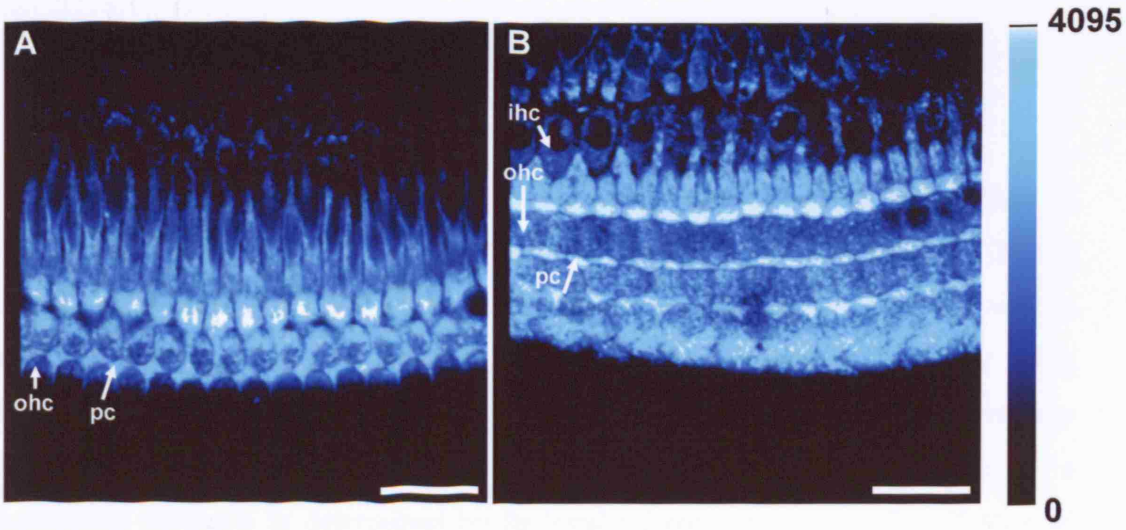

Figure 3. 11 Two-photon image of NAD(P)H intensity measured in a P3 cochlear culture.

Images show the NAD(P)H autofluorescence intensity as excited with 720 nm at two focal planes: (A) close to the surface showing the first row of OHCs and (B) deeper into the tissue showing the base of OHC and 3 rows of OHC bodies. Autofluorescence intensity is mapped according to the look up table shown right. ohc – outer hair cells, pc – phalangeal cell, IHCs – inner hair cell. Scale bar is 20 μm.

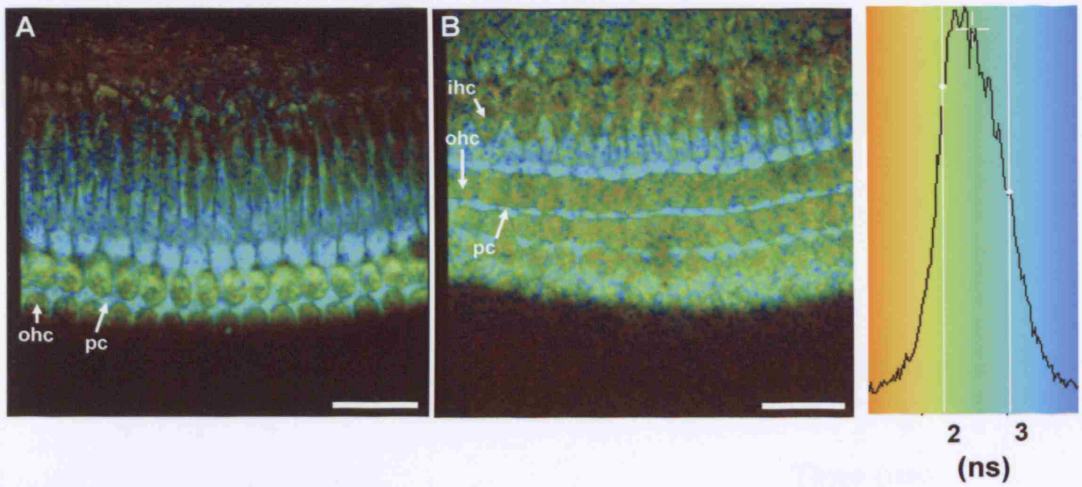

Figure 3. 12 Longer NADH lifetimes evident in cochlear supporting cells

Images show the fluorescence lifetimes of NAD(P)H at two focal planes: **(A)** close to the tissue surface showing the first row of OHCs **(B)** deeper into the tissue showing the OHC base and 3 rows of OHC bodies. Lifetime durations are colour coded (short lifetimes: more green, longer lifetimes: more blue) and scaled as a function of tau 2 (right). Lifetimes are determined from the fluorescent decay of each pixel in the NAD(P)H intensity image (Figure 3.11). Scale bar is 20 µm.

3.1.7 Assessment of mitochondrial metabolism using NAD(P)H lifetime measurements

As described previously (Section 3.1.3), there were clear differences in total NADH autofluorescence between hair cells and supporting cells. Experiments with NaCN and FCCP however did not reveal the reason for these differences. Another way in which to study the properties of NAD(P)H and thus tissue metabolism, is by using the decay of its fluorescence signal. Lifetime imaging is a technique which exploits the inherent variations in the fluorescence decay of a fluorophore. The lifetime of a fluorescent molecule is determined by its local microenvironment. The lifetime of NAD(P)H varies in accordance with its conformational state (Lakowicz et al., 1992). Immobilised NAD(P)H displays a slow fluorescence decay or long lifetime (~1.8 ns) and free cytosolic NAD(P)H, a fast fluorescence decay or short lifetime (~0.4 ns) (Blinova et al., 2005). This is likely due to fewer molecular collisions occurring in the bound conformation, allowing the molecule to retain its energy for longer. For a detailed description of the lifetime imaging system please see Section 2.6.2.

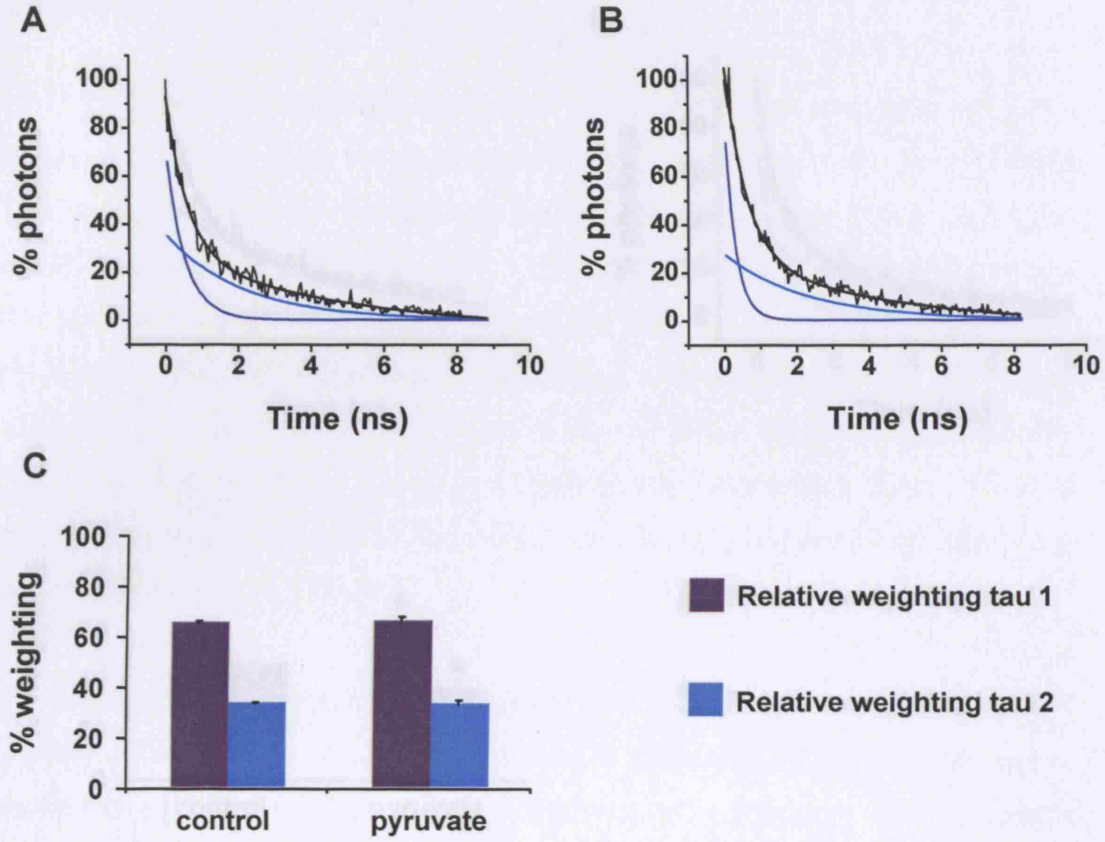

Figure 3. 13 NAD(P) lifetimes measurements for the outer hair cells

(A) Exponential fits to lifetime data from OHCs. Trace shows the raw lifetime data (black trace) and the exponential fits for the two NAD(P)H lifetimes, $\tau 1$ (dark blue) and $\tau 2$ (light blue).

(B) Exponential fits for NAD(P)H lifetime data measured from OHCs following treatment with 10 mM pyruvate. Trace shows the raw lifetime data (black trace) and the exponential decays for $\tau 1$ (dark blue) and $\tau 2$ (light blue).

(C) Relative weighting of the two lifetimes in control and pyruvate treated cultures. The percent weighting of $\tau 1$ and $\tau 2$ are depicted by the dark blue and light blue bars respectively.

Data are mean ± SEM from 4 cultures. p = 0.64 for $\tau 1$ weighting and 0.73 for $\tau 2$ weighting, Students' paired *t*-Test.

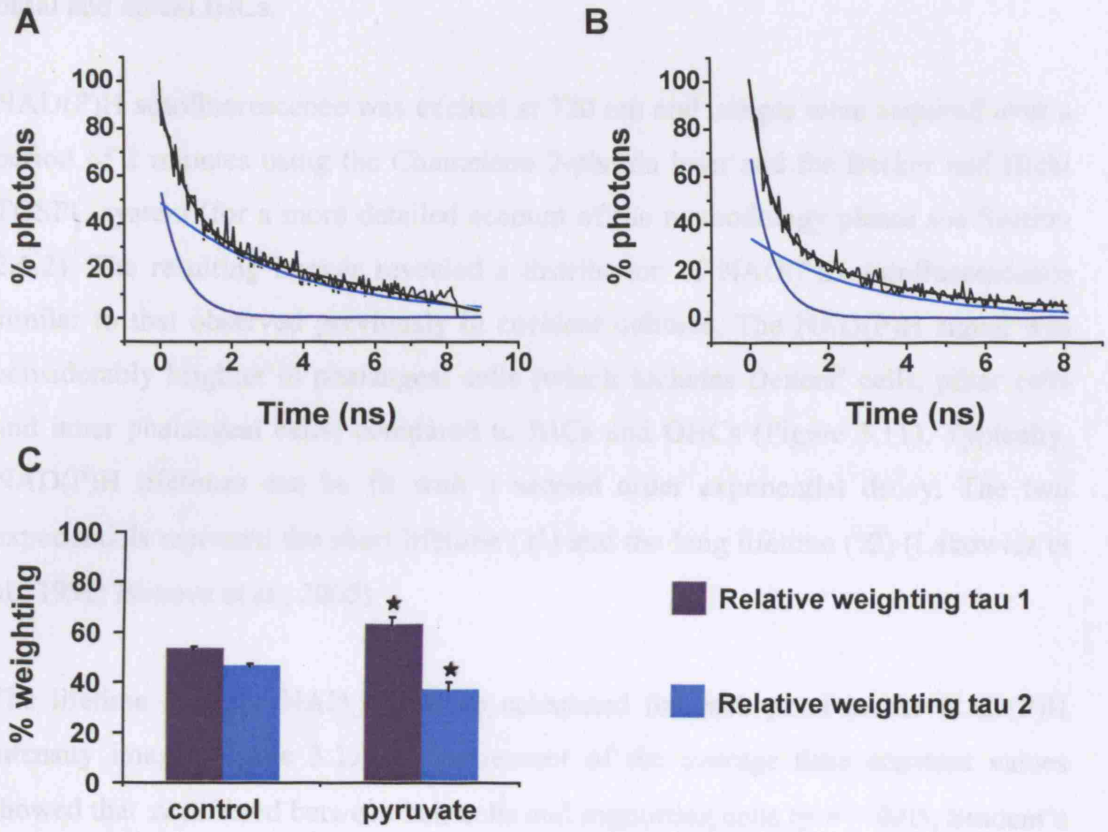

Figure 3. 14 NAD(P) lifetimes measurements for the phalangeal cells

(A) Exponential fits to lifetime data for phalangeal cells. Trace shows the raw lifetime data (black trace) and the exponential fits for the two NAD(P)H lifetimes, $\tau 1$ (dark blue) and $\tau 2$ (light blue).

(B) Exponential fits for NAD(P)H lifetime data measured from phalangeal cells following treatment with 10 mM pyruvate. Trace shows the raw lifetime data (black trace) and the exponential decays for $\tau 1$ (dark blue) and $\tau 2$ (light blue).

(C) Relative weighting of the two lifetimes in control and pyruvate treated cultures. The percent weighting of $\tau 1$ and $\tau 2$ are depicted by the dark blue and light blue bars respectively.

Data are mean ± SEM form 4 cultures. p = 0.01^-12 for $\tau 1$ weighting and 0.05^-12 for $\tau 2$ weighting, Students' paired *t*-Test.

It has been shown in various tissues, that the immobilised NAD(P)H in the cytosol dominates the total fluorescence of the signal (Eng et al., 1989; Blinova et al., 2005). The aim of this experiment was to determine the source of the NADH signal in supporting cells and hair cells (i.e does it originate from mitochondrial or cytosolic

NAD(P)H pools) in attempt to understand the differences in signal intensity between basal and apical IHCs.

NAD(P)H autofluorescence was excited at 720 nm and images were acquired over a period of 2 minutes using the Chameleon 2-photon laser and the Becker and Hickl TCSPC system (for a more detailed account of the methodology please see Section 2.6.2). The resulting images revealed a distribution of NAD(P)H autofluorescence similar to that observed previously in cochlear cultures. The NAD(P)H signal was considerably brighter in phalangeal cells (which includes Deiters' cells, pillar cells and inner phalangeal cells) compared to IHCs and OHCs (Figure 3.11). Typically, NAD(P)H lifetimes can be fit with a second order exponential decay. The two exponentials represent the short lifetime ($\tau 1$) and the long lifetime ($\tau 2$) (Lakowicz et al., 1992; Blinova et al., 2005).

The lifetime data for NAD(P)H were calculated for each pixel in the NAD(P)H intensity image (Figure 3.12). Measurement of the average time constant values showed that $\tau 2$ differed between hair cells and supporting cells ($p = < 0.05$, Student's paired *t*-test). The time constant for $\tau 2$, corresponding to immobilised NAD(P)H was significantly longer in phalangeal cells compared to OHCs (Figure 3.13 & 3.14). In the OHCs, $\tau 1$ was 0.47 ± 0.04 ns and $\tau 2$ 2.5 ± 0.02 ns. In phalangeal cells $\tau 1$ was 0.46 ± 0.02 ns and $\tau 2$ 3 ± 0.02 ns. Differences between hair cells and supporting cells were also evident in the relative weighting of the two NAD(P)H lifetimes (Figures 3.13 & 3.14).

In phalangeal cells, a greater proportion of NAD(P)H seemed to be in the immobilised form ($\tau 2$), indicated by a greater percentage weighting for $\tau 2$. The lifetime weightings were 67 ± 0.4 % $\tau 1$ and 33 ± 0.4 % $\tau 2$ compared to 53 ± 0.7 % $\tau 1$ and 47 ± 0.6 % $\tau 2$ in hair cells and phalangeal cells respectively. This finding suggests supporting cells to have a greater proportion of cytosolic NAD(P)H compared to OHCs.

3.1.8 Pyruvate alters the relative weighting of NAD(P)H lifetimes in phalangeal cells

Pyruvate is a metabolic substrate that can influence both cytosolic and mitochondrial redox states therefore changing the fluorescence signal in each compartment. I investigated the effects of pyruvate on the NAD(P)H lifetime signals in OHCs and supporting cells in attempt to discern the relative contributions of cytosolic and mitochondrial NAD(P)H pools to the overall fluorescence signal. Pyruvate causes oxidation of the cytosolic NAD(P)H pool and reduction of the mitochondrial NADH pool (Scholz et al., 1995; Dumollard et al., 2007). In OHCs, pyruvate had no significant effect on the relative lifetime weighting, whereas in phalangeal cells it caused a shift in the lifetime weighting to one more closely resembling that seen in OHCs.

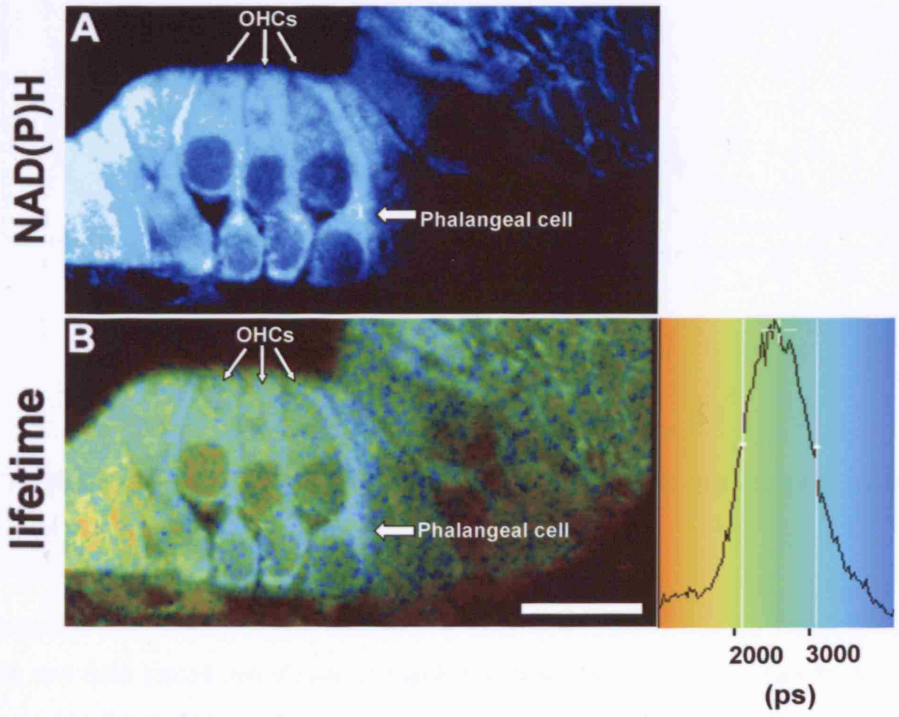

Figure 3. 15 NAD(P)H fluorescence lifetime image taken from a cochlear slice

(A) NAD(P)H intensity image recorded at 720 nm excitation. Image is from a single focal plane 20 µm below the cut surface.**(B)** NAD(P)H lifetime image generated from the intensity data shown in **(A).** Lifetime data in ns are colour-coded according to the scale shown right. Scale bar is 20 µm.

This suggests that in phalangeal cells, pyruvate significantly reduces the relative contribution of immobilised cytosolic NAD(P)H to the overall signal. The weighting in control OHCs was 67 ± 0.4 % τ1 verses 33 ± 0.4 % τ2 whereas in pyruvate treated cultures weightings were 66 ± 0.02 % τ1 verses 34 ± 0.01 % τ2 (Figures 3.13 & 3.14). In phalangeal cells the lifetime weightings were 53 ± 0.7 % τ1 verses 47 ± 0.6 % τ2 in controls and 63 ± 0.6 % τ1 verses 37 ± 0.6 % τ2 following treatment with 10 mM pyruvate (Figures 3.13 & 3.14).

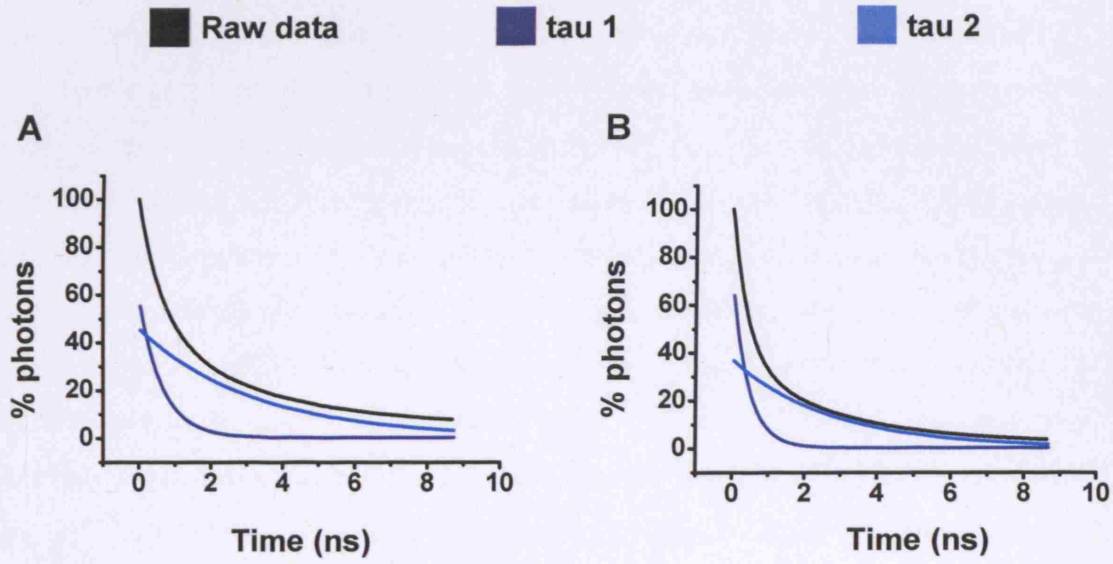

Figure 3. 16 Comparison of NAD(P)H lifetime data between phalangeal cells and OHCs in the cochlear slice preparation

(A) Exponential fits for phalangeal cell lifetime data. **(B)** Exponential fits for OHC lifetime data. The raw data traces are shown in black, the time course of τ1 in dark blue and the time course for τ2 in light blue. Data are representative of 3 slices.

3.1.9 NAD(P)H lifetime imaging in cochlear slices

As described in section 3.1.6, NAD(P)H lifetime were used to assess metabolic differences between the supporting cells and hair cells in the slice preparation. Similar to the explant cultures, in P2 cochlear slices the phalangeal cells had a

brighter NAD(P)H signal compared to the OHCs (Figure 3.15). Lifetime data recorded in the slice preparation were also consistent with that from cultures in that the phalangeal cells have a greater proportion of their NAD(P)H in the long lifetime (immobilised) form (Figure 3.16). Phalangeal cells displayed an average weighting of 56.6% for $t1$ and 43.3 % $t2$ whereas OHCs had a weighting of 68.5% $t1$ and 31.5% $t2$ (Figure 3.16). In agreement with data from explant cultures, differences were also evident in the duration of the longer lifetime between OHCs and phalangeal cells. Phalangeal cells displayed an average $t2$ of 3.1 ns compared to a $t2$ of 2.5 ns in OHCs (Figure 3.16).

3.2 Discussion

In this chapter, I have investigated differences in mitochondrial physiology in various cochlear cell types and have addressed the following questions. 1) Does mitochondrial function vary between basal and apical hair cells or between inner and outer hair cells? 2) Are there any base-to-apex or cell-specific differences in intermediary metabolism in the cochlea? There is substantial evidence implicating mitochondria as key regulators of cellular physiology and pathophysiology. Alongside their predominant role of ATP production, they contribute significantly to $[Ca^{2+}]_c$ homeostasis and signalling (see Section 3.3), oxygen sensing, steroid biosynthesis and the regulation of cell life and cell death. The mitochondrial membrane potential ($\Delta\psi_{mt}$) lies at the heart of most mitochondrial-linked processes and can be monitored using fluorescent probes. In this study, $\Delta\psi_{mt}$ was assessed in different cochlear cell types using the lipophillic cation TMRM. This dye is known to accumulate preferentially into functional mitochondria, in response to their highly negative membrane potential (150-200 mV negative with respect to the cell cytosol) (Johnson et al., 1981). It is assumed, that the fluorescence intensity of the dye corresponds to the activity of the mitochondria. Probes such as this one have been extensively used in a number of cell types to monitor $\Delta\psi_{mt}$ (for review see Duchen et al., 2003). Presently, very little is known about the physiology of mitochondria in the cochlea.

3.2.1 TMRM reveals a base-to-apex difference in mitochondrial function specific to inner hair cells

As documented in other cell types, the pattern of TMRM staining in cochlear cultures was specific to mitochondria and excluded the cell nucleus. In these experiments TMRM fluorescence was used as a direct indicator of mitochondrial function. Quantification of TMRM fluorescence revealed a base-to-apex difference in $\Delta\psi_{mt}$ that was specific to the IHCs, in which the basal IHCs exhibited a significantly lower TMRM fluorescence in comparison to apical IHCs. This indicates that basal IHCs are less polarised than apical IHCs. The extent of mitochondrial polarisation within the different cells was also determined using the variation of the

signal around the mean, the coefficient variation (CV). The CV is calculated by dividing the mean of the fluorescence signal by the standard deviation of the signal. As described previously by Toescu & Verkhratsky (2000) the CV is inversely related to mitochondrial polarisation status in that a higher CV conveys are lower $\Delta\psi_{mt}$. There was a significantly lower standard deviation in the TMRM signal in basal IHCs compared to apical IHCs, consistent with a less polarised population of mitochondria. In contrast, the signal in apical IHCs showed a much higher standard deviation, consistent with a more polarised mitochondrial population. Taken together, these data are indicative of functionally distinct mitochondrial populations in basal and apical IHCs.

Table 4 Underlying causes for differences in mitochondrial membrane potential

$\Delta\psi_{mt}$	**Underlying cause**	**NADH redox index**
more polarised	Cells have lower ATP turnover	More reduced redox index for NADH
	Lower ATP turnover means there is a reduced proton leak	Increased substrate supply to the citric acid cycle
	Reduced proton leak results in a reduced rate of respiration	Slower rate of respiration would mean less consumption of reduced NADH
	Cells could have a lower proton leak due to reduced level of Ca^{2+} cycling through mitochondria	
less polarised	Cells have a higher ATP turnover	More oxidised redox index for NADH
	Higher ATP turnover increases the amount of proton leak	Increased rate of respiration would consume reduced NADH
	Increase in respiratory rate to balance proton leak	May be a reduced substrate supply to the citric acid cycle
	Greater proton leak could also be due to increased Ca^{2+} cycling	

Mitochondrial depolarisation is complicated and in most cases cannot be explained by a single process. The discrepancy in TMRM fluorescence in cochlear IHCs can be attributed to a number of mechanisms. The lower TMRM fluorescence and thus less polarised $\Delta\psi_{mt}$ seen in basal IHCs could result from a higher ATP demand, faster respiratory rate and mild uncoupling within the cell. In an ideal system, where electron transfer and oxidative phosphorylation are fully coupled, a faster rate of

respiration and electron transfer would give a more hyperpolarised $\Delta\psi_{mt}$ and thus brighter TMRM signal (Duchen et al., 2003). In the IHCs however, this is not the case and it can be suggested that the reduced $\Delta\psi_{mt}$ in basal IHCs, as indicated by the lower TMRM signal, results from mild uncoupling and proton leak via the ATP synthase. The higher TMRM signal in apical IHCs indicates a more polarised $\Delta\psi_{mt}$. This could be due to a reduced ATP demand and thus slower rate of respiration in these cells, resulting in a reduced proton leak via the ATP-synthase (Nicholls, 1982). In contrast to the IHCs, no significant differences were observed in TMRM fluorescence between basal and apical outer hair cells (OHCs), suggesting mitochondrial function in this cell type to be conserved along the length of the cochlea.

It should be noted, that the TMRM data discussed previously, were measured from P3 animals in which hearing is not yet established. It is possible therefore that the differences observed in $\Delta\psi_{mt}$ may be subject to developmental modulation up to and subsequent to the onset of hearing (P12). To address the possibility of a developmental gradient in $\Delta\psi_{mt}$ experiments were repeated using the cochlear slice preparation. Initial experiments were conducted using P2 slices so as to optimise the experimental techniques, with the aim of later applying them to slices from P12 animals. Unfortunately, analysis of the TMRM signal in P2 cochlear slices revealed a strikingly different loading in comparison to explant cultures. It is possible that this variation occurs due to differences in the isolation techniques. Following isolation, explant cultures were allowed to recover for at least 24 hours before imaging therefore giving the cells time to recover from the mechanical trauma of dissection. In the acute slice preparation, cells may still be in a stressed state which could alter their metabolism and thus give an erroneous TMRM signal. Additionally, it is feasible that without a sufficient time for recovery, the plasma membrane potential (Vm) of hair cells in the slice is more depolarised. In accordance with the Nernstian distribution of ions across the cell membrane (see Section 2.5.1) this would reduce the TMRM loading.

3.2.2 Base-to-apex differences in mitochondrial redox potential

In order to investigate potential causes of and thereby substantiate the finding of altered potentials in basal and apical IHCs, I investigated differences in mitochondrial redox potential between them. The mitochondrial redox potential refers to the ratio of [NADH/NAD^+] and [$FADH_2$/FAD^{2+}]. Changes in either ratio reflect changes in mitochondrial metabolism. The redox potential for each pair is altered when the transfer of electrons from NADH or $FADH_2$ to oxygen is not matched by the formation of either compound (Houston, 2006). As described in Section 3.1.4, the endogenous fluorescent properties of these molecules change in accordance with their redox state and can therefore be used to estimate the intracellular redox index. Although the localisation of NADH fluorescence has been documented recently in the isolated adult mouse cochlear preparation (Tiede et al., 2007), there are no functional data on intermediary metabolism in the neonatal cochlea. Here, a dynamic assay (Duchen et al., 2003 and Section 3.1.4) was used to determine the resting redox potential in cochlear cells.

To study the relationship between $\Delta\psi_{mt}$ and the cell redox index, basal levels of reduced NADH and oxidised flavoprotein (FAD^{2+}) were determined in IHCs, OHCs and Deiters' cells. It could be predicted, that redox metabolism may well differ between hair cells and supporting cells, due to their distinct physiological functions in the cochlea. In contrast to this hypothesis, no significant differences were observed in the redox index between hair cells and supporting cells. In light of the TMRM data discussed previously (Section 3.2.1) comparisons were also made between basal and apical cells in attempt to uncover the causes for differences in $\Delta\psi_{mt}$ observed along the length of the cochlea. As seen with TMRM, there was no difference in either NADH or FAD^{2+} between basal and apical OHCs, supporting the idea that mitochondrial function is conserved from base to apex in this cell type. Data obtained from IHCs however indicated a more reduced redox state in apical IHCs. This suggests that apical IHCs have a reduced ATP turnover and consequently a slower rate of respiration less proton leak. Additionally, this result may indicate that apical IHCs have a greater substrate supply to the citric acid cycle.

In order to obtain an adequate fluorescent signal from both NADH and FAD^{2+}, the confocal pinhole was left fully open. The effective absence of the pinhole significantly reduces the level of confocality and thus in a complex tissue such as the cochlea it becomes difficult to accurately measure fluorescent signals from different cell types without incorporating signal from cells either above or below the region of interest. If the pinhole was adjusted to a point that achieved sufficient resolution of the different cell types, the NADH fluorescence signal became too low to measure accurately. It is likely therefore that the fluorescence recorded in a specific cell type, within a given focal plane would become contaminated by out of focus light from neighbouring cells. Due to the close packing of cells in the horizontal and vertical planes this methodology provides an estimate of cell-specific base-to-apex differences in redox metabolism within this preparation.

In contrast to data with TMRM, The pattern of NADH autofluorescence was similar between the culture and slice preparations. In both, the NADH signal was brighter in the phalangeal cells (in particular the Deiters' processes) compared to both OHCs and IHCs. Comparison of the flavoprotein signal between slice and culture preparations did reveal a striking difference. Both OHCs and IHCs in the slice had a considerably higher flavoprotein signal compared to those in the culture. This is suggestive of a more oxidised metabolism in hair cells from the acute slice. A more oxidative metabolism would agree with a greater state of stress within the cell.

3.2.3 Influence of oligomycin and BAPTA-AM on $\Delta\psi_{mt}$

Oligomycin is an antibiotic which blocks the proton conductance of the ATP synthase. It has been shown previously that oligomycin causes a hyperpolarisation of $\Delta\psi_{mt}$ in cells where the ATP synthase is contributing to proton leak. This hyperpolarisation is observed as an decrease in the fluorescence of membrane potential probes such as Rh123 or TMRM when used in de-quench mode or as an increase in fluorescence when they are used in re-distribution mode (Duchen, 1992; Duchen et al., 2003). As discussed in Section 3.2.1, an interpretation of the data presented in this chapter would be that apical IHCs have a lower ATP consumption than basal IHCs. A cell displaying a higher rate of ATP consumption would have higher levels of extramitochondrial ADP, which will disrupt state 4 respiration by exchanging matrix ATP for the additional ADP via the adenine nucleotide

translocator. This subsequently reduces the Gibbs energy (ΔG) for the ATP/ADP + pi system leading to perturbation of the ATP synthetase equilibrium (Nicholls, 1982). In attempt to restore ΔG, the ATP synthase operates in the direction of ATP synthesis driving proton re-entry to the matrix (Nicholls, 1982). The influx of protons via the ATP synthase creates a 'shunt' in the proton gradient across the mitochondrial inner membrane and consequently reduces $\Delta\psi_{mt}$. To compensate for the reduction in proton gradient, the electron transfer chain will run at a faster rate. This form of ATP production is referred to as state 3 (ADP-dependent) respiration (Nicholls, 1982). State 3 respiration is completely blocked in the presence of oligomycin. If basal but not apical IHCs were producing ATP predominantly through state 3 respiration one would expect the differences in membrane potential to be abolished in the presence of oligomycin. In the experiments described here, oligomycin did result in hyperpolarisation of $\Delta\psi_{mt}$ in both basal and apical IHCs and normalised the base-to-apex difference in TMRM fluorescence.

A less polarised $\Delta\psi_{mt}$ can also result from a greater rate of mitochondrial Ca^{2+} uptake under resting conditions (Nicholls, 1982). This phenomenon could be due to an increased basal $[Ca^{2+}]_c$ in basal IHCs compared to apical IHCs. In this thesis, treatment of cultures with the membrane permeant Ca^{2+} chelator BAPTA-AM caused hyperpolarisation of $\Delta\psi_{mt}$ in basal and apical IHCs. The extent of the BAPTA-induced hyperpolarisation of $\Delta\psi_{mt}$ was again greater in basal compared to apical IHCs. It is possible therefore that this gradient in $\Delta\psi_{mt}$ between basal and apical IHCs may result from cell-specific differences in both futile mitochondrial Ca^{2+} cycling mitochondria and proton leak via the ATP synthase.

One observation throughout these experiments was the inconsistency of TMRM staining between images taken using the upright Zeiss 510 and those acquired with the inverted Zeiss LSM 510. Images acquired using the upright configuration revealed significant differences in basal and apical IHCs. Those obtained with the inverted set-up followed the same trend, although in this case, were not significant. It is likely that when imaging from the beneath the cochlear preparation, a greater amount of light becomes scattered within the tissue resulting in distortion of the signal. Additionally, the orientation of the hair cells within the preparation can vary

between cultures thus incorporating further variation into measurements made using the inverted system. Data obtained using the upright configuration showed a lower standard deviation throughout. It is feasible, that imaging directly onto the hair cells eliminates or reduces the error and variation seen in the data from the inverted system. This may also explain the insignificant effects of oligomycin on the TMRM signal (these measurements were made using the inverted microscope). The inverted set-up was chosen for these experiments, as it permitted the local application of oligomycin onto the hair cells from a micropipette.

3.2.4 NAD(P)H lifetime imaging reveals metabolic differences between hair cells and phalangeal supporting cells

As described in Section 3.1.6, NAD(P)H fluorescence lifetimes provide additional information regarding the intracellular metabolism of a cell. Changes in the decay of NAD(P)H fluorescence (lifetime) is determined by the local microenvironment of the molecule (Lakowicz et al., 1992). A greater proportion of immobilised NAD(P)H is conveyed by a longer lifetime and free NAD(P)H by a shorter lifetime. The longer lifetime evident in the phalangeal cells is suggestive of a greater proportion of immobilised NAD(P)H in these cells. Contrastingly, in the OHCs a shorter lifetime is dominant, suggesting a greater proportion of free NAD(P)H. These data are also supported by differences in the relative lifetime weightings between the two cell types. Analysis of NAD(P)H in cardiomyocytes reveals an NAH(P)H signal that is predominantly mitochondrial, which is dominated by a short fluorescence lifetime (Duchen MR unpublished data) and consistent with data from the OHCs. Data from phalangeal cells however are more consistent with that from oocytes, which show a mostly cytosolic NAD(P)H signal with a predominantly long fluorescent lifetime (Duchen MR unpublished data). Taken together, this suggests a metabolism that is more oxidative in hair cells compared to one which is more glycolytic in phalangeal cells. This finding is supported by data obtained from slices, in which similar metabolic differences between phalangeal cells and hair cells were observed. The higher flavoprotein signal in hair cells of the slice preparation is also consistent with a more oxidative metabolism.

In summary, assessment of mitochondrial function using confocal, 2-photon and lifetime imaging identifies cell-specific differences in oxidative and intermediary metabolism in the neonatal cochlear preparation. These include base-to-apex variation in $\Delta\psi_{mt}$ and resting redox state specific to the IHCs and metabolic differences between phalangeal supporting cells and OHCs. How these finding relate directly to the physiology of the cochlear remain unclear.

4 Mitochondrial Ca^{2+} buffering influences agonist-induced $[Ca^{2+}]_c$ signalling in cochlear supporting cells

Mitochondrial Ca^{2+} handling is involved in numerous signalling mechanisms within a range of cell types. Mitochondrial Ca^{2+} uptake modulates the magnitude and spatio-temporal properties of Ca^{2+} waves allowing them to modulate the information the Ca^{2+} signal conveys (see Section 1.5.4). Regulation of $[Ca^{2+}]_c$ in cochlear hair cells is likely to be essential for a number of physiological processes which include, amplification, adaptation and synaptic transmission (see Mammano et al., 2007). It is probable that Ca^{2+} homeostasis in supporting cells is of equal importance, as these are the cells that maintain the environment in which the hair cells function. The precise function of $[Ca^{2+}]_c$ waves in supporting cells is at present unclear, although they are thought to play a role in coordinating the response to damage in cochlear epithelia (Gale et al., 2004).

Ototoxicity and acoustic trauma result in damage to and eventually death of the cochlear hair cells. The precise mechanisms by which such stimuli induce hair cell death are unclear. In a number of cell culture models, damage and mechanical stimulation cause increases in $[Ca^{2+}]_c$ that manifest as intercellular $[Ca^{2+}]_c$ waves (Sanderson et al., 1990; Hirose et al., 1999; Gale et al., 2004; Piazza et al., 2007). In auditory epithelia, a Ca^{2+} wave is triggered following damage to a single hair cell (Gale et al., 2004). It has been hypothesised, that damaged hair cells may become leaky and release ATP into the surrounding tissue, eliciting an IP_3-dependent regenerative $[Ca^{2+}]_c$ wave that propagates throughout the neighbouring supporting cells (Gale et al., 2004). These studies focused on the dynamics of the Ca^{2+} wave in the outer sulcus or Claudius cell region which being relatively flat makes this a good model with which to study this phenomenon. This chapter investigates the influence of mitochondrial Ca^{2+} buffering on the properties of agonist-induced changes in $[Ca^{2+}]_c$ and damage-induced intercellular $[Ca^{2+}]_c$ waves in Claudius and Deiters' cells.

4.1.1 *Application of extracellular ATP elicits changes in both $[Ca^{2+}]_c$ and $[Ca^{2+}]_{mt}$*

In this study, extracellular application of ATP was used to induce a reproducible Ca^{2+} response in cochlear Claudius cells of postnatal day three (P3) rats.

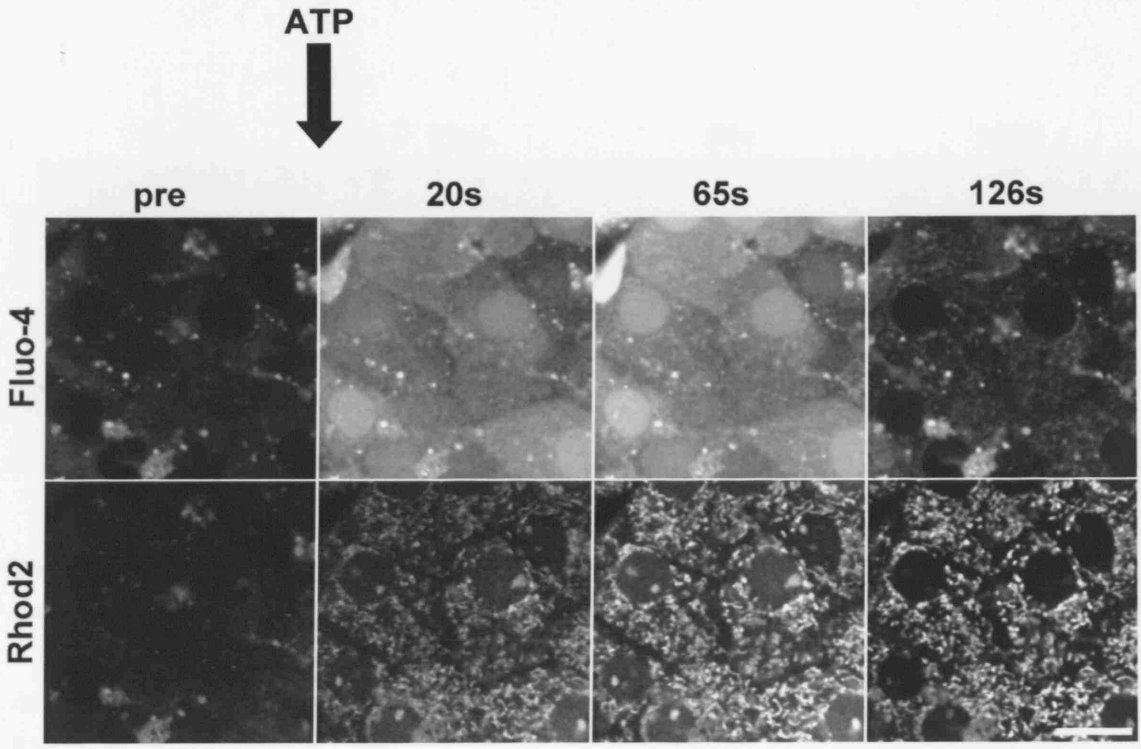

Figure 4. 1 Simultaneous imaging of $[Ca^{2+}]_c$ and $[Ca^{2+}]_{mt}$ reveals coincident Ca^{2+} increase following extracellular ATP application.

Changes in cytosolic Ca^{2+} in response to 50 μM ATP are shown as an increase in fluo-4 fluorescence (top panel). Changes in mitochondrial Ca^{2+} are represented by an increase in Rhod2 fluorescence (bottom panel). Images are averages of three successive frames in a time series. Time post ATP application is indicated top. Scale bar is 20 μm.

The applied concentrations of ATP ([ATP]) were varied from 0.1 up to 100 μM, in order to study the relationship between cytosolic and mitochondrial compartments. ATP was applied for a period of 30 seconds. Throughout these experiments, a higher [ATP] was representative of a greater cytosolic Ca^{2+} load. Changes in $[Ca^{2+}]_c$ were monitored using the high affinity cytosolic Ca^{2+} indicators Fluo4-AM (Figure 4.1), Fura-2-AM (Figure 4.2) and the low affinity indicator Fura-FF-AM (Figure 4.4). $[Ca^{2+}]_{mt}$ was monitored using the high affinity mitochondrial specific Ca^{2+} indicator

Rhod2-AM (Figures 4.1, 4.2) and the low affinity indicator Rhod5N-AM (Figure 4.3).

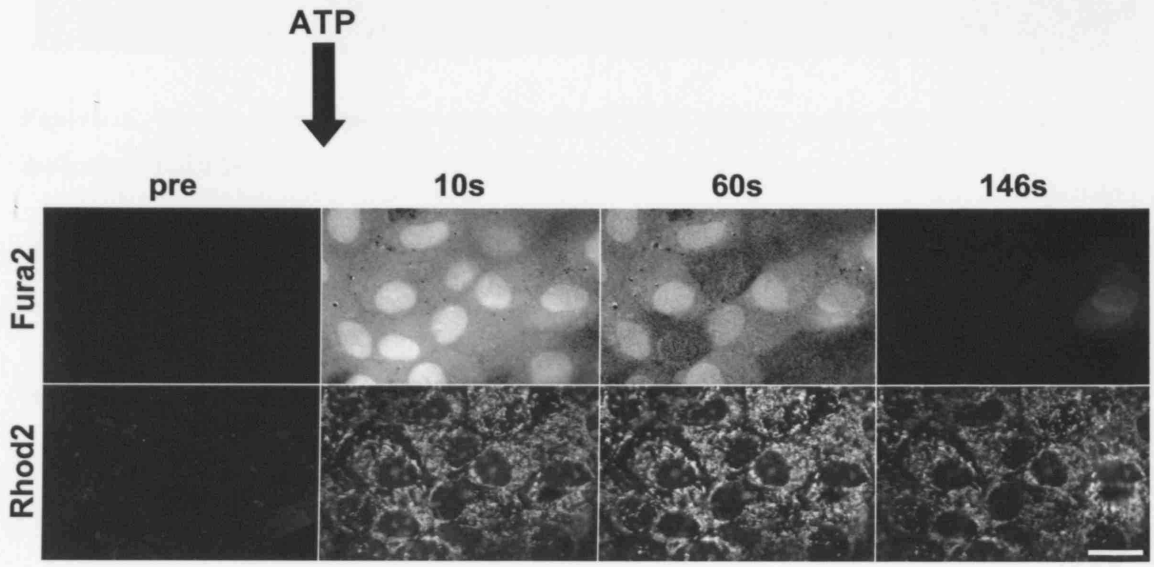

Figure 4. 2 Application of extracellular ATP causes Ca^{2+} elevations in both cytosolic and mitochondrial compartments.

Simultaneous imaging of $[Ca^{2+}]_c$ and $[Ca^{2+}]_{mt}$ in cochlear Claudius cells. Elevation of $[Ca^{2+}]_c$ in response to 50 μM ATP causes a decrease in Fura-2 fluorescence with excitation at 405 nm **(top panel)**. The signal has been inverted and is presented as an increase. Changes in mitochondrial Ca^{2+} are represented by an increase in Rhod2 fluorescence **(bottom panel)**. Images are averages of three successive frames in a time series. Time post ATP application is indicated in seconds. Scale bar is 20 μm.

Uptake of Ca^{2+} into mitochondria was observed in Claudius cells following extracellular application of ATP at all specified concentrations (Figures 4.1, 4.2, 4.3). The relative changes in $[Ca^{2+}]_{mt}$ appeared higher than those seen in $[Ca^{2+}]_c$ (Figures 4.4, 4.5, 4.7) the fluorescent signal in the mitochondria was brighter than that in the cytosol after ATP application. This must be interpreted with caution however, as the signals in cytosolic and mitochondrial compartments were measured using different dyes. The $[Ca^{2+}]_{mt}$ transient was also found to outlast that observed in the cytosol (Figures 4.6, 4.7). The transient duration was defined as the time for the signal fall to 50% of the peak. Step-wise increases in the applied [ATP] revealed a dose-dependent relationship between the [ATP] and relative fluorescence from each cellular compartment (Figure 4.8).

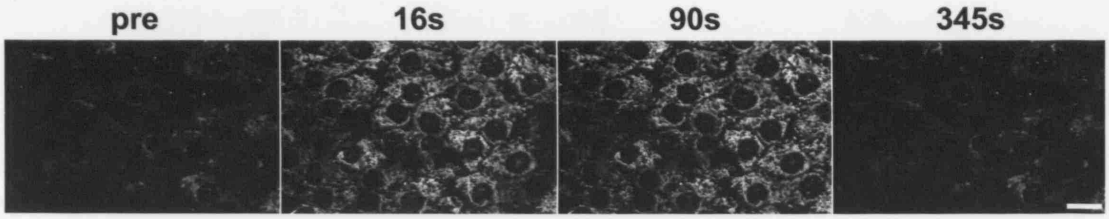

Figure 4. 3 Measurement of mitochondrial Ca^{2+} uptake using the low affinity indicator Rhod 5N.

Changes in mitochondrial Ca^{2+} measured in Claudius cells following the application of 50μM ATP. Raised $[Ca^{2+}]_{mt}$ is represented by an increase in Rhod 5N fluorescence. Images are averages of three successive frames in a time series. Time post ATP application is indicated in seconds. Scale bar is 20 μm.

4.1.2 A dose-dependent relationship exists between $[Ca^{2+}]_c$, $[Ca^{2+}]_{mt}$ and [ATP]

$[Ca^{2+}]_{mt}$ and $[Ca^{2+}]_c$ increase in accordance with [ATP], indicated by the simultaneous increases in both Rhod-5N and Fura-FF fluorescence following ATP application (Figure 4.8). The relative changes in $[Ca^{2+}]_c$ were measured using Fura-2 and Fura-FF over [ATP] ranging from 0.01 to 100 μM. When measured with Fura-2, the dye appeared to become saturated at [ATP] above 1 μM as further increases in fluorescence above this concentration were significantly smaller (Figure 4.8). When measured using Fura-FF however, the fluorescence continued to increase following application of ATP up to concentrations of 100 μM (Figures 4.4, 4.8). Changes in mitochondrial fluorescence were monitored using the low affinity indicator Rhod5N, which also did not saturate with [ATP] up to 100 μM (Figure 4.8).

To investigate the relationship between $[Ca^{2+}]_c$ and $[Ca^{2+}]_{mt}$, extracellular ATP was applied over the concentration range 0.01 – 100 μM to a single cochlear culture. The fluorescent changes occurring at each [ATP] and in each compartment were measured by placing regions of interest over mitochondrial and cytosolic regions. The fluorescence changes at each [ATP] were used to plot $[Ca^{2+}]_{mt}$ as a function of $[Ca^{2+}]_c$ (over the [ATP] range used). The plot of $[Ca^{2+}]_{mt}$ versus $[Ca^{2+}]_c$ revealed a correlation between the two compartments (Figure 4.9). Data was fit with a linear trendline that displayed and R^2 value of 0.89.

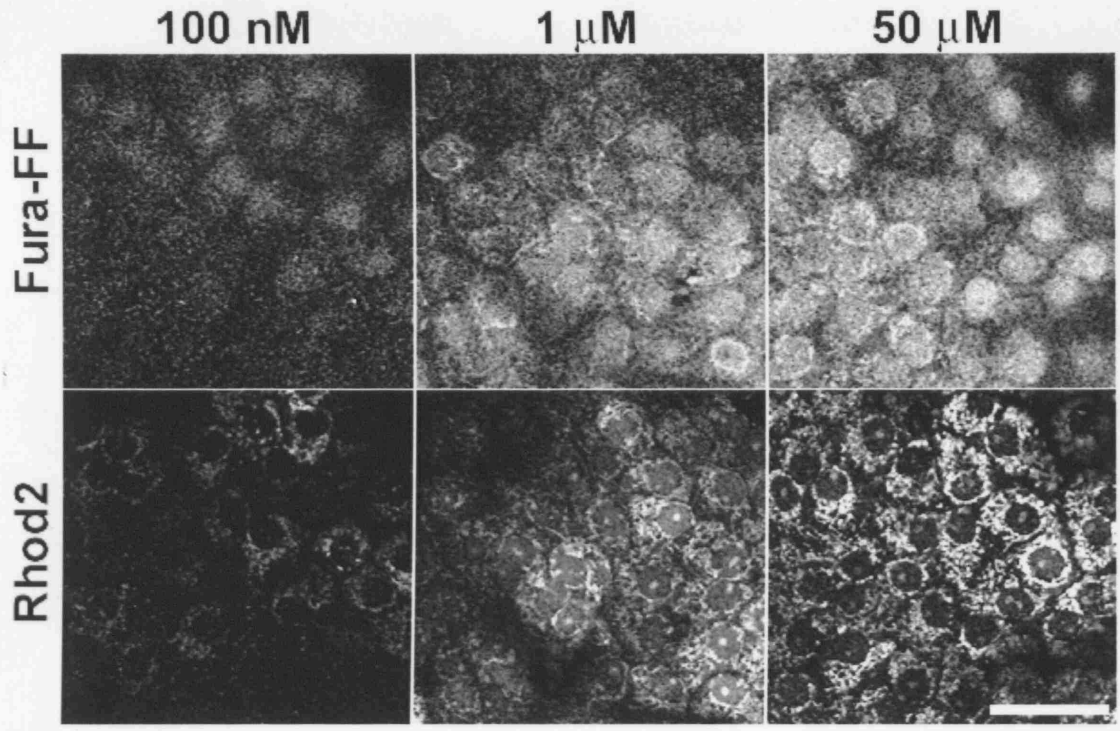

Figure 4. 4 The relationship between cytosolic Ca^{2+}, mitochondrial Ca^{2+} and ATP concentration is dose-dependent.

Image stills indicate the changes in $[Ca^{2+}]_c$ and $[Ca^{2+}]_{mt}$ in response to extracellular ATP application at varying concentrations. Changes in $[Ca^{2+}]_c$ are shown as an decrease (inverted here) in Fura-FF fluorescence with excitation at 405 nm (top panel). Images are displayed as inverted subtracted averages taken from 3 time series at 100 nM, 1 µM and 50 µM (top panel). Elevations in $[Ca^{2+}]_{mt}$ are shown as an increase in Rhod 2 fluorescence (bottom panel) taken from 3 time series at 100 nM, 1 µM and 50 µM. Images are averages of 20 frames recorded post ATP application (duration ~ 30 s) (bottom panel). Scale bar is 50 µm.

4.1.3 Block of mitochondrial Ca^{2+} uptake using CCCP & oligomycin enhances the peak amplitude and duration of ATP-induced Ca^{2+} transients in Claudius cells

The role of mitochondrial Ca^{2+} uptake in $[Ca^{2+}]_c$ signalling in Claudius cells was investigated by blocking the pathway using a cocktail of CCCP and oligomycin (see Section 2.8.3). Uptake of Ca^{2+} into mitochondria is dependent upon on $\Delta\psi_{mt}$ and

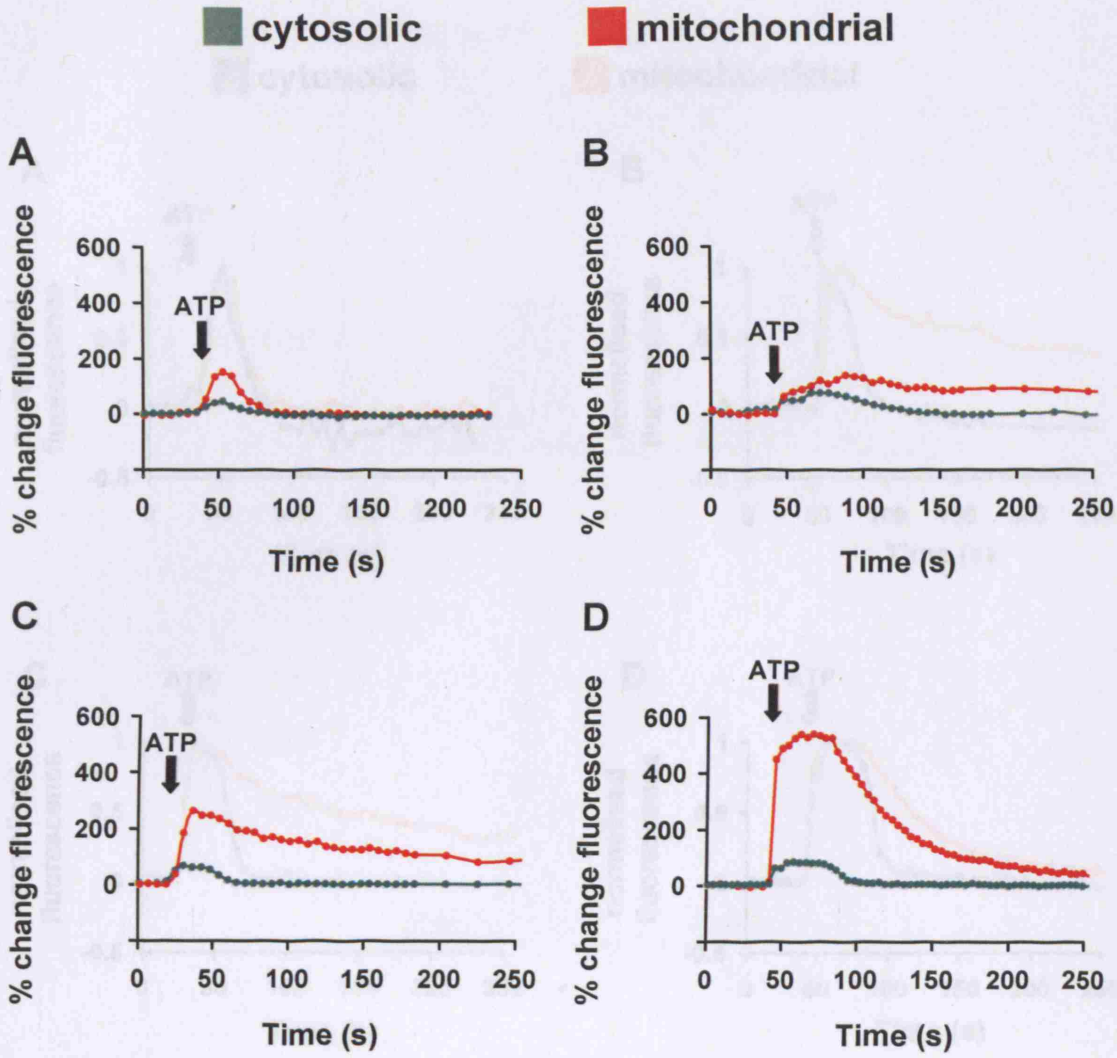

Figure 4. 5 Changes in $[Ca^{2+}]_c$ and $[Ca^{2+}]_{mt}$ in response to extracellular ATP at varying concentrations.

Traces indicate the Ca^{2+} changes in cytosolic and mitochondrial compartments following application of extracellular ATP at 100 nM **(A)**, 500 nM **(B)**, 1 μM **(C)** and 50 μM **(D)**. The changes in $[Ca^{2+}]_c$ is illustrated in green and changes in $[Ca^{2+}]_{mt}$ are shown in red. Data are presented as the percentage change in fluorescence for both signals. ATP application is indicated by the black arrows.

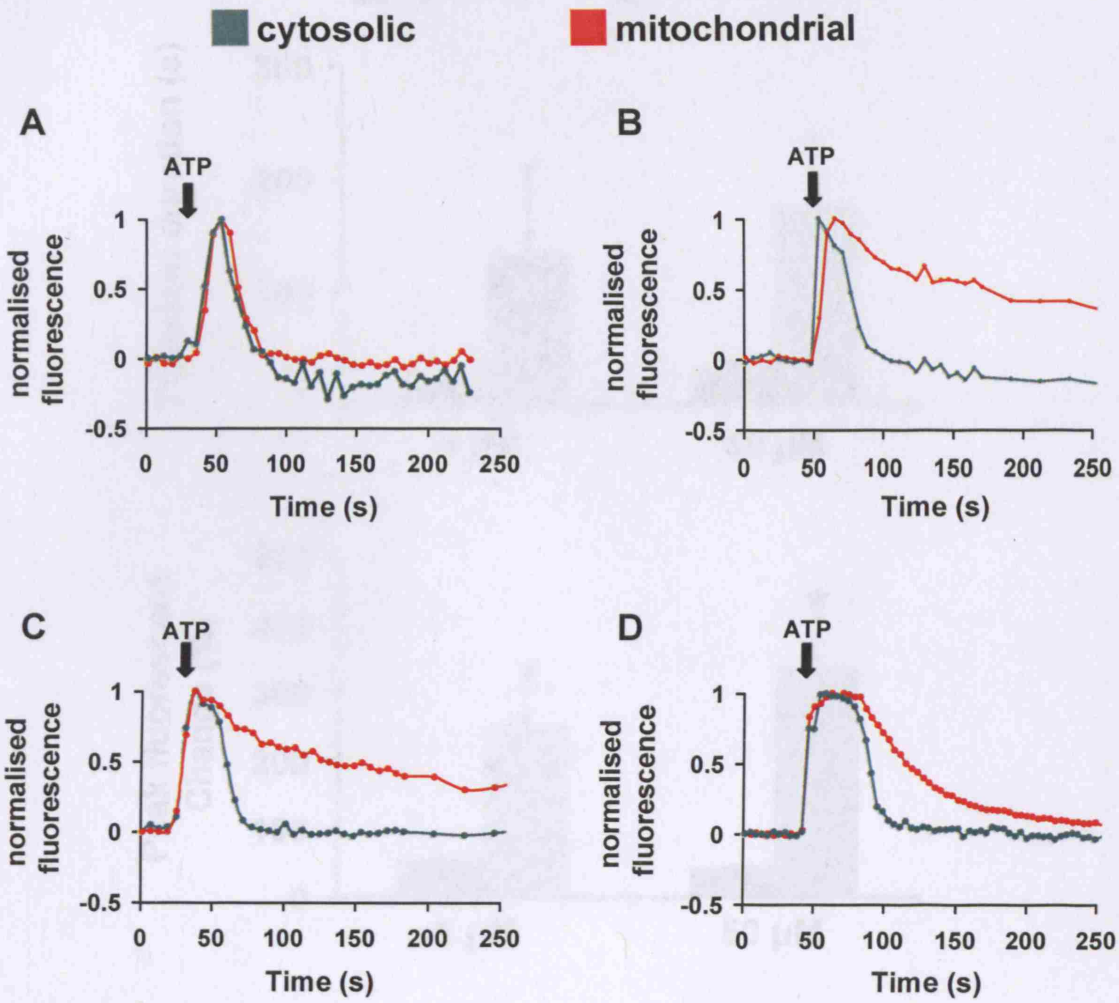

Figure 4. 6 Mitochondrial Ca^{2+} remains elevated for significantly longer than cytosolic Ca^{2+}.

Traces are normalised data illustrating the differences in duration of $[Ca^{2+}]_c$ and $[Ca^{2+}]_{mt}$ transients in response to extracellular ATP. Traces show Ca^{2+} responses at 100 nM **(A)**, 500 nM **(B)**, 1 μM **(C)** and 50 μM **(D).** Changes in $[Ca^{2+}]_c$ and $[Ca^{2+}]_{mt}$ are shown in green and red respectively. Time of ATP application is indicated by the black arrows.

therefore activity of the electron transfer chain (see Duchen, 2004 and Section 1.5). By incubating cultures with the uncoupler CCCP (see Section 2.5.5), $\Delta\psi_{mt}$ is dissipated and Ca^{2+} uptake is prevented. Oligomycin ensures complete collapse of $\Delta\psi_{mt}$ by inhibiting the reverse mode function of the mitochondrial ATP-synthase and consumption of cellular ATP.

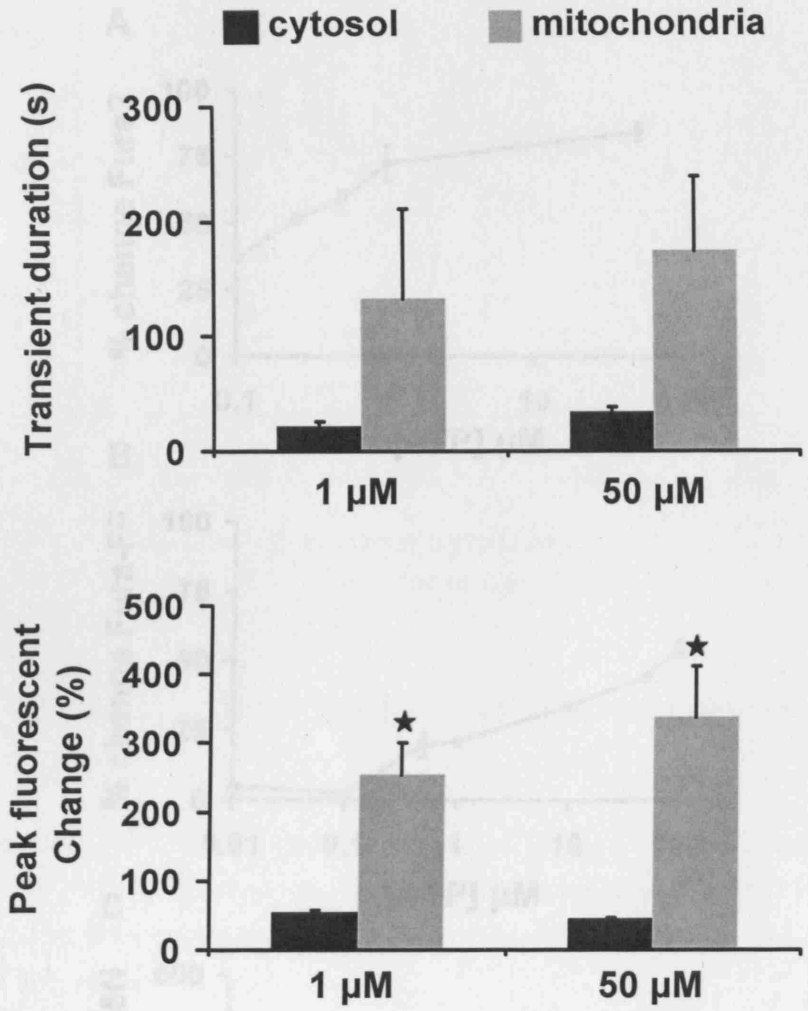

Figure 4. 7 Differences in ATP-induced Ca^{2+} transients between mitochondrial and cytosolic compartments.

Top panel Pooled data showing the duration of the ATP-induced Ca^{2+} transient in the cytosol **(black bars)** and mitochondria **(grey bars)** at 1 and 50 μM ATP**.** Data for 1 μM are mean ± SEM from 6 cultures. Data for 50 μM are mean ± SEM from 4 cultures.
Bottom panel Pooled data to show differences in the peak Ca^{2+} changes in cytosolic and mitochondrial compartments at 1 and 50 μM. Data for 1 μM are from 6 cultures. p=<0.008, Student's paired *t*-test. Data for 50 μM from 4 cultures. p = < 0.02, Student's paired *t*-test. All data are mean ± SEM.

During periods of elevated $[Ca^{2+}]_c$, Ca^{2+} uptake into energised mitochondria is an important mechanism by which Ca^{2+} is cleared from the cytosol (see Section 1.5.4). Interference with this pathway would therefore be expected to modulate various parameters of the $[Ca^{2+}]_c$ signal. $[Ca^{2+}]_c$ was mobilised using extracellular application

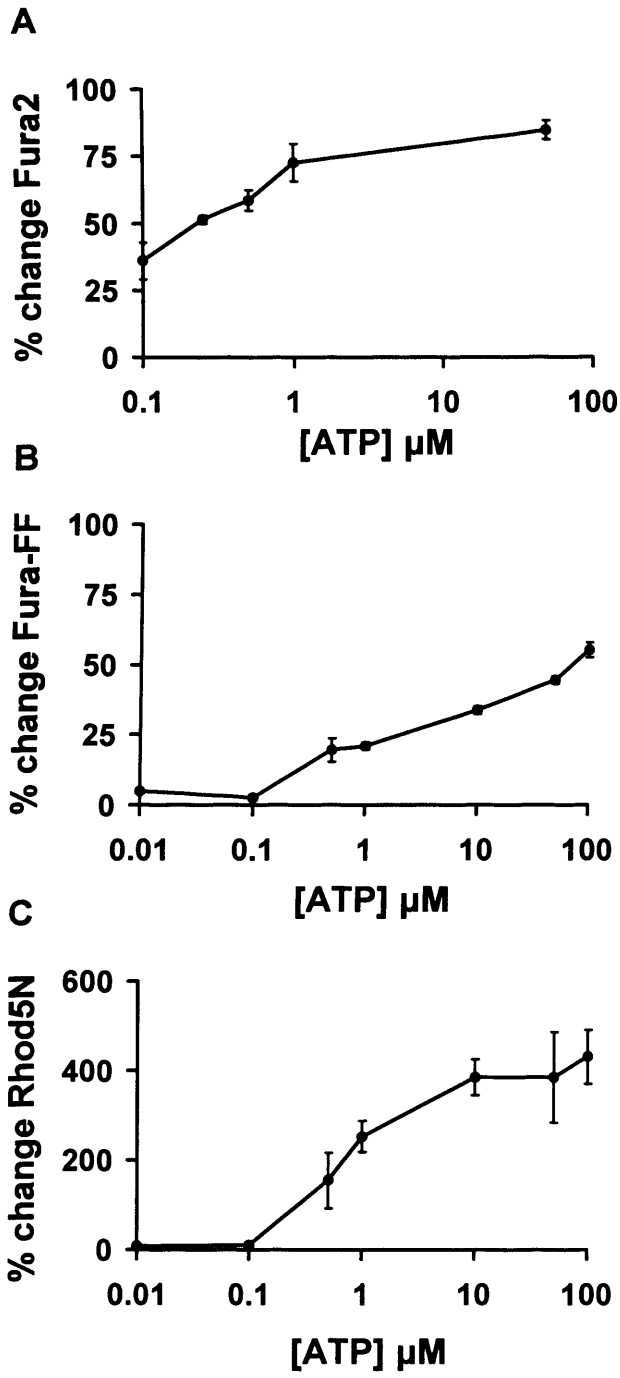

Figure 4. 8 Semi-log_{10} plots of average changes in $[Ca^{2+}]_c$ and $[Ca^{2+}]_{mt}$ as a function of [ATP] using Fura-2, Fura-FF and Rhod 5N.

Changes in $[Ca^{2+}]_c$ in response to 0.01, 0.1, 1, 10 and 100 µM ATP are represented by the increases in Fura-2 **(A)** and Fura-FF fluorescence **(B)**. Changes in $[Ca^{2+}]_{mt}$ are presented as an increase in Rhod-5N fluorescence **(C)**. Data are mean ± SEM from 4 individual experiments.

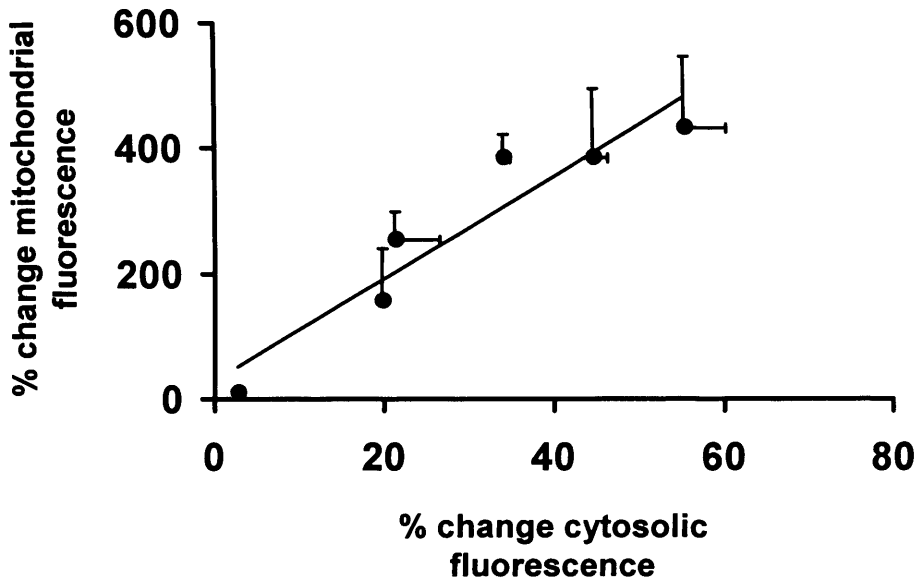

Figure 4. 9 Relationship between $[Ca^{2+}]_c$ and $[Ca^{2+}]_{mt}$ during agonist-induced $[Ca^{2+}]_c$ signalling.

The graph shows $[Ca^{2+}]_{mt}$ plotted as a function of $[Ca^{2+}]_c$ over ATP concentrations ranging from 0.01 – 50 μM. $[Ca^{2+}]_{mt}$ levels are represented by percentage Rhod-5N fluorescence and $[Ca^{2+}]_c$ levels are represented by percentage Fura-FF fluorescence. Data are mean ± SEM from 4 separate experiments.

of ATP from a micropipette under pressure. Elevations in $[Ca^{2+}]_c$ in response to [ATP] ranging from 0.01 – 50 μM were monitored using Fura-FF. ROIs were placed on cells in close proximity to the puff site so as to obtain an accurate representation of $[Ca^{2+}]_c$ changes at each [ATP]. The magnitude of the $[Ca^{2+}]_c$ signal increased with ATP concentration (Figure 4.10).

The peak amplitudes of ATP-induced transients in the cytosolic compartment were compared at 1, 10 and 50 μM between control and CCCP treated cultures. Transients were monitored using Fura-FF and Rhod 5N. The ATP-induced Ca^{2+} transient was increased in the presence of CCCP (5 μM) at all concentrations studied. The effects of CCCP and oligomycin were most pronounced at 50 μM ATP (Figure 4.10). The duration of ATP-induced Ca^{2+} transients were compared between control and CCCP treated cultures at 1 and 50 μM, as these were the concentrations at which mitochondrial Ca^{2+} buffering had the most influence (Figures 4.11, 4.12).

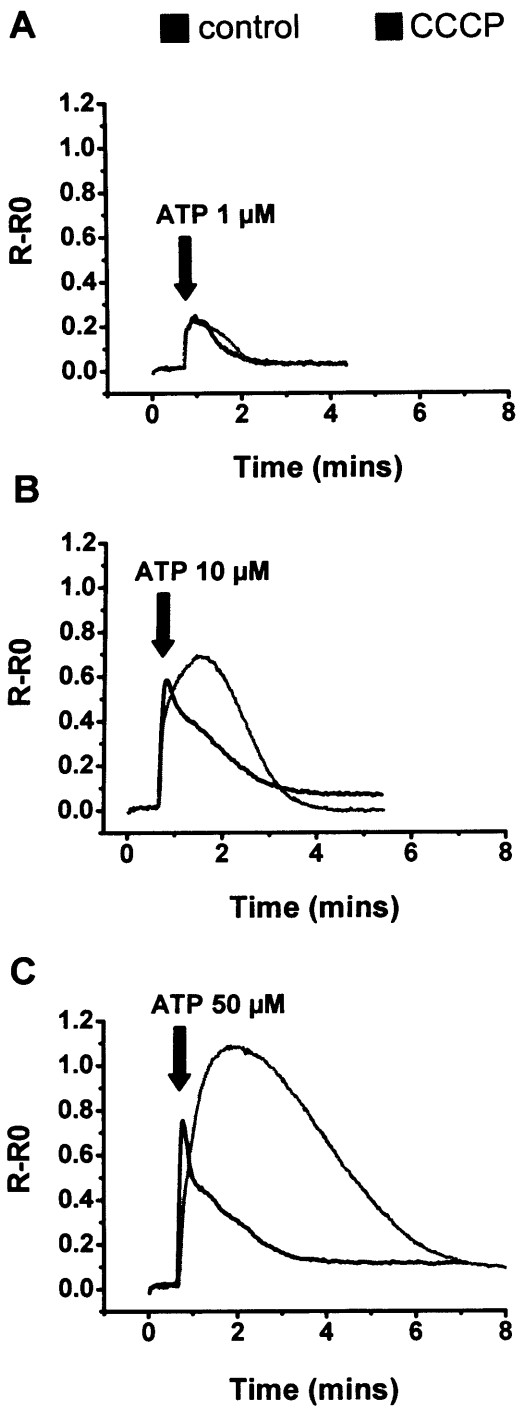

Figure 4. 10 CCCP enhances the peak amplitude and duration of ATP-induced $[Ca^{2+}]_c$ transients in cochlear Claudius cells.

Traces show average responses measured from a field of 15 cells. Control responses (black) to 1 µM **(A)** 10 µM **(B)** and 50 µM **(C)** ATP. $[Ca^{2+}]_c$ responses to 1 µM **(A)** 10 µM **(B)** and 50 µM **(C)** ATP in the presence of 5 µM CCCP (grey). Changes in $[Ca^{2+}]_c$ are represented by ratio changes in Fura-FF fluorescence. Time of ATP application is indicated by the black arrows.

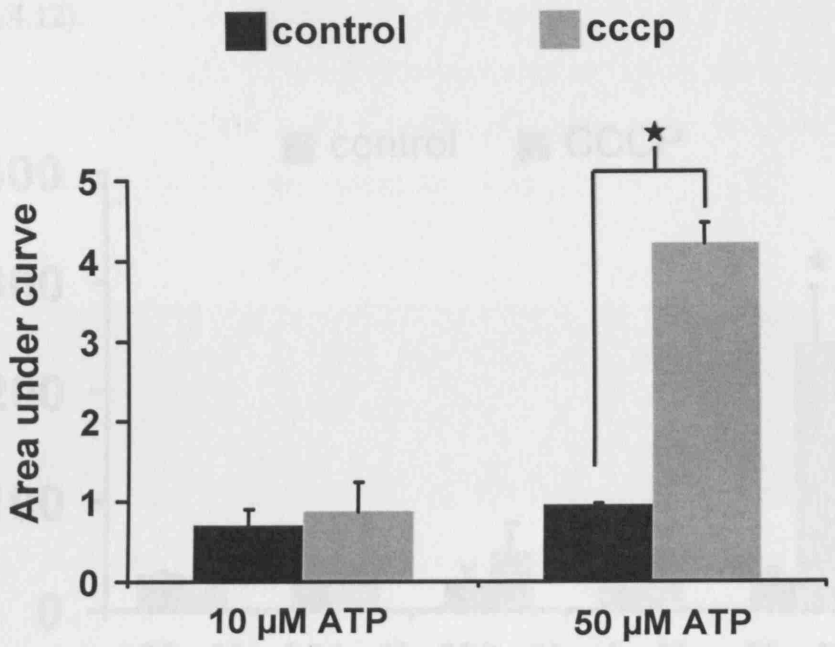

Figure 4. 11 CCCP prolongs ATP-induced $[Ca^{2+}]_c$ elevations in Claudius cells.

Chart shows the integrated area under the Ca^{2+} transient curves at 10 µM **(A)** and 50 µM ATP **(B)**. Control responses (black bars) and those in the presence of CCCP (grey bars) are shown for each concentration. For 10 µM, data are from 2 cultures, 38 cells. p = 0.6, Student's paired *t*-test. For 50 µM, data are from 3 cultures, 57 cells. p = 0.003, Student's paired *t*-test. All data are mean ± SEM.

At 10 µM a 1 fold increase in duration (p = 0.11, Student's paired *t*-test) was observed and at 50 µM, a 4 fold increase (p = 0.02, Student's paired *t*-test) was seen between control transients and those in the presence of CCCP (Figure 4.11). The transient duration was calculated as the area under each ATP-induced curve.

As measured using Fura-FF, control $[Ca^{2+}]_c$ transients lasted for 33 ± 2 s, 22 ± 1 s, 29 ± 12 s, 28 ± 4 s and 31 ± 3s at 0.1, 0.25, 0.5, 1 and 50 µM respectively. In the presence of CCCP and oligomycin, transient durations increased to 31 ± 5 s, 29 ± 12 s, 52 ± 26 s, 48 ± 5 s and 244 ± 49 s at 0.1, 0.25, 0.5, 1 and 50 µM respectively (Figure 4.12). The influence of mitochondrial Ca^{2+} buffering was negligible at [ATP] below 500 nM, as no differences were observed in transient duration between control and CCCP treated cultures (Figure 4.12). A significant increase in the duration of the ATP-induced $[Ca^{2+}]_c$ was only evident at 1 and 50 µM ATP (Figure 4.12). CCCP-

induced modulation of the Ca^{2+} signal was also most robust at 50 μM ATP (Figures 4.10, 4.11, 4.12).

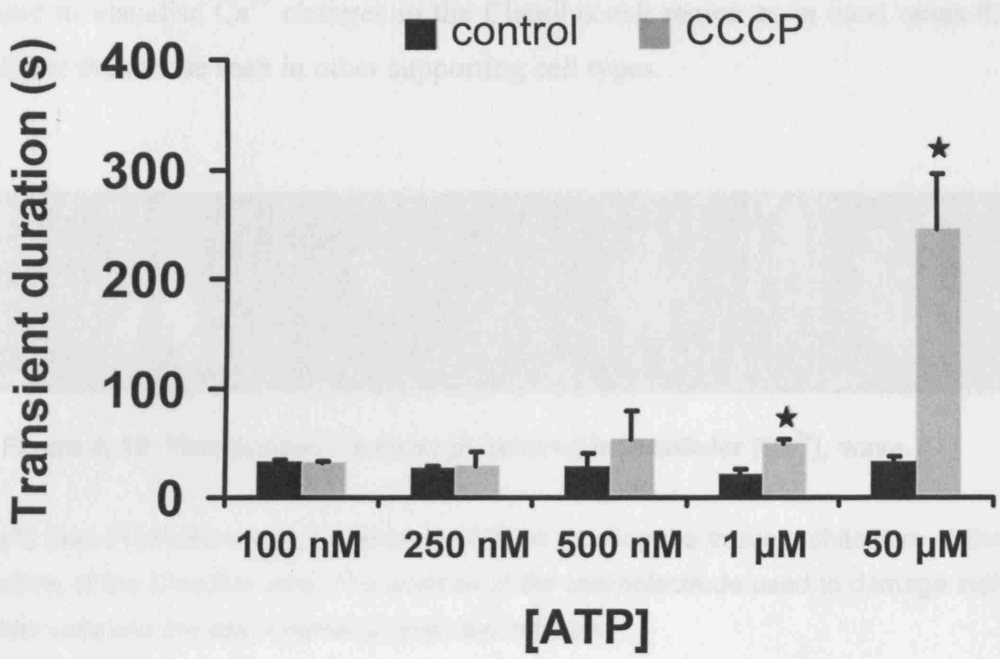

Figure 4. 12 CCCP enhances the duration of ATP-induced $[Ca^{2+}]_c$ transients in cochlear Claudius cells at [ATP] above 500 nM.

Chart displays the pooled data for control (black bars) and CCCP treated cultures (grey bars) in response to varying ATP concentrations. The transient duration is defined here, as the time taken for the signal to fall to 50% of its peak. Data are presented as mean ± SEM. P = < 0.05, Student's paired t-test.

4.2 Mitochondrial modulation of damage-induced intercellular $[Ca^{2+}]_c$ waves in Claudius and Deiters' cells

4.2.1 Blocking mitochondrial Ca^{2+} uptake enhances both extent of spread and propagation velocity of damage-induced intercellular Ca^{2+} waves

Mechanical damage of individual hair cells was used to elicit reproducible intercellular $[Ca^{2+}]_c$ waves in cochlear explants. Mechanically-induced Ca^{2+} waves were visualised using Fura-2 and spread from the site of damage out into the

surrounding supporting cells (Figure 4.13). The rate of propagation of the intercellular Ca^{2+} wave (measured with Fura-FF or Fura-2) was 13.5 ± 3 μm/s in the Claudius and 12.8 ± 2.4 μm/s in the Deiters' cell regions (Figure 4.14). Fura-FF was used to visualise Ca^{2+} changes in the Claudius cell region as in most cases they are higher than those seen in other supporting cell types.

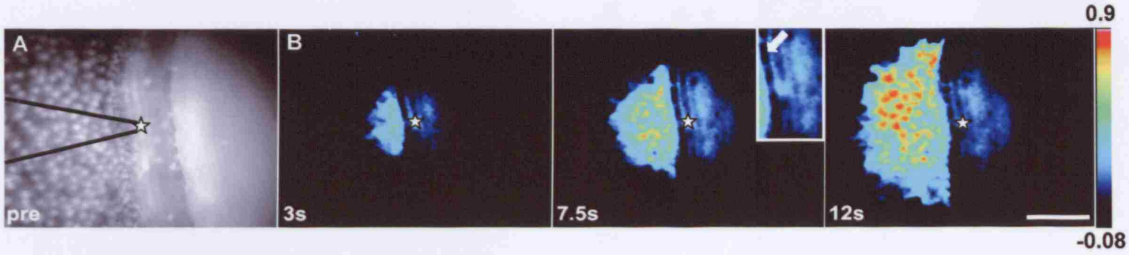

Figure 4. 13 Time series of a damage induced intercellular $[Ca^{2+}]_c$ wave.

(A) Fura-FF fluorescence recorded at 380 nm showing the tissue architecture at the focal plane of the Claudius cells. The position of the microelectrode used to damage individual hair cells and the site of damage (star) are indicated.

(B) Series of subtracted ratio images (R-R0) illustrating the propagation of the damage-induced intercellular $[Ca^{2+}]_c$ wave. Panel inset highlights the predominance of the wave in the Deiters' cells and the significantly reduced magnitude of the wave in the hair cells (white arrow). Scale bar is 100 μm. Fluorescence intensity levels are mapped according to the scale indicated right.

Blocking mitochondrial Ca^{2+} uptake (see Section 2.8.4) with Ru360 significantly increased the propagation velocity to 18.8 ± 5.4 μm/s in Claudius cells ($p = < 0.05$) and 16.8 ± 2.8 μm/s in Deiters cells ($p = < 0.05$) (Figure 4.14). Ru360 also increased the extent of wave spread. The spread of the Ca^{2+} wave was determined using line scan analysis as described in Section 2.11.3. The total distance travelled by the Ca^{2+} wave was increased from 114 ± 11 μm to 152 ± 11 μm in the Claudius cell region ($p =< 0.05$, Student's paired *t*-test) and from 154 ± 5 μm to 164 ± 8 μm in the Deiters' cell region ($p = <0.05$, Student's paired *t*-test) (Figure 4.15).

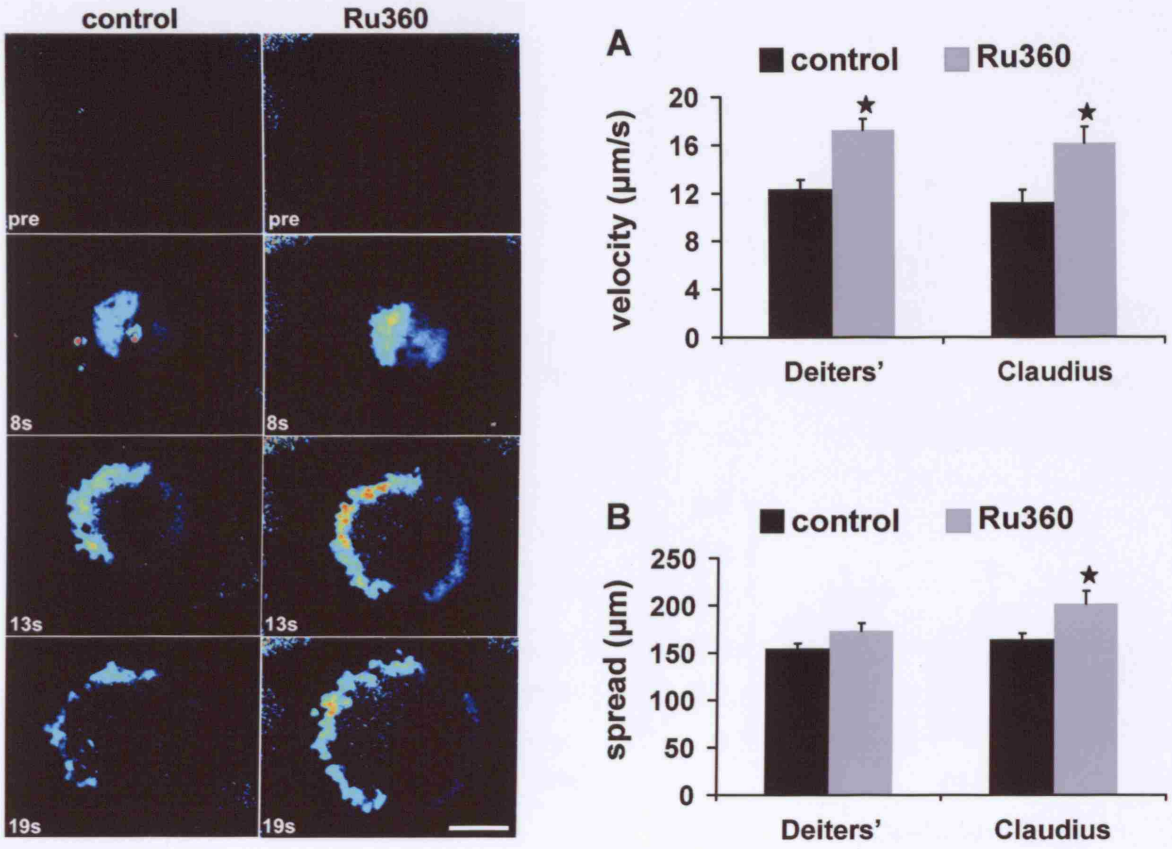

Figure 4. 14 Ru360 increases the propagation velocity and extent of spread of the intercellular $[Ca^{2+}]_c$ wave.

Left panel. Images illustrate the velocity and spread of the wave-front in control (left images) and Ru360 treated (right images) cultures. Image stills are averages from differentiated images at time post damage (indicated)

(A) Velocity of the Ca^{2+} wave in Deiters' and Claudius cell regions in control (black bars) and Ru360 treated (grey bars) cultures. Data are mean ± SEM from 10 and 13 experiments respectively. **(B)** Extent of spread of the Ca^{2+} wave in Deiters' and Claudius cell regions in control (black bars) and Ru360 treated (grey bars) cultures. Data are mean ± SEM from 10 and 13 experiments respectively. Star indicates $p < 0.05$, Student's paired t-test.

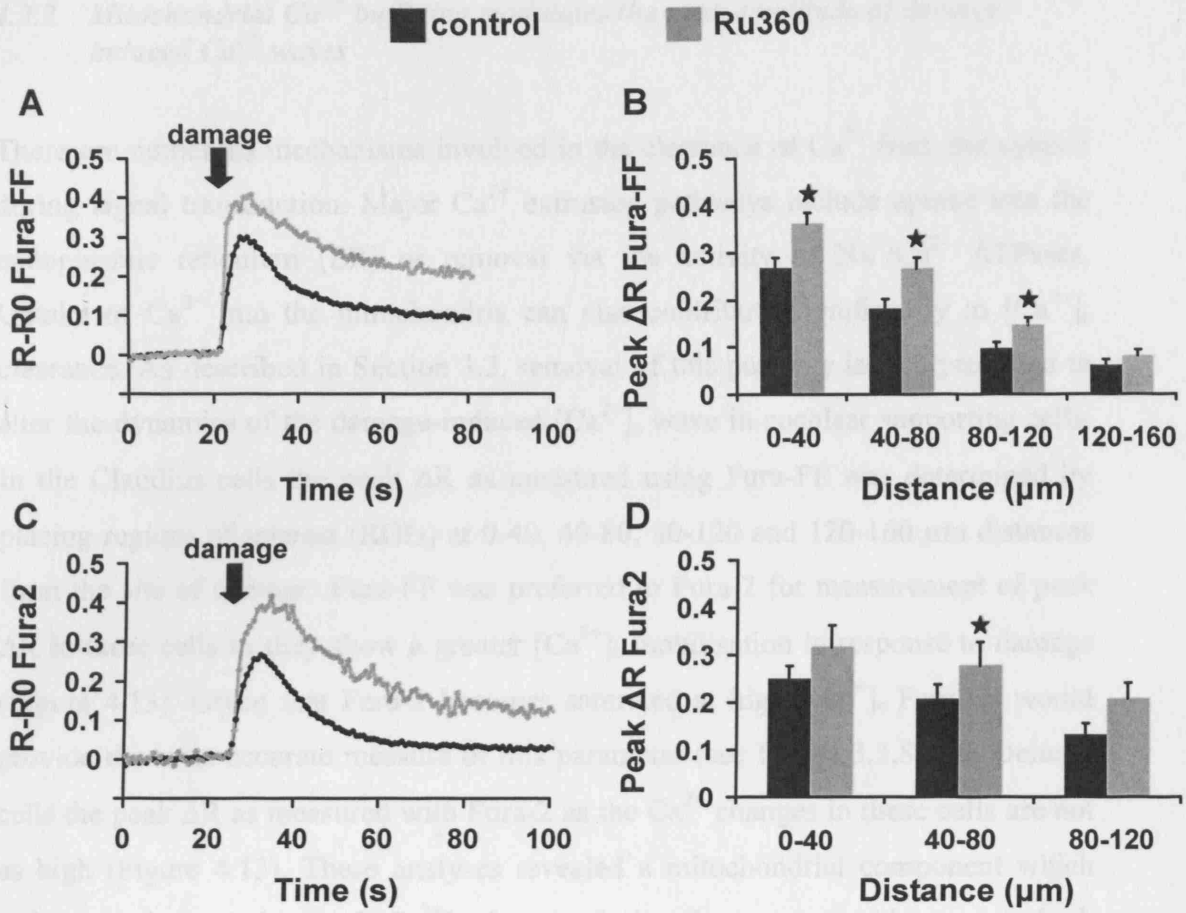

Figure 4. 15 Ru360 enhances the amplitude of damage-induced $[Ca^{2+}]_c$ transients in cochlear supporting cells.

(A) Damage-induced Ca^{2+} transient in Claudius cells for control (black) and Ru360 treated (grey) cultures measured at 60 μm from the damage site.

(B) Peak ΔR Fura-FF for damage-induced Ca^{2+} transients in Claudius cells at increasing distance from the damage site. Data are mean ± SEM from 13 experiments.

(C) Damage-induced Ca^{2+} transient in Deiters' cell region for control (black) and Ru360 treated (grey) cultures 60 μm from the site of damage.

(D) Peak ΔR Fura-FF for damage-induced Ca^{2+} transients in the Deiters' cell region at increasing distances from the site of damage. Data are mean ± SEM from 10 experiments. Stars indicate $p < 0.05$; Student's paired t-test.

4.2.2 *Mitochondrial Ca^{2+} buffering modulates the peak amplitude of damage-induced Ca^{2+} waves*

There are numerous mechanisms involved in the clearance of Ca^{2+} from the cytosol during signal transduction. Major Ca^{2+} extrusion pathways include uptake into the endoplasmic reticulum (ER) or removal via the activity of Na^{+}/Ca^{2+} ATPases. Uptake of Ca^{2+} into the mitochondria can also contribute significantly to $[Ca^{2+}]_c$ clearance. As described in Section 3.3, removal of this pathway is also predicted to alter the dynamics of the damage-induced $[Ca^{2+}]_c$ wave in cochlear supporting cells. In the Claudius cells the peak ΔR as measured using Fura-FF was determined by placing regions of interest (ROIs) at 0-40, 40-80, 80-120 and 120-160 μm distances from the site of damage. Fura-FF was preferred to Fura-2 for measurement of peak ΔR in these cells as they show a greater $[Ca^{2+}]_c$ mobilisation in response to damage (Figure 4.13). Given that Fura-2 becomes saturated at high $[Ca^{2+}]_c$ Fura-FF would provide the most accurate measure of this parameter (see Figure 3.3.8). In Deiters' cells the peak ΔR as measured with Fura-2 as the Ca^{2+} changes in these cells are not as high (Figure 4.13). These analyses revealed a mitochondrial component which influences the magnitude of $[Ca^{2+}]_c$ changes during damage-induced waves in both Claudius and Deiters' cell regions (Figure 4.15).

4.2.3 *Mitochondrial Ca^{2+} uptake is important for recovery to baseline $[Ca^{2+}]_c$ levels*

Uptake of Ca^{2+} is important for restoration of $[Ca^{2+}]_c$ back to baseline levels. The role of mitochondria in restoring $[Ca^{2+}]_c$ levels post-damage was investigated by administering mechanical damage to single hair cells. The half life of the Ca^{2+} wave ($T_{1/2}$) was calculated as the time taken to recover to 50% of its peak amplitude and was measured at 0-40 μm, 40-80 μm, 80-120 μm and 120-160 μm in Claudius cells and at 0-40 μm, 40-80 μm and 80-120 μm in Deiters' cells.

Table 5 Ratio changes for the damage-induced intercellular $[Ca^{2+}]_c$ waves in Claudius cells, measured at increasing distances from the lesion site in controls and Ru360 treated cultures

Distance from damage site (μm)	Peak ΔR (Claudius cells)	Peak ΔR (Claudius cells) With Ru360
0-40	0.26 ± 0.07	0.36 ± 0.08
40-80	0.2 ± 0.07	0.27 ± 0.09
80-120	0.09 ± 0.04	0.14 ± 0.05
120-160	0.06 ± 0.04	0.08 ± 0.04

Table 6 Ratio changes for the damage-induced intercellular $[Ca^{2+}]_c$ waves in Deiters' cells, measured at increasing distances from the lesion site in controls and Ru360 treated cultures

Distance from damage site (μm)	Peak ΔR (Deiters' cells)	Peak ΔR (Deiters' cells) With Ru360
0-40	0.25 ± 0.02	0.32 ± 0.04
40-80	0.21 ± 0.03	0.38 ± 0.05
80-120	0.11 ± 0.02	0.34 ± 0.03

4.2.4 Mitochondrial Ca^{2+} in buffering is important in recovery of $[Ca^{2+}]_c$ after hair cell damage.

The influence of mitochondrial Ca^{2+} buffering is greater in the Claudius cell region compared to the Deiters' cell region (Figure 4.16). Ru360 increased the duration of the signal (time to reach 50 % of its peak) from 13.4 ± 1.4 s to 14.5 ± 1.1 s and 19.6 ± 1.5 s in Deiters' and Claudius cell regions respectively at 40 μm from the site of damage ($p = < 0.05$, Student's paired *t*-test) (Figure 4.16). Ru360 had no significant effect on the duration of the $[Ca^{2+}]_c$ wave at distances greater than 60 μm (data not shown). No significant prolonging of the damage-induced $[Ca^{2+}]_c$ wave was observed at any distance in the Deiters' cell region (Figure 4.16).

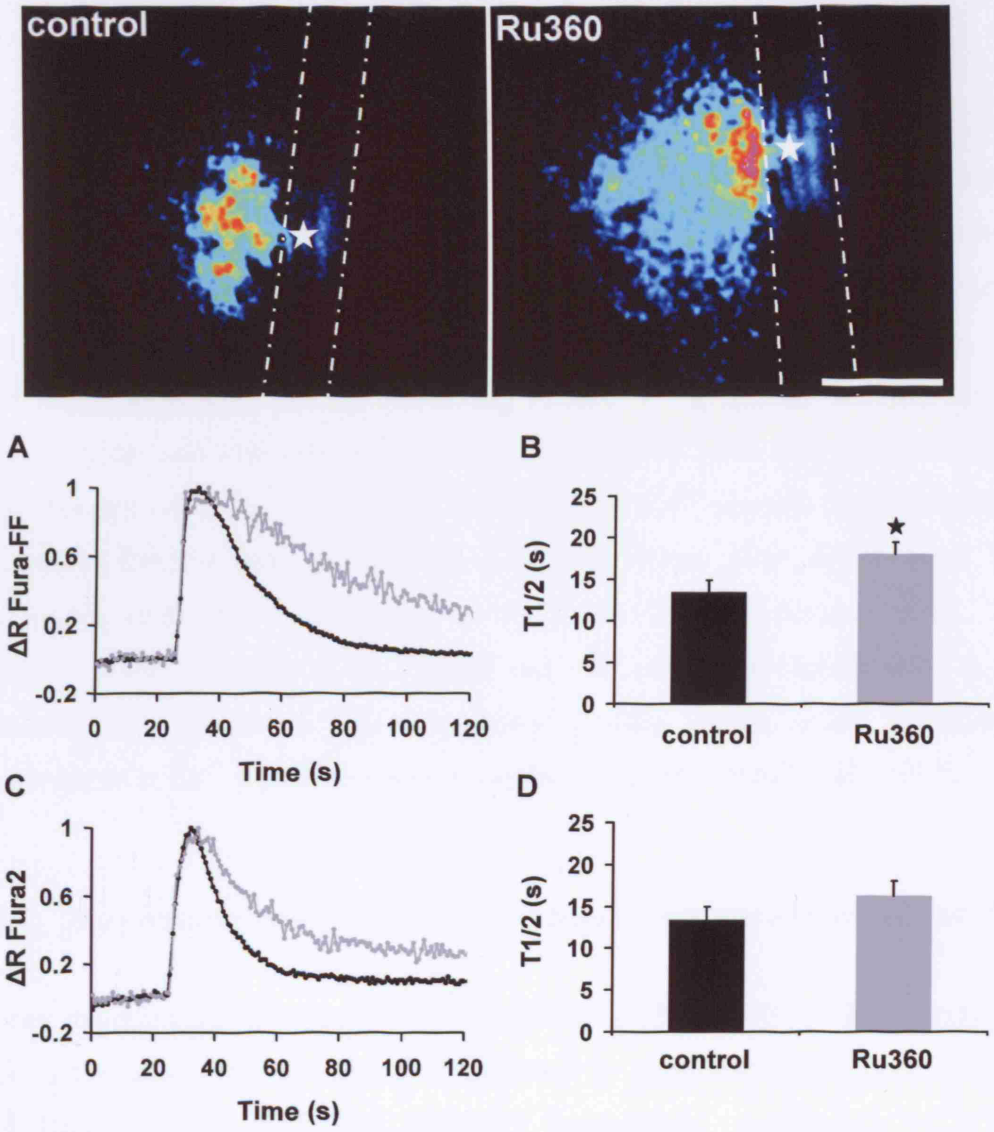

Figure 4. 16 Ru360 prolongs recovery of $[Ca^{2+}]_c$ back to baseline levels.

(Top panel) 15 frame averages from the end of the experiment in control (left) and Ru360 treated (right) cultures. Dotted lines indicate the Deiters' cell region. The damage site is shown by the white star. Scale bar is 100 μm. **(A)** Normalised traces showing duration of the damage-induced Ca^{2+} transient in Claudius cells under control (black) and Ru360 treated (grey) conditions. **(B)** Pooled data for the Claudius cell region indicating the duration of damage-induced Ca^{2+} transients in control and Ru360 treated cultures. Data are mean ± SEM. $P < 0.05$, Student's paired t-test. **(C)** Normalised traces showing duration of the damage-induced Ca^{2+} transient in the Deiters' cell region under control (black) and Ru360 treated (grey) conditions.

(D) Pooled data for the Deiters' cell region indicating the duration of damage-induced Ca^{2+} transients in control and Ru360 treated cultures. Data are mean ± SEM, $p > 0.05$, Student's paired *t*-test.

4.3 Discussion

In the present study I have addressed the following: 1) Do mitochondria sequester Ca^{2+} from the cytosol in cochlear supporting cells during ATP-induced Ca^{2+} signals? 2) What is the relationship between cytosolic and mitochondrial compartments during periods of raised $[Ca^{2+}]_c$? 3) Are mitochondria involved in shaping the spatio-temporal properties of intercellular $[Ca^{2+}]_c$ waves in cochlear supporting cells? Elevations in $[Ca^{2+}]_c$ are key signalling events which activate a wide range of physiological and pathophysiological processes. It is now well documented that mitochondria take up Ca^{2+} during physiological Ca^{2+} signals (see Nicholls and Crompton, 1980; Rizzuto et al., 1994; Werth and Thayer, 1994; Boitier et al., 1999; Hajnoczky et al., 1999; Hajnoczky et al., 2000a; Camello-Almaraz et al., 2002; Duchen, 2004; Andrade et al., 2005) and can contribute significantly to their spatiotemporal properties. There is currently little known about mitochondrial involvement in Ca^{2+} signals in cochlear epithelia (see Mammano et al., 2007).

4.3.1 Mitochondrial and cytosolic Ca^{2+} changes in response to extracellular ATP

In my experiments, application of extracellular ATP reliably evoked increases in $[Ca^{2+}]_c$ throughout the Claudius cells indicated by simultaneous increases in Fura-2 and Rhod-2, or Fura-FF and Rhod-5N fluorescence. Application of ATP at concentrations ranging from 0.01-100 μM was used as a means studying the relationship between mitochondrial and cytosolic compartments at different $[Ca^{2+}]_c$ loads. The ATP-induced $[Ca^{2+}]_c$ signals elicited in cytosolic and mitochondrial compartments displayed distinct amplitudes and temporal properties. On average $[Ca^{2+}]_{mt}$ responses displayed longer half lives compared to those seen in the cytosol. At lower ATP concentrations, a 5 fold difference was apparent between the transient duration of cytosolic and mitochondrial signals. A similar prolongation of the $[Ca^{2+}]_{mt}$ signal has been documented in other cell models (Hajnoczky et al., 1995; Herrington et al., 1996; Jou et al., 1996; Simpson and Russell, 1998; Boitier et al., 1999). Measurement of the peak amplitude of cytosolic and mitochondrial Ca^{2+} transients using Fura-FF and Rhod-2 respectively, revealed a clear difference in magnitude between the two although it must be noted that these measurements were

made using different Ca^{2+} dyes with distinct fluorescent properties and Kd values (Fura-FF 5.6 μM, Rhod-5N 320 μM). The latter would suggest levels of Ca^{2+} accumulated by mitochondria from the cytosol during agonist-induced signalling are greater then those mobilised in the cytosol in response to ATP.

When changes in $[Ca^{2+}]_{mt}$ in response to ATP application were monitored using the high affinity Ca^{2+} indicator Rhod-2 (Kd 1μM), no further increase in fluorescence was observed at concentrations above 1 μM (data not shown). This could be due to either saturation of the mitochondrial Ca^{2+} uptake pathway or saturation of the dye. To test this hypothesis, experiments were repeated using the low affinity Ca^{2+} indicator Rhod-5N (Kd 320 μM). Rhod-5N showed $[Ca^{2+}]_{mt}$ to increase in accordance with ATP concentration up to 10 μM. Large variations in the signal intensity were evident at 50 μM, making it difficult to determine whether it is at this concentration that the signal begins to plateau. Rhod-5N was therefore used to measure changes in $[Ca^{2+}]_{mt}$ throughout the experiments discussed subsequently.

As discussed in Section 1.5.1, the major pathway for Ca^{2+} uptake into mitochondria occurs via the Ca^{2+} uniporter situated on the inner mitochondrial membrane. Ca^{2+} uptake via the uniporter relies on the presence of a Ca^{2+} electrochemical gradient across the mitochondrial inner membrane which provides the driving force for Ca^{2+} entry (see Gunter and Pfeiffer, 1990). The latter is based on the idea that resting $[Ca^{2+}]_{mt}$ is significantly lower than $[Ca^{2+}]_c$ (Puskin and Gunter, 1973). It is not surprising therefore that a greater degree of mitochondrial Ca^{2+} uptake occurs at higher ATP concentrations. In Claudius cells, the effects of CCCP on the properties of $[Ca^{2+}]_c$ transients (discussed in the next section) appeared negligible at ATP concentrations below 1 μM. This suggests that the levels of $[Ca^{2+}]_c$ mobilised at ATP concentrations below 1 μM are not sufficient for uniporter activation. The threshold for net Ca^{2+} uptake via the uniporter is thought to lie within the range of ~100-500 nM $[Ca^{2+}]_c$ (Toescu et al., 1993; Gunter and Gunter, 1994; Moreau et al., 2006).

In Claudius cells, Fura-FF and Rhod-5N fluorescence increased as a function of ATP above concentrations of 0.1 μM. The mobilisation of $[Ca^{2+}]_c$ and uptake of Ca^{2+} into mitochondria at 0.01 μM (indicated by an increase in either Fura-FF or Rhod-5N) were negligible most likely due to the low affinity of both Fura-FF and Rhod-5N.

The steady increase in Fura-FF fluorescence between 0.1 μM and 100 μM ATP shows a continued increase in $[Ca^{2+}]_c$ over this concentration range. In the mitochondria however, a plateau of the Rhod-5N fluorescence was observed at concentrations above 10 μM ATP, indicating either inactivation of the uniporter, no further changes in matrix Ca^{2+} or saturation of Rhod-5N. The Ca^{2+} uniporter can become inactivated at high $[Ca^{2+}]_c$ thus preventing uptake (Moreau et al., 2006). Matrix Ca^{2+} can also be buffered by phosphate (PO_4^{3-}) within the mitochondria. These Ca^{2+} phosphate complexes are thought to buffer matrix Ca^{2+} in the range of 1-5 μM but not at concentrations in the millimolar range (Nicholls and Chalmers, 2004), which might suggest that in this study ATP does not mobilise $[Ca^{2+}]_c$ loads above the micromolar range. The different buffering capacities of the matrix Ca^{2+} phosphate complex at micromolar and millimolar $[Ca^{2+}]_{mt}$ is attributable to changes in matrix pH that accompany the influx of Ca^{2+} into mitochondria (Nicholls and Chalmers, 2004). It is possible that buffering of matix Ca^{2+} by PO_4^{3-} accounts for the plateau in fluorescent signal. Another explanation would be that Rhod-5N becomes saturated at ATP concentrations above 10 μM as in some cell types matrix Ca^{2+} is documented to reach millimolar levels (Montero et al., 2000).

4.3.2 Mitochondrial modulation of ATP-induced Ca^{2+} transients

As discussed in Section 3.3.1, Claudius cell mitochondria take up Ca^{2+} in response to extracellular ATP. Similarly to the mitochondrial Ca^{2+} buffering identified in other cell types (Herrington et al., 1996; Jou et al., 1996; Boitier et al., 1999; Gonzalez et al., 2000), sequestered Ca^{2+} is retained in Claudius cell mitochondria for prolonged periods of time. The prolonged retention of Ca^{2+} in the mitochondria has been linked with modulation of $[Ca^{2+}]_c$ signals in multiple cell types (Werth and Thayer, 1994; Herrington et al., 1996; Boitier et al., 1999; Kennedy, 2002). Under control conditions, $[Ca^{2+}]_c$ and $[Ca^{2+}]_{mt}$ increased in parallel with [ATP]. Blocking of mitochondrial Ca^{2+} uptake with CCCP and oligomycin, enhanced both peak amplitude and duration of the agonist-induced transient at 1, 10 and 50 μM ATP. To rule out the modulation of transients occurring as a result of CCCP-induced cellular ATP depletion, experiments were conducted in the presence of 12.5 μg/μl oligomycin. As described in Section 3.3.1, varying ATP concentrations were used to elicit different $[Ca^{2+}]_c$ loads. Prolongation of the ATP-induced Ca^{2+} signal was most

pronounced at high [ATP]. This highlights a central role for mitochondrial Ca^{2+} buffering under conditions of high $[Ca^{2+}]_c$ load. Although prolonging of the transient was also observed at lower concentrations, it occurred to a lesser extent and was not significant.

It was difficult to accurately determine the exponential time course of ATP-induced Ca^{2+} transients as measurements were made in an epithelium. ATP responses between cells close to the site of application differed from those in cells further away suggesting the [ATP] to vary throughout the epithelium. In a most cases $[Ca^{2+}]_c$ transient evoked by application of ATP recovered with an mono-exponential time course that remained unaltered by CCCP. This finding is consistent with data reported in astrocytes and supports a prolonged retention of Ca^{2+} in the mitochondria (Boitier et al., 1999). In other cell types, Ca^{2+} release from mitochondria subsequent to uptake can shape the $[Ca^{2+}]_c$ (Thayer and Miller, 1990). In astrocytes and Claudius cells, it is possible that because Ca^{2+} remains in the mitochondria for such long periods its efflux is too slow to significantly shape the $[Ca^{2+}]_c$ transient. Taken together, these data show the presence of a mitochondrial buffering mechanism, which is activated at the $[Ca^{2+}]_c$ levels mobilised in responses to [ATP] > 500 nM. Enhancement of the peak amplitude in the presence of CCCP and oligomycin is conflicting with data reported from other cell types. In astrocytes (Boitier et al., 1999), adrenal chromaffin cells (Babcock et al., 1997), HeLa cells (Rizzuto et al., 1992), T lymphocytes (Hoth et al., 1997) and gonadotrophs (Hehl et al., 1996) loss $\Delta\psi_{mt}$ has no effect on the peak amplitude of $[Ca^{2+}]_c$ signals.

4.3.3 Mitochondrial modulation of damage-induced Ca^{2+} waves

Mitochondrial Ca^{2+} uptake is known to be important in determining the amplitude (Herrington et al., 1996; Kennedy, 2002) and spatio-temporal properties (Boitier et al., 1999; Hajnoczky et al., 1999) of $[Ca^{2+}]_c$ signals. As reported by Gale *et al.*, (2004) and Piazza *et al.*, (2007), mechanical damage administered to single hair cells elicited an intercellular $[Ca^{2+}]_c$ wave that propagated away from the damage site into the Claudius and Deiters' cell regions. It has been suggested, that such waves may play a role in proliferation (Piazza et al., 2007), the activation of programmes controlling gene transcription (Gale et al., 2004) and the regulation of K^+ recycling

(Piazza et al., 2007). One aspect investigated in this chapter, was the ability of mitochondria to regulate the spatiotemporal properties and amplitude of these waves. In this study, mitochondria Ca^{2+} buffering was found to modulate the localised spread, amplitude and duration of damage-induced intercellular Ca^{2+} waves in cochlear supporting cells

Mechanical damage to single outer hair cells was used to induce intercellular $[Ca^{2+}]_c$ waves in the Claudius and Deiters' cell regions. Mechanical damage is known to elicit a regenerative, IP_3-dependent Ca^{2+} wave thought to depend on ATP release from compromised cells (Gale et al., 2004; Piazza et al., 2007). As measured with Fura-2, control waves propagated with an average velocity of 11.2 and 12.3 μm/s and spread up to 164 and 154 μm in Claudius and Deiters' cell regions respectively. These parameters are characteristic of mechanically-induced intercellular Ca^{2+} waves observed in astrocytes (Wang et al., 1997). To address the question of whether mitochondria play a functional role in the propagation of these waves, the Ca^{2+} uniporter was blocked using the selective inhibitor Ru360. This inhibitor was chosen in place of CCCP, as positive controls showed the uncoupler to alter baseline $[Ca^{2+}]_c$ levels in some cultures. In the absence of mitochondrial Ca^{2+} buffering, waves displayed a similar regenerative behaviour but with significant changes in the spatio-temporal properties to controls. In both Claudius and Deiters' cell regions, waves elicited in the presence of Ru360 presented with a 1.4 fold increase in propagation velocity. This demonstrates that mitochondria exert a negative influence on the propagation velocity of intercellular $[Ca^{2+}]_c$ waves and is consistent with data reported previously for the propagation of intracellular $[Ca^{2+}]_c$ waves in cortical astrocytes (Boitier et al., 1999).

The negative feedback effect exerted by mitochondria can be explained through their ability to influence the activity of IP_3 receptor (IP_3R) Ca^{2+}-release channels. As described in Section 1.5.4, the initiation and propagation of Ca^{2+} waves is thought to depend on the release of IP_3 in stimulated cells (see Section 1.5.4). Released IP_3 can then diffuse via intra and intercellular pathways (Hajnoczky et al., 1999; Beltramello et al., 2005) away from the release site. Regulation of IP_3Rs can thus be considered a major determinant of Ca^{2+} wave propagation. In hepatocytes, mitochondria are positioned in close proximity to the ER, which is enriched with IP_3R Ca^{2+}-release

channels (Hajnoczky et al., 1999). In these cells, removal of mitochondrial Ca^{2+} buffering sensitises IP_3R Ca^{2+}-release channels to sub maximal concentrations of IP_3. This results in amplification of Ca^{2+} release from the ER. When mitochondrial Ca^{2+} buffering is active, Ca^{2+} release from the ER is reduced. This phenomenon would therefore explain the slowed propagation velocity of control waves. It is possible therefore that mitochondria in supporting cells suppress the positive feedback effects exerted by Ca^{2+} on the IP_3R allowing them to shape patterns of Ca^{2+} release. This would agree with observations made in the hepatocyte cell model (Hajnoczky et al., 1999). Similar to data obtained using endogenous Ca^{2+} chelators (Wang et al., 1997), Claudius cell mitochondria function as spatial buffers. The mitochondrial Ca^{2+} buffering capacity is low enough to permit wave propagation, but sufficient to restrict Ca^{2+} signalling to a localised range in cochlear epithelia.

$[Ca^{2+}]_c$ has distinct regulatory effects on type 1 and type 2 IP_3Rs. The type 1 IP_3Rs exhibit inactivation at high $[Ca^{2+}]_c$, whereas the type 2 IP_3Rs do not. The determinant of whether mitochondria exert a positive or negative effect on $[Ca^{2+}]_c$ wave propagation is likely to depend on the IP_3R expression profile. The type 2 IP_3R is the predominant subtype expressed is cultured cortical astrocytes (see Boitier et al., 1999). Astrocytic mitochondria are also located in close proximity to IP_3Rs, allowing them to modulate receptor sensitivity (Sheppard et al., 1997). In this model, local buffering of Ca^{2+} by mitochondria can regulate the gating kinetics of the type 2 IP_3R. A reduction in $[Ca^{2+}]_c$ around the mouth of the IP_3 channel results in desensitisation of the receptor to IP_3. This reduces levels of IP_3-dependent Ca^{2+} release and consequently the magnitude of IP_3-induced $[Ca^{2+}]_c$ transients. Reduced $[Ca^{2+}]_c$ will also restrict the amount of Ca^{2+} available for diffusion to other IP_3Rs thus dampening the regenerative intracellular $[Ca^{2+}]_c$ wave propagation (Boitier et al., 1999). As removal of mitochondrial Ca^{2+} buffering had similar effects in Claudius cells, Deiters' cells and astrocytes it is proposed that the IP_3 receptor profile between astrocytes and cochlear supporting cells is comparable.

In addition to the effects on propagation velocity, Ru360 also prolonged recovery of $[Ca^{2+}]_c$ back to baseline levels, the peak amplitude of the signal and the extent by which the signal spread. This demonstrates that mitochondria also regulate the temporal properties of damage-induced Ca^{2+} waves. Mitochondrial regulation of

$[Ca^{2+}]_c$ changes in Claudius and Deiters' cells was similar for both ATP induced Ca^{2+} mobilisation (see Section 3.3.2) and damage-induced responses. This indicates that once initiated, the $[Ca^{2+}]_c$ wave in cochlear supporting cells may be regulated by a conserved mechanism.

Dysregulation of intercellular Ca^{2+} waves in Claudius and Deiters cells may affect a number of processes within the cochlea. Firstly, amplification of Ca^{2+} waves may alter the homeostatic environment necessary for hair cell function, leading to impairment of mechanosensory transduction. In another model, the propagation of intercellular Ca^{2+} waves throughout the supporting cell syncytium is suggested to modulate sound-induced gene expression through activation of downstream effectors such as MAP-kinases (Gale et al., 2004). The differential activation of transcription factors in B lymphocytes has also been linked with the amplitude and duration of $[Ca^{2+}]_c$ transients. In that study, the transcriptional regulators NF-κB and c-Jun N-terminal kinase (JNK) were activated at high amplitude $[Ca^{2+}]_c$ and the ubiquitous transcription factor NFAT (involved in cell-cell interactions) in response to low amplitude signals (Dolmetsch et al., 1997). The differential activation of these pathways by $[Ca^{2+}]_c$ reflects intrinsic differences in Ca^{2+} sensitivity (Dolmetsch et al., 1997). In neonatal cochlear explants, both JNK (Gale et al., 2004) and extracellularly regulated kinase 1/2 (ERK 1/2) (Lahne M., Gale J.E. unpublished data) are activated following mechanical damage in localised areas surrounding the lesion site. It is possible therefore that the extent of MAP-kinase activation and the specific kinase activated may be altered by modulating the spatio-temporal profile of damage-induced Ca^{2+} waves.

5 Early signalling events in neomycin-induced hair cell toxicity

Aminoglycosides are the most commonly used antibiotics worldwide for the treatment of gram negative bacterial infections. Their broad antibacterial spectrum and bactericidal properties allow them to kill and prevent the growth of a wide range of pathogenic bacteria. One of the major complications of aminoglycoside use in patients is ototoxicity, in which both cochlear and vestibular systems are vulnerable. Treatment of cochlear and vestibular cultures with aminoglycosides results in the selective loss of hair cells. The hair cells in both cochlear and vestibular systems display a differential sensitivity to aminoglycosides. In the cochlea, basal hair cells are more vulnerable than apical hair cells and in the vestibular system, type I hair cells are more sensitive than type II hair cells (see Forge and Schacht, 2000). In this chapter I describe my studies of the acute effects of the aminoglycoside neomycin on the cellular patho-physiology of cochlear explant cultures. Previous studies have linked aminoglycoside toxicity with release of the mitochondrial matrix proteins cytochrome c, AIF and EndoG (Wang et al., 2004; Jiang et al., 2006), all of which promote apoptotic cell death. There are also data to suggest that Ca^{2+} overload and activation of the MAPK pathways play an important role in the pathology associated with these drugs (Hirose et al., 1999; Gale et al., 2001; Matsui et al., 2004). I therefore set out to investigate the acute effects of neomycin on $[Ca^{2+}]_c$ and $[Ca^{2+}]_{mt}$ and on mitochondrial physiology.

5.1.1 Neomycin induces rapid changes in $[Ca^{2+}]_c$ in OHCs

Until recently (Owens et al., 2007), there have been few studies investigating the early signalling mechanisms involved in aminoglycoside toxicity. In the present study, Fura-2 was used to monitor changes in $[Ca^{2+}]_c$ in cochlear explants over 4 hours of neomycin treatment. Although previous studies show neomycin to modulate the transducer current at concentrations between 3μM - 50μM (Marcotti et al., 2005), in my experiments, a supramaximal dose of 1 mM neomycin was used. This concentration is known to reliably induce hair cell death under *in vitro* conditions. In patients, it is difficult to determine the concentration of aminoglycosides that cause

deafness as there is currently no non-invasive method by which to sample cochlear fluids in which neomycin is believed to become concentrated. The time course of hair cell death in patients also occurs over much longer time periods, presumably because doses of drug used clinically are much lower (Forge and Schacht, 2000).

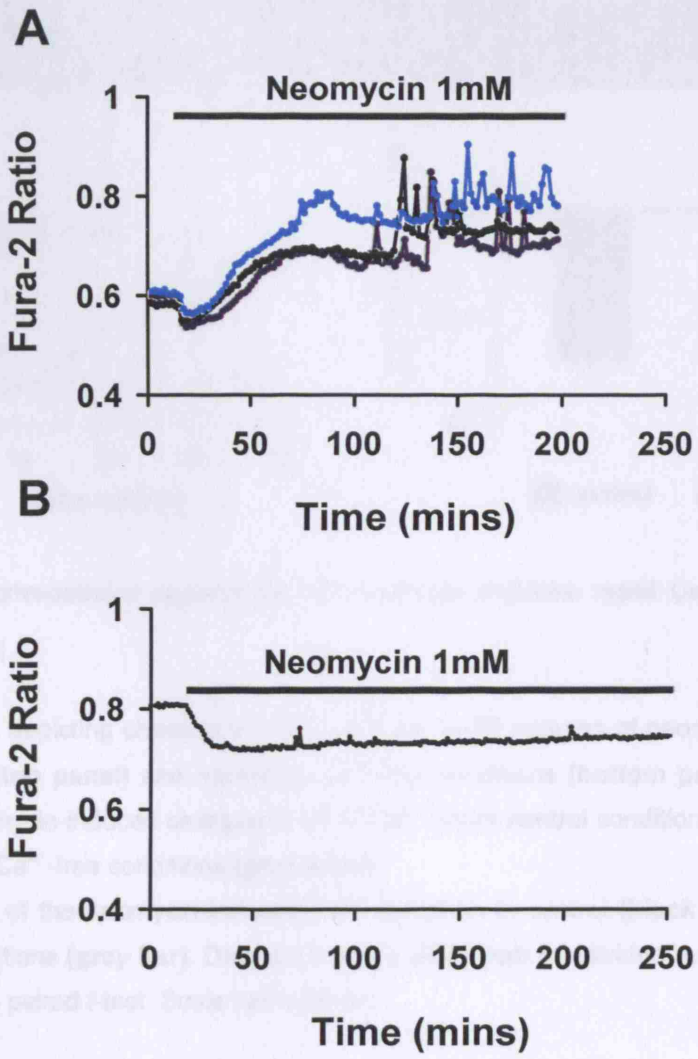

Figure 5. 1 Neomycin-induces a biphasic $[Ca^{2+}]_c$ response in OHCs

(A) Representative traces of neomycin-induced Ca^{2+} changes measured from 3 OHCs over a period of 3.3h. Black bar represents the presence of neomycin. Note that some Ca^{2+} signal is incorporated from the surrounding Deiters' cells between 100-200 mins.
(B) Averaged trace from 6 OHCs showing the changes in $[Ca^{2+}]_c$ following neomycin application in nominally Ca^{2+}-free conditions. Black bar represents the presence of neomycin. Traces are representative of responses in OHCs measured from 6 cultures. Black bars indicate the presence of neomycin.

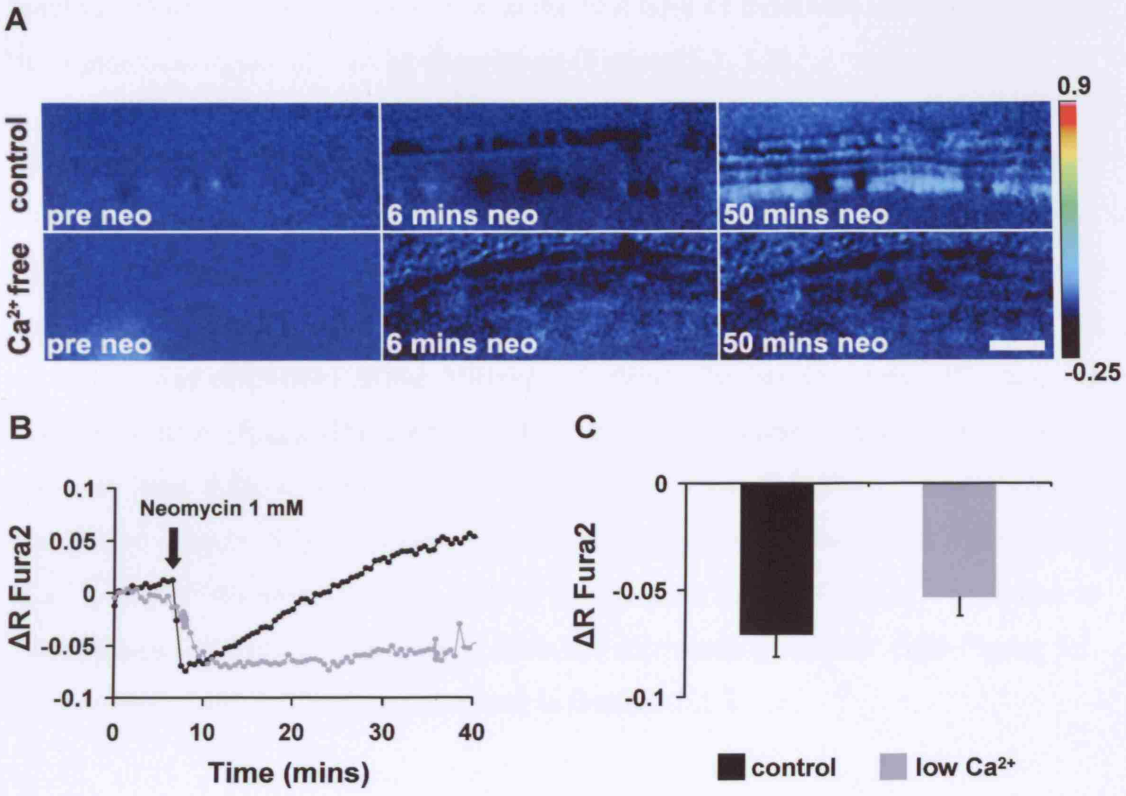

Figure 5. 2 Extracellular application of neomycin induces rapid Ca^{2+} changes in OHCs.

(A) ΔR images depicting changes in OHC Ca^{2+} during 50 minutes of neomycin treatment under control **(top panel)** and nominally Ca^{2+}-free conditions **(bottom panel)**. **(B)** Time course of Neomycin-induced changes in OHC Ca^{2+} under control conditions **(black trace)** and nominally Ca^{2+}-free conditions **(grey trace)**.
(C) Magnitude of the neomycin-induced Ca^{2+} reduction in control **(black bar)** nominally Ca^{2+}-free conditions **(grey bar)**. Data are mean ± SEM from 6 individual experiments. p = 0.22, Student's paired *t*-test. Scale bar is 50 um.

In neonatal rat cochlear cultures, bath application of 1 mM neomycin induced a biphasic change in $[Ca^{2+}]_c$ in OHCs (Figure 5.1). The response was characterised by an immediate reduction in $[Ca^{2+}]_c$ in OHCs (phase 1) followed by a progressive and sustained increase in $[Ca^{2+}]_c$ (phase 2).

In control recording media (HBSS pH 7.4 containing 1.2 mM Ca^{2+}) the average drop in Fura-2 fluorescence (measured from responding cells in 4 cultures) was 0.07 ± 0.01 ratio units (Figure 5.2). Phase 1 was followed by an increase in $[Ca^{2+}]_c$ above

baseline, which reached a plateau within the first hour of treatment and was sustained throughout the remainder of the experiment (Figures 5.1, 5.2).

The kinetics of the neomycin-induced increase (phase 2) in $[Ca^{2+}]_c$ were determined by calculating the time taken to reach 50% of the peak Fura-2 ratio ($t_{1/2}$) (over the first hour of neomycin treatment). The $t_{1/2}$ for the neomycin-induced $[Ca^{2+}]_c$ increase was 21 ± 3 s as measured from 4 cultures. The peak ratio change in response to neomycin was calculated as the difference between the baseline ratio (R0) and the maximum ratio (R_{max}). The increase in Fura-2 fluorescence during phase 2 of the response was 0.06 ± 0.01 ratio units (measured from 4 cultures) under control conditions (Figure 5.2). Towards the end of recordings in neomycin intercellular $[Ca^{2+}]_c$ waves (displayed as Ca^{2+} spikes) can be seen in the OHC Ca^{2+} trace due to incorporation of Fura-2 fluorescence from the surrounding Deiters' cells Figure 5.1. These phenomena will be discussed later in Section 5.1.3.

5.1.2 Reduction of external Ca^{2+} alters the neomycin-induced Ca^{2+} increase in OHCs but not the decrease

Phase 1 of the neomycin-induced $[Ca^{2+}]_c$ response observed in OHCs persisted under nominally Ca^{2+}-free conditions (estimated to be 20 μM). There was also no significant difference ($p = 0.22$, Student's paired *t*-test) in the extent of the reduction in $[Ca^{2+}]_c$ between control and nominally Ca^{2+}-free conditions. In nominally Ca^{2+}-free conditions the drop in Fura-2 ratio was 0.053 ± 0.008 ratio units (Figure 5.2). However, phase 2, the increase in $[Ca^{2+}]_c$ was no longer observed in nominally Ca^{2+}-free conditions (Figure 5.2). These observations indicate that phase 2 of the neomycin response is dependent upon Ca^{2+} influx.

5.1.3 Neomycin-induced hair cell death correlates with $[Ca^{2+}]_c$ waves in cochlear supporting cells

It has been documented that aminoglycosides can induce membrane permeablisation and subsequent apoptosis in cochlear hair cells (Forge, 1985; Dehne et al., 2002). Aminoglycoside-induced hair cell death has also been linked previously with increased $[Ca^{2+}]_c$ within hair cells of utricular epithelia (Matsui et al., 2004).

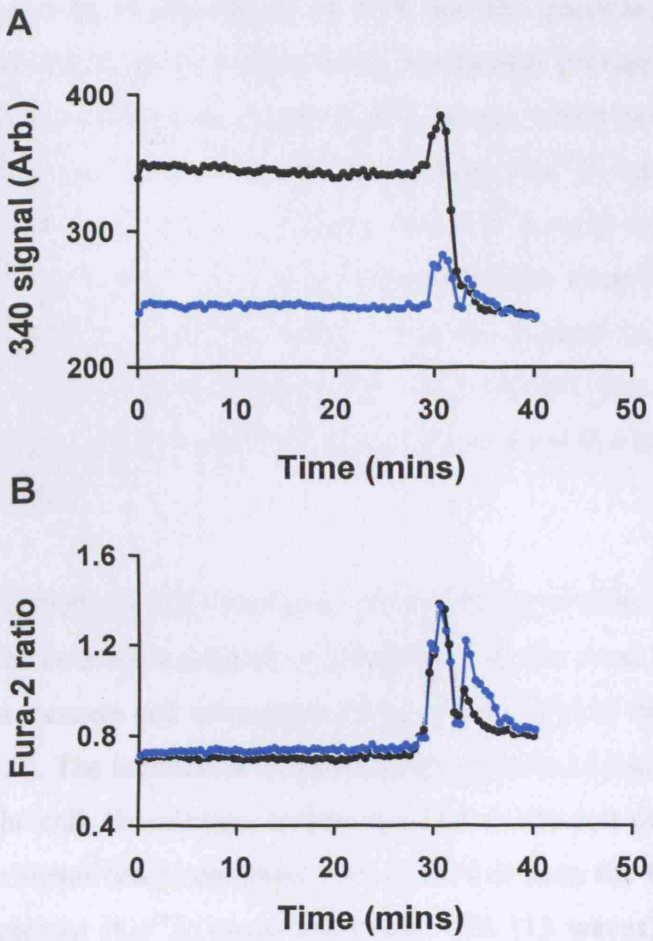

Figure 5. 3 Neomycin-induced changes in OHC $[Ca^{2+}]_c$ prior to the onset of intercellular $[Ca^{2+}]_c$ waves

Traces depict the changes occurring in $[Ca^{2+}]_c$ in a single OHC and the associated intercellular $[Ca^{2+}]_c$ wave occurring at 3h 25 minutes after neomycin addition.

(A) Neomycin-induced changes in $[Ca^{2+}]_c$ as indicated by changes in Fura-2 fluorescence excited at 340 nm. **Black trace** shows the increase and subsequent decrease in 340 signal in OHCs immediately prior to onset of an intercellular $[Ca^{2+}]_c$ wave in the surrounding supporting cells. **Blue trace** shows the changes in $[Ca^{2+}]_c$ in the Deiters' cells following lysis of the compromised OHC.

(B) Neomycin-induced changes in $[Ca^{2+}]_c$ as indicated by changes in the Fura-2 ratio. **Black trace** shows the neomycin-induced ratio changes in a compromised OHC prior to onset of the wave. **Blue trace** shows the intercellular $[Ca^{2+}]_c$ wave in the Deiters' cell region. Traces are representative of responses measured in 53 OHCs from 6 independent experiments.

The hypothesis explored here is whether neomycin-induced hair cell permeabilisation results in the release of ATP and the generation of intercellular $[Ca^{2+}]_c$ waves. As discussed in Section 4.3.3, mechanical damage to a single OHC elicited an ATP-dependent intercellular $[Ca^{2+}]_c$ wave, which propagated into the surrounding supporting cells. A similar intercellular $[Ca^{2+}]_c$ was observed in the supporting cells during neomycin treatment. This $[Ca^{2+}]_c$ wave was associated with the death or lysis of an OHC. The loss of OHC membrane integrity was determined by monitoring the 340 and 380 nm Fura-2 signals. A drop in both signals was considered to indicate a permeabilisation of the cell and thus loss of the dye. Analysing in this way revealed that these events did occur with a peak between 2 and 3 hours of treatment.

Coincident loss of both signals (excited at 340 and 380 nm) from an OHC was used to indicate loss of membrane integrity. Coincident with the onset of an intercellular $[Ca^{2+}]_c$ wave, an increase and subsequent drop was observed in the 340nm signal in OHCs (Figure 5.3). The increase in 340 nm signal indicates an increase in OHC Ca^{2+} before lysis of the cell. On average, an increase of 8 ± 2 % was observed in the 340 nm fluorescence signal before complete loss of the dye from the OHC (Figure 5.3). Of the 76 intercellular $[Ca^{2+}]_c$ waves measured, 17% (13 waves) did not coincide with a loss of 340 nm fluorescence from the compromised OHC 13% (10 waves) coincided with only a drop in 340 nm fluorescence and 70% (53 waves) were preceded by the late bi-phasic change in OHC $[Ca^{2+}]_c$ shown Figure 5.3.

Neomycin-induced intercellular $[Ca^{2+}]_c$ waves that occurred in cochlear cultures treated with 1 mM neomycin (Figures 5.4, 5.5) had similar characteristics to those elicited using mechanical damage in that they propagated from single OHCs into the Deiters' cells (Figure 5.4), Claudius cells (Figure 5.5) or both regions simultaneously (image not shown). As stated previously, 83% (10 waves showing only a loss of 340 nm fluorescence and 53 waves displaying the bi-phasic change in 340 nm signal) of waves correlated with the loss of Fura-2 fluorescence excited at 340 nm from the OHCs. Analysis of the frequency of this event was limited to 4 hours of neomycin treatment, as all 6 experiments covered this time period. Over the time period of 4-8 hours, an additional 13 out of 13 waves were also found to correlate with loss of 340 and 380 nm Fura-2 fluorescence (data not shown). The first intercellular $[Ca^{2+}]_c$

waves were observed most frequently at ~ 90-120 minutes after the addition of neomycin (Figure 5.6).

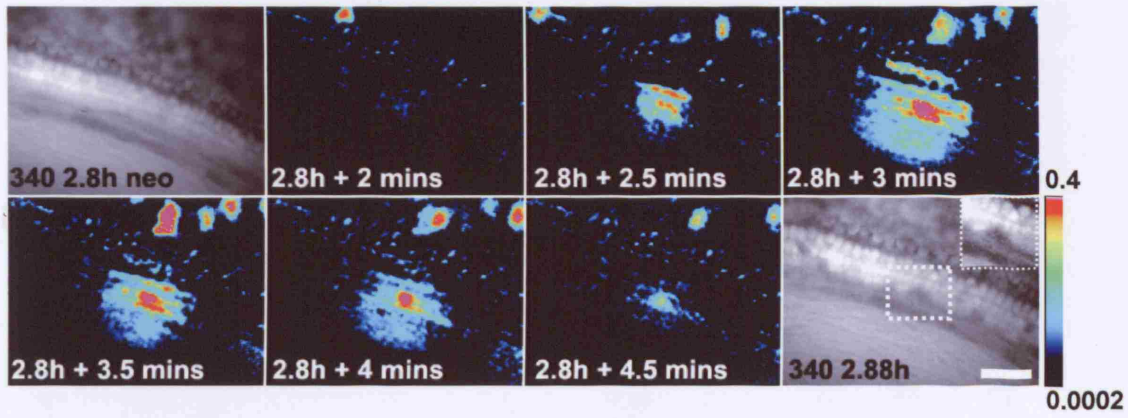

Figure 5. 4 Neomycin causes $[Ca^{2+}]_c$ waves in the Deiters' cell region of cochlear cultures.

Single R-R0 images from a time series. Image sequence left to right depicts the time-course of a neomycin-induced $[Ca^{2+}]_c$ wave in the Deiters' cell region. First and last images show the Fura-2 fluorescence excited at 340 nm at the start and end of the event. Inset shows loss of 340 nm fluorescence from a single OHC, representing the origin of the Ca^{2+} wave. Scale bar is 50 um.

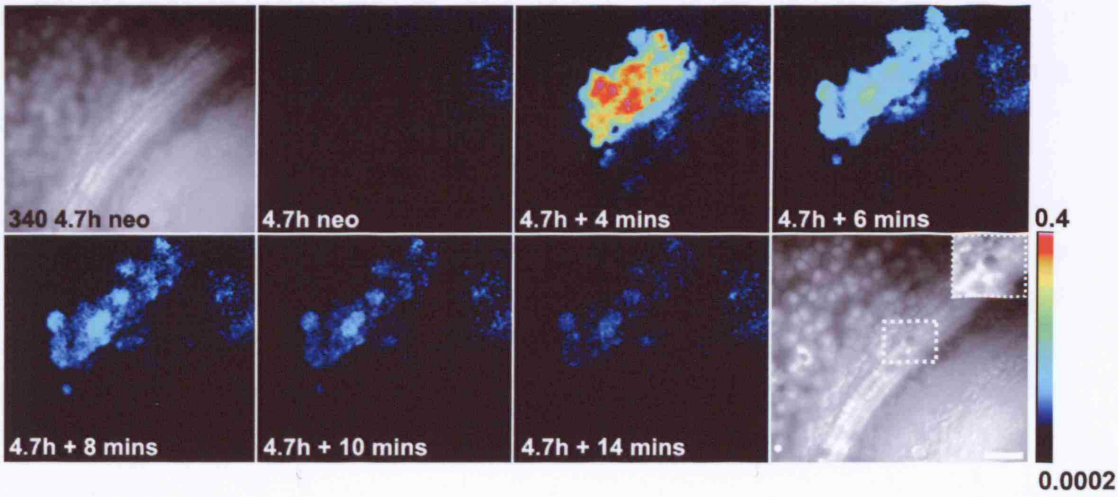

Figure 5. 5 Neomycin causes $[Ca^{2+}]_c$ waves in the Claudius cell region of explant cochlear cultures.

Single R-R0 images from a time series. Image sequence left to right depicts the time-course of a neomycin-induced $[Ca^{2+}]_c$ wave in the Claudius cell region. The first and last images show the Fura-2 fluorescence excited at 340 nm, before and after the Ca^{2+} wave. The inset shows loss of 340 nm fluorescence from a single OHC, depicting the origin of the wave. Scale bar is 50 um.

A frequency histogram (Figure 5.6) was generated by separating the individual events (intercellular Ca^{2+} wave or loss of 340 signal) into time bins of 30 minutes over a period of 0-240 minutes (4h).

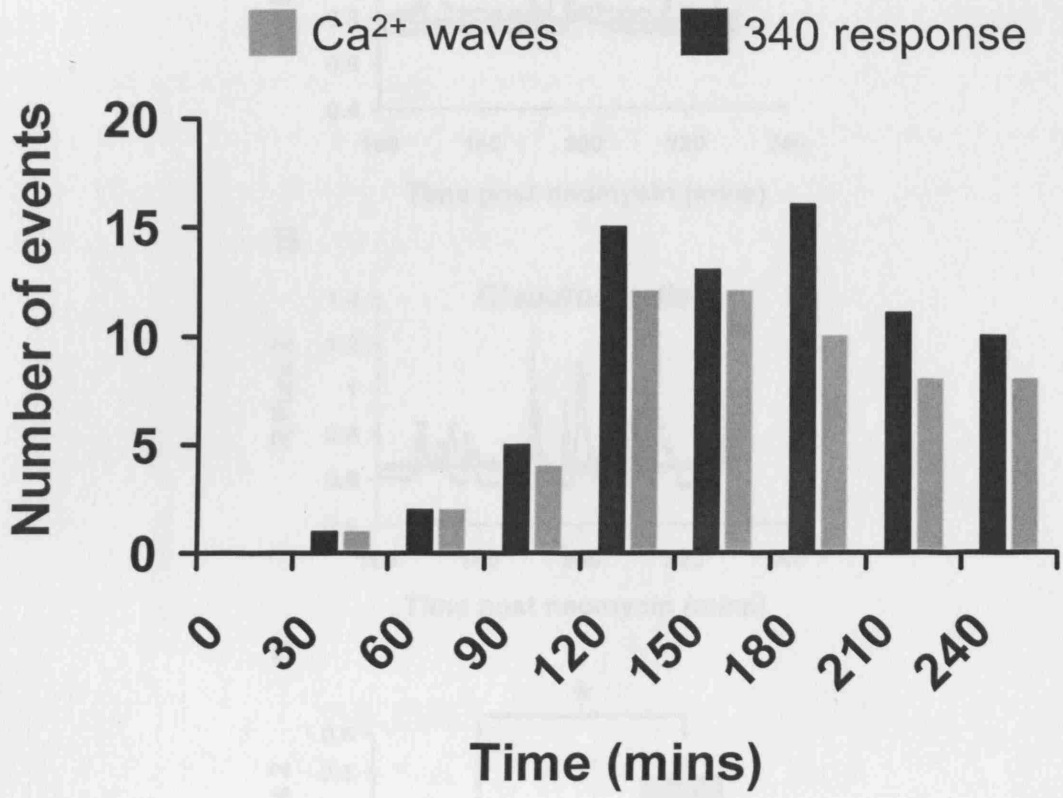

Figure 5. 6 $[Ca^{2+}]_c$ waves in Deiters' and Claudius cells correlate with permeabilisation of ohcs.

Frequency histogram showing the timing of neomycin-induced events in the Deiters' and Claudius cell regions over a period of 4 hours (30 minute bins). **Black bars** represent the onset of an intercellular $[Ca^{2+}]_c$ wave. **Grey bars** indicate the loss of 340 nm Fura-2 fluorescence due to permeabilisation of an OHC. Histogram represents pooled data from 76 waves measured from 6 individual experiments over 4 hours of neomycin treatment.

To study the properties of the neomycin-induced Ca^{2+} wave in more detail, the interval time between sequential images was reduced from 2 minutes to 30 seconds. From a total of 8 waves measured from 4 cultures (with the 30 second time interval), the peak amplitude of $[Ca^{2+}]_c$ transient was significantly ($p < 0.01$, Student's paired *t*-test) greater in the Claudius cells (peak Fura-2 ratio 1.48, 0.5) compared to Deiters' cells (peak Fura-2 ratio 1.01, ΔR 0.33) (Figure 5.7).

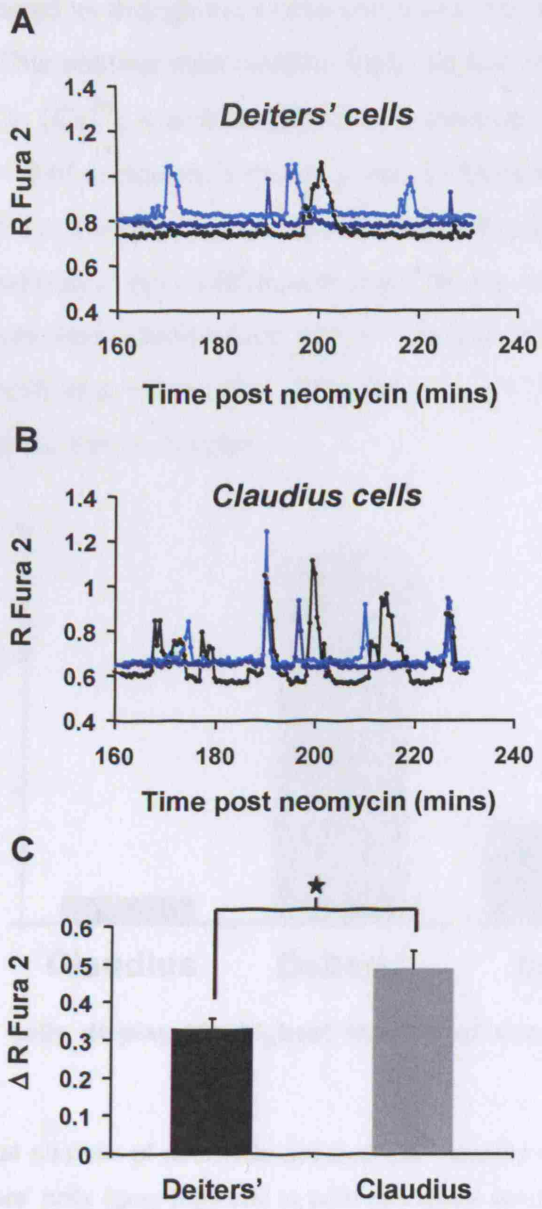

Figure 5. 7 Amplitude of neomycin-induced $[Ca^{2+}]_c$ is greater in Claudius cells than Deiters' cells.

(A) Fura-2 ratio changes (ΔR) recorded from 6 $[Ca^{2+}]_c$ waves occurring in three Deiters' cells during the 80 minute time period.

(B) Fura-2 ratio changes for 12 neomycin-induced $[Ca^{2+}]_c$ waves measured from three ROIs in the Claudius cell region over the 80 minute time period.

(C) Pooled data showing the amplitude of neomycin-induced $[Ca^{2+}]_c$ in the Deiters' **(black)** and Claudius cell **(grey)** regions. Data are mean ± SEM, from 8 waves originating from 8 OHCs in 4 cultures for Deiters' and Claudius cells. p = 0.014, Student's paired *t*-test.

In some cases it appeared as though more than one wave was occurring in the same region (Figure 5.8). This phenomenon resulted from the loss of membrane integrity in neighbouring OHCs. $[Ca^{2+}]_c$ waves displayed ratio changes (ΔR) of 0.33 ± 0.02 and 0.48 ± 0.08 ($p = 0.014$, Student's paired *t*-test) in Deiters' and Claudius cells respectively (Figure 5.8). These data show that the two cell types respond differently to the same damage stimulus. Such differences could be due to variation in receptor expression profiles and thus mechanisms of Ca^{2+} mobilisation between the two. These differences could also result from differences in ER Ca^{2+} content or Ca^{2+} buffering mechanisms between cell types.

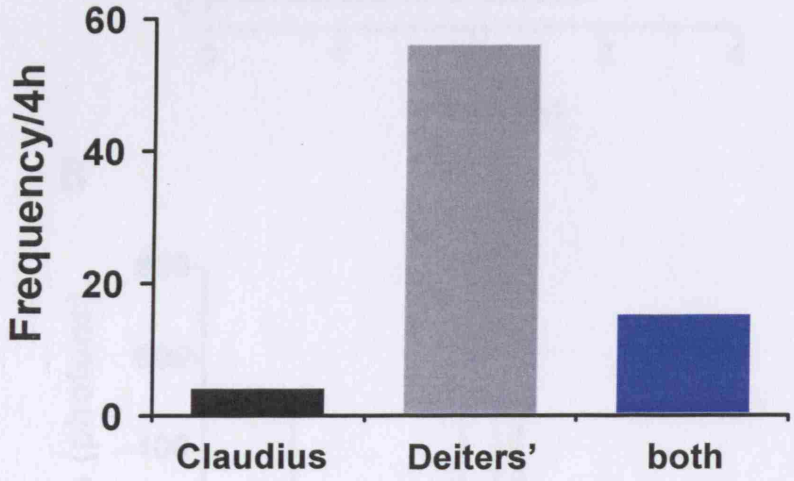

Figure 5. 8 Deiters' cells display the highest number of neomycin-induced Ca^{2+} waves.

Chart displays the total number of neomycin-induced Ca^{2+} events occurring in Claudius cells (black bar), Deiters' cells (grey bar) and in both cell types simultaneously (blue bar). Data are from a total of 76 waves measured in 6 cultures.

Of the total number of neomycin-induced events (76) recorded over 4h of neomycin treatment in 6 separate experiments (including waves imaged using slow and fast time intervals), 56 occurred in the Dieters' cell region, 8 in the Claudius cell region and 12 in both regions simultaneously (Figure 5.8). The intercellular Ca^{2+} waves occuring exclusively in the Claudius cells (Figure 5.8) and those that propagated into both regions simultaneously coincided predominantly with the loss of 340 fluorescence (see Section 5.1.3) from multiple OHCs in close proximity.

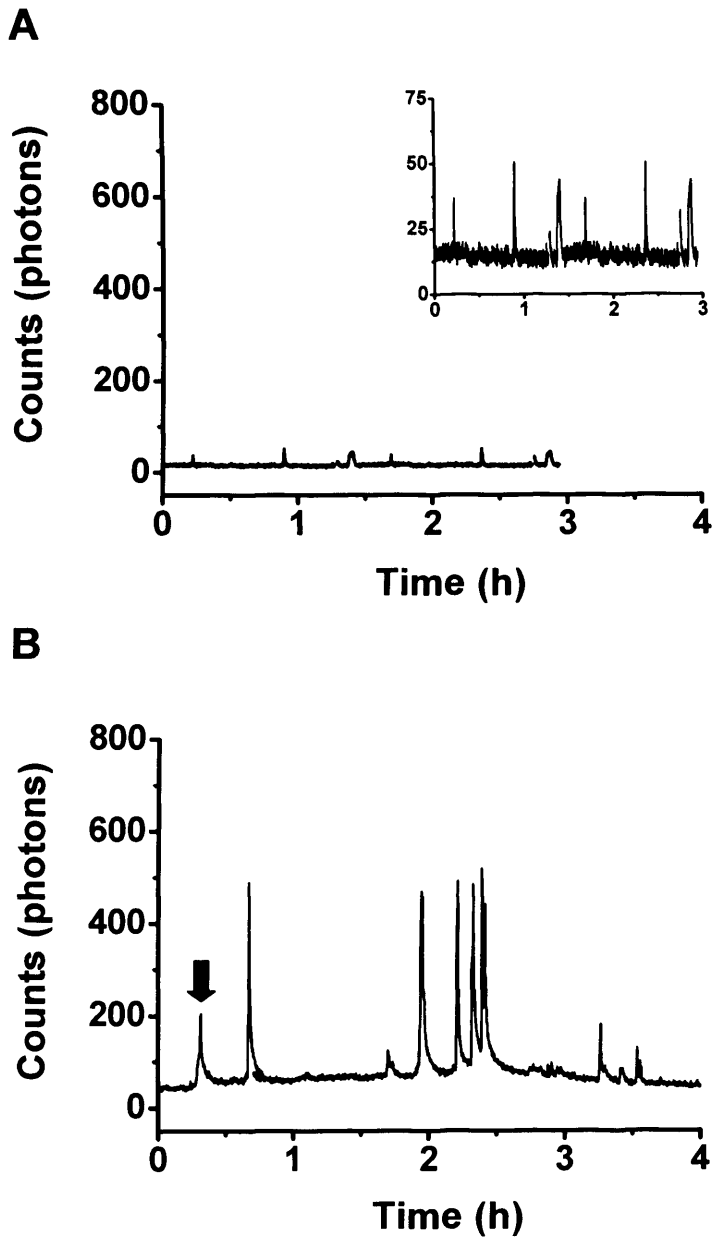

Figure 5. 9 Neomycin treatment causes transient increases in extracellular ATP

(A) Spontaneous changes in extracellular ATP in a cochlear explant under control conditions measured using the luciferin-luciferase assay. Changes in luminescence were recorded using a highly sensitive photon counting PMT system (see Methods). **Inset** shows the same trace on an expanded Y axis. **(B)** Neomycin-induced changes in extracellular ATP recorded from a cochlear culture over a period of 4 h following exposure to 1mM neomycin. ATP release was monitored using the luciferin-luciferase bioluminescence assay. An increase in extracellular ATP is represented by a greater number of photons. The time of neomycin addition is represented by the black arrow.

Those recorded in the Deiters' cells were due to the loss of membrane integrity from a single OHC. These observations suggest that a larger damage stimulus is required to elicit intercellular $[Ca^{2+}]_c$ waves in Claudius cells or both Deiters' and Claudius cells simultaneously compared to in the Deiters' cell region alone.

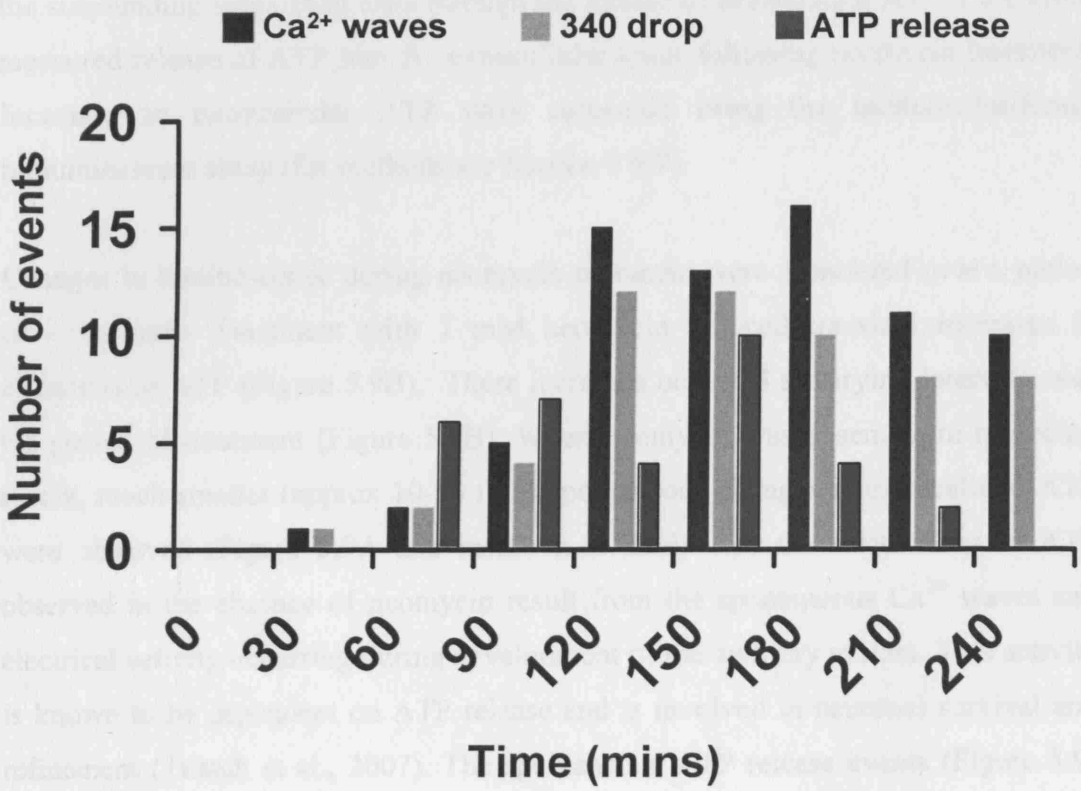

Figure 5. 10 Correlation between $[Ca^{2+}]_c$ waves, OHC permeabilisation and release of extracellular ATP.

Histogram showing the frequency and timing of neomycin-induced events in cochlear explants. **(Black bars)** indicate the number of neomycin-induced $[Ca^{2+}]_c$ waves occurring at various intervals over a period of 4h after neomycin addition. **(Grey bars)** The number of cells in which loss of 340 nm Fura-2 fluorescence is observed due to permeabilisation of an OHC. **(Blue bars)** The number of ATP release event occurring at various time intervals over a period of 4h.

Those recorded in the Deiters' cells were due to the loss of membrane integrity from a single OHC. These observations suggest that a larger damage stimulus is required to elicit intercellular $[Ca^{2+}]_c$ waves in Claudius cells or both Deiters' and Claudius cells simultaneously compared to in the Deiters' cell region alone.

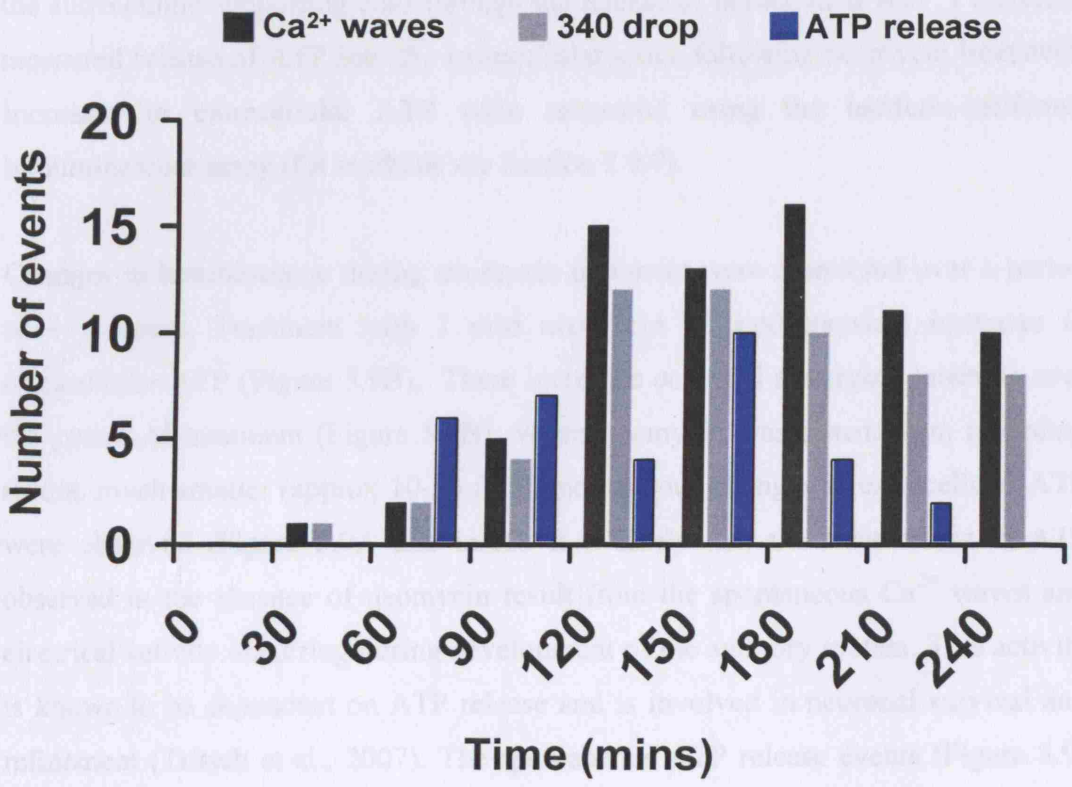

Figure 5. 10 Correlation between $[Ca^{2+}]_c$ waves, OHC permeabilisation and release of extracellular ATP.

Histogram showing the frequency and timing of neomycin-induced events in cochlear explants. **(Black bars)** indicate the number of neomycin-induced $[Ca^{2+}]_c$ waves occurring at various intervals over a period of 4h after neomycin addition. **(Grey bars)** The number of cells in which loss of 340 nm Fura-2 fluorescence is observed due to permeabilisation of an OHC. **(Blue bars)** The number of ATP release event occurring at various time intervals over a period of 4h.

5.1.4 Neomycin treatment causes transient increases in extracellular ATP

It has been shown in a number of cell types, including cochlear epithelia, that Ca^{2+} waves are both initiated by and require the release of extracellular ATP, which acts on purinergic receptors (Newman, 2001; Gale et al., 2004; Pearson et al., 2005). It is possible that the loss of OHC membrane integrity elicits intercellular Ca^{2+} waves in the surrounding supporting cells through the release of intracellular ATP. I therefore measured release of ATP into the extracellular space following neomycin treatment. Increases in extracellular ATP were measured using the luciferin-luciferase bioluminescent assay (for methods see Section 2.9.7).

Changes in luminescence during neomycin treatment were monitored over a period of ~ 4 hours. Treatment with 1 mM neomycin induced transient increases in extracellular ATP (Figure 5.9B). These increases occurred at varying intervals over the period of treatment (Figure 5.9B). When neomycin was absent from recording media, much smaller (approx 10-20 fold) spontaneous changes in extracellular ATP were observed (Figure 5.9A and inset). It is likely that the fluctuations in ATP observed in the absence of neomycin result from the spontaneous Ca^{2+} waves and electrical activity occurring during development of the auditory system. This activity is known to be dependent on ATP release and is involved in neuronal survival and refinement (Tritsch et al., 2007). The spontaneous ATP release events (Figure 5.9) were not observed in the presence of apyrase (data not shown). The temporal profile of luminescence changes suggested that the highest number of neomycin induced ATP release events (for quantification see Section 2.11.6) to occur between 150-180 minutes neomycin treatment (Figures 5.10). The release of extracellular ATP, the establishment of $[Ca^{2+}]_c$ waves and the loss of 340 nm fluorescence from OHCs were found to correlate temporally with one another (Figure 5.10).

5.1.5 Effects of apyrase on neomycin-induced $[Ca^{2+}]_c$ changes

Apyrase acts by degrading extracellular ATP and was thus used to determine the requirement for ATP in the generation of neomycin-induced changes in OHC $[Ca^{2+}]_c$ and the generation of intercellular Ca^{2+} waves. The acute biphasic change in OHC

$[Ca^{2+}]_c$ (see Section 5.1.1) was still evident following treatment with 80 U/ml apyrase (Figure 5.11).

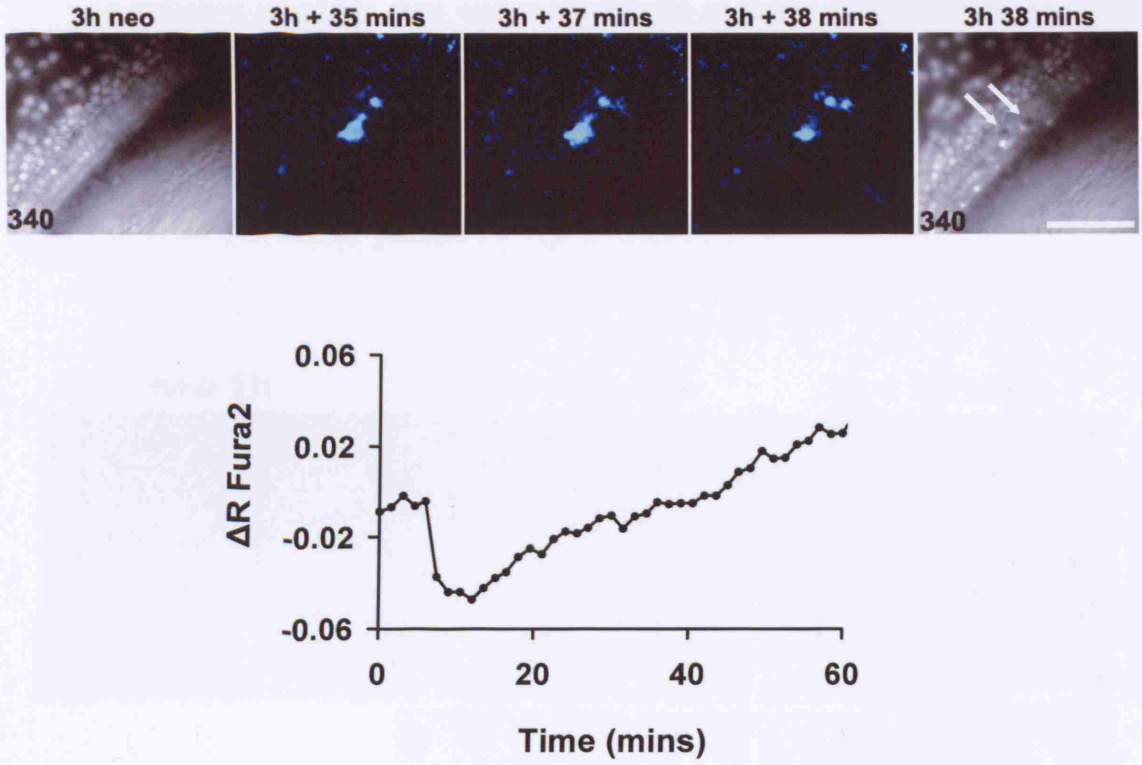

Figure 5. 11 Apyrase does not influence the early bi-phasic response in OHC $[Ca^{2+}]_c$ but attenuates the neomycin-induced intercellular Ca^{2+} wave

Raw 340 nm Fura-2 fluorescence image **(left)** recorded 3 hours after neomycin addition. **Colour mapped images**, R-R0 images show the reduced intercellular Ca^{2+} wave elicited during OHC permeabilisation/death. Raw 340 nm Fura-2 image **(right)** recorded subsequent to the neomycin-induced event, illustrating the loss of dye from the compromised OHC. Responding cells are indicated by the white arrows. Images are single frames taken from R-R0 ratios. Scale bar is 100 µm.
Bottom trace the bi-phasic changes in OHC $[Ca^{2+}]_c$ in the first hour of neomycin treatment persist in the presence of apyrase. Graph is representative of responses measured from OHCs in 3 separate experiments.

For the first phase of the response, Fura-2 fluorescence dropped by 0.06 ± 0.01 ratio units and was not significantly different ($p = 0.22$, Student's paired *t*-test) to changes observed in controls. The second phase of the OHC $[Ca^{2+}]_c$ response (the increasing above baseline) was also unaltered by apyrase and began to reach a plateau within an

hour of neomycin treatment (Figure 5.12). In apyrase experiments, cell death was again determined by the coincident loss of Fura 2 fluorescence at 340 nm and 380 nm. The increase in $[Ca^{2+}]_c$ (see Figure 5.3), which preceded complete loss of the dye from the compromised OHC was also evident in the presence of apyrase and had a mean ΔR of 0.13 ± 0.02. In dramatic contrast to controls however, no intercellular Ca^{2+} waves were observed in response to neomycin when apyrase was present in the extracellular solution (Figure 5.11).

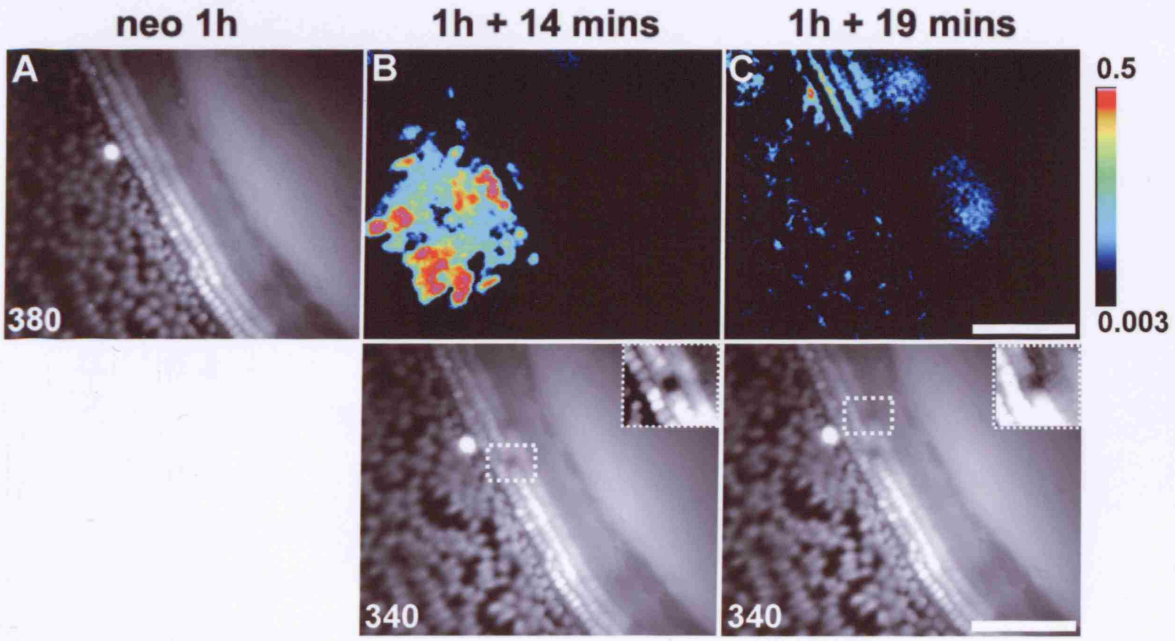

Figure 5. 12 Nominally Ca^{2+} free conditions do not abolish neomycin-induced intercellular Ca^{2+} waves.

(A) 380 nm Fura-2 fluorescence image showing the cellular pattern at the recording site. **(B-C)** R-R0 images from a time series showing an intercellular Ca^{2+} wave in Claudius **(B)** and Deiter's **(C)** cell regions in nominally Ca^{2+}-free conditions. **Panel (B) top** shows an intercellular Ca^{2+} wave in the Claudius cell region. **Panel (B) bottom** 340 nm fluorescence image showing the loss of signal from a compromised OHC. **Panel (C) top** shows an intercellular Ca^{2+} wave in the Deiters' cell region. **Panel (C) bottom** 340 nm fluorescence image showing loss of dye from the compromised OHC. Scale bar is 100 µm.

5.1.6 *Neomycin-induced intercellular Ca^{2+} waves are not dependent on external Ca^{2+}*

In order to determine the role of Ca^{2+} influx in the generation of neomycin-induced intercellular Ca^{2+} waves and investigate the cause for differences in the magnitude of Ca^{2+} waves in the two cell types, $Ca^{2+}$was substituted by Mg^{2+} in the extracellular solution. The nominally Ca^{2+} free solution was estimated to be 20 μM. In nominally Ca^{2+} free conditions, intercellular Ca^{2+} waves were still evident in both Deiters' and Claudius cell regions (Figure 5.12).

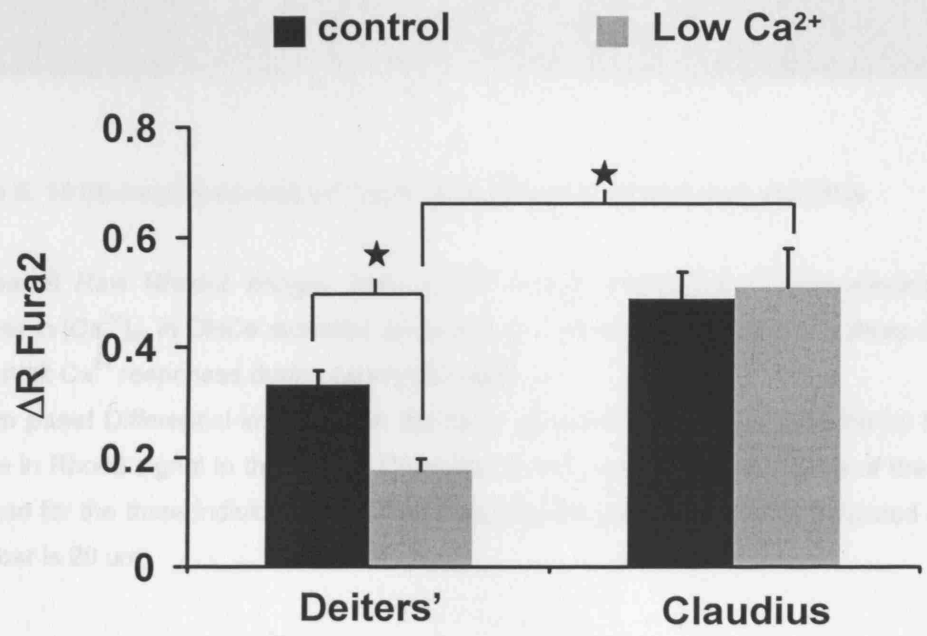

Figure 5. 13 Lowering external Ca^{2+} reduced the magnitude of the $[Ca^{2+}]_c$ changes during neomycin-induced Ca^{2+} waves in the Deiters' but not Claudius cell regions

(Black bars) Average ΔR values recorded during neomycin-induced Ca^{2+} waves recorded in the Deiter's and Claudius cell regions in 1.2 mM external Ca^{2+}.

(Grey bars) Average ΔR values recorded during neomycin-induced Ca^{2+} waves recorded in the Deiter's and Claudius cell regions in nominally Ca^{2+}-free conditions.

Data are mean ± SEM from 8 waves (in both Claudius and Deiters' cell regions). For Deiters' cells p = 0.0004, Student's paired *t*-test. For Deiters' verses Claudius cells p=0.004, Student's paired *t*-test.

The significant difference ($p = 0.004$, Student's paired *t*-test) was still observed in the neomycin-induced ΔR between Deiters' and Claudius cells (Figure 5.13). The ratio changes were 0.17 ± 0.019 and 0.5 ± 0.07 in the Deiters' and Claudius cell regions respectively (Figure 5.13).

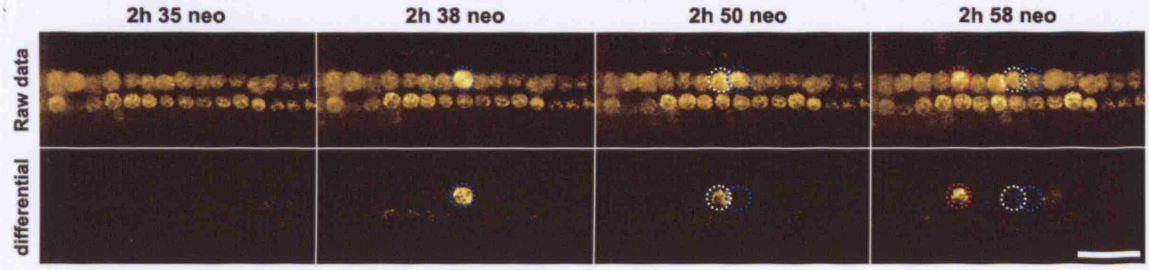

Figure 5. 14 Neomycin causes an increase in Rhod2 fluorescence in OHCs

Top panel Raw Rhod-2 images from a time series showing the neomycin-induced changes in $[Ca^{2+}]_{mt}$ in OHCs recorded using Rhod2. Coloured circles indicate three OHCs that exhibit Ca^{2+} responses during neomycin treatment.
Bottom panel Differential images from the same sequence, showing the frame by frame change in Rhod2 signal in the OHCs. Coloured circles depict the time-course of the Ca^{2+} response for the three individual cells. The time post neomycin addition is indicated (top). Scale bar is 20 um.

Decreasing the external Ca^{2+} did however significantly reduced the magnitude of $[Ca^{2+}]_c$ changes during neomycin-induced Ca^{2+} waves in the Deiters' cell region ($p=0.0004$, Student's paired *t*-test). In control Ca^{2+} conditions, Ca^{2+} waves recorded in the Deiters' cell region had a mean ΔR of 0.33 ± 0.02 whereas those recorded in nominally Ca^{2+} free had a mean ΔR of 0.17 ± 0.019 (Figure 5.13). Reducing the external Ca^{2+} had no significant effect on the magnitude of $[Ca^{2+}]_c$ changes during neomycin-induced Ca^{2+} waves in the Claudius cell region (Figure 5.13). These data suggest that neomycin-induced intercellular Ca^{2+} waves in the Deiters' cell region partially require Ca^{2+} influx, whereas those in the Claudius cell region depend predominantly on Ca^{2+} release from internal stores.

5.1.7 *Mitochondrial Ca^{2+} transients were observed in OHCs and Claudius cells in response to neomycin*

It has been suggested previously, that aminoglycoside-induced ototoxicity is associated with prolonged increases in $[Ca^{2+}]_c$ (Matsui et al., 2004). The sustained elevation in $[Ca^{2+}]_c$ in cochlear cultures over the 4 hour period of neomycin treatment (see Section 5.1.1) is likely to result in a similar $[Ca^{2+}]$ increase within the mitochondrial matrix. It is also likely that mitochondria sequester Ca^{2+} from the cytosol during the neomycin-induced intercellular Ca^{2+} waves describes herein. Prolonged elevations in $[Ca^{2+}]_{mt}$ has been linked with induction of mPTP and consequently cell death (for review see Halestrap, 2006a) which could potentially play an important role in aminoglycoside toxicity. I therefore investigated neomycin-induced uptake of Ca^{2+} into mitochondria using the Ca^{2+} indicator Rhod2 (see Section 2.8.2).

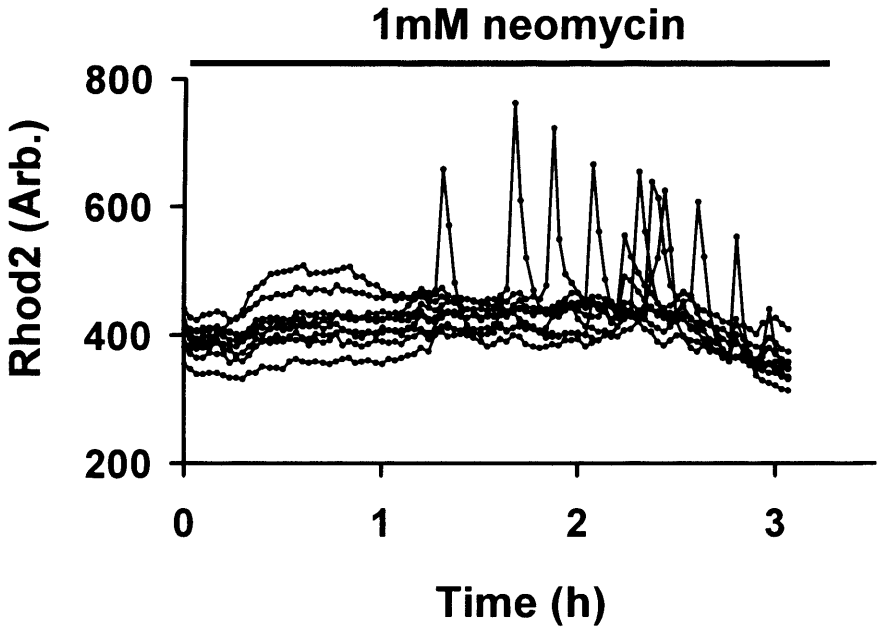

Figure 5. 15 Neomycin induces Ca^{2+} transients in OHCs

Graph shows the increase in Rhod2 fluorescence in OHCs during 3h of neomycin treatment. The presence of neomycin is indicated by the black bar. Traces show the responses measured from 11 OHCs in one experiment. Responses are representative of signals from 24 OHCs measured in 3 separate experiments.

In these experiments, an increase in mitochondrial Ca^{2+} was represented by an increase in Rhod2 fluorescence, although it is likely that a significant amount of the signal was due to changes in $[Ca^{2+}]_c$ as the dye also reports changes in $[Ca^{2+}]_c$. This made it difficult to determine how much of the signal was mitochondrial and how much was cytosolic. Increases in Rhod2 fluorescence were seen in OHCs at various time points over 4 hours of neomycin treatment (Figures 5.14, 5.15). The average duration of the neomycin-induced Ca^{2+} transient in OHCs was 18 ± 8 minutes (n = 15 cells from 3 separate experiments). In one experiment, the increase in Rhod2 fluorescence in OHCs coincided with the onset of a mitochondrial Ca^{2+} wave throughout the Claudius cell region (Figure 5.16). The average duration of changes in $[Ca^{2+}]_{mt}$ during waves was 8 ± 1.4 minutes (n = 10). The recovery of $[Ca^{2+}]_{mt}$ to baseline in the Claudius cells did not in all cases coincide with recovery of Rhod2 fluorescence in the OHCs (Figure 5.16).

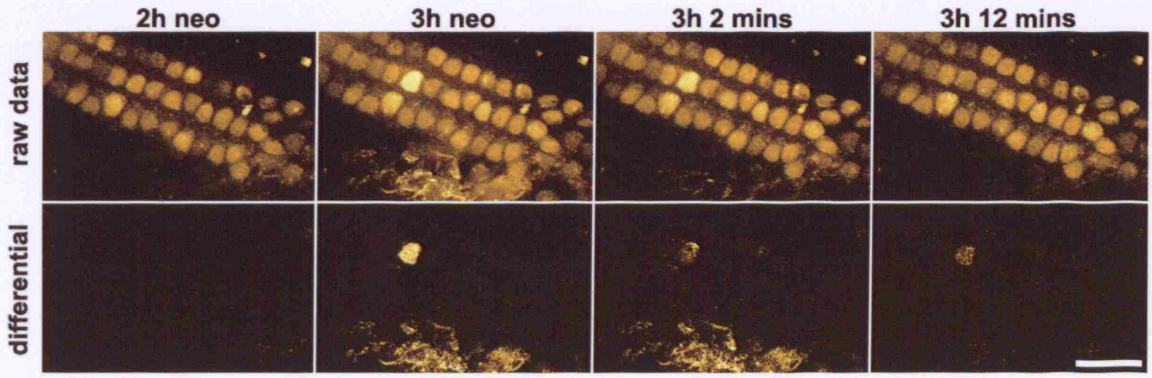

Figure 5. 16 Neomycin-induced Ca^{2+} elevations in OHCs correlate with an increased mitochondrial Ca^{2+} in Claudius cells.

Top panel Single frames from a raw Rhod-2 series showing the correlation between the increased Rhod2 fluorescence in OHCs and Claudius cells. Time post neomycin addition is indicated top.**Bottom Panel** Differential images from the same sequence showing the frame by frame change in Rhod-2. The Ca^{2+} increase within a single OHC induces a wave of mitochondrial Ca^{2+} uptake in cochlear Claudius cells. Time post neomycin addition is indicated top. Scale bar is 20 µm.

For each individual event, the changes in $[Ca^{2+}]_{mt}$ measured using Rhod2 also appeared to increase by a greater amount in Claudius cells compared to OHCs

(Figure 5.17). When comparing responses across the entire data set (10 waves from 1 experiment) however, there was no significant difference in the fluorescent changes between the two cell types (p = 0.41, Student's paired *t*-test) but note, this data is only from one experiment.

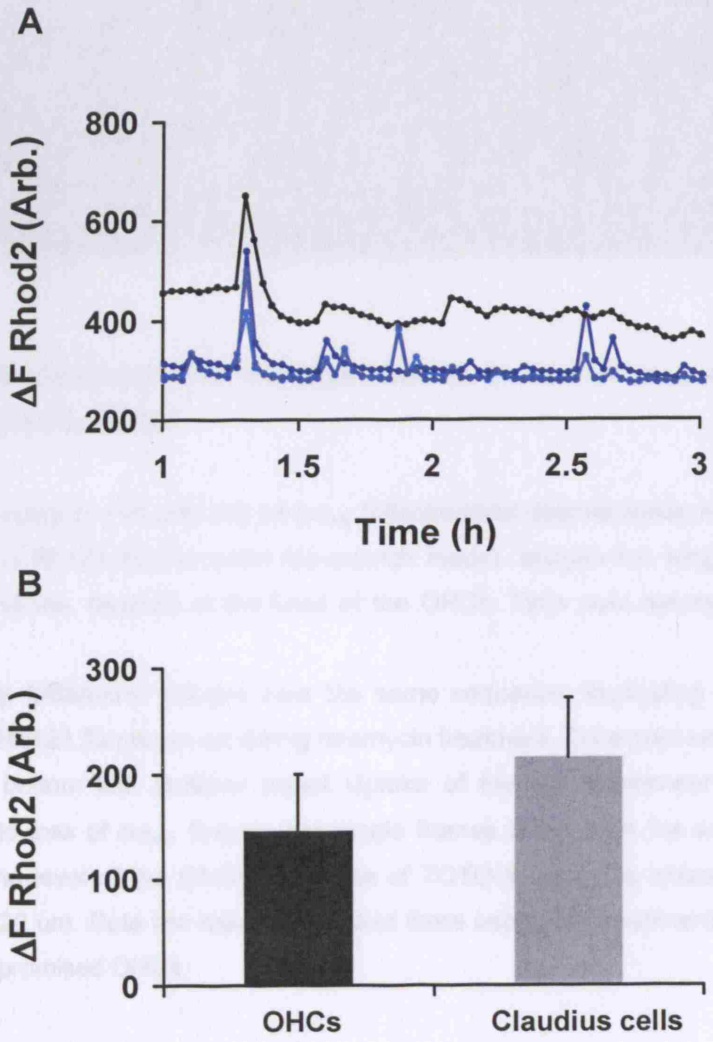

Figure 5. 17 The magnitude of neomycin-induced $[Ca^{2+}]_{mt}$ transients are similar in OHCs and Claudius cells.

(A) Neomycin induced-changes in $[Ca^{2+}]_{mt}$ measured using Rhod2. The $[Ca^{2+}]_{mt}$ transient in the OHCs is shown in black. Mitochondrial $[Ca^{2+}]_{mt}$ transients occurring in the Claudius cells are shown in blue. Note that the graph the starts 1 h into neomycin treatment.
(B) Pooled data indicating the peak Rhod2 fluorescence change in OHCs (black) and Claudius cells (grey). Data are mean ± SEM from 10 waves measured from 1 experiment. p = 0.411, Student's paired *t*-test.

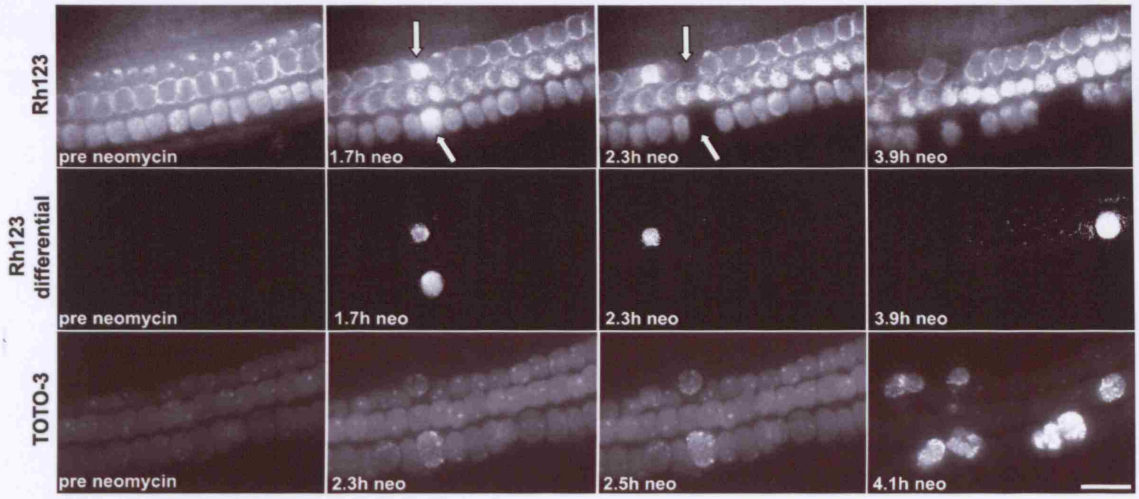

Figure 5. 18 Treatment with neomycin results in loss of $\Delta\psi_{mt}$ and membrane permeabilisation in OHCs.

Top panel Neomycin-induced loss of $\Delta\psi_{mt}$. Mitochondrial depolarisation is represented by an increase in Rh123 fluorescence (de-quench mode). Images are single frames taken from a time series, focused at the level of the OHCs. Time post neomycin is indicated bottom left.

Middle panel Differential images from the same sequence, illustrating the cell-specific increases in Rh123 fluorescence during neomycin treatment. Time post neomycin addition is indicated bottom left. **Bottom panel** Uptake of the cell impermeant dye TOTO-3, subsequent to loss of $\Delta\psi_{mt}$. Images are single frames taken from the same time series focused at the level of the OHCs. The time of TOTO-3 uptake is indicated bottom left. Scale bar is 20 um. Data are representative of three separate experiments. White arrows indicate compromised OHCs.

5.1.8 Neomycin-induced hair cell death is associated with loss of $\Delta\psi_{mt}$

As described in Section 5.1.7, neomycin results in mitochondrial Ca^{2+} uptake in both OHCs and Claudius cells. When mitochondria are exposed to increased $[Ca^{2+}]$ levels for prolonged periods, they may undergo swelling and become uncoupled (see Halestrap, 2006a). Uncoupling of the mitochondria will result in loss of $\Delta\psi_{mt}$, a phenomenon that can be studied using potentiometric cationic dyes. In the experiments discussed below, the fluorescent dye Rhodamine 123 (Rh123) was used to investigate the effects of the aminoglycoside neomycin on $\Delta\psi_{mt}$ in cochlear OHCs.

Rh123 was used in de-quench mode (see Section 2.5.1) at a final concentration of 1 μM, permitting the measurement of dynamic changes in $\Delta\psi_{mt}$ (see Duchen et al., 2003). In this mode, loss of $\Delta\psi_{mt}$ is conveyed by an increase in fluorescence.

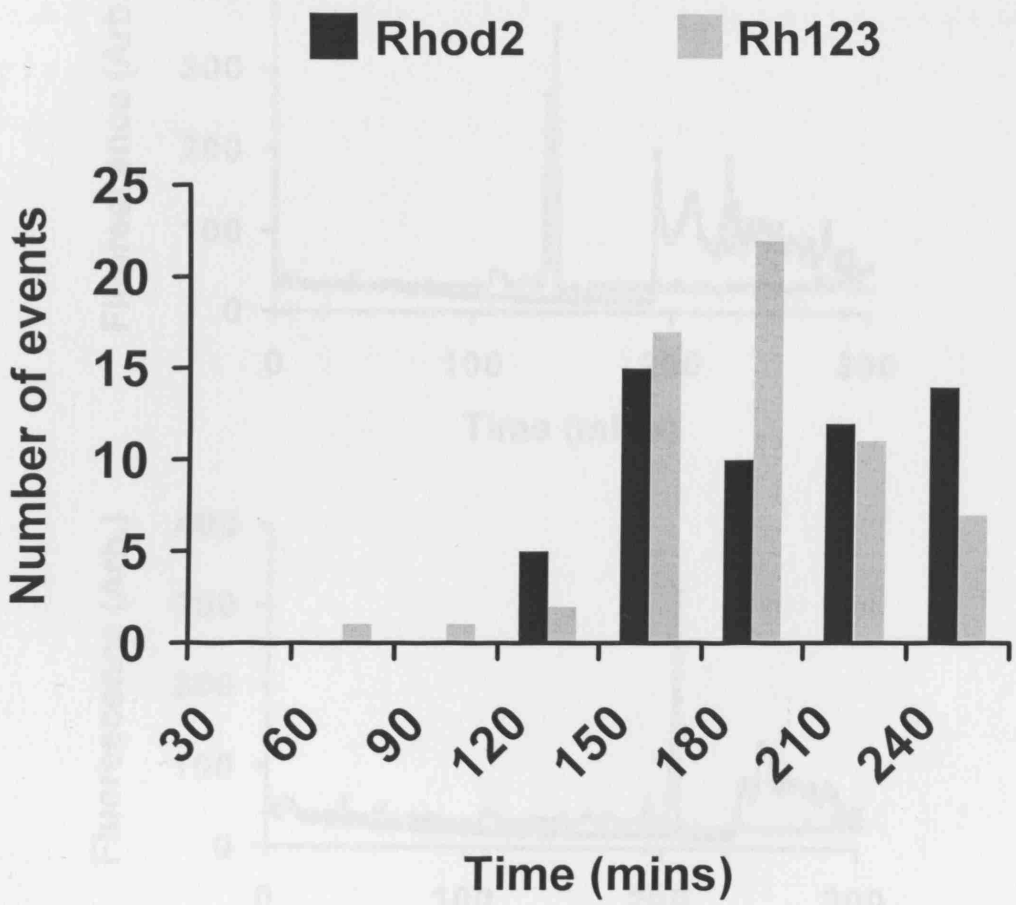

Figure 5. 19 Correlation between elevated $[Ca^{2+}]_{mt}$ and loss of $\Delta\psi_{mt}$

Combined data from individual experiments show a correlation between the increase in Rhod-2 signal and the loss of $\Delta\psi_{mt}$. **Black bars** Timing and frequency of neomycin-induced increases in $[Ca^{2+}]_{mt}$ measured in OHCs using Rhod2.
Grey bars The timing and frequency of neomycin-induced loss of $\Delta\psi_{mt}$ in OHCs measured using Rh123. Histogram shows the pooled data Rhod 2 (n = 4) and Rh123 (n = 3).

To determine whether loss of $\Delta\psi_{mt}$ coincided with cell death, cultures were dual loaded with the live-dead marker TOTO-3 and Rh123 and imaged using the Nipkow spinning disc confocal system. Loss of $\Delta\psi_{mt}$ was observed in OHCs, during neomycin treatment (Figure 5.18). Mitochondrial depolarisation was evident in some OHCs as early as 60 minutes post neomycin addition (Figure 5.18). The highest

number of neomycin-induced depolarisations occurred between 180 – 210 minutes (Figure 5.19).

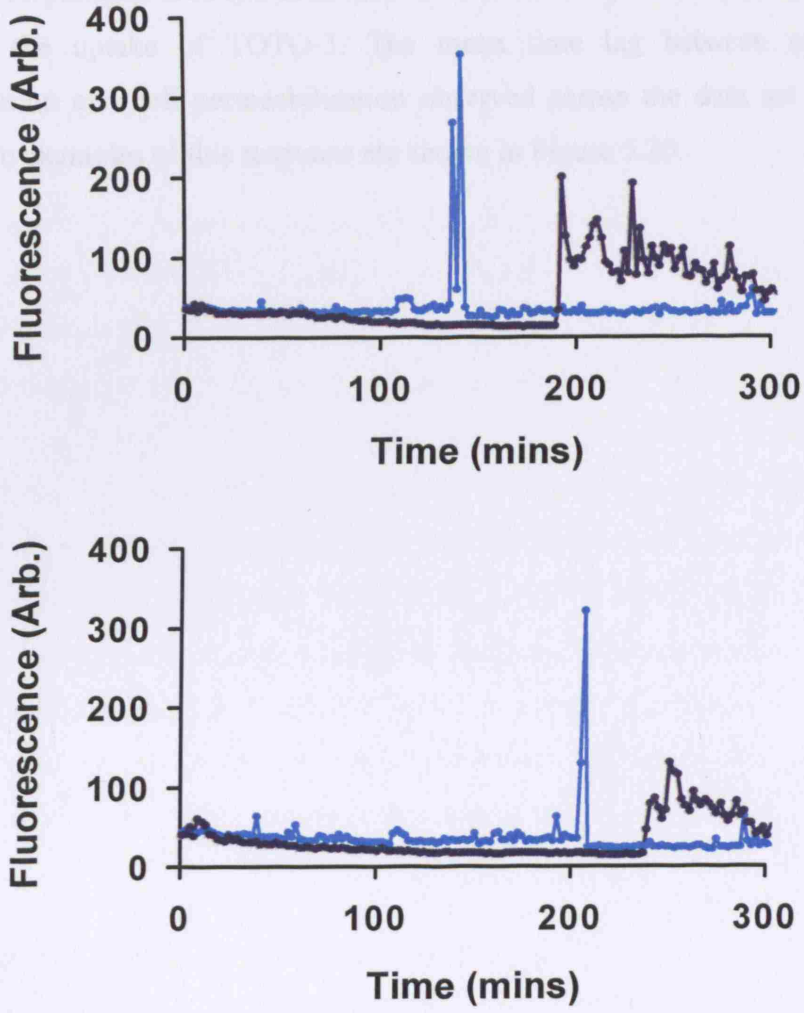

Figure 5. 20 Loss of $\Delta\psi_{mt}$ precedes cell permeabilisation.

The neomycin-induced increases in Rh123 and TOTO-3 fluorescence displayed above are measured from raw data traces. Graphs depict the neomycin-induced increases in Rh123 **(light blue)** and TOTO-3 fluorescence **(dark blue)** in OHCs. Trace shows 2 responses in OHCs from 1 experiment. Data are representative of responses measured from 15 OHCs in 2 separate cultures.

In order to determine whether loss of $\Delta\psi_{mt}$ was associated with mitochondrial Ca^{2+} overload, the onset times of mitochondrial depolarisations and the number of OHCs in which they occurred were compared with those of Rhod2 (Figure 5.19). This

frequency histogram was generated by dividing the individual events (de-quench of Rh123 signal or increase in Rhod2 signal) into time bins of 30 minutes over a period of 0-240 minutes (4h). An interesting observation throughout these experiments, was that in all responding cells (15 cells from 2 individual experiments), the loss of $\Delta\psi_{mt}$ preceded the uptake of TOTO-3. The mean time lag between mitochondrial depolarisation and cell permeabilisation observed across the data set was 34 ± 6 mins. Two examples of this response are shown in Figure 5.20.

5.2 Discussion

In this chapter I have described my investigations of the following hypotheses: **1)** Does neomycin induce changes in $[Ca^{2+}]_c$ and $[Ca^{2+}]_{mt}$ in cochlear hair cells? **2)** Does neomycin affect mitochondrial physiology? In these experiments, a supramaximal dose of 1 mM neomycin was used to selectively induce hair cell death. It has been shown previously, that local application of a single dose of the drug to the middle ear cavity induces effects almost identical to those observed after systemic administration (Wersall et al., 1969). The cellular selectivity of aminoglycosides *in vitro* is similar to that seen under *in vivo* conditions (Richardson and Russell, 1991) thus providing support for the validity of the explant model. Before aminoglycosides can execute cell death, they must be internalised within the hair cells. The precise mechanism by which aminoglycosides enter the hair cells remains unclear, however the recent data suggest the predominant mechanism to occur through entry via the transduction channel itself (Gale et al., 2001; Marcotti et al., 2005). There is also evidence from previous studies suggesting that internalisation results from receptor mediated endocytosis at the hair cell apical membrane (Richardson et al., 1997). Nothing is known about changes in mitochondrial physiology and $[Ca^{2+}]_c$ during aminoglycoside-induced ototoxicity in the mammalian auditory system.

5.2.1 *Neomycin induces rapid changes in OHC $[Ca^{2+}]_c$*

The effects of neomycin on hair cell $[Ca^{2+}]_c$ were investigated in OHCs. Unfortunatly, it is difficult to get OHCs and IHCs in the same focal plane during live imaging. The focal plane of the OHCs was chosen preferentially over that of IHCs, as in P3 explant cultures OHCs respond more quickly to aminoglycosides than IHCs. Additionally, the supporting cells surrounding the OHCs are more accessible for imaging than those in the IHC region. A slight yet significant reduction in OHC $[Ca^{2+}]_c$ was observed almost immediately in response to bath application of 1 mM neomycin. Earlier studies have shown that aminoglycosides reduce the magnitude of $[Ca^{2+}]_c$ transients elicited in hair cells during K^+-induced depolarisations (Tan et al., 2001). Reduction of depolarisation-induced $[Ca^{2+}]_c$ transients was originally attributed to a reduced influx of Ca^{2+} through the transduction channel in the

presence of aminoglycosides. This hypothesis has recently been confirmed by data showing the antibiotics block the transduction channel directly (Kimitsuki and Ohmori, 1993; Gale et al., 2001; Marcotti et al., 2005). As the transduction channel has been linked with Ca^{2+} influx to the hair cell (Lumpkin et al., 1997; Ricci and Fettiplace, 1998) its elimination may result in a reduction of $[Ca^{2+}]_c$ over a prolonged period of time. It is unlikely however that the transduction channel itself could be responsible for setting up the resting $[Ca^{2+}]_c$ in OHCs. There have also been reports that aminoglycosides can reduce $[Ca^{2+}]_c$ levels in unstimulated guinea pig hair cells by interacting with L-type voltage-gated Ca^{2+} channels (Dulon et al., 1989). Blocking of the transduction channel by neomycin could result in hyperpolarisation of the OHC. Hyperpolarisation of the cell could consequently inhibit the activity of voltage-gated Ca^{2+} channels at the basolateral end of the cell, preventing Ca^{2+} influx and thus giving a global reduction of OHC $[Ca^{2+}]_c$.

When external Ca^{2+} was lowered to ~ 20 μM (a concentration similar to that in the endolymph *in vivo*), the rapid reduction in OHC $[Ca^{2+}]_c$ was still observed. The magnitude of the drop in low external Ca^{2+} was slightly but not significantly reduced.This is a somewhat surprising result, as one would predict the drop to be eliminated or at least significantly attenuated in low external Ca^{2+}. Reducing external Ca^{2+} would lower basal Ca^{2+} influx through both voltage-gated Ca^{2+} channels and the MET channel meaning the neomycin-induced OHC hyperpolarisation or channel block would have less influence over OHC $[Ca^{2+}]_c$. A possible explanation for the persistence of the response is that the external Ca^{2+} at the basolateral end of the cell is not as easily reduced. This could be attributed to the presence of tight junctions between the apical and basal portion of the cell and the small extracellular volume basolaterally due to the surrounding supporting cells.

It has also been reported that in conditions of low external Ca^{2+} there is still a significant flux of the ion through the channel (Lumpkin et al., 1997). The persistence of phase 1 of the neomycin-induced bi-phasic response (Section 5.1.1) could also be due to neomycin blocking Ca^{2+} influx through the channel under low Ca^{2+} conditions. It is also a possibility that because the levels of Ca^{2+} influx to the hair cells are relatively low under normal conditions (Ricci and Fettiplace, 1998), the effect of reducing external Ca^{2+} is negligible. The drop in OHC $[Ca^{2+}]_c$ could also be

attributed to the continued acivity of the Ca^{2+}-ATPase (PMCA) expressed in the OHCs. Expression of PMCAs has been documented in immature and mature OHCs and IHCs (Crouch and Schulte, 1995) and has been implicated in regulation of hair cell $[Ca^{2+}]_c$ subsequent to Ca^{2+} loads (Kennedy, 2002). If the Ca^{2+} efflux pathway were active in the absence of the influx pathway (via the MET channel) it may cause a net reduction in OHC $[Ca^{2+}]_c$. The initial drop in OHC Ca^{2+} was also clearly evident in the presence of apyrase, showing no requirement for extracellular ATP.

The reduction in OHC $[Ca^{2+}]_c$ was followed by an increase in $[Ca^{2+}]_c$ above baseline values. This increase in $[Ca^{2+}]_c$ is likely due to a mechanism that does not involve Ca^{2+} influx via the transduction channel, as one would expect it to be blocked in the presence of 1mM neomycin. However, it must also be noted that neomycin is a permeant channel blocker and so the MET channel will not be blocked all the time. (Kimitsuki and Ohmori, 1993; Gale et al., 2001; Marcotti et al., 2005). The effects of neomycin on $[Ca^{2+}]_c$ have been investigated previously in nephrotoxicity, using the opossum kidney (OK) cell line model. Here, the elevation in $[Ca^{2+}]_c$ resulted from direct activation of the extracellular Ca^{2+} sensing receptor (CaR) by neomycin. Activation of the receptor led to a sustained increase in $[Ca^{2+}]_c$, that was associated with activation of the PLC-IP_3 pathway (Ward et al., 2002). In the cochlear hair cells however, the sustained elevation of $[Ca^{2+}]_c$ was abolished when extracellular Ca^{2+} was lowered to 20 μM suggesting that Ca^{2+} release from stores plays an insignificant role. The role of $[Ca^{2+}]_c$ overload in aminoglycoside-induced ototoxicity has also been studied in hair cells of the mature avian auditory system (basal papilla). In these experiments, treatment with gentamicin resulted in a significant increase in $[Ca^{2+}]_c$ within 15 minutes of application. The response was attributed to influx of Ca^{2+} through voltage-gated Ca^{2+} channels, as was abolished by nifiedipine (Hirose et al., 1999). The similarity in the time-course of the neomycin-induced increase in $[Ca^{2+}]_c$ between avian and mammalian hair cells suggests a conserved action of neomycin in both models. The precise mechanism by which neomycin would activate L-type voltage-gated Ca^{2+} is presently unknown. L-type Ca^{2+} channels activate upon membrane depolarisation (see Marcantoni et al., 2007). One hypothesis could therefore be that neomycin activates L-type channels by depolarising the OHC plasma membrane directly. Another mechanism could be activation of voltage-gated Ca^{2+} channels in response to changes in cell redox state or activation of redox-gated

TRP channels (see Groschner et al., 2004). A well documented side effect of aminoglycosides is the generation of free radicals, the precise source of which is unclear (Forge and Schacht, 2000).

5.2.2 Neomycin treatment elicits $[Ca^{2+}]_c$ waves in cochlear supporting cells

Cochlear supporting cells respond to hair cell damage with elevations in intracellular Ca^{2+}. These Ca^{2+} elevations propagate out away from the hair cell into the surrounding supporting cells as a regenerative intercellular $[Ca^{2+}]_c$ wave (Gale et al., 2004). Pharmacological dissection of this response revealed initiation of a purinergic/IP_3 signalling pathway dependent predominantly on P2Y receptor activation (Gale et al., 2004; Piazza et al., 2007). It is not clear whether these waves propagate via diffusion of IP_3 between neighbouring cells through gap junctions, release of ATP that acts as an extracellular messenger or through a combination of both processes.

In my experiments, prolonged treatment of cochlear cultures with 1mM neomycin induced relatively small intercellular Ca^{2+} waves that propagated into the Deiters' and Claudius cell regions and in the latter the $[Ca^{2+}]_c$ changes were of greater amplitude. The difference in amplitude between $[Ca^{2+}]_c$ waves in Deiters' and Claudius cells may result from variation in their receptor expression profiles and thus differences in their sensitivity to ATP. Such differences could also be due to differences in ER Ca^{2+} content or Ca^{2+} buffering between cell types. A particularly high sensitivity to ATP has been described previously in the Claudius cell region and was ascribed to a unique assembly of purinergic receptor subtypes (Gale et al., 2004; Piazza et al., 2007). Persistence of $[Ca^{2+}]_c$ waves in nominally Ca^{2+} free solution indicates a mechanism involving release of Ca^{2+} from internal stores. Although reduction of external Ca^{2+} did not eliminate neomycin-induced $[Ca^{2+}]_c$ waves, it did significantly reduce their amplitude in the Deiters' cell region but not the Claudius cell region. This suggests a requirement for both store release and Ca^{2+} influx in the generation of intercellular Ca^{2+} waves in Deiters' cells. The differential effect of low external Ca^{2+} seen in Deiters' and Claudius cells is again likely to result from different receptor expression profiles between the two cell types.

Previous studies in cochlear supporting cells showed that intercellular $[Ca^{2+}]_c$ waves rely almost exclusively on IP_3 dependent release of Ca^{2+} from the ER. Although there is evidence for expression of ryanodine receptors in the cochlea (Grant et al., 2006), their contribution in the propagation of intercellular Ca^{2+} waves is thought to be minimal (Piazza et al., 2007). Throughout experiments presented in this chapter, the onset of intercellular waves correlated with the loss of 340 and 380 nm fluorescence from OHCs and were blocked by apyrase, suggesting that intercellular Ca^{2+} waves triggered by neomycin result from the release of ATP from damaged or dying hair cells. The highest frequency of neomycin-induced Ca^{2+} waves occurred in the Deiter's cell region. Ca^{2+} waves were only elicited in the Claudius cell region following loss of OHCs in the outermost row or lysis of multiple OHCs in the first and second rows. It is possible, that ATP released from single OHCs in the first and second rows becomes degraded by the highly active ectonucleotidases expressed in the OHC region (Vlajkovic et al., 2002). ATP release from OHCs in the outermost row also can also easily diffuse more easily to the Claudius cell region.

ATP release occurs in response to mechanical stimulation in retinal astrocytes and Müller cells, leading to the generation of intercellular Ca^{2+} waves (Newman, 2001). An essential role for extracellular ATP in the generation of neomycin-induced intercellular Ca^{2+} waves in the cochlea is shown by the significant reduction in wave propagation throughout the supporting cells in the presence of apyrase. Apyrase acts by degrading extracellular ATP and would thus prevent ATP diffusion between neighbouring cells. The release of cellular ATP during neomycin toxicity is further supported by data obtained using the luciferin-luciferase assay showing that ATP release occurs throughout the period of treatment. These events were abolished in the presence of apyrase and were not observed in the absence of neomycin.

The precise role of intercellular Ca^{2+} waves in cochlear supporting cells is at present undefined. It is possible they may function to activate Ca^{2+}-dependent protein kinases that in turn can regulate processes such as proliferation or repair and programmes associated with gene expression (Gale et al., 2004; Matsui et al., 2004; Scemes and Giaume, 2006). The ATP-induced Ca^{2+} waves described in Claudius cells have also been suggested to play a role in cochlear homeostasis by regulating K^+ recycling (Piazza et al., 2007).

5.2.3 *Neomycin promotes mitochondrial Ca^{2+} uptake*

Uptake of Ca^{2+} from the cytosol into mitochondria has been documented in a number of cell types during multiple signalling cascades (see Section 1.5.4). Ca^{2+} enters the mitochondria down its electrochemical gradient established by the highly negative $\Delta\psi_{mt}$ and low intramitochondrial Ca^{2+}. Calcium ions cross the outer mitochondrial membrane (OMM) via the voltage dependent anion-selective channel (VDAC) and the inner membrane (IMM) via the Ca^{2+} uniporter (see Hajnoczky et al., 2006). Once sequestered in the mitochondria, Ca^{2+} will activate Ca^{2+}-sensitive dehydrogenases resulting in a greater ATP production (McCormack et al., 1990; Duchen, 1992; Hajnoczky et al., 1995; Robb-Gaspers et al., 1998; Jouaville et al., 1999). Under various pathophysiological conditions, an increase in matrix Ca^{2+} will lead ultimately to cell death (see Hajnoczky et al., 2006). Under normal conditions, Ca^{2+} is cleared from the mitochondrial matrix via activity of the Na^{+}/Ca^{2+} exchanger, preventing a net increase in mitochondrial Ca^{2+} (Halestrap, 2006b). Once $[Ca^{2+}]_c$ has exceeded a certain concentration, mitochondria can no longer regulate their matrix Ca^{2+} and thus become Ca^{2+} overloaded. Prolonged periods of elevated $[Ca^{2+}]_{mt}$ can activate the mitochondrial permeability transition pore (mPTP) which results in cell death (Gunter et al., 2000).

In cochlear explants, elevations in $[Ca^{2+}]_{mt}$ (measured using the Ca^{2+} indicator Rhod2) were observed in both hair cells and supporting cells during neomycin treatment. The observations made in OHCs must be interpreted with caution, as in this cell type it was difficult to distinguish between mitochondrial and cytosolic compartments. It is likely therefore, that measurements made in OHCs using Rhod2 included a significant cytosolic signal. As described previously, 1mM neomycin induced a prolonged increase in $[Ca^{2+}]_c$ in OHCs, potentially due to Ca^{2+} influx through L-type voltage-gated Ca^{2+} channels as it was not observed when external Ca^{2+} was lowered. Raised $[Ca^{2+}]_{mt}$ can induce mPTP in a number of ways, including interaction with cyclophillin D (CyP-D) (Basso et al., 2005) and the VDAC (Bathori et al., 2006), both of which are constituents of the mPTP. In contrast to hair cells, neomycin caused no prolonged rise in $[Ca^{2+}]_c$ in supporting cells, but instead elicited Ca^{2+} waves, which resulted in waves of mitochondrial Ca^{2+} uptake. The onset of $[Ca^{2+}]_{mt}$ waves occurred simultaneously with stochastic increase in $[Ca^{2+}]_{mt}$ in OHCs.

This supports a mechanism in which a factor (most likely ATP) is released from the damaged hair cell, where it subsequently elicits $[Ca^{2+}]_c$ and $[Ca^{2+}]_{mt}$ responses in the surrounding supporting cells. The wave of mitochondrial Ca^{2+} uptake seen in Claudius cells could be involved in the execution cell death by activating members of the MAPK signalling cascade. It has recently been suggested by Lahne *et* al., 2007 (unpublished data) that neomycin-induced activation of extracellularly regulated kinase 1/2 (ERK 1/2) leads to the release of a pathogenic factor that promotes hair cell death (Lahne, 2007). Additonally $[Ca^{2+}]_{mt}$ waves in supporting cells may serve a metabolic function by increasing the rate of mitochondrial ATP production through the activation of Ca^{2+}-dependent dehydrogenases (McCormack et al., 1990; Jouaville et al., 1999). It has been proposed, that in order for increased $[Ca^{2+}]_{mt}$ to be converted from a physiological to a pathological stimulus, it must be accompanied by a coincident pathological effector. In this case, the effector is likely to be the ROS produced as a result of neomycin treatment (see Forge and Schacht, 2000). Neomycin-induced cell death is only observed in the hair cells, primarily because it is these cells which take it up at levels high enough to reach a critical threshold. Although taken up be supporting cells (Dai et al., 2006) it is likely that aminoglycosides do ot reach the critical level to induce toxicity and thus the $[Ca^{2+}]_{mt}$ may play a physiological role in the absence of a pathological effector.

5.2.4 Neomycin treatment results in loss of $\Delta\psi_{mt}$

The membrane potential lies at the centre of virtually all processes in which the mitochondria participate. Loss of $\Delta\psi_{mt}$ can occur in response to many factors and can be both transient and prolonged. Irreversible loss of $\Delta\psi_{mt}$ will lead to cell death by either apoptosis or necrosis (Green and Kroemer, 2004). It is the metabolic and ionic integrity of the cell and the nature of the death-inducing stimulus which determine whether it dies by apoptosis or necrosis (Green and Reed, 1998; Halestrap et al., 2004). OHCs treated with 1mM neomycin show loss of $\Delta\psi_{mt}$ 2.5h. The subsequent cell death however did not coincide with the loss of $\Delta\psi_{mt}$ and a typical delay of 30 minutes was observed. This suggests that mitochondrial depolarisation may not directly result in cell death, but instead may activate a secondary process that does. Mitochondrial depolarisation is a common feature of cell death (see Green and

Kroemer, 2004) however this measurement alone is not sufficient to determine whether the mPTP has been activated or if the cell dies through necrosis or apoptosis.

Changes in $\Delta\psi_{mt}$ have been studied previously in cochlear OHCs during gentamicin ototoxicity. In this study, it was suggested that mitochondrial depolarisation indicated induction of mPTP in that cell death could be blocked by cyclosporine A (Dehne et al., 2002). It is possible that neomycin-induced hair cell death results from mPTP activation. The fact that neomycin causes an increase in $[Ca^{2+}]_{mt}$ within a similar time (see Section 5.2.3) period would support a role for mPTP induction as Ca^{2+} overload is a major trigger in its activation (Basso et al., 2005; Hajnoczky et al., 2006). Induction of mPTP would result in loss of $\Delta\psi_{mt}$, mitochondrial swelling and permeabilisation of the outer mitochondrial membrane, leading ultimately to release of matrix proteins such as cytochrome c (see Green and Reed, 1998; and Halestrap, 2006b). Opening of the permeability transition pore also leads to a reduction in cellular ATP, by inhibiting mitochondrial ATP production (Halestrap et al., 2004). Without knowing whether mPTP inhibitors significantly promote hair cell survival, the apoptotic pathway cannot be ruled out.

Apoptosis is consistent with loss of $\Delta\psi_{mt}$ and cytochrome c release, but does not require induction of mPTP (Vander Heiden et al., 1997; Goldstein et al., 2000; Kim et al., 2000; Basso et al., 2005; Baines et al., 2007). If cell death were initiated subsequent to mPTP activation one might expect cell death to proceed through necrosis as the cell would have insufficient ATP levels to support progression of the apoptotic pathway (Eguchi et al., 1997). However, studies of aminoglycoside toxicity in both vestibular and cochlear hair cell however suggest an important role for apoptosis, as cell death is blocked by broad spectrum caspase inhibitors (Forge and Li, 2000; Cheng et al., 2005). Data from mouse vestibular and cochlear cultures have implicated the Bcl-2 protein family in the execution of cell death (Cunningham et al., 2004; Vicente-Torres and Schacht, 2006). One cannot rule out the possibility of species-specific differences between mammalian and avian cultures, allowing aminoglycoside-induced mPTP activation during hair cell death to remain a plausible mechanism. In summary, it is presently unclear whether aminoglycoside toxicity results in cell death through apoptosis, necrosis or through a combination of the two pathways.

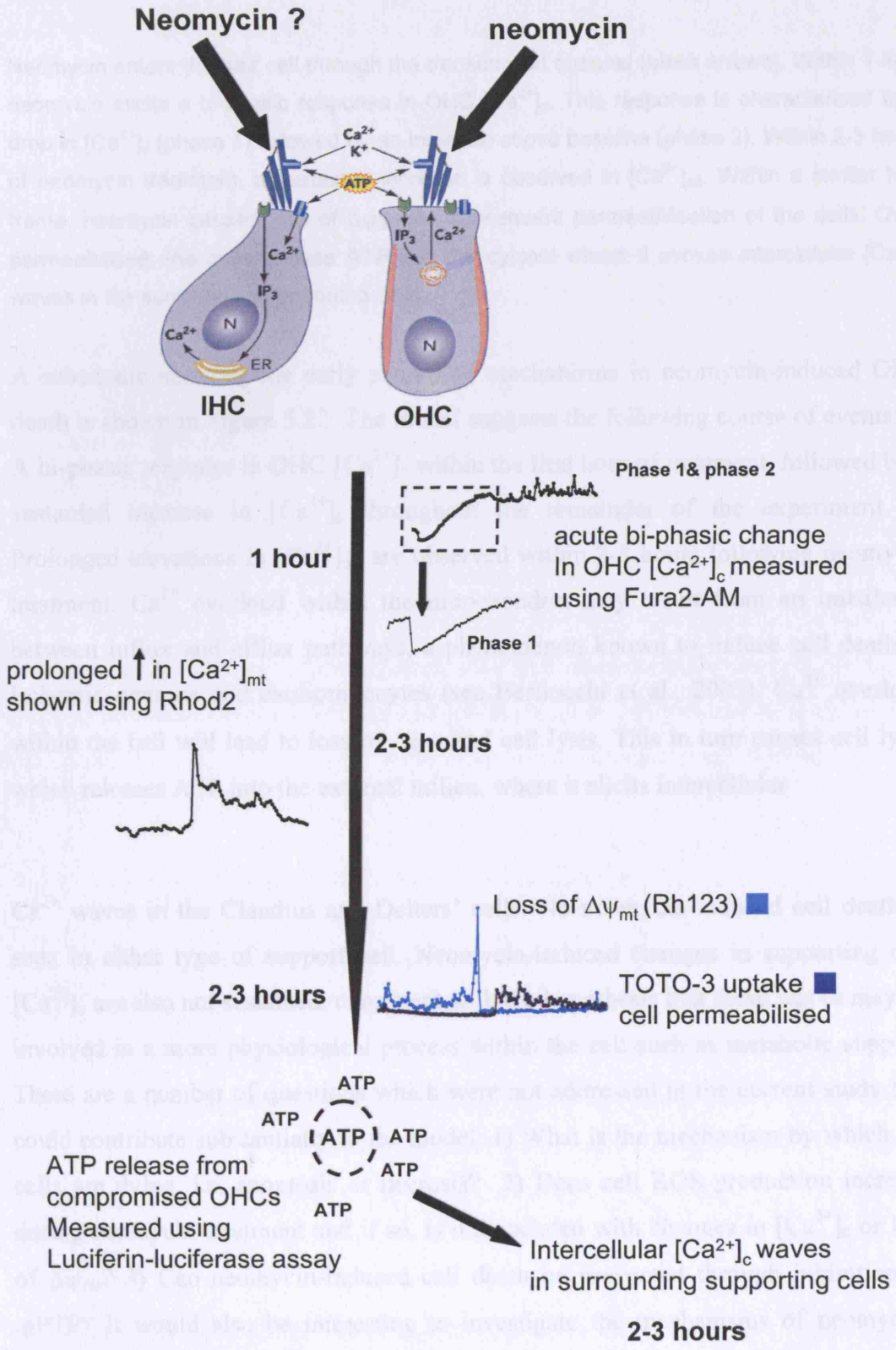
Neomycin ?
neomycin
Ca2+
K+
ATP
IP3
Ca2+
N
ER
IHC
OHC
Phase 1& phase 2
acute bi-phasic change
In OHC [Ca2+]c measured
using Fura2-AM
Phase 1
1 hour
prolonged ↑ in [Ca2+]mt
shown using Rhod2
2-3 hours
Loss of Δψmt (Rh123)
TOTO-3 uptake
cell permeabilised
2-3 hours
ATP release from
compromised OHCs
Measured using
Luciferin-luciferase assay
Intercellular [Ca2+]c waves
in surrounding supporting cells
2-3 hours

Figure 5. 22 Schematic of the early signalling events involved in neomycin-induced OHC death.

Neomycin enters the hair cell through the transduction channel (black arrows). Within 1 hour neomycin elicits a bi-phasic response in OHC $[Ca^{2+}]_c$. This response is characterised by a drop in $[Ca^{2+}]_c$ (phase 1) followed by an increase above baseline (phase 2). Within 2-3 hours of neomycin treatment, a sustained increase is observed in $[Ca^{2+}]_{mt}$. Within a similar time frame, neomycin causes loss of $\Delta\psi_{mt}$ and subsequent permeabilisation of the cells. Once permeabilised, the cells release ATP into the cytosol where it evokes intercellular $[Ca^{2+}]_c$ waves in the surrounding supporting cells.

A schematic showing the early signalling mechanisms in neomycin-induced OHC death is shown in Figure 5.22. The model suggests the following course of events: **1)** A bi-phasic response in OHC $[Ca^{2+}]_c$ within the first hour of treatment, followed by a sustained increase in $[Ca^{2+}]_c$ throughout the remainder of the experiment. **2)** Prolonged elevations in $[Ca^{2+}]_{mt}$ are observed within 2-3 hours following neomycin treatment. Ca^{2+} overload within the mitochondria may result from an imbalance between influx and efflux pathways, a phenomenon known to induce cell death in ischemic neurons and cardiomyocytes (see Berliocchi et al., 2005). Ca^{2+} overload within the cell will lead to loss of $\Delta\psi_{mt}$ and cell lysis. This in turn causes cell lysis which releases ATP into the external milieu, where it elicits intercellular

Ca^{2+} waves in the Claudius and Deiters' cells. No neomycin-induced cell death is seen in either type of support cell. Neomycin-induced changes in supporting cell $[Ca^{2+}]_c$ are also not sustained, consistent with the hypothesis that these waves may be involved in a more physiological process within the cell such as metabolic support. There are a number of questions which were not addressed in the current study that could contribute substantially to the model. **1)** What is the mechanism by which the cells are dying, i.e. apoptosis or necrosis? **2)** Does cell ROS production increase during neomycin treatment and if so, is it associated with changes in $[Ca^{2+}]_c$ or loss of $\Delta\psi_{mt}$? **3)** Can neomycin-induced cell death be prevented through inhibition of mPTP? It would also be interesting to investigate the mechanisms of neomycin-induced cell death in the inner hair cells.

6 General discussion

Aside from their role in ATP production, little is known about the physiology of and function of mitochondria in the cochlea. The work presented in this thesis was prompted by observations that mutations occurring in the mitochondrial genome can result in deafness and a hypersensitivity to ototoxic agents (see Fischel-Ghodsian, 1999). Such mitochondrial mutations are expressed in all tissues, yet in a number of cases, the phenotype is seen exclusively in the ear suggesting a uniquely important role for mitochondria in cochlear physiology and pathophysiology. Without an understanding of mitochondrial function in the cochlea and the role they play in its physiology, it becomes challenging to determine precisely how such mutations result in deafness. The pathology of mitochondrial mutations resulting in deafness is at present unclear, although it has been suggested that they result in impaired ATP production (Li et al., 2004; Zhao et al., 2005). Why then would such a mutation produce a phenotype only in the ear, as there are many tissues throughout the body with a high demand for ATP? The experiments presented in this thesis were designed to study the physiology of mitochondria and their involvement in physiological and pathophysiological processes in the mammalian cochlea. Mitochondrial function was investigated in hair cells and supporting cells, as deafness can result from dysfunction in either.

6.1.1 Base-to-apex differences in mitochondrial function

Mitochondrial function in the cochlea was assessed using the potentiometric probe TMRM and the endogenous fluorescence of NAD(P)H and flavoproteins. TMRM is a lipophilic cation which loads readily into mitochondria in response to their highly negative membrane potential ($\Delta\psi_{mt}$). The TMRM fluorescence intensity is therefore used as an indicator of mitochondrial polarisation status (see Section 2.5). Confocal imaging of TMRM in cochlear explant cultures from post-natal day 3 (+ 1 day *in vitro*) revealed a significantly higher fluorescent signal in apical IHCs compared to basal IHCs but not in OHCs or supporting cells, demonstrating a base-to-apex difference in mitochondrial function specific to IHCs. Differences in $\Delta\psi_{mt}$ may result from a range of possible metabolic differences between cells including differences in substrate supply, respiratory rate, mitochondrial 'leak' or an increased rate of Ca^{2+}

cycling across the mitochondrial membrane. While one would ideally measure oxygen consumption in the various cells in order to differentiate between these possibilities and elucidate the functional significance of a base-to-apex gradient in $\Delta\psi_{mt}$, such experiments are not possible in the cochlear preparation. An alternative approach is provided by the measurement of endogenous autofluorescence from NADH and flavoproteins, allowing mitochondrial function to be assessed at the level of single identifiable cells. Base-to-apex differences in mitochondrial metabolism in IHCs were investigated by establishing the resting 'redox index' of the different cell types with reference to the dynamic range of the signals defined by changes in NADH and FAD^{2+} autofluorescence to the metabolic inhibitors CN and FCCP. These experiments revealed a more reduced redox state in apical IHCs compared to basal IHCs. A higher $\Delta\psi_{mt}$ associated with a more reduced redox state in apical IHCs could result from a lower ATP turnover and consequently reduced proton leak through the ATP-synthase (increasing $\Delta\psi_{mt}$ and thus TMRM fluorescence) coupled with a slower resting respiratory rate compared to basal IHCs (see Nicholls, 1982). The base-to-apex gradient in $\Delta\psi_{mt}$ could also be attributed to differences in the basal rate of Ca^{2+} cycling across the mitochondrial membrane in the two cochlear regions (see Nicholls, 1982). If basal IHCs had a greater rate of Ca^{2+} cycling at rest, it would tend to reduce $\Delta\psi_{mt}$ and thus be seen as a lower TMRM signal. The more reduced redox sate seen in apical compared to basal IHCs could also be attributed to a greater substrate supply to the citric acid cycle, which maintains the pool of reduced NAD(P)H.

6.1.2 Oligomycin and BAPTA-AM do normalise the base-to-apex difference in $\Delta\psi_{mt}$

To investigate the hypothesis that basal IHCs have a greater proton leak via the ATP-synthase, basal and apical cultures were treated with oligomycin. If the latter was the underlying mechanism for the difference in mitochondrial function between base and apex, oligomycin would normalise the difference in $\Delta\psi_{mt}$ and thus TMRM fluorescence. In my experiments, oligomycin caused a significant increase in $\Delta\psi_{mt}$ in basal but not apical IHCs and normalised the base-to-apex gradient in $\Delta\psi_{mt}$. This finding suggests base-to-apex differences in mitochondrial function. The effects of

oligomycin on $\Delta\psi_{mt}$ in IHCs of the base and apex of the cochlea indicate a greater ATP turnover and increased proton leak via the ATP synthase in basal compared to apical IHCs.

The less polarised $\Delta\psi_{mt}$ in basal IHCs could also result from a greater futile Ca^{2+} cycling in mitochondria under resting conditions (see Nicholls, 1982). The entry of Ca^{2+} into mitochondria results in depolarisation of $\Delta\psi_{mt}$ which is subsequently compensated for by proton extrusion via the electron transfer chain (Nicholls, 1982). Although there are no base-to-apex studies on IHC $[Ca^{2+}]_c$, there is evidence to suggest that resting $[Ca^{2+}]_c$ is higher in basal OHCs compared to apical OHCs (in guinea pig) (Tan et al., 2001). It is possible that this difference in $[Ca^{2+}]_c$ is due to a base-to-apex variation in Ca^{2+} binding proteins (Papakostas et al., 2000). If like OHCs, basal IHCs also have an elevated resting $[Ca^{2+}]_c$, it is possible that the plasma membrane ATPases may be more active in attempt to regulate $[Ca^{2+}]_c$ levels. An increased pump activity would require more ATP and thus account for the increased rate of ATP consumption in basal IHCs. A greater ATP consumption would reduce the ATP/ADP ratio and consequently stimulate respiration, which would lead to an increased proton leak via the ATP synthase. To test the hypothesis that futile Ca^{2+} cycling contributes to the less polarised $\Delta\psi_{mt}$ in basal IHCs, cultures were treated with the membrane permeant Ca^{2+} chelator BAPTA-AM, which will bind both cytosolic and mitochondrial Ca^{2+}. The effects of BAPTA-AM on basal and apical IHCs were similar to those of oligomycin in that it significantly hyperpolarised $\Delta\psi_{mt}$ in basal but not apical IHCs. BAPTA-AM did not however normalise the base-to-apex gradient in TMRM fluorescence. The combined effects of greater futile Ca^{2+} cycling and increased ATP turnover and proton leak would be consistent with the more oxidised redox state (Section 3.2.2) and a less polarised $\Delta\psi_{mt}$ (3.2.1) seen in basal IHCs.

6.1.3 Assessment of mitochondrial function in the cochlear slice preparation

Analysis of the same parameters in the cochlea slice preparation gave somewhat different results. The TMRM loading in hair cells (both OHCs and IHCs) was significantly lower than that observed in cultures suggesting that hair cell

mitochondria in the slice are less polarised than in the explant culture. Another striking difference between the slice and culture preparation was seen in the flavoprotein signal. Hair cells in the slice displayed an elevated FAD^{2+} fluorescence which is consistent with a degree of uncoupling. Taken together, the reduced TMRM loading and increase FAD^{2+} signal suggest that hair cells in the slice have a higher resting rate of oxygen consumption (Duchen, 1992) which is often an indicator of cellular stress (see Duchen, 2004). The most plausible explanation for the differences between the two models is that in the slice, which is an acute preparation the tissue is still damaged, whilst in the explant culture, cells have had time to recover from the stresses induced by the isolation process.

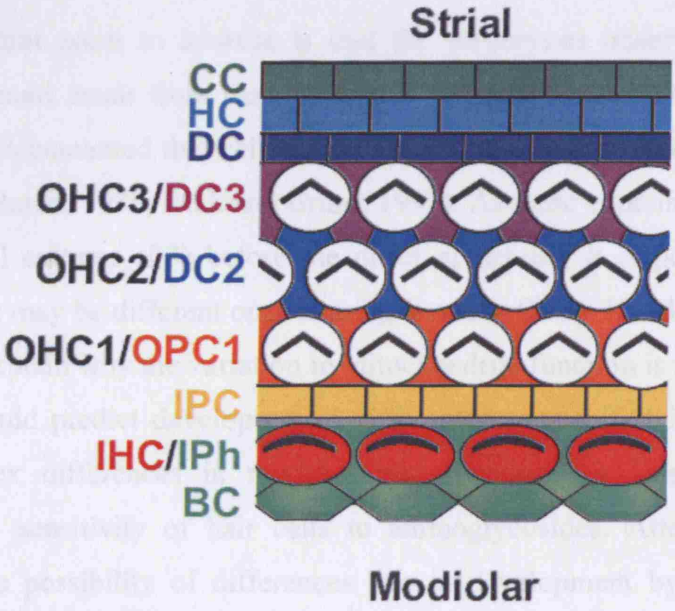

Figure 6. 1 The cellular patterning in the Organ of Corti at P0

A single row of inner hair cells (IHCs) is present on the modiolar side (green). IHCs are surrounded by border cells (BC) on their modiolar sides (green) and inner phalangeal cells (IPh), inner pillar cells (IPC) and outer pillar cells (OPC) on their strial sides (grey). The three outer hair cell (OHC) rows are separated from the IHCs by a single row of IPCs. The neighbouring OHC rows are divided by Deiters' cells (DC). The third OHC row is separated from the Hensen's (HC)/ Claudius cell (CC) region by a single row of Deiters' cells. *Schematic from Kelley 2007.*

At P0, when the pattern of the organ of Corti is essentially complete, inner hair cells are surrounded by border cells on their modiolar sides and inner phalangeal cells, inner pillar cells and outer pillar cells on their lateral and strial sides. The OHC rows are separated by rows of Deiters' cells and the third row of Deiters' cells forms the boundary between the third outer hair cell row and the Hensen's/Claudius cell region (see Kelley, 2007). When imaging NADH and FAD^{2+} I kept the confocal pinhole fully open in order to maximise collection of the weak signals and limit photobleaching. This significantly reduces the confocality of the system making it different to clearly distinguish between the hair cells and the numerous types of supporting cell. The complexity of the cochlear preparation is shown in the schematic below.

An important point to address is that the differences observed in mitochondrial function could result from developmental variation between base and apex. It has been well documented that cells in the base of the cochlea mature ahead of those in the apex (Burda, 1985; Roth and Bruns, 1992). As these experiments were conducted in neonatal cultures (P3) before the onset of hearing it is possible mitochondrial physiology may be different once hearing is active (P15). If indeed this is the case, it does not explain why the variation in mitochondrial function is restricted to the IHCs as one would predict developmental differences to manifest in all cell types. The base-to-apex differences in mitochondrial function may also contribute to the differential sensitivity of hair cells to aminoglycosides. Attempts were made to address the possibility of differences due to development by repeating the same experiments in the cochlear slice preparation. Whilst it is not possible to culture cochlear explants from animals older then P5-P8, cochlear slices can be obtained from neonatal and adult tissue. Experiments in cochlear slices were perhaps disappointing, as there were clear differences in both TMRM, and flavoprotein signals between hair cells in cultures and slices. These differences could suggest a state of stress in mitochondria within hair cells of the slice preparation.

6.1.4 NAD(P)H lifetime imaging reveals metabolic differences between hair cells and supporting cells in the neonatal cochlea

In order to investigate the base-to-apex differences in mitochondrial NADH further I employed NAD(P)H lifetime imaging. These experiments were carried out using 2-photon excitation of NAD(P)H at 720 nm. 2-photon excitation microscopy establishes confocality within the tissue, due to the highly localised mechanism of excitation (Helmchen and Denk, 2005). The restricted volume in which the fluorophore is excited eliminates a large proportion of out of focus light from surrounding cells thus improving the resolution of structures and organelles within the tissues. The fluorescence lifetime imaging system allows one to distinguish between NAD(P)H in different pools, separately identifying the relative contributions of bound and free NAD(P)H to the signal (Blinova et al., 2005). In preliminary data from the lab, this seems largely to translate into differences in cytosolic and mitochondrial compartments respectively (Duchen MR unpublished). Lifetime imaging of NAD(P)H in P3 cochlea cultures revealed metabolic differences between hair cells and supporting cells. It has been suggested previously, that cochlear hair cells have a high capacity for ATP production (Tiede et al., 2007) although the precise mechanism for ATP synthesis remains unknown. There are currently no data investigating metabolic function in cochlear supporting cells. In this thesis, the data from NAD(P)H lifetime imaging suggest that in P3 cochlea cultures hair cells depend predominantly on oxidative metabolism while supporting cells seem to have a higher glycolytic capacity. The metabolic differences observed between hair cells and supporting cells are similar to those documented between neurons and astrocytes (see Pellerin et al., 2007). There are also reports that astrocytes provide neurons with supplementary metabolic substrate via the astrocyte-neuron lactate shuttle. Lactate is then used as the preferential oxidative substrate in neurons (Pellerin et al., 2007). It is possible therefore that supporting cells in the cochlea function in a similar way by providing hair cells with the necessary trophic support.

6.1.5 *Mitochondria regulate the spatio-temporal properties and magnitude of agonisit and damage-induced intercellular $[Ca^{2+}]_c$ signals in the neonatal cochlea*

The differences in mitochondrial function between hair cells and supporting cells prompted the hypothesis that physiological processes regulated by mitochondria such as Ca^{2+} signalling, may differ between the two cell types. Previous studies have documented intracellular (Mammano et al., 1999; Kennedy, 2002) and intercellular (Gale et al., 2004; Piazza et al., 2007; Tritsch et al., 2007) Ca^{2+} waves in the organ of Corti preparation. I therefore investigated the role of mitochondrial Ca^{2+} buffering in the regulation of both agonist-induced and damage-induced Ca^{2+} signalling by blocking the mitochondrial Ca^{2+} uptake pathway with CCCP and oligomycin or with Ru360. Similar to studies in other cell types including astrocytes (Boitier et al., 1999), oligodendrocytes (Simpson and Russell, 1996), hepatocytes (Hajnoczky et al., 1999), adrenal chromaffin cells (Herrington et al., 1996) and gonadotrophs (Hehl et al., 1996) my experiments show that mitochondrial Ca^{2+} buffering plays an important role in governing the spatio-temporal properties and amplitude of intercellular Ca^{2+} waves in cochlear supporting cells. Intercellular Ca^{2+} waves have been documented in supporting cells in response to mechanical damage (Gale et al., 2004 and Lahne M & Gale J.E. in press), extracellular ATP application (Piazza et al., 2007) and occur spontaneously during development (Tritsch et al., 2007). The precise physiological role of any of the latter are at present unclear, however it has been suggested that such waves may play a role in the regulation of proliferation and K^+ recycling (see Mammano et al., 2007) and control of gene expression (Gale et al., 2004). It is also possible, that intercellular Ca^{2+} waves in the cochlear may stimulate a greater mitochondrial ATP production in an attempt to match cellular energy production with demand (Jouaville et al., 1999).

It has been shown previously, that mitochondria play a role in regulation of $[Ca^{2+}]_c$ levels close to synaptic sites in IHCs in response to depolarisation-induced $[Ca^{2+}]_c$ loads (Kennedy, 2002). I therefore attempted to investigate the role of mitochondrial Ca^{2+} buffering in the regulation of intracellular $[Ca^{2+}]_c$ signals in hair cells in response to ATP application and mechanical damage. In both OHCs and IHCs, it was not possible to accurately resolve mitochondrial and cytosolic compartments, thus making it difficult to study the relationship between $[Ca^{2+}]_c$ and $[Ca^{2+}]_{mt}$.

Additionally, $[Ca^{2+}]_c$ transients in hair cells were only elicited at ATP concentrations exceeding 100 μM so that their Ca^{2+} signal was often masked by that occurring in the neighbouring supporting cells. This was mainly because supporting cells responded maximally at much lower ATP concentrations. It may be possible, in future experiments, to more accurately study mitochondrial regulation of $[Ca^{2+}]_c$ signals in hair cells using the mitochondrially targeted Ca^{2+}-sensitive fluorescent protein reporters such as cameleon, or pericam. In place of focal ATP application, it may also prove more effective to use Ca^{2+} uncaging within the hair cells specifically as a means of inducing a $[Ca^{2+}]_c$ load.

6.1.6 Prolonged elevations in mitochondrial Ca^{2+} are associated with neomycin-induced OHC death

Aminoglycoside antibiotics are used for treating gram negative bacterial infections. Over the last few years, clinical use of these drugs has dramatically declined in developed countries, due to their significant ototoxic and nephrotoxic effects. Aminoglycosides such as neomycin enter the cochlea following systemic administration. The preferential toxicity of the drug (basal hair cells are more susceptible than apical hair cells) does not correlate with its distribution throughout cochlear tissues (see Rybak and Ramkumar, 2007). The precise mechanism by which aminoglycosides induce hair cell death remains unclear. There is a large body of evidence suggesting that ROS generation is important in aminoglycoside-induced cell death however its involvement in ototoxicity and nephrotoxicity is controversial (Rybak and Ramkumar, 2007). Previous studies have shown that aminoglycoside-induced ROS generation occurs in isolated renal mitochondria (Yang et al., 1995) however *in vitro* experiments failed to link this phenomenon directly with nephrotoxicity (Stratta et al., 1994). Similarly, in ototoxicity the role of ROS generation remained controversial: in one study, free radical scavengers were found inefficient in protecting against aminoglycoside-induced hair cell death (see Forge and Schacht, 2000) while more recent data suggested that antioxidant administration can significantly reduce aminoglycoside toxicity in the cochlea (for review see Lesniak et al., 2005). Members of the MAPK signalling pathway, predominantly JNK have been identified as down-stream targets of aminoglycoside-generated ROS both *in vitro* (Sugahara et al., 2006) and *in vivo* (Ylikoski et al., 2002).

Additionally, aminoglycoside toxicity has been linked with prolonged increases in $[Ca^{2+}]_c$ (Hirose et al., 1999; Ward et al., 2002) and the establishment of Ca^{2+} waves in vestibular (Matsui et al., 2004) and cochlear (Section 5.1.4) epithelia. These changes in $[Ca^{2+}]_c$ have also been linked with activation of members of the MAPK signalling pathway (Ward and Riccardi, 2002; Gale et al., 2004 Lahne & Gale unpublished data). In my experiments, I used the cochlea explant model to study mitochondrial Ca^{2+} signalling during aminoglycoside toxicity as mitochondria are known to modulate $[Ca^{2+}]_c$ signals in the cochlea (see C hapter 4). Rhod2 was used to measure mitochondrial Ca^{2+} buffering in aminoglycoside toxicity. Although used predominantly to study changes in mitochondrial Ca^{2+}, Rhod2 can also be used to monitor cytosolic Ca^{2+} (see Boitier et al., 1999; Gerasimenko and Tepikin, 2005). Neomycin caused large elevations in hair cell $[Ca^{2+}]_c$ however it was again not possible to accurately separate mitochondrial and cytosolic Ca^{2+} signals. Such elevations in $[Ca^{2+}]_c$ have been linked previously with the activation of L-type voltage gated Ca^{2+} channels in avian hair cells (Hirose et al., 1999). The mechanism by which neomycin activates these channels in not known, although it could be suggested that neomycin directly depolarises the hair cell plasma membrane leading to activation of voltage-gated Ca^{2+} channels. In order to more accurately resolve cytosolic and mitochondrial compartments, experiments could be repeated using mitochondrially targeted Ca^{2+} sensitive fluorescent indicators such as cameleon and pericam. This would permit the study of Ca^{2+} exclusively in the mitochondrial compartment (Rizzuto et al., 1992; Szabadkai et al., 2003), although transfection of explant cultures is difficult. An additional drawback in these experiments was the time-course over which neomycin was effective. Cultures had to be treated for a minimum of 3 hours before the effects of neomycin were apparent. This made it impossible to study the role of mitochondrial Ca^{2+} uptake in aminoglycoside toxicity using conventional methods (Ru360, Ruthenium red or a combination of FCCP and oligomycin). It may also be interesting to monitor the level and rate of ROS production in both hair cells and supporting cells during aminoglycosides treatment and determine whether either of the latter are modulated by the changes in $[Ca^{2+}]_c$. These experiments could be conducted using fluorescent ROS indicators such as dihydroethidium, mitosox red in combination with $[Ca^{2+}]_{c/mt}$ indicators.

6.1.7 *Neomycin causes intercellular $[Ca^{2+}]_c$ waves in cochlear supporting cells*

Neomycin also consistently caused the appearance $[Ca^{2+}]_c$ waves in the Deiters' and Claudius cell regions after 2-3 hours of treatment. These waves were dependent on ATP release from compromised OHCs. In hair cells from cultured chick utricles, changes in $[Ca^{2+}]_c$ were suggested to precede caspase-3 activation in hair cells and thus play a role in neomycin-induced hair cell death (Matsui et al., 2004). In my experiments changes in OHC $[Ca^{2+}]_c$ preceded the onset of intercellular Ca^{2+} waves. It is possible therefore that the neomycin-induced increase in OHC $[Ca^{2+}]_c$ may result in caspase activation through a similar mechanism. The role of the intercellular Ca^{2+} waves in cochlear supporting cells is at present unclear. However, as supporting cells are generally thought to provide hair cells with trophic support, neomycin-induced Ca^{2+} waves could be playing a metabolic role attempting to match cellular energy with demand. As discussed in Section 4.3, mitochondria accumulate Ca^{2+} from the cytosol during damage-induced intercellular $[Ca^{2+}]_c$ signalling. Ca^{2+} uptake into mitochondria could then act to increase the rate of ATP production (Jouaville et al., 1999).

6.1.8 *Loss of $\Delta\psi_{mt}$ precedes uptake of vital dyes in neomycin-induced OHC death*

Using the potentiometric cationic fluorescent probe Rhodamine 123 (Rh123) I also studied changes in $\Delta\psi_{mt}$ during aminoglycoside treatment. Despite many reports suggesting a mitochondrial involvement in aminoglycoside-induced hair cell death (Dehne et al., 2002; Vicente-Torres and Schacht, 2006; Owens et al., 2007; Wang et al., 2007), there are no studies investigating dynamic changes in $\Delta\psi_{mt}$ in response to the drugs. In my experiments, Rh123 was used in de-quench mode (see Section 2.5.1) to study changes in $\Delta\psi_{mt}$ in response to neomycin. Treatment with neomycin (1 mM) induced substantial increases in Rh123 fluorescence in OHCs, suggesting the loss of $\Delta\psi_{mt}$ after 2-3 hours of neomycin treatment. The time-course of aminoglycoside toxicity varies between models and species. Data from *in vivo* experiments shows hair cell degeneration within 8-12 hours (Hirose et al., 2004) whereas *in vitro* data from both mammalian and zebra fish tissue demonstrates the effects of aminoglycosides over a significantly shorter time period (Hirose et al., 1997; Dehne et al., 2002; Owens et al., 2007). The large variation in time course

observed under *in vivo* and *in vitro* conditions could be attributed to differences in the extracellular environment as cell culture has been shown to impose a state of oxidative stress on cells (see Halliwell, 2003). Although an important parameter to study, measurement of $\Delta\psi_{mt}$ alone is not sufficient to determine the mechanism of cell death, since both apoptosis and necrosis are associated with mitochondrial depolarisation (see Section 5.2.4). Data presented here using Rhod-2 suggest that neomycin results in prolonged increases in $[Ca^{2+}]_{mt}$. As prolonged periods of elevated $[Ca^{2+}]_{mt}$ can induce mPTP activation (see Gunter et al., 2000) it is possible this is the mechanism underlying loss of $\Delta\psi_{mt}$. Activation of mPTP has been implicated previously during aminoglycoside-induced hair cell death (Dehne et al., 2002), however the stimulus for induction is not clear. Further experiments are therefore required to establish the precise involvement and activation of mPTP in aminoglycoside toxicity. Investigating the effects of cyclosporine A (an inhibitor of mPTP) on neomycin toxicity would be a valuable experiment as would establishing a link between neomycin-induced Ca^{2+} elevation and the loss of $\Delta\psi_{mt}$. It would also be interesting to study aminoglycoside toxicity in CyP-D and VDAC knock out animals. Such experiments would give a greater insight into the role of mitochondria in aminoglycoside ototoxicity and perhaps lead to the development of a therapeutic agent that can be administered clinically to counteract the toxic effects of aminoglycosides.

7 References

Alberts B, Bray D, Lewis J, Raff M, Roberts K, Watson J (1994) Molecular Biology of the Cell: Garland Publishing, NY.

Andrade FH, McMullen CA, Rumbaut RE (2005) Mitochondria are fast Ca2+ sinks in rat extraocular muscles: a novel regulatory influence on contractile function and metabolism. Invest Ophthalmol Vis Sci 46:4541-4547.

Ashmore JF (1987) A fast motile response in guinea-pig outer hair cells: the cellular basis of the cochlear amplifier. J Physiol 388:323-347.

Ashmore JF, Ohmori H (1990) Control of intracellular calcium by ATP in isolated outer hair cells of the guinea-pig cochlea. J Physiol 428:109-131.

Babcock DF, Herrington J, Goodwin PC, Park YB, Hille B (1997) Mitochondrial participation in the intracellular Ca2+ network. J Cell Biol 136:833-844.

Baffy G, Miyashita T, Williamson JR, Reed JC (1993) Apoptosis induced by withdrawal of interleukin-3 (IL-3) from an IL-3-dependent hematopoietic cell line is associated with repartitioning of intracellular calcium and is blocked by enforced Bcl-2 oncoprotein production. J Biol Chem 268:6511-6519.

Baines CP, Kaiser RA, Sheiko T, Craigen WJ, Molkentin JD (2007) Voltage-dependent anion channels are dispensable for mitochondrial-dependent cell death. Nat Cell Biol 9:550-555.

Baines CP, Kaiser RA, Purcell NH, Blair NS, Osinska H, Hambleton MA, Brunskill EW, Sayen MR, Gottlieb RA, Dorn GW, Robbins J, Molkentin JD (2005) Loss of cyclophilin D reveals a critical role for mitochondrial permeability transition in cell death. Nature 434:658-662.

Bakowski D, Burgoyne RD, Parekh AB (2003) Activation of the store-operated calcium current ICRAC can be dissociated from regulated exocytosis in rat basophilic leukaemia (RBL-1) cells. J Physiol 553:387-393.

Basso E, Fante L, Fowlkes J, Petronilli V, Forte MA, Bernardi P (2005) Properties of the permeability transition pore in mitochondria devoid of Cyclophilin D. J Biol Chem 280:18558-18561.

Bathori G, Csordas G, Garcia-Perez C, Davies E, Hajnoczky G (2006) Ca2+-dependent control of the permeability properties of the mitochondrial outer membrane and voltage-dependent anion-selective channel (VDAC). J Biol Chem 281:17347-17358.

Beal MF (2005) Mitochondria take center stage in aging and neurodegeneration. Ann Neurol 58:495-505.

Beatrice MC, Palmer JW, Pfeiffer DR (1980) The relationship between mitochondrial membrane permeability, membrane potential, and the retention of Ca2+ by mitochondria. J Biol Chem 255:8663-8671.

Becker W, Hickl (2006) TCSPC Handbook.

Beltramello M, Piazza V, Bukauskas FF, Pozzan T, Mammano F (2005) Impaired permeability to Ins(1,4,5)P3 in a mutant connexin underlies recessive hereditary deafness. Nat Cell Biol 7:63-69.

Berliocchi L, Bano D, Nicotera P (2005) Ca2+ signals and death programmes in neurons. Philos Trans R Soc Lond B Biol Sci 360:2255-2258.

Bernardi P, Vassanelli S, Veronese P, Colonna R, Szabo I, Zoratti M (1992) Modulation of the mitochondrial permeability transition pore. Effect of protons and divalent cations. J Biol Chem 267:2934-2939.

Berridge MJ (1995) Capacitative calcium entry. Biochem J 312 (Pt 1):1-11.

Beutner D, Voets T, Neher E, Moser T (2001) Calcium dependence of exocytosis and endocytosis at the cochlear inner hair cell afferent synapse. Neuron 29:681-690.
Bezprozvanny I, Watras J, Ehrlich BE (1991) Bell-shaped calcium-response curves of Ins(1,4,5)P3- and calcium-gated channels from endoplasmic reticulum of cerebellum. Nature 351:751-754.
Blinova K, Carroll S, Bose S, Smirnov AV, Harvey JJ, Knutson JR, Balaban RS (2005) Distribution of mitochondrial NADH fluorescence lifetimes: steady-state kinetics of matrix NADH interactions. Biochemistry 44:2585-2594.
Bodmer D, Brors D, Pak K, Bodmer M, Ryan AF (2003) Gentamicin-induced hair cell death is not dependent on the apoptosis receptor Fas. Laryngoscope 113:452-455.
Bogenhagen D, Clayton DA (1977) Mouse L cell mitochondrial DNA molecules are selected randomly for replication throughout the cell cycle. Cell 11:719-727.
Boitier E, Rea R, Duchen MR (1999) Mitochondria exert a negative feedback on the propagation of intracellular Ca2+ waves in rat cortical astrocytes. J Cell Biol 145:795-808.
Bosher SK, Warren RL (1978) Very low calcium content of cochlear endolymph, an extracellular fluid. Nature 273:377-378.
Buntinas L, Gunter KK, Sparagna GC, Gunter TE (2001) The rapid mode of calcium uptake into heart mitochondria (RaM): comparison to RaM in liver mitochondria. Biochim Biophys Acta 1504:248-261.
Burda H (1985) Qualitative assessment of postnatal maturation of the organ of Corti in two rat strains. Hear Res 17:201-208.
Burnstock G (1972) Purinergic nerves. Pharmacol Rev 24:509-581.
Burnstock G (2007) Physiology and pathophysiology of purinergic neurotransmission. Physiol Rev 87:659-797.
Camello-Almaraz C, Salido GM, Pariente JA, Camello PJ (2002) Role of mitochondria in Ca(2+) oscillations and shape of Ca(2+) signals in pancreatic acinar cells. Biochem Pharmacol 63:283-292.
Capaldi RA, Aggeler R (2002) Mechanism of the F(1)F(0)-type ATP synthase, a biological rotary motor. Trends Biochem Sci 27:154-160.
Casano RA, Bykhovskaya Y, Johnson DF, Hamon M, Torricelli F, Bigozzi M, Fischel-Ghodsian N (1998) Hearing loss due to the mitochondrial A1555G mutation in Italian families. Am J Med Genet 79:388-391.
Chabbert C, Canitrot Y, Sans A, Lehouelleur J (1995) Calcium homeostasis in guinea pig type-I vestibular hair cell: possible involvement of an Na(+)-Ca2+ exchanger. Hear Res 89:101-108.
Chan DC (2006) Mitochondria: dynamic organelles in disease, aging, and development. Cell 125:1241-1252.
Cheng AG, Cunningham LL, Rubel EW (2005) Mechanisms of hair cell death and protection. Curr Opin Otolaryngol Head Neck Surg 13:343-348.
Collins TJ, Bootman MD (2003) Mitochondria are morphologically heterogeneous within cells. J Exp Biol 206:1993-2000.
Collins TJ, Berridge MJ, Lipp P, Bootman MD (2002) Mitochondria are morphologically and functionally heterogeneous within cells. Embo J 21:1616-1627.
Corey DP, Hudspeth AJ (1983) Kinetics of the receptor current in bullfrog saccular hair cells. J Neurosci 3:962-976.
Crawford AC, Fettiplace R (1985) The mechanical properties of ciliary bundles of turtle cochlear hair cells. J Physiol 364:359-379.

Crawford AC, Evans MG, Fettiplace R (1989) Activation and adaptation of transducer currents in turtle hair cells. J Physiol 419:405-434.
Crompton M (2003) On the involvement of mitochondrial intermembrane junctional complexes in apoptosis. Curr Med Chem 10:1473-1484.
Crompton M, Capano M, Carafoli E (1976) Respiration-dependent efflux of magnesium ions from heart mitochondria. Biochem J 154:735-742.
Crouch JJ, Schulte BA (1995) Expression of plasma membrane Ca-ATPase in the adult and developing gerbil cochlea. Hear Res 92:112-119.
Cunningham LL, Cheng AG, Rubel EW (2002) Caspase activation in hair cells of the mouse utricle exposed to neomycin. J Neurosci 22:8532-8540.
Cunningham LL, Matsui JI, Warchol ME, Rubel EW (2004) Overexpression of Bcl-2 prevents neomycin-induced hair cell death and caspase-9 activation in the adult mouse utricle in vitro. J Neurobiol 60:89-100.
Dai CF, Mangiardi D, Cotanche DA, Steyger PS (2006) Uptake of fluorescent gentamicin by vertebrate sensory cells in vivo. Hear Res 213:64-78.
Dallos P, He DZ, Lin X, Sziklai I, Mehta S, Evans BN (1997) Acetylcholine, outer hair cell electromotility, and the cochlear amplifier. J Neurosci 17:2212-2226.
Davis AF, Clayton DA (1996) In situ localization of mitochondrial DNA replication in intact mammalian cells. J Cell Biol 135:883-893.
De Giorgi F, Lartigue L, Ichas F (2000) Electrical coupling and plasticity of the mitochondrial network. Cell Calcium 28:365-370.
Dehne N, Rauen U, de Groot H, Lautermann J (2002) Involvement of the mitochondrial permeability transition in gentamicin ototoxicity. Hear Res 169:47-55.
DiMauro S (2004) Mitochondrial diseases. Biochim Biophys Acta 1658:80-88.
DiMauro S (2007) Mitochondrial DNA medicine. Biosci Rep 27:5-9.
Dolmetsch RE, Lewis RS, Goodnow CC, Healy JI (1997) Differential activation of transcription factors induced by Ca2+ response amplitude and duration. Nature 386:855-858.
Drahota Z, Gazzotti P, Carafoli E, Rossi CS (1969) A comparison of the effects of different divalent cations on a number of mitochondrial reactions linked to ion translocation. Arch Biochem Biophys 130:267-273.
Duchen MR (1992) Ca(2+)-dependent changes in the mitochondrial energetics in single dissociated mouse sensory neurons. Biochem J 283 (Pt 1):41-50.
Duchen MR (2000a) Mitochondria and Ca(2+)in cell physiology and pathophysiology. Cell Calcium 28:339-348.
Duchen MR (2000b) Mitochondria and calcium: from cell signalling to cell death. J Physiol 529 Pt 1:57-68.
Duchen MR (2004) Mitochondria in health and disease: perspectives on a new mitochondrial biology. Mol Aspects Med 25:365-451.
Duchen MR, Biscoe TJ (1992) Relative mitochondrial membrane potential and [Ca2+]i in type I cells isolated from the rabbit carotid body. J Physiol 450:33-61.
Duchen MR, Leyssens A, Crompton M (1998) Transient mitochondrial depolarizations reflect focal sarcoplasmic reticular calcium release in single rat cardiomyocytes. J Cell Biol 142:975-988.
Duchen MR, Surin A, Jacobson J (2003) Imaging mitochondrial function in intact cells. Methods Enzymol 361:353-389.
Dulon D, Mollard P, Aran JM (1991) Extracellular ATP elevates cytosolic Ca2+ in cochlear inner hair cells. Neuroreport 2:69-72.

Dulon D, Zajic G, Aran JM, Schacht J (1989) Aminoglycoside antibiotics impair calcium entry but not viability and motility in isolated cochlear outer hair cells. J Neurosci Res 24:338-346.
Dumollard R, Ward Z, Carroll J, Duchen MR (2007) Regulation of redox metabolism in the mouse oocyte and embryo. Development 134:455-465.
Dumont RA, Lins U, Filoteo AG, Penniston JT, Kachar B, Gillespie PG (2001) Plasma membrane Ca2+-ATPase isoform 2a is the PMCA of hair bundles. J Neurosci 21:5066-5078.
Eatock RA (2000) Adaptation in hair cells. Annu Rev Neurosci 23:285-314.
Eatock RA, Corey DP, Hudspeth AJ (1987) Adaptation of mechanoelectrical transduction in hair cells of the bullfrog's sacculus. J Neurosci 7:2821-2836.
Echtay KS (2007) Mitochondrial uncoupling proteins--what is their physiological role? Free Radic Biol Med 43:1351-1371.
Eguchi Y, Shimizu S, Tsujimoto Y (1997) Intracellular ATP levels determine cell death fate by apoptosis or necrosis. Cancer Res 57:1835-1840.
Eng J, Lynch RM, Balaban RS (1989) Nicotinamide adenine dinucleotide fluorescence spectroscopy and imaging of isolated cardiac myocytes. Biophys J 55:621-630.
Fettiplace R, Ricci A (2006) Mechanoelectrical transduction in auditory hair cells. In: Vertebrate Hair Cells: Springer.
Fettiplace R, Ricci AJ, Hackney CM (2001) Clues to the cochlear amplifier from the turtle ear. Trends Neurosci 24:169-175.
Fischel-Ghodsian N (1999) Mitochondrial deafness mutations reviewed. Hum Mutat 13:261-270.
Fischel-Ghodsian N, Prezant TR, Bu X, Oztas S (1993) Mitochondrial ribosomal RNA gene mutation in a patient with sporadic aminoglycoside ototoxicity. Am J Otolaryngol 14:399-403.
Forge A (1985) Outer hair cell loss and supporting cell expansion following chronic gentamicin treatment. Hear Res 19:171-182.
Forge A, Li L (2000) Apoptotic death of hair cells in mammalian vestibular sensory epithelia. Hear Res 139:97-115.
Forge A, Schacht J (2000) Aminoglycoside antibiotics. Audiol Neurootol 5:3-22.
Frey TG, Mannella CA (2000) The internal structure of mitochondria. Trends Biochem Sci 25:319-324.
Frolenkov GI, Mammano F, Kachar B (2003) Regulation of outer hair cell cytoskeletal stiffness by intracellular Ca2+: underlying mechanism and implications for cochlear mechanics. Cell Calcium 33:185-195.
Fuchs PA, Glowatzki E, Moser T (2003) The afferent synapse of cochlear hair cells. Curr Opin Neurobiol 13:452-458.
Furuta H, Luo L, Hepler K, Ryan AF (1998) Evidence for differential regulation of calcium by outer versus inner hair cells: plasma membrane Ca-ATPase gene expression. Hear Res 123:10-26.
Gale JE, Piazza V, Ciubotaru CD, Mammano F (2004) A mechanism for sensing noise damage in the inner ear. Curr Biol 14:526-529.
Gale JE, Marcotti W, Kennedy HJ, Kros CJ, Richardson GP (2001) FM1-43 dye behaves as a permeant blocker of the hair-cell mechanotransducer channel. J Neurosci 21:7013-7025.
Galluzzi L, Kroemer G (2007) Mitochondrial apoptosis without VDAC. Nat Cell Biol 9:487-489.

Garcia JA, Yee AG, Gillespie PG, Corey DP (1998) Localization of myosin-Ibeta near both ends of tip links in frog saccular hair cells. J Neurosci 18:8637-8647.
Geleoc GS, Holt JR (2003) Auditory amplification: outer hair cells pres the issue. Trends Neurosci 26:115-117.
Gerasimenko O, Tepikin A (2005) How to measure Ca2+ in cellular organelles? Cell Calcium 38:201-211.
Gillespie PG (2004) Myosin I and adaptation of mechanical transduction by the inner ear. Philos Trans R Soc Lond B Biol Sci 359:1945-1951.
Goldstein JC, Waterhouse NJ, Juin P, Evan GI, Green DR (2000) The coordinate release of cytochrome c during apoptosis is rapid, complete and kinetically invariant. Nat Cell Biol 2:156-162.
Gonzalez A, Schulz I, Schmid A (2000) Agonist-evoked mitochondrial Ca2+ signals in mouse pancreatic acinar cells. J Biol Chem 275:38680-38686.
Grant L, Slapnick S, Kennedy H, Hackney C (2006) Ryanodine receptor localisation in the mammalian cochlea: an ultrastructural study. Hear Res 219:101-109.
Green DR, Reed JC (1998) Mitochondria and apoptosis. Science 281:1309-1312.
Green DR, Kroemer G (2004) The pathophysiology of mitochondrial cell death. Science 305:626-629.
Greenwood D, Jagger DJ, Huang LC, Hoya N, Thorne PR, Wildman SS, King BF, Pak K, Ryan AF, Housley GD (2007) P2X receptor signaling inhibits BDNF-mediated spiral ganglion neuron development in the neonatal rat cochlea. Development 134:1407-1417.
Griesinger CB, Richards CD, Ashmore JF (2005) Fast vesicle replenishment allows indefatigable signalling at the first auditory synapse. Nature 435:212-215.
Groschner K, Rosker C, Lukas M (2004) Role of TRP channels in oxidative stress. Novartis Found Symp 258:222-230; discussion 231-225, 263-226.
Guan MX, Fischel-Ghodsian N, Attardi G (1996) Biochemical evidence for nuclear gene involvement in phenotype of non-syndromic deafness associated with mitochondrial 12S rRNA mutation. Hum Mol Genet 5:963-971.
Gunter KK, Gunter TE (1994) Transport of calcium by mitochondria. J Bioenerg Biomembr 26:471-485.
Gunter TE, Pfeiffer DR (1990) Mechanisms by which mitochondria transport calcium. Am J Physiol 258:C755-786.
Gunter TE, Buntinas L, Sparagna G, Eliseev R, Gunter K (2000) Mitochondrial calcium transport: mechanisms and functions. Cell Calcium 28:285-296.
Hajnoczky G, Hager R, Thomas AP (1999) Mitochondria suppress local feedback activation of inositol 1,4, 5-trisphosphate receptors by Ca2+. J Biol Chem 274:14157-14162.
Hajnoczky G, Robb-Gaspers LD, Seitz MB, Thomas AP (1995) Decoding of cytosolic calcium oscillations in the mitochondria. Cell 82:415-424.
Hajnoczky G, Csordas G, Krishnamurthy R, Szalai G (2000a) Mitochondrial calcium signaling driven by the IP3 receptor. J Bioenerg Biomembr 32:15-25.
Hajnoczky G, Csordas G, Madesh M, Pacher P (2000b) The machinery of local Ca2+ signalling between sarco-endoplasmic reticulum and mitochondria. J Physiol 529 Pt 1:69-81.
Hajnoczky G, Csordas G, Das S, Garcia-Perez C, Saotome M, Sinha Roy S, Yi M (2006) Mitochondrial calcium signalling and cell death: approaches for assessing the role of mitochondrial Ca2+ uptake in apoptosis. Cell Calcium 40:553-560.

Halestrap AP (2006a) Mitochondria and preconditioning: a connexin connection? Circ Res 99:10-12.
Halestrap AP (2006b) Calcium, mitochondria and reperfusion injury: a pore way to die. Biochem Soc Trans 34:232-237.
Halestrap AP, McStay GP, Clarke SJ (2002) The permeability transition pore complex: another view. Biochimie 84:153-166.
Halestrap AP, Clarke SJ, Javadov SA (2004) Mitochondrial permeability transition pore opening during myocardial reperfusion--a target for cardioprotection. Cardiovasc Res 61:372-385.
Hallap T, Nagy S, Jaakma U, Johannisson A, Rodriguez-Martinez H (2005) Mitochondrial activity of frozen-thawed spermatozoa assessed by MitoTracker Deep Red 633. Theriogenology 63:2311-2322.
Halliwell B (2003) Oxidative stress in cell culture: an under-appreciated problem? FEBS Lett 540:3-6.
Han W, Shi X, Nuttall AL (2006) AIF and endoG translocation in noise exposure induced hair cell death. Hear Res 211:85-95.
Hehl S, Golard A, Hille B (1996) Involvement of mitochondria in intracellular calcium sequestration by rat gonadotropes. Cell Calcium 20:515-524.
Helmchen F, Denk W (2005) Deep tissue two-photon microscopy. Nat Methods 2:932-940.
Henderson D, Bielefeld EC, Harris KC, Hu BH (2006) The role of oxidative stress in noise-induced hearing loss. Ear Hear 27:1-19.
Hengartner MO (2000) The biochemistry of apoptosis. Nature 407:770-776.
Herrington J, Park YB, Babcock DF, Hille B (1996) Dominant role of mitochondria in clearance of large Ca2+ loads from rat adrenal chromaffin cells. Neuron 16:219-228.
Hirose K, Hockenbery DM, Rubel EW (1997) Reactive oxygen species in chick hair cells after gentamicin exposure in vitro. Hear Res 104:1-14.
Hirose K, Westrum LE, Cunningham DE, Rubel EW (2004) Electron microscopy of degenerative changes in the chick basilar papilla after gentamicin exposure. J Comp Neurol 470:164-180.
Hirose K, Westrum LE, Stone JS, Zirpel L, Rubel EW (1999) Dynamic studies of ototoxicity in mature avian auditory epithelium. Ann N Y Acad Sci 884:389-409.
Holt JR, Corey DP (2000) Two mechanisms for transducer adaptation in vertebrate hair cells. Proc Natl Acad Sci U S A 97:11730-11735.
Holt JR, Gillespie SK, Provance DW, Shah K, Shokat KM, Corey DP, Mercer JA, Gillespie PG (2002) A chemical-genetic strategy implicates myosin-1c in adaptation by hair cells. Cell 108:371-381.
Hornig H, Woolley P, Luhrmann R (1987) Decoding at the ribosomal A site: antibiotics, misreading and energy of aminoacyl-tRNA binding. Biochimie 69:803-813.
Hosler JP, Ferguson-Miller S, Mills DA (2006) Energy transduction: proton transfer through the respiratory complexes. Annu Rev Biochem 75:165-187.
Hoth M, Penner R (1992) Depletion of intracellular calcium stores activates a calcium current in mast cells. Nature 355:353-356.
Hoth M, Fanger CM, Lewis RS (1997) Mitochondrial regulation of store-operated calcium signaling in T lymphocytes. J Cell Biol 137:633-648.
Housley GD (2000) Physiological effects of extracellular nucleotides in the inner ear. Clin Exp Pharmacol Physiol 27:575-580.

Housley GD, Greenwood D, Ashmore JF (1992) Localization of cholinergic and purinergic receptors on outer hair cells isolated from the guinea-pig cochlea. Proc Biol Sci 249:265-273.
Housley GD, Marcotti W, Navaratnam D, Yamoah EN (2006) Hair cells--beyond the transducer. J Membr Biol 209:89-118.
Housley GD, Kanjhan R, Raybould NP, Greenwood D, Salih SG, Jarlebark L, Burton LD, Setz VC, Cannell MB, Soeller C, Christie DL, Usami S, Matsubara A, Yoshie H, Ryan AF, Thorne PR (1999) Expression of the P2X(2) receptor subunit of the ATP-gated ion channel in the cochlea: implications for sound transduction and auditory neurotransmission. J Neurosci 19:8377-8388.
Houston ME (2006) Biochemistry primer for exercise science: Human Kinetics Publishers.
Howard J, Hudspeth AJ (1987) Mechanical relaxation of the hair bundle mediates adaptation in mechanoelectrical transduction by the bullfrog's saccular hair cell. Proc Natl Acad Sci U S A 84:3064-3068.
Howard J, Hudspeth AJ (1988) Compliance of the hair bundle associated with gating of mechanoelectrical transduction channels in the bullfrog's saccular hair cell. Neuron 1:189-199.
Hudspeth AJ, Choe Y, Mehta AD, Martin P (2000) Putting ion channels to work: mechanoelectrical transduction, adaptation, and amplification by hair cells. Proc Natl Acad Sci U S A 97:11765-11772.
Ichas F, Mazat JP (1998) From calcium signaling to cell death: two conformations for the mitochondrial permeability transition pore. Switching from low- to high-conductance state. Biochim Biophys Acta 1366:33-50.
Ichas F, Jouaville LS, Mazat JP (1997) Mitochondria are excitable organelles capable of generating and conveying electrical and calcium signals. Cell 89:1145-1153.
Ikeda K, Saito Y, Nishiyama A, Takasaka T (1992) Na(+)-Ca2+ exchange in the isolated cochlear outer hair cells of the guinea-pig studied by fluorescence image microscopy. Pflugers Arch 420:493-499.
Jacobson J, Duchen MR (2001) 'What nourishes me, destroys me': towards a new mitochondrial biology. Cell Death Differ 8:963-966.
Jagger DJ, Robertson D, Housley GD (2000) A technique for slicing the rat cochlea around the onset of hearing. J Neurosci Methods 104:77-86.
Jiang H, Sha SH, Forge A, Schacht J (2006) Caspase-independent pathways of hair cell death induced by kanamycin in vivo. Cell Death Differ 13:20-30.
Johnson LV, Walsh ML, Bockus BJ, Chen LB (1981) Monitoring of relative mitochondrial membrane potential in living cells by fluorescence microscopy. J Cell Biol 88:526-535.
Jou MJ, Peng TI, Sheu SS (1996) Histamine induces oscillations of mitochondrial free Ca2+ concentration in single cultured rat brain astrocytes. J Physiol 497 (Pt 2):299-308.
Jouaville LS, Ichas F, Holmuhamedov EL, Camacho P, Lechleiter JD (1995) Synchronization of calcium waves by mitochondrial substrates in Xenopus laevis oocytes. Nature 377:438-441.
Jouaville LS, Pinton P, Bastianutto C, Rutter GA, Rizzuto R (1999) Regulation of mitochondrial ATP synthesis by calcium: evidence for a long-term metabolic priming. Proc Natl Acad Sci U S A 96:13807-13812.
Kamimura T, Whitworth CA, Rybak LP (1999) Effect of 4-methylthiobenzoic acid on cisplatin-induced ototoxicity in the rat. Hear Res 131:117-127.

Kataoka Y, Ohmori H (1994) Activation of glutamate receptors in response to membrane depolarization of hair cells isolated from chick cochlea. J Physiol 477 (Pt 3):403-414.
Kelley MW (2007) Cellular commitment and differentiation in the organ of Corti. Int J Dev Biol 51:571-583.
Kennedy HJ (2002) Intracellular calcium regulation in inner hair cells from neonatal mice. Cell Calcium 31:127-136.
Kennedy HJ, Crawford AC, Fettiplace R (2005) Force generation by mammalian hair bundles supports a role in cochlear amplification. Nature 433:880-883.
Kennedy HJ, Evans MG, Crawford AC, Fettiplace R (2003) Fast adaptation of mechanoelectrical transducer channels in mammalian cochlear hair cells. Nat Neurosci 6:832-836.
Kim TH, Zhao Y, Barber MJ, Kuharsky DK, Yin XM (2000) Bid-induced cytochrome c release is mediated by a pathway independent of mitochondrial permeability transition pore and Bax. J Biol Chem 275:39474-39481.
Kimitsuki T, Ohmori H (1992) The effect of caged calcium release on the adaptation of the transduction current in chick hair cells. J Physiol 458:27-40.
Kimitsuki T, Ohmori H (1993) Dihydrostreptomycin modifies adaptation and blocks the mechano-electric transducer in chick cochlear hair cells. Brain Res 624:143-150.
Kirichok Y, Krapivinsky G, Clapham DE (2004) The mitochondrial calcium uniporter is a highly selective ion channel. Nature 427:360-364.
Kitahara T, Li-Korotky HS, Balaban CD (2005) Regulation of mitochondrial uncoupling proteins in mouse inner ear ganglion cells in response to systemic kanamycin challenge. Neuroscience 135:639-653.
Kokoszka JE, Waymire KG, Levy SE, Sligh JE, Cai J, Jones DP, MacGregor GR, Wallace DC (2004) The ADP/ATP translocator is not essential for the mitochondrial permeability transition pore. Nature 427:461-465.
Kopke RD, Liu W, Gabaizadeh R, Jacono A, Feghali J, Spray D, Garcia P, Steinman H, Malgrange B, Ruben RJ, Rybak L, Van de Water TR (1997) Use of organotypic cultures of Corti's organ to study the protective effects of antioxidant molecules on cisplatin-induced damage of auditory hair cells. Am J Otol 18:559-571.
Kroemer G, Reed JC (2000) Mitochondrial control of cell death. Nat Med 6:513-519.
Kros CJ, Rusch A, Richardson GP (1992) Mechano-electrical transducer currents in hair cells of the cultured neonatal mouse cochlea. Proc Biol Sci 249:185-193.
Lagostena L, Cicuttin A, Inda J, Kachar B, Mammano F (2001) Frequency dependence of electrical coupling in Deiters' cells of the guinea pig cochlea. Cell Commun Adhes 8:393-399.
Lahne M (2007) Damage-induced signalling mechanisms in the neonatal cochlea. PhD thesis.
Lakowicz JR, Szmacinski H, Nowaczyk K, Johnson ML (1992) Fluorescence lifetime imaging of free and protein-bound NADH. Proc Natl Acad Sci U S A 89:1271-1275.
Lesniak W, Pecoraro VL, Schacht J (2005) Ternary complexes of gentamicin with iron and lipid catalyze formation of reactive oxygen species. Chem Res Toxicol 18:357-364.
Li X, Fischel-Ghodsian N, Schwartz F, Yan Q, Friedman RA, Guan MX (2004) Biochemical characterization of the mitochondrial tRNASer(UCN) T7511C mutation associated with nonsyndromic deafness. Nucleic Acids Res 32:867-877.

Liberman MC, Gao J, He DZ, Wu X, Jia S, Zuo J (2002) Prestin is required for electromotility of the outer hair cell and for the cochlear amplifier. Nature 419:300-304.
Lin HW, Schneider ME, Kachar B (2005) When size matters: the dynamic regulation of stereocilia lengths. Curr Opin Cell Biol 17:55-61.
Lumpkin EA, Marquis RE, Hudspeth AJ (1997) The selectivity of the hair cell's mechanoelectrical-transduction channel promotes Ca2+ flux at low Ca2+ concentrations. Proc Natl Acad Sci U S A 94:10997-11002.
Ly JD, Grubb DR, Lawen A (2003) The mitochondrial membrane potential (deltapsi(m)) in apoptosis; an update. Apoptosis 8:115-128.
Mammano F, Kros CJ, Ashmore JF (1995) Patch clamped responses from outer hair cells in the intact adult organ of Corti. Pflugers Arch 430:745-750.
Mammano F, Bortolozzi M, Ortolano S, Anselmi F (2007) Ca2+ signaling in the inner ear. Physiology (Bethesda) 22:131-144.
Mammano F, Frolenkov GI, Lagostena L, Belyantseva IA, Kurc M, Dodane V, Colavita A, Kachar B (1999) ATP-Induced Ca(2+) release in cochlear outer hair cells: localization of an inositol triphosphate-gated Ca(2+) store to the base of the sensory hair bundle. J Neurosci 19:6918-6929.
Mangiardi DA, McLaughlin-Williamson K, May KE, Messana EP, Mountain DC, Cotanche DA (2004) Progression of hair cell ejection and molecular markers of apoptosis in the avian cochlea following gentamicin treatment. J Comp Neurol 475:1-18.
Marcantoni A, Baldelli P, Hernandez-Guijo JM, Comunanza V, Carabelli V, Carbone E (2007) L-type calcium channels in adrenal chromaffin cells: role in pace-making and secretion. Cell Calcium 42:397-408.
Marchetti P, Castedo M, Susin SA, Zamzami N, Hirsch T, Macho A, Haeffner A, Hirsch F, Geuskens M, Kroemer G (1996) Mitochondrial permeability transition is a central coordinating event of apoptosis. J Exp Med 184:1155-1160.
Marcotti W, van Netten SM, Kros CJ (2005) The aminoglycoside antibiotic dihydrostreptomycin rapidly enters mouse outer hair cells through the mechano-electrical transducer channels. J Physiol 567:505-521.
Marcus DC, Thalmann R, Marcus NY (1978) Respiratory rate and ATP content of stria vascularis of guinea pig in vitro. Laryngoscope 88:1825-1835.
Marcus DC, Wu T, Wangemann P, Kofuji P (2002) KCNJ10 (Kir4.1) potassium channel knockout abolishes endocochlear potential. Am J Physiol Cell Physiol 282:C403-407.
Margulis L (1996) Archaeal-eubacterial mergers in the origin of Eukarya: phylogenetic classification of life. Proc Natl Acad Sci U S A 93:1071-1076.
Martin P, Hudspeth AJ (1999) Active hair-bundle movements can amplify a hair cell's response to oscillatory mechanical stimuli. Proc Natl Acad Sci U S A 96:14306-14311.
Marzo I, Brenner C, Zamzami N, Susin SA, Beutner G, Brdiczka D, Remy R, Xie ZH, Reed JC, Kroemer G (1998) The permeability transition pore complex: a target for apoptosis regulation by caspases and bcl-2-related proteins. J Exp Med 187:1261-1271.
Matlib MA, Zhou Z, Knight S, Ahmed S, Choi KM, Krause-Bauer J, Phillips R, Altschuld R, Katsube Y, Sperelakis N, Bers DM (1998) Oxygen-bridged dinuclear ruthenium amine complex specifically inhibits Ca2+ uptake into mitochondria in vitro and in situ in single cardiac myocytes. J Biol Chem 273:10223-10231.

Matsui JI, Gale JE, Warchol ME (2004) Critical signaling events during the aminoglycoside-induced death of sensory hair cells in vitro. J Neurobiol 61:250-266.
Matsunaga T, Kumanomido H, Shiroma M, Ohtsuka A, Asamura K, Usami S (2004) Deafness due to A1555G mitochondrial mutation without use of aminoglycoside. Laryngoscope 114:1085-1091.
McCormack JG, Denton RM (1984) Role of Ca2+ ions in the regulation of intramitochondrial metabolism in rat heart. Evidence from studies with isolated mitochondria that adrenaline activates the pyruvate dehydrogenase and 2-oxoglutarate dehydrogenase complexes by increasing the intramitochondrial concentration of Ca2+. Biochem J 218:235-247.
McCormack JG, Halestrap AP, Denton RM (1990) Role of calcium ions in regulation of mammalian intramitochondrial metabolism. Physiol Rev 70:391-425.
McFadden SL, Ding D, Reaume AG, Flood DG, Salvi RJ (1999) Age-related cochlear hair cell loss is enhanced in mice lacking copper/zinc superoxide dismutase. Neurobiol Aging 20:1-8.
McKenzie M, Liolitsa D, Hanna MG (2004) Mitochondrial disease: mutations and mechanisms. Neurochem Res 29:589-600.
Mitchell P (1961) Coupling of phosphorylation to electron and hydrogen transfer by a chemi-osmotic type of mechanism. Nature 191:144-148.
Miyata H, Silverman HS, Sollott SJ, Lakatta EG, Stern MD, Hansford RG (1991) Measurement of mitochondrial free Ca2+ concentration in living single rat cardiac myocytes. Am J Physiol 261:H1123-1134.
Mockett BG, Housley GD, Thorne PR (1994) Fluorescence imaging of extracellular purinergic receptor sites and putative ecto-ATPase sites on isolated cochlear hair cells. J Neurosci 14:6992-7007.
Moller A (2000) Hearing: Its Physiology and Pathophysiology: Academic press.
Montero M, Alonso MT, Carnicero E, Cuchillo-Ibanez I, Albillos A, Garcia AG, Garcia-Sancho J, Alvarez J (2000) Chromaffin-cell stimulation triggers fast millimolar mitochondrial Ca2+ transients that modulate secretion. Nat Cell Biol 2:57-61.
Moreau B, Nelson C, Parekh AB (2006) Biphasic regulation of mitochondrial Ca2+ uptake by cytosolic Ca2+ concentration. Curr Biol 16:1672-1677.
Moser T, Beutner D (2000) Kinetics of exocytosis and endocytosis at the cochlear inner hair cell afferent synapse of the mouse. Proc Natl Acad Sci U S A 97:883-888.
Nakagawa T, Akaike N, Kimitsuki T, Komune S, Arima T (1990) ATP-induced current in isolated outer hair cells of guinea pig cochlea. J Neurophysiol 63:1068-1074.
Nakagawa T, Shimizu S, Watanabe T, Yamaguchi O, Otsu K, Yamagata H, Inohara H, Kubo T, Tsujimoto Y (2005) Cyclophilin D-dependent mitochondrial permeability transition regulates some necrotic but not apoptotic cell death. Nature 434:652-658.
Newman EA (2001) Propagation of intercellular calcium waves in retinal astrocytes and Muller cells. J Neurosci 21:2215-2223.
Nicholls DG (1982) Bioenergetics, An introduction to the chemiosmotic theory: Academic press.
Nicholls DG, Crompton M (1980) Mitochondrial calcium transport. FEBS Lett 111:261-268.

Nicholls DG, Chalmers S (2004) The integration of mitochondrial calcium transport and storage. J Bioenerg Biomembr 36:277-281.
Nicotera TM, Hu BH, Henderson D (2003) The caspase pathway in noise-induced apoptosis of the chinchilla cochlea. J Assoc Res Otolaryngol 4:466-477.
Noguchi Y, Yashima T, Ito T, Sumi T, Tsuzuku T, Kitamura K (2004) Audiovestibular findings in patients with mitochondrial A1555G mutation. Laryngoscope 114:344-348.
Nomiya S, Nishizaki K, Anniko M, Karita K, Ogawa T, Masuda Y (1998) Appearance and distribution of two Ca2+-binding proteins during development of the cochlea in the musk shrew. Brain Res Dev Brain Res 110:7-19.
North RA, Barnard EA (1997) Nucleotide receptors. Curr Opin Neurobiol 7:346-357.
Orrenius S (2004) Mitochondrial regulation of apoptotic cell death. Toxicol Lett 149:19-23.
Owens KN, Cunningham DE, MacDonald G, Rubel EW, Raible DW, Pujol R (2007) Ultrastructural analysis of aminoglycoside-induced hair cell death in the zebrafish lateral line reveals an early mitochondrial response. J Comp Neurol 502:522-543.
Pack AK, Slepecky NB (1995) Cytoskeletal and calcium-binding proteins in the mammalian organ of Corti: cell type-specific proteins displaying longitudinal and radial gradients. Hear Res 91:119-135.
Papakostas K, Hackney CM, Furness DN (2000) The distribution of the calcium buffer calbindin in the cochlea of the guinea-pig. Clin Otolaryngol Allied Sci 25:570-576.
Parekh AB (2003) Store-operated Ca2+ entry: dynamic interplay between endoplasmic reticulum, mitochondria and plasma membrane. J Physiol 547:333-348.
Pearson RA, Dale N, Llaudet E, Mobbs P (2005) ATP released via gap junction hemichannels from the pigment epithelium regulates neural retinal progenitor proliferation. Neuron 46:731-744.
Pellerin L, Bouzier-Sore AK, Aubert A, Serres S, Merle M, Costalat R, Magistretti PJ (2007) Activity-dependent regulation of energy metabolism by astrocytes: an update. Glia 55:1251-1262.
Petit PX, Goubern M, Diolez P, Susin SA, Zamzami N, Kroemer G (1998) Disruption of the outer mitochondrial membrane as a result of large amplitude swelling: the impact of irreversible permeability transition. FEBS Lett 426:111-116.
Petronilli V, Cola C, Massari S, Colonna R, Bernardi P (1993) Physiological effectors modify voltage sensing by the cyclosporin A-sensitive permeability transition pore of mitochondria. J Biol Chem 268:21939-21945.
Peuchen S, Clark JB, Duchen MR (1996) Mechanisms of intracellular calcium regulation in adult astrocytes. Neuroscience 71:871-883.
Piantadosi CA, Suliman HB (2006) Mitochondrial transcription factor A induction by redox activation of nuclear respiratory factor 1. J Biol Chem 281:324-333.
Piazza V, Ciubotaru CD, Gale JE, Mammano F (2007) Purinergic signalling and intercellular Ca2+ wave propagation in the organ of Corti. Cell Calcium 41:77-86.
Pickles JO (1988) An Introduction to the Physiology of Hearing: Academic Press.
Poot M, Zhang YZ, Kramer JA, Wells KS, Jones LJ, Hanzel DK, Lugade AG, Singer VL, Haugland RP (1996) Analysis of mitochondrial morphology and function with novel fixable fluorescent stains. J Histochem Cytochem 44:1363-1372.

Prezant TR, Agapian JV, Bohlman MC, Bu X, Oztas S, Qiu WQ, Arnos KS, Cortopassi GA, Jaber L, Rotter JI, et al. (1993) Mitochondrial ribosomal RNA mutation associated with both antibiotic-induced and non-syndromic deafness. Nat Genet 4:289-294.

Puskin JS, Gunter TE (1973) Ion and pH gradients across the transport membrane of mitochondria following Mn ++ uptake in the presence of acetate. Biochem Biophys Res Commun 51:797-803.

Putney JW, Jr. (1986) A model for receptor-regulated calcium entry. Cell Calcium 7:1-12.

Ramos-Franco J, Fill M, Mignery GA (1998) Isoform-specific function of single inositol 1,4,5-trisphosphate receptor channels. Biophys J 75:834-839.

Raphael Y (2002) Cochlear pathology, sensory cell death and regeneration. Br Med Bull 63:25-38.

Raphael Y, Altschuler RA (2003) Structure and innervation of the cochlea. Brain Res Bull 60:397-422.

Reed KC, Bygrave FL (1974) The inhibition of mitochondrial calcium transport by lanthanides and ruthenium red. Biochem J 140:143-155.

Ricci AJ, Fettiplace R (1997) The effects of calcium buffering and cyclic AMP on mechano-electrical transduction in turtle auditory hair cells. J Physiol 501 (Pt 1):111-124.

Ricci AJ, Fettiplace R (1998) Calcium permeation of the turtle hair cell mechanotransducer channel and its relation to the composition of endolymph. J Physiol 506 (Pt 1):159-173.

Ricci AJ, Crawford AC, Fettiplace R (2000) Active hair bundle motion linked to fast transducer adaptation in auditory hair cells. J Neurosci 20:7131-7142.

Richardson GP, Russell IJ (1991) Cochlear cultures as a model system for studying aminoglycoside induced ototoxicity. Hear Res 53:293-311.

Richardson GP, Forge A, Kros CJ, Fleming J, Brown SD, Steel KP (1997) Myosin VIIA is required for aminoglycoside accumulation in cochlear hair cells. J Neurosci 17:9506-9519.

Rizzuto R, Bernardi P, Pozzan T (2000) Mitochondria as all-round players of the calcium game. J Physiol 529 Pt 1:37-47.

Rizzuto R, Simpson AW, Brini M, Pozzan T (1992) Rapid changes of mitochondrial Ca2+ revealed by specifically targeted recombinant aequorin. Nature 358:325-327.

Rizzuto R, Bastianutto C, Brini M, Murgia M, Pozzan T (1994) Mitochondrial Ca2+ homeostasis in intact cells. J Cell Biol 126:1183-1194.

Rizzuto R, Pinton P, Carrington W, Fay FS, Fogarty KE, Lifshitz LM, Tuft RA, Pozzan T (1998) Close contacts with the endoplasmic reticulum as determinants of mitochondrial Ca2+ responses. Science 280:1763-1766.

Robb-Gaspers LD, Burnett P, Rutter GA, Denton RM, Rizzuto R, Thomas AP (1998) Integrating cytosolic calcium signals into mitochondrial metabolic responses. Embo J 17:4987-5000.

Roth B, Bruns V (1992) Postnatal development of the rat organ of Corti. II. Hair cell receptors and their supporting elements. Anat Embryol (Berl) 185:571-581.

Russell IJ, Sellick PM (1978) Intracellular studies of hair cells in the mammalian cochlea. J Physiol 284:261-290.

Rutter GA, Rizzuto R (2000) Regulation of mitochondrial metabolism by ER Ca2+ release: an intimate connection. Trends Biochem Sci 25:215-221.

Rybak LP, Ramkumar V (2007) Ototoxicity. Kidney Int 72:931-935.

Rybak LP, Whitworth C, Somani S (1999) Application of antioxidants and other agents to prevent cisplatin ototoxicity. Laryngoscope 109:1740-1744.
Salt AN, Melichar I, Thalmann R (1987) Mechanisms of endocochlear potential generation by stria vascularis. Laryngoscope 97:984-991.
Sanchez JA, Garcia MC, Sharma VK, Young KC, Matlib MA, Sheu SS (2001) Mitochondria regulate inactivation of L-type Ca2+ channels in rat heart. J Physiol 536:387-396.
Sanderson MJ, Charles AC, Dirksen ER (1990) Mechanical stimulation and intercellular communication increases intracellular Ca2+ in epithelial cells. Cell Regul 1:585-596.
Scaduto RC, Jr., Grotyohann LW (1999) Measurement of mitochondrial membrane potential using fluorescent rhodamine derivatives. Biophys J 76:469-477.
Scarpa A, Azzone GF (1970) The mechanism of ion translocation in mitochondria. 4. Coupling of K+ efflux with Ca2+ uptake. Eur J Biochem 12:328-335.
Scarpulla RC (2002) Nuclear activators and coactivators in mammalian mitochondrial biogenesis. Biochim Biophys Acta 1576:1-14.
Scemes E, Giaume C (2006) Astrocyte calcium waves: what they are and what they do. Glia 54:716-725.
Schapira AH (2006) Mitochondrial disease. Lancet 368:70-82.
Scholz TD, Laughlin MR, Balaban RS, Kupriyanov VV, Heineman FW (1995) Effect of substrate on mitochondrial NADH, cytosolic redox state, and phosphorylated compounds in isolated hearts. Am J Physiol 268:H82-91.
Sha SH, Taylor R, Forge A, Schacht J (2001) Differential vulnerability of basal and apical hair cells is based on intrinsic susceptibility to free radicals. Hear Res 155:1-8.
Sharma VK, Ramesh V, Franzini-Armstrong C, Sheu SS (2000) Transport of Ca2+ from sarcoplasmic reticulum to mitochondria in rat ventricular myocytes. J Bioenerg Biomembr 32:97-104.
Sheppard CA, Simpson PB, Sharp AH, Nucifora FC, Ross CA, Lange GD, Russell JT (1997) Comparison of type 2 inositol 1,4,5-trisphosphate receptor distribution and subcellular Ca2+ release sites that support Ca2+ waves in cultured astrocytes. J Neurochem 68:2317-2327.
Shigemoto T, Ohmori H (1990) Muscarinic agonists and ATP increase the intracellular Ca2+ concentration in chick cochlear hair cells. J Physiol 420:127-148.
Shimizu S, Narita M, Tsujimoto Y (1999) Bcl-2 family proteins regulate the release of apoptogenic cytochrome c by the mitochondrial channel VDAC. Nature 399:483-487.
Shimizu S, Eguchi Y, Kamiike W, Funahashi Y, Mignon A, Lacronique V, Matsuda H, Tsujimoto Y (1998) Bcl-2 prevents apoptotic mitochondrial dysfunction by regulating proton flux. Proc Natl Acad Sci U S A 95:1455-1459.
Simpson PB, Russell JT (1996) Mitochondria support inositol 1,4,5-trisphosphate-mediated Ca2+ waves in cultured oligodendrocytes. J Biol Chem 271:33493-33501.
Simpson PB, Russell JT (1998) Mitochondrial Ca2+ uptake and release influence metabotropic and ionotropic cytosolic Ca2+ responses in rat oligodendrocyte progenitors. J Physiol 508 (Pt 2):413-426.
Skellett RA, Chen C, Fallon M, Nenov AP, Bobbin RP (1997) Pharmacological evidence that endogenous ATP modulates cochlear mechanics. Hear Res 111:42-54.

Sparagna GC, Gunter KK, Sheu SS, Gunter TE (1995) Mitochondrial calcium uptake from physiological-type pulses of calcium. A description of the rapid uptake mode. J Biol Chem 270:27510-27515.
Spassova MA, Soboloff J, He LP, Xu W, Dziadek MA, Gill DL (2006) STIM1 has a plasma membrane role in the activation of store-operated Ca(2+) channels. Proc Natl Acad Sci U S A 103:4040-4045.
Steyger PS, Gillespie PG, Baird RA (1998) Myosin Ibeta is located at tip link anchors in vestibular hair bundles. J Neurosci 18:4603-4615.
Stratta P, Segoloni GP, Canavese C, Muzio G, Dogliani M, Serra A, Allemandi P, Salomone M, Caramellino C, Canuto R (1994) Oxygen free radicals are not the main factor in experimental gentamicin nephrotoxicity. Ren Fail 16:445-455.
Sugahara K, Rubel EW, Cunningham LL (2006) JNK signaling in neomycin-induced vestibular hair cell death. Hear Res 221:128-135.
Susin SA, Zamzami N, Castedo M, Hirsch T, Marchetti P, Macho A, Daugas E, Geuskens M, Kroemer G (1996) Bcl-2 inhibits the mitochondrial release of an apoptogenic protease. J Exp Med 184:1331-1341.
Szabadkai G, Simoni AM, Rizzuto R (2003) Mitochondrial Ca2+ uptake requires sustained Ca2+ release from the endoplasmic reticulum. J Biol Chem 278:15153-15161.
Szabo I, Bernardi P, Zoratti M (1992) Modulation of the mitochondrial megachannel by divalent cations and protons. J Biol Chem 267:2940-2946.
Tager JM, Veldsema-Currie RD, Slater EC (1966) Chemi-osmotic theory of oxidative phosphorylation. Nature 212:376-379.
Takeuchi S, Ando M (1997) Marginal cells of the stria vascularis of gerbils take up glucose via the facilitated transporter GLUT: application of autofluorescence. Hear Res 114:69-74.
Tan CT, Lee SY, Yao CJ, Liu SH, Lin-Shiau SY (2001) Effects of gentamicin and pH on [Ca2+]i in apical and basal outer hair cells from guinea pigs. Hear Res 154:81-87.
Thayer SA, Miller RJ (1990) Regulation of the intracellular free calcium concentration in single rat dorsal root ganglion neurones in vitro. J Physiol 425:85-115.
Tiede LM, Rocha-Sanchez SM, Hallworth R, Nichols MG, Beisel K (2007) Determination of hair cell metabolic state in isolated cochlear preparations by two-photon microscopy. J Biomed Opt 12:021004.
Toescu EC, Verkhratsky A (2000) Assessment of mitochondrial polarization status in living cells based on analysis of the spatial heterogeneity of rhodamine 123 fluorescence staining. Pflugers Arch 440:941-947.
Toescu EC, Gardner JM, Petersen OH (1993) Mitochondrial Ca2+ uptake at submicromolar [Ca2+]i in permeabilised pancreatic acinar cells. Biochem Biophys Res Commun 192:854-859.
Trenker M, Malli R, Fertschai I, Levak-Frank S, Graier WF (2007) Uncoupling proteins 2 and 3 are fundamental for mitochondrial Ca2+ uniport. Nat Cell Biol 9:445-452.
Tritsch NX, Yi E, Gale JE, Glowatzki E, Bergles DE (2007) The origin of spontaneous activity in the developing auditory system. Nature 450:50-55.
Usami S, Takumi Y, Fujita S, Shinkawa H, Hosokawa M (1997) Cell death in the inner ear associated with aging is apoptosis? Brain Res 747:147-150.

Vander Heiden MG, Chandel NS, Williamson EK, Schumacker PT, Thompson CB (1997) Bcl-xL regulates the membrane potential and volume homeostasis of mitochondria. Cell 91:627-637.
Vicente-Torres MA, Schacht J (2006) A BAD link to mitochondrial cell death in the cochlea of mice with noise-induced hearing loss. J Neurosci Res 83:1564-1572.
Vlajkovic SM, Thorne PR, Housley GD, Munoz DJ, Kendrick IS (1998) Ecto-nucleotidases terminate purinergic signalling in the cochlear endolymphatic compartment. Neuroreport 9:1559-1565.
Vlajkovic SM, Thorne PR, Sevigny J, Robson SC, Housley GD (2002) NTPDase1 and NTPDase2 immunolocalization in mouse cochlea: implications for regulation of p2 receptor signaling. J Histochem Cytochem 50:1435-1442.
Voets T, Neher E, Moser T (1999) Mechanisms underlying phasic and sustained secretion in chromaffin cells from mouse adrenal slices. Neuron 23:607-615.
von Gersdorff H, Vardi E, Matthews G, Sterling P (1996) Evidence that vesicles on the synaptic ribbon of retinal bipolar neurons can be rapidly released. Neuron 16:1221-1227.
Wallace DC (1999) Mitochondrial diseases in man and mouse. Science 283:1482-1488.
Wang J, Ladrech S, Pujol R, Brabet P, Van De Water TR, Puel JL (2004) Caspase inhibitors, but not c-Jun NH2-terminal kinase inhibitor treatment, prevent cisplatin-induced hearing loss. Cancer Res 64:9217-9224.
Wang J, Ruel J, Ladrech S, Bonny C, van de Water TR, Puel JL (2007) Inhibition of the c-Jun N-terminal kinase-mediated mitochondrial cell death pathway restores auditory function in sound-exposed animals. Mol Pharmacol 71:654-666.
Wang Z, Tymianski M, Jones OT, Nedergaard M (1997) Impact of cytoplasmic calcium buffering on the spatial and temporal characteristics of intercellular calcium signals in astrocytes. J Neurosci 17:7359-7371.
Wangemann P (2006) Supporting sensory transduction: cochlear fluid homeostasis and the endocochlear potential. J Physiol 576:11-21.
Ward DT, Riccardi D (2002) Renal physiology of the extracellular calcium-sensing receptor. Pflugers Arch 445:169-176.
Ward DT, McLarnon SJ, Riccardi D (2002) Aminoglycosides increase intracellular calcium levels and ERK activity in proximal tubular OK cells expressing the extracellular calcium-sensing receptor. J Am Soc Nephrol 13:1481-1489.
Wendt-Gallitelli MF, Isenberg G (1991) Total and free myoplasmic calcium during a contraction cycle: x-ray microanalysis in guinea-pig ventricular myocytes. J Physiol 435:349-372.
Wersall J, Lundquist PG, Bjorkroth B (1969) Ototoxicity of gentamicin. J Infect Dis 119:410-416.
Werth JL, Thayer SA (1994) Mitochondria buffer physiological calcium loads in cultured rat dorsal root ganglion neurons. J Neurosci 14:348-356.
White PN, Thorne PR, Housley GD, Mockett B, Billett TE, Burnstock G (1995) Quinacrine staining of marginal cells in the stria vascularis of the guinea-pig cochlea: a possible source of extracellular ATP? Hear Res 90:97-105.
Wu MM, Luik RM, Lewis RS (2007) Some assembly required: constructing the elementary units of store-operated Ca2+ entry. Cell Calcium 42:163-172.
Wu YC, Ricci AJ, Fettiplace R (1999) Two components of transducer adaptation in auditory hair cells. J Neurophysiol 82:2171-2181.

Xiang J, Chao DT, Korsmeyer SJ (1996) BAX-induced cell death may not require interleukin 1 beta-converting enzyme-like proteases. Proc Natl Acad Sci U S A 93:14559-14563.

Yamashita D, Miller JM, Jiang HY, Minami SB, Schacht J (2004) AIF and EndoG in noise-induced hearing loss. Neuroreport 15:2719-2722.

Yang CL, Du XH, Han YX (1995) Renal cortical mitochondria are the source of oxygen free radicals enhanced by gentamicin. Ren Fail 17:21-26.

Yang J, Liu X, Bhalla K, Kim CN, Ibrado AM, Cai J, Peng TI, Jones DP, Wang X (1997) Prevention of apoptosis by Bcl-2: release of cytochrome c from mitochondria blocked. Science 275:1129-1132.

Ylikoski J, Xing-Qun L, Virkkala J, Pirvola U (2002) Blockade of c-Jun N-terminal kinase pathway attenuates gentamicin-induced cochlear and vestibular hair cell death. Hear Res 166:33-43.

Zhao H, Young WY, Yan Q, Li R, Cao J, Wang Q, Li X, Peters JL, Han D, Guan MX (2005) Functional characterization of the mitochondrial 12S rRNA C1494T mutation associated with aminoglycoside-induced and non-syndromic hearing loss. Nucleic Acids Res 33:1132-1139.

Zorov DB, Filburn CR, Klotz LO, Zweier JL, Sollott SJ (2000) Reactive oxygen species (ROS)-induced ROS release: a new phenomenon accompanying induction of the mitochondrial permeability transition in cardiac myocytes. J Exp Med 192:1001-1014.

Zwirner P, Wilichowski E (2001) Progressive sensorineural hearing loss in children with mitochondrial encephalomyopathies. Laryngoscope 111:515-521.